PhD Thesis R-386
Institut for Byggeri og Anlæg

# Challenges when retrofitting multi-storey buildings with interior thermal insulation

Tommy Riviere Odgaard

**Challenges when retrofitting multi-storey buildings consisting of solid masonry facades and embedded wood with interior thermal insulation**

**Supervisors**
Associate Professor Søren Peter Bjarløv, The Technical University of Denmark
Professor Carsten Rode, The Technical University of Denmark
Senior specialist Michael Per Vesterløkke†, COWI Denmark
Section leader and senior specialist Peter Schjørmann Thorsen, COWI Denmark
Senior specialist Jens Brendstrup, COWI Denmark
Senior specialist Merete Hjorth Rasmussen, COWI Denmark

**Assessment Committee**
Professor Svend Højgaard Svendsen (Chair), The Technical University of Denmark
Senior Lecturer Lars-Erik Harderup, Lund University, Moisture Research Centre
Dr Ernst Jan de Place Hansen, Aalborg University, Danish Building Research Institute

**Start date:**
December 15, 2013

**Submission date:**
January 26, 2018

**Re-submission date, revised after comments from assessment committee:**
February 14, 2019

Minor changes have been incorporated in the Thesis after the thesis defence, based on comments from the assessment committee. The changes have been approved by the assessment committee.



**Department of Civil Engineering**
Technical University of Denmark
Building 118
DK-2800 Kgs. Lyngby
Denmark

ISBN: 9788778774811
Report R-386

# PREFACE

This Thesis was initially submitted after the equivalent of three years full time industrial PhD study at the Technical University of Denmark and COWI A/S. The Thesis has been revised and re-submitted based on comments from the assessment committee, as it was deemed not suitable for defence in its original form.

The Thesis is the basis of the fulfilment of requirements for the Danish industrial PhD degree. The Thesis is written as a paper-based dissemination, based on a number of papers, where the ones submitted for peer-reviewed journals are appended.

Kgs. Lyngby, February 14, 2019.

_____

Tommy Riviere Odgaard

# ACKNOWLEDGEMENTS

This industrial PhD project have been carried out in cooperation with, with office space at both locations:

- The Technical University of Denmark, department of Civil Engineering, section of building design.
- COWI Denmark, department of Buildings (Eastern Denmark), section of Building Physics and Refurbishment.

The project was supported through the Danish industrial PhD program by Innovationsfonden [grant number 1355-00129]; COWIfonden [grant number C-123.01]; and COWI A/S.

The experimental setup for the 8-wall container was supported by Realdania, planned in cooperation with Xella Denmark. Xella and Ytong have not had any influence on the results and analyses of the experiment.

The experimental setup for the 16-wall container was supported by Grundejernes Investeringsfond, planned in cooperation with the Danish Technological Institute and COWI Denmark.

Supplementary work was supported through the RIBuild project under the European research programme Horizon 2020, [call H2020-EE-2014-1-PPP, topic EE-03-2014].

I would like to thank my team of supervisors for discussions and sparring during the project: Søren Peter Bjarløv, Carsten Rode, Michael Vesterløkke†, Peter Schjørmann Thorsen, Merete Hjorth Rasmussen, and Jens Brendstrup. I will be ever grateful for the assistance of Michael Vesterløkke, and am sorry that he did not live through the last 14 days to see the finished thesis. All my colleagues in COWI deserve a special thank you, for always providing a good working atmosphere.

I would like to thank the assessment committee for their invaluable comments to the 1st (rejected) edition of this thesis. The comments were an invaluable help to make a better and improved 2nd edition.

Furthermore, I would like to thank:

- Lab technician in metrology, Lars Kokholm Andersen, for the development of the physical monitoring system with good comprehension for my needs.

- PhD student Tessa Kvist Hansen for the good cooperation in the office and with the development of wind driven rain systems, but also for the many academic discussions, later joined by new PhD student Nickolaj Feldt Jensen.

- The staff at the Institute of Building Climatology, Technische Universität Dresden, for the collaboration regarding material measurements of materials used in the container projects (partly funded by the RIBuild project), and the initial consideration of the Delphin model setup for future collaborative simulation studies between the technical universities of Dresden and Denmark.

- Phillip Skov Halding for his support regarding the outline of the Thesis and for allowing to use his PhD Thesis (Halding et al., 2016) as a base for my own Thesis.

- Jule Christensen for her invaluable help in proofreading my Thesis.

Finally, I would like to thank my wife and two kids for always being ready with a smile and a hug, and for allowing me to work insane hours, especially during the last ½ year, while home and social life have been on standby.

# ABSTRACT

Today, approximately 25 % of the apartments in the Danish multi-storey stock of more than two stories are found in buildings with masonry facades erected in the period 1850-1930. Of these apartments, 71 % are situated in Copenhagen, the Danish capital. The building traditions and norms in force during the period entail that these buildings share similar characteristics, including solid masonry walls and embedded wooden components. The energy use and indoor climate was not in focus during construction, wherefore the current occupants cannot expect modern levels of thermal comfort and the section include a considerable energy saving potential. It is evident that thermal comfort and energy use can be improved by increasing the thermal resistance of the façade. With focus on the masonry part of the total façade area, this can be achieved with thermal insulation applied to the interior or exterior surface. While application to the exterior surface is the best solution from a building physics point of view, the retention of the exterior façade expression is often a desire from the owner or a preservation requirement, leaving application to the interior surface as the only possibility.

The buildings from the period have been investigated to determine the degree of shared characteristics within the building segment, showing similar building techniques with consistent thin spandrels under the windows and a low share of available interior surface area for the application of insulation. There were performed thermal simulations of characteristic façade sections in 3-dimensional models, finding that insulation of the spandrel can achieve up to 40 % of the maximum possible reduction achievable from reducing the thermal transmittance by retrofitting the masonry with interior insulation.

The influence on the hygrothermal conditions when applying interior thermal insulation to solid masonry walls have been investigated experimentally in a case study and by comparative analyses of results from two field experiments.

The case study was 2 rooms in a dormitory with a normal indoor moisture load, situated at an urban location. The study showed how retrofitting the interior surface of a solid masonry spandrel with a diffusion open thermal insulation system changed the hygrothermal balance in the wall, resulting in a colder and wetter wall with similar conditions throughout the wall. Evaluation of the case study, based on measurements and on-site investigations, showed no calculated or observed risks of moisture-induced damage.

The field experiments were designed and constructed with an extensive measurement program, exposed to a high indoor moisture load and located in a

rural area. The measurements were used for comparative analyses, to investigate the difference in hygrothermal performance of different interior thermal insulation systems, applied to the entire masonry surface or with some variations within the systems. The comparative analyses were based on the measured relative humidity, temperature and on mathematical damage models able to take exposure time into consideration. The damage models were used to compare the calculated risks of moisture-induced damage in the different systems. The results of the comparative analyses with the boundary conditions of the field experiments showed:

- Application of a thermal insulation system depending on a tight vapour barrier or a diffusion open thermal insulation system resulted in an increase in calculated mould germination and growth on the masonry surface behind the insulation.

- Application of a thermal insulation system depending on a tight vapour barrier resulted in an increase in calculated irreversible wooden decay in the wooden beam (floor joist), compared to other insulation systems and an un-insulated wall.

- Hydrophobizing the exterior masonry surface with a hydrophobic façade treatment had an overall positive effect on the hygrothermal conditions, and can be further improved by replacing a part of the moisture-open insulation with autoclaved aerated concrete.

# RESUME

Omtrentligt 25 % af lejlighederne i den danske etage-boligmasse over to etager er placeret i historiske bygninger med en blank murværksfacade, opført i perioden 1850-1930. Af disse lejligheder er 71 % placeret i København/Frederiksberg. Bygningerne er grundet bygningstraditioner og normer opført med en ens byggeskik igennem perioden, bestående af blandt andet massive murstensvægge og bærende træelementer der ligger af i murværket.

Der var under opførslen af bygningerne ikke fokus på energiforbrug og komfort, og nuværende beboere kan derfor ikke forvente et moderne niveau af blandt andet termisk komfort. Potentialet for forbedring af netop termisk komfort er betydeligt for bygninger i dette segment, med stort potentiale for ligeledes at forbedre bygningens energiforbrug igennem øget isoleringsevne af facaden. Fokus i dette erhvervs-ph.d. projekt har været på murværks-andelen af facaderne, hvor komfortforbedringer og energibesparelser kan opnås ved at opsætte enten ind- eller udvendig efterisolering. Ud fra et bygningsfysisk synspunkt vil den bedste løsning være at efterisolere den udvendig side, men da facadens oprindelige udtryk ofte ønskes bibeholdt af ejer, eller er krævet grundet bevaringsværdighed, er det kun muligt at efterisolere den indvendige overflade.

Opbygningen af etageejendomme fra perioden 1850-1930 er blevet undersøgt og har vist at der er benyttet en ensartet byggeteknik igennem perioden, bestående af tynde brystningspartier og en lav procentdel af det indvendige overfladeareal med mulighed for efterisolering. Der er blevet udført termiske simuleringer af typiske facadesektioner, som viste at 40 % af den teoretisk opnåelige energibesparelse ved isolering af hele den indvendige overflade, vil kunne opnås ved udelukkende at isolere de tynde brystningspartier.

De hygrotermiske ændringer der introduceres ved opsætning af indvendig efterisolering på massivt murværk er blevet undersøgt i et casestudie og ved komparativ analyse af resultater fra to store eksperimentelle opsætninger.

Casestudiet bestod af 2 værelser i et kollegie med en normal indendørs fugtbelastningsgrad, beliggende i et byområde. Undersøgelsen viste at indvendig efterisolering af et brystningsparti med et diffusionsåbent materiale ændrede den hygrotermiske balance i væggen, resulterende i en koldere og vådere mur med ens værdier i hele murens dybde. Casestudiet blev undersøgt baseret på målinger og fysiske in-situ undersøgelser, og viste ingen beregnet eller observeret udvikling af skimmelvækst, trænedbrydning eller frostskader.

De eksperimentelle opsætninger blev designet og opbygget med et omfattende måleprogram, udsat for en høj indendørs fugtbelastningsgrad, beliggende i Kongens Lyngby. Eksperimenterne gik ud på at vurdere forskellige eksisterende indvendige termiske isoleringssystemer, installeret på hele den indvendige overflade og variationer heraf. Vurderingerne blev baseret på en komparativ analyse af måleresultater: Relativ luftfugtighed og temperatur, samt matematiske skademodeller der inkluderede eksponeringstid. Skadesmodellerne blev brugt til at indikere og sammenligne risikoen for udvikling af skimmelvækst og trænedbrydning. Resultaterne af de komparative analyser med de randbetingelser der gør sig gældende i de eksperimentelle opsætninger viste:

- Anvendelse af et indvendige efterisoleringssystem afhængigt af enten tæt dampspærre eller diffusionsåbenhed resulterede i forværring a beregnet skimmelvækst på murværksoverfladen bag isoleringen.

- Anvendelse af et indvendigt efterisoleringssystem afhængigt af tæt dampspærre resulterede i forværring af beregnet irreversibel trænedbrydning i træbjælkeenden, sammenlignet med andre efterisoleringsløsninger og en u-isoleret væg.

- Imprægnering af det udvendige murværk med en hydrofob facadebehandling havde en overordnet positiv indvirkning på de hygrotermiske forhold, og kan forbedres yderligere ved at erstatte en del af den diffusionsåbne isolering med gasbeton med en højere varmeledningsevne.

# ABBREVIATIONS, SYMBOLS AND DEFINITIONS

## *Abbreviations*

AAC = Autoclaved Aerated Concrete

BBR = the Danish Building and Dwelling Register

DTU = Technical University of Denmark

IST = Innovative Sensor Technology IST AG

**SH(#)** = Sub-hypothesis(followed by number)

TI = Danish Technological Institute

TUD = Technische Universität Dresden

TUT = Tampere University of Technology

VTT = VTT Technical Research centre of Finland

WDR = Wind Driven Rain

## *Symbols and units*

| Symbol | Description | Unit |
|---|---|---|
| $\alpha$ | Activation index for wooden decay mass loss | $-$ |
| $\alpha_V$ | Exposure coefficient | $-$ |
| $C_{th}$ | Thermal conductance | $\frac{W}{K}$ |
| $d$ | Thickness | $m$ |
| $DRF$ | Driving rain factor | $-$ |
| $\mathrm{Factor_b}$ | Building/environment factors, transforming $r_v$ *to* $r_{vb}$ | $-$ |

| | | |
|---|---|---|
| $h$ | Height | $m$ |
| $\lambda$ | Transport coefficient for thermal conductivity | $\frac{W}{m \cdot K}$ |
| $MI$ | Mould index | $-$ |
| $ML$ | Wooden decay mass loss | % |
| $p$ | Vapour pressure | $Pa$ |
| $p_{sat}$ | Saturated vapour pressure | $Pa$ |
| $\varphi$ | Relative humidity | $-$ |
| $\Psi$ | Linear thermal transmittance | $\frac{\mathrm{W}}{\mathrm{m} \cdot \mathrm{K}}$ |
| $R$ | Thermal resistance | $\frac{\mathrm{m}^2\mathrm{K}}{\mathrm{W}}$ |
| $R$ | DC electrical resistance | $log10M\Omega$ |
| $R_{adjusted}$ | DC electrical resistance, adjusted to 20°C | $log10M\Omega$ |
| $\mathrm{r_v}$ | Rain moving towards a vertical surface | $\frac{l}{m^2}$ |
| $R_v$ | Gas constant for water vapour = 462 | $\frac{Pa \cdot m^3}{K \cdot kg}$ |
| $r_{vb}$ | Rain deposited on a vertical building surface | $\frac{l}{m^2}$ |
| $r_h$ | Horizontal rain | $\frac{\mathrm{l}}{\mathrm{m}^2}$ or mm |
| $r_{h,intensity}$ | Horizontal rainfall intensity | $\frac{\mathrm{l}}{\mathrm{m}^2 \cdot \mathrm{h}}$ or $\frac{\mathrm{mm}}{\mathrm{h}}$ |
| $R_s$ | Convective heat transfer resistance | $\frac{\mathrm{m}^2\mathrm{K}}{\mathrm{W}}$ |

| | | |
|---|---|---|
| $RH$ | Relative humidity | % |
| $T$ | Absolute temperature | $K$ |
| $\theta$ | Celsius temperature | $°C$ |
| $\Theta$ | Angle between wind direction and wall surface | [°] |
| $u$ | Wooden moisture content (weight-%) | % |
| $U$ or $U-value$ | Thermal transmittance | $\frac{\mathrm{W}}{\mathrm{m}^2 \cdot \mathrm{K}}$ |
| $v$ | Humidity by volume | $\frac{kg}{m^3}$ |
| $\mathrm{V}_{10}$ | Standard wind speed from weather station | $\frac{m}{s}$ |
| $V_t$ | Terminal fall speed of raindrop | $\mathrm{m/s}$ |
| $\mathrm{V(z)}$ | Wind speed at height of interest | $\frac{m}{s}$ |
| $w$ | Width | $m$ |
| $z$ | Height of interest | $m$ |
| $\emptyset$ | Raindrop diameter | $mm$ |
| $\overline{\emptyset}$ | Median raindrop diameter | $mm$ |

## *Subscripts*

*s* = Surface resistance

*i* = Interior

*e* = Exterior

## *Definitions*

I have chosen to use the following definitions throughout the PhD Thesis, acknowledging that other words/definitions exist in literature:

> Moisture-tight system:

Traditional thermal insulation strategy when retrofitted an existing interior surface with thermal insulation. Based on a framework, usually comprised of wood or steel, with thermal insulation in between and finished with a vapour barrier on the warm side of the thermal insulation material.

> Moisture-open system:

Thermal insulation system designed for the interior and/or exterior side of an existing construction, without a vapour barrier. Many different thermal insulation materials exist, all open for some degree of moisture transport. The materials have various material parameters, and the moisture transport take place by a combination of capillary transport in pores and moisture diffusion through the material.

> Interior (thermal) insulation:

A thermal insulation material retrofitted to the existing interior surface of a buildings outer leaf.

> Hydrophobic façade treatment, hydrophobation of material and hydrophobized material:

Relating to the impregnation of an exterior façade, thereby reducing the capillary transport of water in the outmost layer of the thermal envelope (both in- and outwards). The defined words define the material, the process and the result.

> Multi-storey building:

A multi-storey building is defined as a building with individual households on different floors.

> Wooden beam (end)

Wooden beams used in the floor structure spanning between the exterior masonry facades or composed of various trimming due to openings in the floor. The beams rest on wall plates embedded along the façade, with flooring resting on top of the wooden beams. The end of the wooden beam relates to the part situated in the façade, on the exterior side of the wall plate. A wooden beam is also known as a floor joist.

> Hygrothermal (conditions):

The combination of moisture and heat. The hygrothermal conditions include temperature and relative humidity.

# TABLE OF CONTENTS

# APPENDED PAPERS

**Paper #1** (Odgaard et al., 2018a)**:**
Interior insulation – Characterisation of the historic, solid masonry building segment and analysis of the heat saving potential by 1d, 2d, and 3d simulation

**Authors:**
Tommy Odgaard (DTU/COWI), Søren Peter Bjarløv (DTU), Carsten Rode (DTU).

**Publication:**
Published in Energy and Buildings, Volume 162, Pages 1-11, 1 March 2018.

**Outline:**
The paper presents and analyses 3 subjects: The composition of the characteristic historic Danish multi-storey buildings, erected in the period 1850-1930 and 1930–1950; the segment size and distribution of multi-storey buildings in Denmark; the potential theoretical heat saving from installing interior thermal insulation to a façade window section, including comparative analyses using 1-, 2- and 3-dimensional thermal simulation.

---

**Paper #2** (Odgaard et al., 2018b)**:**
Interior insulation - Experimental investigation of hygrothermal conditions and damage evaluation of solid masonry façades in a listed building

**Authors:**
Tommy Odgaard (DTU/COWI), Søren Peter Bjarløv (DTU), Carsten Rode (DTU).

**Publication:**
Published in Building and Environment, Volume 129, Pages 1-14, 1 February 2018.

**Outline:**
The paper presents and analyses the results from 2 years and 8 months of measurements in a case study, where the interior surface of a solid masonry spandrel was retrofitted with thermal insulation. The work includes thermal comfort considerations based on interior surface temperatures, mould risk evaluation based on a mathematical model and physical measurements, wooden decay risk evaluation based on a mathematical model and frost risk evaluation based on visual inspections and an analysis of measurements.

**Paper #3** (Odgaard et al., 2018c)**:**
Influence of hydrophobation and deliberate thermal bridge on hygrothermal conditions of internally insulated historic solid masonry walls with built-in wood

**Authors:**
Tommy Odgaard (DTU/COWI), Søren Peter Bjarløv (DTU), Carsten Rode (DTU).

**Publication:**
Published in Energy and Buildings, Volume 173, Pages 530-546, 15 August 2018.

**Outline:**
This paper presents the first results from one of two large experimental setups with solid masonry walls and wooden elements in refrigerated containers at the Technical University of Denmark. The paper includes comparative analyses with a point of reference in an un-insulated wall, focusing on the influence in the hygrothermal balance of the construction and the risk of damage when applying three variants of the same interior thermal insulation system.

# 1 INTRODUCTION

## 1.1 Incentive for action

A large share of the building mass in the major cities of Denmark consist of historic multi-storey buildings, built in the period 1850-1930 with solid masonry walls at a time with no regulations regarding energy consumption. Especially the city centres are characterised by mostly consisting of this type of building, most of which have a bare brick exterior surface. It is in general desired to maintain this typical and characteristic facade expression, in some cases preferred by the owner, in other cases controlled by legislation.

However, considering that the buildings now, in the year 2018, were constructed between 88 and 168 years ago, it is obvious that they do not live up to modern standards within energy use or indoor environment. Three main types of stakeholders have been identified, with different agendas regarding the current state of the historic multi-storey buildings:

- Government and building owners
- Tenants
- Professionals within the building sector

### 1.1.1 Government and building owners

On a governmental level, the Danish government has a vision of becoming fossil fuel free by year 2050. Different means exist to achieve this aim for the Danish capital (Harrestrup and Svendsen, 2014): By investing in renovation of the current building mass or the energy supply. Harrestrup and Svendsen emphasised the need to invest in energy renovations as early as possible, thereby reducing the future needed heat supply capacity and thereby investment. This need was emphasised, as investment solely into the supply side would result in too expensive and oversized supply.

Looking into the energy consumption for space heating and domestic hot water, it was found that multi-storey building from the period 1851-1930 consumed 4.4 TWh/year, corresponding to approximately 3.2 % of the total energy used for space heating and domestic hot water in Denmark. Comparing to the specific energy used for space heating and domestic hot water in all multi-storey buildings, the energy use of buildings from this period correspond to 38.3 % (Kragh and Wittchen, 2014; Odgaard et al., 2018a).

With the governments vision to become free of fossil fuels for energy production, the Danish multi-storey buildings with solid masonry walls therefore receive increasing attention for their large potential for heat loss reduction and consequent reduction of $CO_2$ emissions (Kragh and Wittchen, 2014; Wittchen et al., 2011).

The building owners are influenced by the government's aim to reduce energy consumption through utility companies. This demand to reduce energy was imposed upon the Danish utility companies in 2016, directed towards building owners primarily through consultancy or subsidy for energy saving measures (Danish Energy Agency, 2017).

### *1.1.2* Tenants

On a tenant level, the multi-storey buildings from 1850-1930 cannot provide comfort equivalent to that of modern buildings. These multi-storey buildings were built in a period when regulations dictated the structural design, with no consideration in thermal insulation. From the time of erection to now, energy prices have risen considerably, starting with the first international oil crisis in 1973, and occupants are generally expecting more comfort with higher indoor temperatures.

The masonry part of the traditional multi-storey building façade can be summarized as masonry columns and the part of the façade over the windows, varying in thickness depending on the floor, and a thin non-varying spandrel underneath the windows (Engelmark, 2013, 1983). The spandrel is responsible for a considerable part of the façades overall heat loss.

While it might be possible to increase the comfort of tenants by supplying heat and thereby increase the ambient air temperature to that expected in modern buildings, a minimum of 20 $^0$C, the thin walls still present a risk of discomfort from cold surfaces. An investigation based on 1d hygrothermal simulation in WUFI by Finken et al. of an un-insulated spandrel with a Danish design year (DS 418:2011,

2011) showed a minimum temperature on the inside surface of 9.2 $^0$C (Finken et al., 2016). This temperature difference can cause discomfort for occupants based on asymmetric radiation larger than 10 $^0$C from surfaces (Fanger et al., 2006, 1985), cold floors (DS/EN ISO 7730:2006, 2006; DS/ISO/TS 13732-2:2011, 2011) and risk of draught occurring from cold air drop down from the cold interior surfaces.

### *1.1.3* Professionals within the building sector

On the consultant and entrepreneur level, there is a lack of knowledge and best practices to provide safe solutions for fulfilling the needs of the government, building owners and tenants, described in Section 1.1.1 and 1.1.2 respectively.

Guidelines regarding interior thermal insulation in Denmark only contain information on moisture-tight systems (Brandt et al., 2013). It is however often discovered that vapour barriers are not vapour tight in joints due to design or execution errors. With the current structure of the Danish building sector, I will claim that it is not possible to install a tight vapour barrier during normal refurbishment of existing multi-storey buildings from 1850-1930.

Multiple cases with moisture-induced damage in buildings related to retrofitted thermal insulation on the interior surface have been seen, including one experimental setup describing the reason presented later in Section 5.3 on page 133. The extent of damage caused by interior insulation in Denmark is difficult to clarify, as investigations performed by consultancy firms are performed under client confidentiality and no data has yet been distributed. Some examples of mould growth behind moisture-tight systems have been presented by a researcher at the Danish Technological Institute (TI) (Høegh, 2015), and cases with damage in connection with moisture-open systems have also been seen. A unique Danish organization, BYG-ERFA, gathers and distributes examples and documented constructional experiences. This organization aims to distribute knowledge to enhance the quality and limit risks within the building sector. BYG-ERFA is well-respected and their short brochures are used by students, consultants and practitioners within the building industry as common knowledge, which entails that it is a very powerful statement when they recommend to avoid interior thermal insulation and instead recommend to accept a higher heat expense or to install exterior thermal insulation where it is possible (BYG-ERFA, 2009; Christensen et al., 2015).

## *1.2* ***Method to fulfil stakeholder agendas***

The overall incentive for action clarified in Section 1.1 relates to the high heat loss and thereby energy consumption of historic multi-storey buildings. The multi-storey buildings from 1850-1930 have been shown to consume 150-155 kWh/m² (Kragh and Wittchen, 2014; Wittchen et al., 2011), which could potentially be reduced to less than half, approximately 60 kWh/m² (Wittchen et al., 2011), where a large share of the reduction relates to reduction of heat loss.

When considering how to reduce the heat loss of existing buildings, it has been established that the best solution from a building physics point of view is to apply thermal insulation on the exterior surface when possible (Brandt et al., 2013; Kuenzel, 1998; Munch-Andersen, 2008). The choice of installing thermal insulation to the interior or exterior side must therefore be based on the wish or mandatory requirements for preservation of the individual exterior façade expression, versus the risk when applying thermal insulation to the interior side of the thermal envelope.

It must be noted that preservation regulations in Denmark prohibit changes of the construction for listed buildings and demands for preservation of the original architectural features of the exterior façade in worth-to-preserve buildings. The following thereby applies to worth-to-preserve and non-preserved buildings.

The heat loss of all types of buildings can basically be simplified to totals in vertical and horizontal direction. The heat loss from a typical historic multi-storey building from the period 1850-1930 have been simplified by Jesper Engelmark in Figure 1. Looking into the individual heat losses, the following considerations regarding each loss must be acknowledges:

> Roof

The Danish multi-storey buildings typically have a cold loft. Well-established solutions exist, increasing the amount of insulation between the top apartment and the cold loft.

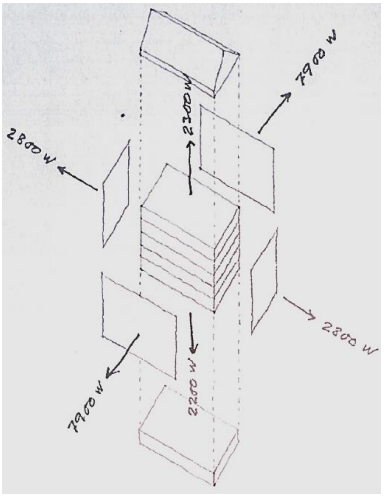


*Figure 1 Sketch of heat loss from typical historic multi-storey building. Courtesy of J. Engelmark.*

> Basement

The application of insulation to the exterior surface of basements are costly, but not hindered by aesthetics.

> Gabel

Multi-storey buildings constructed in the period of 1850-1930 were built with a gable towards the next building. The thickness of the gable was typically 1-1½ brick thick (240-360 mm) and the masonry were typically of bad quality, as it was built towards the gable of the next multi-storey building. Gables connecting to another multi-storey building will have a negligible heat loss. Some multi-storey buildings have been torn down, leaving gables with boundary conditions they were not designed for.

Freestanding original gables should be renovated to withstand temperature and wind driven rain, possibly via exterior thermal insulation. The gables are typically not preserved, illustrated by the tendency of applying art to the gables, as illustrated in Figure 2.

> Façade

Research shows that considerable energy saving potential can be achieved from applying thermal insulation to the solid masonry façade of historic multi-storey buildings (Morelli et al., 2012; Morelli and Svendsen, 2012).

Considerations regarding the application of thermal insulation on the exterior or interior side of the façade should depend on if the façade is facing towards the street or the court.

1. Towards court

As preservation requirements for worth-to-preserve buildings only apply to the expression towards the street, it is possibly to make an architectonic update to the façade towards the court. This could include modern options such as elevators and balconies, and in this process include exterior thermal insulation.

2. Towards street

Changes are not allowed to an exterior surface defined as worthy of preservation. The application of interior insulation is in this case a possibility for occupants to obtain indoor environment and comfort levels that meet modern standards, while preserving the exterior expression of the building.


*Figure 2 Example of gables in Copenhagen, modified with art. Last picture from Tullinsgade is painted on a retrofitted (thermal insulation) board, usually paintings are applied directly to masonry/rendering. Photos courtesy of Thea Gregersen.*

By using various strategies for thermal insulation in the different exterior areas shown in Figure 1, the needs of the government, building owners and tenants can be achieved. To fulfil the needs of the professionals within the building sector, safe and robust solutions to install thermal insulation to the buildings need to be found. As stated in the bullets above, the different vertical and horizontal areas of the building can be solved with different thermal insulation strategies, where investigating the retrofitting of thermal insulation to the interior solid masonry surface is within the scope of this PhD study.

### *1.2.1* Current state of research within interior thermal insulation

When considering retrofitting the interior surface of historic masonry facades with thermal insulation, a range of disadvantages compared to exterior systems must be acknowledged. The following disadvantages are natural and influences all types of interior thermal insulation systems.

- Thermal bridges cannot be eliminated.
- Reduction of the indoor space.
- Alteration of interior expression.
- The temperature in the original wall drops severely, as the heat flow from the room to the original wall is reduced (Straube and Schumacher, 2007; Ueno et al., 2013).
- Two-sided evaporation of moisture is limited (Scheffler et al., 2014), depending on how permeable the insulation systems are to diffusion of water vapour. Moisture will still enter the wall (e.g. wind driven rain, rising damp and condensation).
- There will be a risk of condensation at the original interior masonry surface behind moisture-open insulation or un-tight moisture-tight systems (Kuenzel, 1998; Straube and Schumacher, 2007).
- The moisture content will increase in the original wall, leading to high moisture content on the cold side, behind the interior thermal insulation material (Hamid and Wallent En, 2017; Kuenzel, 1998; Mets et al., 2017; Saïd et al., 2003; Scheffler et al., 2014; Ueno et al., 2013; Vereecken and Roels, 2015, 2014).
- Especially for diffusion open systems (sub-type of moisture-open system):
    - The system relies on diffusion open materials that allow for diffusion of moisture from the original wall towards the interior, but such systems will also allow for diffusion from the inside climate to the original wall during cold periods.

> Especially for moisture-tight systems:

    - The systems should theoretically have no diffusion to or from indoor climate, although most cases show that completely tight vapour barriers are rarely possible to achieve in practice. Perforations and un-tight joints in vapour barriers result in intensified moisture point loads, especially combined with thermal stack in the higher storeys.

The degree in which the conditions are worsened are influenced by:

- The interior and exterior boundary conditions, increasing with thickness of insulation (Finken et al., 2016).
- The extent of interior surface coverage.
- The amount of moisture entering the construction from both sides.

A case study with application of interior thermal insulation to a limited area below a window, in a room with low moisture load, has been shown possible in the appended Paper #2. The evaluation of moisture-induced damage from mould, wooden decay and frost was evaluated showing no risk of such damages. Based on a theoretical study into thermal transmittance in the appended Paper #1, this solution was shown able to achieve 40 % of the potential reduction of thermal transmittance from a full covering strategy, while only covering 17 % of the total interior surface area.

An experimental study in the appended Paper #3, applying thermal insulation to the interior masonry surface with a full covering strategy, showed the possibility to decrease the risk of moisture-induced damage by varying a thermal insulation system.

Previous researches have focused on how to add interior thermal insulation to old masonry constructions and the performance of the insulation material (Christensen et al., 2015; Hamid and Wallent En, 2017; Harrestrup and Svendsen, 2015; Morelli and Svendsen, 2012; Pavlik, 2009; Scheffler, 2011; Toman et al., 2009; Zhao et al., 2017).

## *1.3* ***Scope of industrial PhD study***

The industrial PhD study was initiated based on a large public interest in reducing heating expenses, while preserving the exterior building expression. The industrial partner identified this as a field of interest with great potential, but also a field involving many risks based on examples where projects with retrofitted interior insulation have shown not to function properly, resulting in mould, fungi and frost damage. Nevertheless, retrofitting existing constructions with interior thermal insulation is in many cases the only possibility when considering increasing the thermal resistance of worth-to-preserve buildings, why further investigations were needed to reduce the risks.

The scope of the industrial PhD project was to investigate measures to increase the occupant comfort and at the same time reduce energy loss in historic multi-storey buildings with a bare brick exterior leaf. This building type is characteristic for bigger Danish cities, especially the inner city of Copenhagen, but are also seen in different varieties in other countries. The investigated measures were limited to thermal insulation, retrofitted to the interior surface of a characteristic construction. This method has historically shown to be problematic, since it constitutes a risk of introducing moisture-induced damage. The scope of this industrial PhD project was investigated by working with the following three main topics, emphasized with bold text in the following: **Investigating the existing Danish multi-storey building stock** with solid masonry walls and embedded wooden elements, as a basis for the design of the field experiments. This topic aims to clarify the characteristic composition of the segment together with the amount and distribution of the segment's dwellings and buildings. **Establishing and testing large scale, reliable, controlled and long-term field experiments exposed to an outdoor climate** able to produce high quality measurement data, to increase the understanding of the changed hygrothermal conditions when retrofitting thermal insulation to an interior surface. The large and long-term field experiments were designed to resemble multi-storey dwellings with solid masonry walls, embedded wooden elements and a partition wall, retrofitted with selected moisture-open interior thermal insulation systems available at the time of constructing the experiment. The work involved simultaneous design of an advanced measurement system and extensive programming of a script to sort, evaluate and output the massive amounts of experimental data. The data output was designed as easily accessible formats and reduced package sizes as basis for subsequent analysis and hygrothermal simulation-based studies. The field experiment was reported after the first 2½ years of monitoring, evaluating the first measurements from the setup by comparative analysis of data from different walls and sensor points based on the

raw data and moisture-induced damage models for mould and wooden decay. **Carrying out a case study in an inhabited dormitory** building with a construction similar to that of the field experiments, insulated with one thermal insulation system thoroughly tested in the field experiments. The case study included; an investigation of the existing conditions in a dwelling, with focus on risk of occupant discomfort from cold surfaces; the hygrothermal response when retrofitting interior thermal insulation, by monitoring the hygrothermal balance of two spandrels when exposed to varying occupancy over 2 years and 8 months.

The aim of this Thesis is to present the findings of the PhD study and document the construction of the long-term large scale field experiments and the case study. The findings include:

- Presentation of the characteristic composition of the building segment, as a basis for work within multi-storey buildings with solid masonry walls and embedded wood, found to be constructed in the period 1850-1930.
- Clarification of potential reduction in average thermal transmittance from different thermal insulation strategies, based on parameterized 1-, 2- and 3-dimensional thermal simulation models.
- Description of the magnitude and nationwide distribution of dwellings and buildings to illustrate the relevance of focusing on this part of the Danish building stock.
- Presentation of comparative analyses from the field experiments, using measurements from 33 unique measurement points composed from combinations of 6 unique walls and 9 unique sensor points in the appended Paper #3 and Section 5 of this PhD Thesis. The measurement points presented in the appended Paper #3 have been picked out to investigate how implementation of a hydrophobic façade treatment and a deliberate thermal bridge influence the hygrothermal balance in a solid masonry wall retrofitted with an interior insulation system. The measurement points presented in Section 5 of this Thesis have been selected to illustrate the hygrothermal balance occurring in a moisture-tight interior insulation system during the course of a year.
    - Beside the presented results, measurements exist for a total of 24 walls with 7-12 sensor points per wall, resulting in 228 unique measurement points in the field experiments. The used methodology for treating measurement data has been developed generically, treating all data similarly and thereby creating a catalogue of cases derived from this PhD study.

> Presentation of results from a case study, where an interior surface of an existing dormitory building with normal occupancy was retrofitted with a thermal insulation system similar to the systems extensively tested in one container of the field experiments.

The current state of measurements from the field experiments form the basis for a comparative analysis, illustrating how different thermal insulation systems perform compared to others and a reference wall. The measurements can be used to indicate how similar measurements at the same location will react when exposed to an identical climate. Performing a full hygrothermal assessment of the effect when retrofitting thermal insulation to the interior surface of Danish multi-storey housing, consisting of solid masonry walls and embedded wooden elements, would need extensive hygrothermal simulations with various locations and climate loads. The catalogue of cases derived from this PhD study provide quality input for such parametric hygrothermal simulations, serving as a basis to perform full hygrothermal assessment in subsequent simulation-based studies within the field.

### *1.3.1* Research hypothesis

The main hypothesis of the industrial PhD project was:

> Techniques to solve the building physical challenges when retrofitting the high share of solid masonry facade walls in Denmark with interior thermal insulation can be found by comparative evaluation, based on reliable quality measurement data from long-term laboratory experiments and a case study. Retrofitting of interior insulation to a representative selection of such walls can increase occupant comfort and reduce the thermal transmittance, without the risk of moisture-induced damage occurring in the construction.

The main hypothesis is rephrased into sub-hypotheses (**SH**) and an independent-hypothesis (**IH**), listed in the following paragraphs. Each sub- and independent-hypothesis are followed by a range of goals used to evaluate if they can be rejected. The individual **SH** and **IH** are treated in the appended papers and sections as defined in Table 1, with a conclusion in the respective defined sections of this Thesis. The main hypothesis is concluded on in Section 8.

Sub-hypothesis #1 (**SH1**): A characteristic composition and period of erection can be determined for Danish multi-storey buildings with solid masonry walls and embedded wooden elements, illustrating that the areas available for retrofitting interior insulation is limited.

If one of the following goals do not apply, then Sub-hypothesis #1 can be rejected:

> A period of erection for characteristic Danish multi-storey buildings with solid masonry walls and embedded wooden elements can be determined based on a literature study.

> Multi-storey buildings constructed within the period of erection share a characteristic composition, which can be determined based on a literature study and validated against existing constructions.

> More than 33 % of the total exterior leaf for a typical façade wall from the period are unavailable for retrofitting interior thermal insulation.

Sub-hypothesis #2 (**SH2**): The share of Danish multi-storey dwellings with solid masonry walls and embedded wooden elements is substantial compared to the total Danish multi-storey building stock, with a nationwide distribution showing a large degree of dwellings situated in major cities at the time of erection.

If one of the following goals do not apply, then Sub-hypothesis #2 can be rejected:

> The share of the investigated multi-storey dwellings and buildings are substantial if more than 20 % share a characteristic composition, originating from a specific period of erection.

> A large degree of the investigated multi-storey dwellings is situated in the capitol of Denmark. A large degree is for this goal defined as more than 60%.

Sub-hypothesis #3 (**SH3**): The potential reduction in average thermal transmittance by various interior thermal insulation strategies, retrofitted to Danish multi-storey buildings with solid masonry walls and embedded wooden elements, can be determined by thermal simulation.

If one of the following goals do not apply, then Sub-hypothesis #3 can be rejected:

> A 3-dimensional parametric thermal simulation model show that:
  - More than 25 % of the potential reduction in average thermal transmittance from full coverage thermal insulation of the interior masonry surface can be achieved by only insulating the spandrel.
  - Creating a deliberate thermal bridge with AAC next to the wall plate will decrease the reduction in average thermal transmittance obtained from full coverage interior thermal insulation by less than 5 %.
  - The thermal bridge introduced by an intersecting wall is a comfort issue and do only influence the average thermal transmittance of an interior insulated wall section insignificantly. Insignificantly is for this goal defined as a decrease of the reduction by less than 2.5 %.

Sub-hypothesis #4 (**SH4**): The hygrothermal balance in solid masonry walls with embedded wooden elements, combined with various types of interior thermal insulation systems and exterior surface treatments, can be evaluated in controlled field experiments exposed to real weather conditions.

If one of the following goals do not apply, then Sub-hypothesis #4 can be rejected:

> A clear difference between the initial stabilization period and stabilized measurements can be identified for relative humidity and temperature measurements.

> Comparative analyses show clear and explainable differences for measurements obtained from variations of an interior thermal insulation system.

> There is a clear and explainable difference in hygrothermal behaviour for moisture-tight and moisture-open insulation systems when retrofitted to an interior masonry surface.

> The effect of wind driven rain can be observed by relative humidity measurements in the embedded wooden elements.

Sub-hypothesis #5 (**SH5**): The worsening of the hygrothermal balance when retrofitting the interior masonry surface with thermal insulation can be reduced by introducing a hydrophobic treatment to the exterior surface or a deliberate thermal bridge on the interior side.

If one of the following goals do not apply, then Sub-hypothesis #5 can be rejected:

> The introduction of a deliberate thermal bridge, replacing insulation material next to the wall plate and wooden beam end, reduce the worsening of the hygrothermal conditions from retrofitting with interior thermal insulation.

> Hydrophobation of the exterior masonry surface reduce the worsening of the hygrothermal conditions introduced from retrofitting with interior thermal insulation.

Sub-hypothesis #6 (**SH6**): The thin solid masonry spandrel in existing multi-storey dwellings can be retrofitted with interior thermal insulation without risking moisture-induced damage from neither the initial response, nor the long-term changed hygrothermal balance.

If one of the following goals do not apply, then Sub-hypothesis #6 can be rejected:

> Reliable measurements from a case study can be obtained, despite the many uncertainties in such an experiment, showing clear and explainable hygrothermal distinctions between a reference and an internally insulated spandrel.

> Clear distinction can be made, separating the initial hygrothermal response and the long-term effect on the hygrothermal balance when retrofitting an interior masonry surface with thermal insulation.

> Retrofitting the existing interior surface of a solid masonry spandrel with a thermal insulation system must not result in moisture-induced damage. The risk of moisture-induced damage is evaluated by:

    - Mould growth is evaluated mathematically and by in-situ measurements. The results must be within acceptable boundaries defined by the respective methods.

    - Wooden decay is evaluated mathematically, the results must show no occurrence of irreversible decay.

    - Frost is evaluated based on measurements and visual observations, observation must show no frost damage of the exterior surface.

Independent-hypothesis #1 (**IH1**): DC electrical resistance measurements in wooden dowels can be used to monitor the development of relative humidity during a transient experiment.

If the following goal do not apply, then Independent-hypothesis #1 can be rejected:

> Calculated relative humidity from DC electrical resistance measurements in wooden dowels and digital relative humidity sensors, installed in the same wooden element, show similar results during a transient experiment. In this goal, similar is defined as +/5 %-points in relative humidity.

### *1.3.2* Thesis guide

As the Thesis is the outcome of an industrial PhD study, the focus has been on dissemination of applied science, with dissemination of theory, methods and results in the Thesis in the most non-scientific level possible. It has been attempted to increase the readability of the Thesis by including a large amount of figures when describing constructions and experimental setups. The method of dissemination in the appended papers is on a scientific level.

The Thesis deals with a range of subjects within the application of thermal insulation to the interior surface of multi-storey buildings.

- The first section focuses on the incentive to consider retrofitting the interior surface of the thermal envelope with thermal insulation, clarification of where this might be needed, the current state of research within the field and the overall scope of the industrial PhD study.
- The second section introduce relevant building physics as a basis for the work done in the PhD study. The section includes a description of the hygrothermal changes occurring in a construction when applying interior thermal insulation; the boundary conditions affecting the construction; the damage models used in comparative analyses to evaluate risks; and the use of wooden dowels to monitor development of moisture in constructions.
- The third section include a segment investigation of the amount, national distribution and the characteristics of historic multi-storey buildings.
- The fourth section concern a theoretical investigation into the potential for reducing heat loss of characteristic multi-storey building façades from the period 1850-1930. The investigation includes variations of insulation thickness, offset from floor/ceiling and a situation with a solid partition

wall. The section further includes a reference to an investigation of simulating in 1, 2 and 3 dimensions in the appended Paper #1.

- The fifth section documents the construction of a large scale field experiment, developed and built at the Technical University of Denmark in Kgs. Lyngby, and a comparative analysis of measurements obtained in the experiment.
- The sixth section present experimental results from a case study, where a spandrel in a historic multi-storey building with solid masonry walls was retrofitted with thermal insulation on the interior surface.
- The seventh section contain a cross-section discussion of the research conducted in the industrial PhD study. The section connects the content of the preceding sections.
- The eight section concludes on the main hypothesis based on sub-hypotheses and provides ideas for future research.

In general, the sections include short summaries of the appended papers relevant for the section, additional research fitting the research in a broader context, research that could not fit into the short and strict format of peer-reviewed journals and extracts from presentations performed over the period of the PhD study.

The connection between the sub-hypotheses, independent-hypothesis, main hypothesis, sections and the appended papers are illustrated in Table 1. The hypotheses are used to focus the summaries of relevant appended papers in Section 3-6, to lead the discussion in these sections and are finally concluded on in the individual sub-conclusions. The main hypothesis is concluded on in the conclusion in Section 8, based on the hypotheses treated in Section 3-6.

Hyperlinks have been incorporated in the digital version of this Thesis, allowing for easy transition to:

> Sub-, independent- and main hypotheses.
> The appended papers.
> Sections in the Thesis and appended papers.
    - Sections in the Thesis are referred to as "Section #"
    - Sections in the appended papers are referred to as "Sec. #"
> Figures in the Thesis and appended papers.
    - Figures in the Thesis are referred to as "Figure #"
    - Figures in the appended papers are referred to as "Fig. #"

| Content of PhD thesis | Section | Hypotheses | | | | | | | |
|---|---|---|---|---|---|---|---|---|---|
| | | **SH1** | **SH2** | **SH3** | **SH4** | **SH5** | **SH6** | **IH1** | Main |
| **Introduction**<br>Incentive, state of the art, scope, hypotheses, research questions, structure | 1 | | | | | | | | |
| **Methods and theory**<br>Effect of interior insulation, hygrothermal conditions, moisture-induced damage models, monitoring with wooden dowels | 2 | | | | | | | | |
| **Characteristics, amount and distribution of buildings**<br>Litterature review, historic, masonry, multi-storey, floorplan investigation, segment analyse, distribution | 3 | X | X | | | | | | |
| **Potential for reducing thermal transmittance**<br>Interior insulation, historic, masonry, surface area considerations, multi-dimensional parametric thermal simulation, saving potential | 4 | | | X | | | | | |
| **Large scale field experiment**<br>Experimental field study, experimental setup, masonry, interior insulation, measurements | 5 | | | | X | X | | X | |
| **Case study**<br>Full-scale experiment, interior insulation, historic, masonry, occupant comfort, moisture-induced damage evaluation, in-situ damage measurements, frost | 6 | | | | | | X | | |
| **Discussion**<br>Cross section discussion of results from preceding sections | 7 | | | | | | | | |
| **Conclusion**<br>Conclusion on main hypothesis, future research | 8 | | | | | | | | X |
| | | | | | | | | | |
| Appended paper: Paper #1: Interior insulation – Characterisation of the historic, solid masonry building segment and analysis of the heat saving potential by 1d, 2d, and 3d simulation | | X | X | X | | | | | |
| Appended paper: Paper #2: Interior insulation - Experimental investigation of hygrothermal conditions and damage evaluation of solid masonry façades in a listed building | | | | | | | X | | |
| Appended paper: Paper #3: Influence of hydrophobation and deliberate thermal bridge on hygrothermal conditions of internally insulated historic solid masonry walls with built-in wood | | | | | X | X | | X | |

*Table 1 Thesis guide: Connection between sections, hypotheses and appended papers.*

### *1.3.3* The contributions of the PhD student

The study has included, reported and disseminated the following in papers submitted to international peer-reviewed journals and in present Thesis:

- Description of amount, distribution and characteristics of multi-storey buildings from the periods 1850-1930 and 1930-1950.
- Investigation into the theoretical savings from applying interior thermal insulation to historic multi-storey buildings from Denmark, including description on how the largest share of the potential reduction in relative thermal transmittance is achieved from the first millimetres of thermal insulation.
- Reported a case study where a thermal insulation system has been installed to the interior masonry surface of a spandrel in a historic multi-storey building, without resulting in moisture-induced damage.
- The set-up of large field experiments under a project concerning interior insulation at DTU, involving multiple PhD students, as presented in Section 1.3.4. Some of the results from the experiment is published in the appended Paper #3 and present Thesis, to document that the field experiments works as intended and can produce high quality measurements as an input for subsequent work. The findings from the experimental study presented in the appended Paper #3 and this Thesis include:
    - Comparative analyses of the measured hygrothermal conditions in masonry walls, wooden beam ends, wall plates and thermal insulation with combinations of the following variations:
        - Application of moisture-tight or moisture-open thermal insulation to the interior masonry surface.
        - Replacing thermal insulation with a deliberate thermal bridge next to the wall plate.
        - Applying a hydrophobic façade treatment to the exterior masonry surface.

Experiments regarding robustness, e.g. impact resistance, load-carrying capacity and microclimate of the interior insulation systems have been performed in a Danish bachelor project (Jacobsen and Dabelsteen, 2016). The state of the research is mentioned as future research in Section 8.1, but results have not yet made it into international peer-reviewed journals and have not been included in this Thesis.

### *1.3.4* Structure of project with multiple PhD students regarding interior insulation at DTU

I have been part of a range of projects within interior insulation led by Associate Professor Søren Peter Bjarløv, at the building design section under the department of civil engineering at DTU. At the time of initial submission of my PhD Thesis, the project members under Associate Professor Bjarløv comprised of three PhD students and one scientific assistant. The three PhD students have had different focus areas, summarized as:

PhD student Tessa Kvist Hansen: The focus was on 1:1 experiments based on case studies, with special focus on materials.

PhD student Nickolaj Feldt Jensen: Will continue the work with unpublished results from the field experiments started by Tommy R. Odgaard, along with other projects under Associate Professor Bjarløv.

Industrial PhD student Tommy Odgaard: The main focus was the setup of field experiments, aiming to provide experimental data for further analysis and comparison with simulation models. This work have demanded a substantial work within construction of the experimental facilities, but also development of a Matlab script which can transfer experimental data into an usable data format, as presented in Appendix B on page 231. This work was concluded with comparative analyses of data from some walls in the field experiments, to illustrate the quality of measurements and the future possibilities. The desktop work within segment analyses and thermal simulation was a prerequisite for the construction of the experiments. The case study was a side-project used to test the real-life conditions in a dwelling and the performance of an insulation system.

I have summarized the main work I have had with the field experiments situated at DTU in the following:

- In collaboration with Associate Professor Bjarløv:
  - Work with initial budgets and grant applications for the two individual field experiments.
  - Plan the construction of the field experiments and supervise the construction, from plain field to working field experiments.
  - Installation of sensors in the field experiments.
  - Plan which insulation systems should be investigated, take contact to suppliers and supervise the installation in the field experiments.

- On my own:
    - Planning and implementation of sensor equipment: Investigation of available sensors on market, initial tests, purchasing sensors, protection of sensors with shrink tubing and calibration.
        - The development and construction of the physical system from sensor cable at walls → experimental computer in containers, illustrated in Figure 169 on page 234, was done by lab assistant Lars Kokholm Andersen.
    - Develop Matlab script, reading 3 .txt files with sensor addresses, measured relative humidity and measured temperature, producing outputs as calibrated measurements and moisture-induced damage models in form of graphs, .csv and .out files. The script was developed with usability in mind, contained approximately 11.500 lines of code/comments and is described in Appendix B, starting from page 231.
    - Maintain field experiments by controlling that the measurement system worked on a weekly basis, the water tanks for humidifiers had a sufficient water content and occasionally replace malfunctioning sensors.
    - Production of foam concrete.
    - Dissemination of results from field experiments in papers and various workshops/conferences.

Other projects within interior insulation ran in other sections under the department of civil engineering at DTU, but I have not had the possibility to collaborate with these projects due to time constraints.

# 2 THEORY FOR EVALUATING HYGROTHERMAL CONDITIONS AND DAMAGE MODELS

Section 2 revolves the building physics affecting the hygrothermal conditions in historic multi-storey buildings built in the period 1850-1930, and methods to evaluate and monitor the hygrothermal conditions. The section is based on the appended Paper #2 and Paper #3, as well as the multiple presentations performed throughout the PhD study and unpublished research.

The section starts with a general introduction to the building physics affecting both the original historic constructions and the retrofitted cases, directed towards readers that are not familiar with building physics. As the section progress, the level of complexity increases into a scientific level, going further into description of the boundary conditions, evaluating the risk of moisture-induced damage and finally a description of the measurement technique used.

While some of the content can seem very basic, it serves as a general and illustrative introduction to the hygrothermal conditions in the constructions. There is a large amount of literature going further in-depth into the different hygrothermal mechanisms (Brandt et al., 2013; Hagentoft, 2001; Hens, 2012; Pedersen, 1989; Rode and Lund, 2016). It is not intended to challenge such textbooks, but should instead serve as a basic introduction to the field. This section forms the foundation for the following sections, with references to and from relevant sections.

## 2.1 Hygrothermal conditions in historic multi-storey buildings from a building physics point of view

To understand how the building physics affect the historic multi-storey buildings constructed in the period 1850-1930, it is vital to understand the composition of this building segment. The description of the building composition will be kept to a minimum in this section, as a thorough description is done in Section 3, starting from page 49.

The composition of the façade is complex and thereby not possible to simplify to 2-dimensional cross sections, something with is often done anyway. One specific detail impossible to simplify to a 2-dimensional cross section concern the wooden beams in the façade, repeating with a 175 x 175 mm or 200 x 200 mm beam approximately every 1000 mm, with a pugging/air layer in between the beams.

The 3-dimensional composition of the construction entails that the wooden beam has a natural way of evaporating moisture absorbed at the wooden beam end, closest to the exterior surface, as illustrated in Figure 3. This effect has been sketched in Figure 4 with convection along the wooden beam/pugging layer, infiltrating into the wooden floor structure, forced by a pumping effect due to movement on the floor. The structure allows indoor moist air to access the cold masonry surface and wooden beam end, but also to ventilate the volume through façade cracks, increasing with thermal stack effect towards the upper floors.

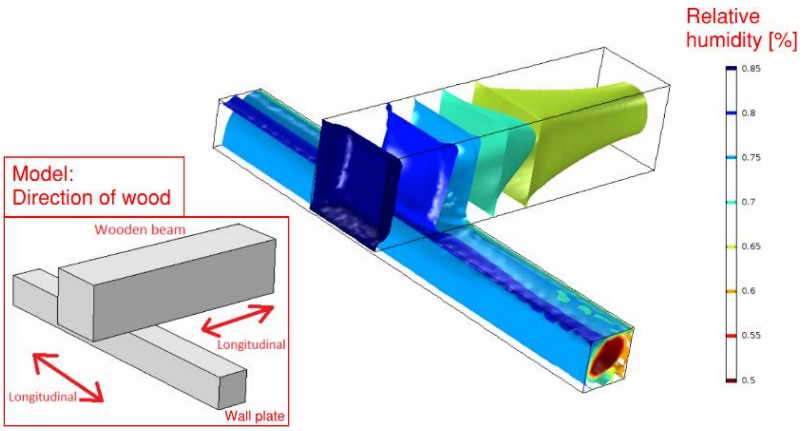


*Figure 3 Un-published simulative study of anisotropic moisture transport in wooden elements, done as part of PhD summer school* (Odgaard, 2014).

The original, un-insulated wall will have convection along the interior surface of the masonry wall, allowing for evaporation of moisture from the masonry wall. Looking at the illustration in Figure 4, the introduction of interior thermal insulation lowers the temperature of the masonry and hinders this natural evaporation to the indoor environment, from no transport in moisture-tight systems, to decreased transport towards and from the masonry in moisture-open systems. The outdoor moisture sources are less influenced by the dimensional differences, being:

- Wind driven rain (WDR). The combination of vertical rain and wind pressure on the wall.
- Sun that can dry out the wall, but also drive moisture transport towards the inside.
- Rising damp in the lower storeys.

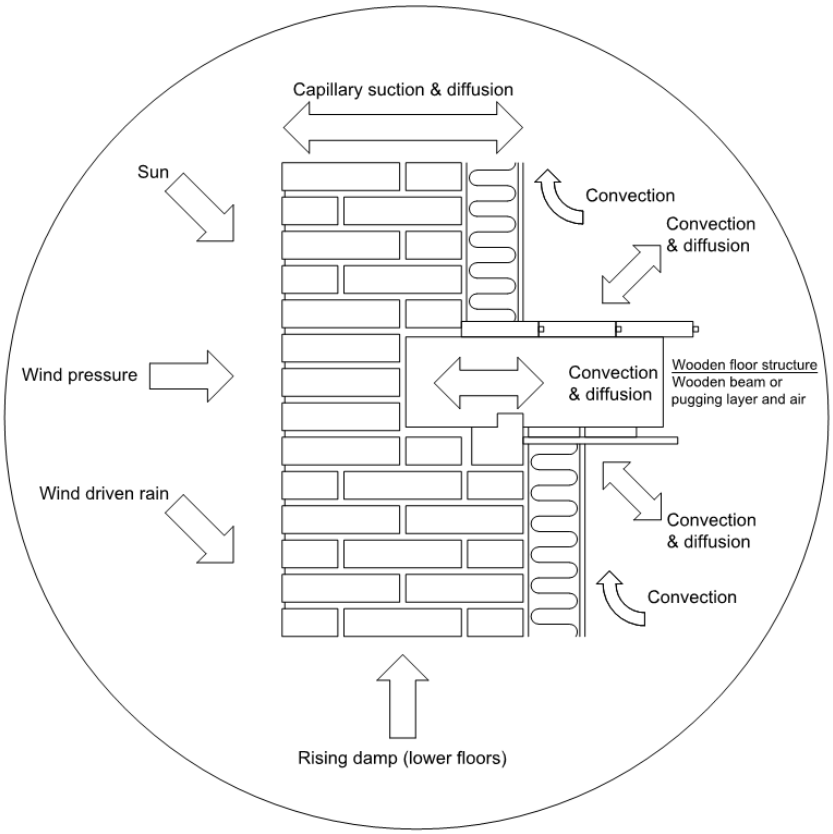


*Figure 4 Hygrothermal processes in vertical cross-section of solid masonry column in traditional facade wall of multi-storey built in the period 1850-1930.*

### *2.1.1* Change in hygrothermal conditions by the introduction of thermal insulation to the interior surface

By introducing thermal insulation to the interior masonry surface, there are introduced changes to the original hygrothermal conditions in the walls. Some of these changes have been presented earlier with the state of the art in Section 1.2.1 on page 7, but briefly summing up:

- Decreased two-sided evaporation.

Introducing thermal insulation on the interior surface hinders direct evaporation to the indoor environment, with different behaviour for capillary active, diffusion open or moisture-tight systems.

- Decrease of temperature in winter, increase in summer.

Heat exchange rate towards the indoor environment is reduced.

- The location of the dewpoint is changed.

In the original wall, the dewpoint will normally be in the masonry wall. By applying interior thermal insulation, the dewpoint will often be in the insulation layer. The purpose of the moisture-tight system is to avoid condensation at this new dewpoint location.

- The moisture level in the masonry wall increases.

As the same amount of moisture enters the wall (WDR, rising damp and solar driven moisture transport towards the interior), but the ability to evaporate from the wall has been reduced.

- The airtightness of the construction is increased.

When applying a layer on the interior surface, the airtightness of the construction will be increased. While it is not necessarily negative to increase the airtightness, then this can result in lowered natural ventilation of the indoor environment, hence increased risk of increased moisture content and worsened indoor comfort.

A further illustrative description of the changed dewpoint has been done by first illustrating how the temperature profile through the wall changes when applying thermal insulation to a solid masonry spandrel in Section 2.1.2, evaluating the condensation risk when retrofitting the interior surface with thermal insulation in Section 2.1.3.

### *2.1.2* Temperature distribution in solid masonry spandrel



The solid masonry spandrel is characteristic for historic multi-storey building from the period 1850-1930. The spandrel is the façade part located in between the masonry columns, between the window and the floor, and has a thickness of 1 brick with rendering on the interior side (238 mm).

This section includes a minor steady state conductive heat transfer investigation, concerning the temperature profiles of:

- An original spandrel.
- A spandrel retrofitted with 100 mm of thermal insulation on the exterior masonry surface.
- A spandrel retrofitted with 100 mm of thermal insulation on the interior masonry surface.

The constructions are designed based on identical material thickness and transport coefficient for thermal conductivity:

- Brick: Thickness = 0.228 m, $\lambda$ = 0.8 $\frac{W}{m \cdot K}$.
- Rendering: Thickness = 0.010 m, $\lambda$ = 0.3 $\frac{W}{m \cdot K}$.
- Insulation: Thickness = 0.100 m, $\lambda$ = 0.042 $\frac{W}{m \cdot K}$.
- 2 x adhesive mortar: Thickness = 0.008 m, $\lambda$ = 0.18 $\frac{W}{m \cdot K}$.
- Convective heat transfer coefficients: $R_{si}$ = 0.13 $\frac{m^2 \cdot K}{W}$, $R_{se}$ = 0.04 $\frac{m^2 \cdot K}{W}$.

The calculated temperature distribution for the original un-insulated spandrel with realistic interior and exterior temperatures of +20 °C and -1.1 °C respectively is illustrated in Figure 5 (-1.1 °C = month-mean outdoor temperature in TRY-dataset in February, the dimensioning temperature outdoor in Denmark is -12 °C (DS 418:2011, 2011)). The convective surface resistance on the interior surface do in this example account for ¼ of the total thermal resistance in the construction, due to the low thermal resistance in the un-insulated spandrel. Because of this, a similar ¼ of the temperature drop takes place before reaching the interior surface, resulting in an interior surface temperature highly influenced by the outdoor temperature.

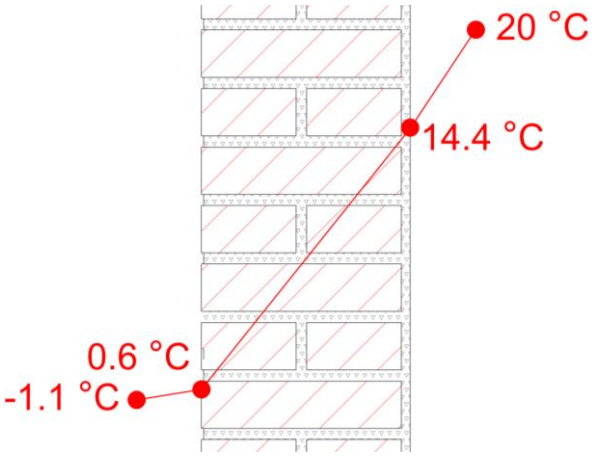


*Figure 5 Temperature distribution in 1 brick (238 mm) solid masonry spandrel.*

The second case concerns an identical spandrel as illustrated in Figure 5, retrofitted with 100 mm thermal insulation on the exterior masonry surface, illustrated in Figure 6. Because of the decrease in the total thermal transmittance of the construction, the influence of the convective surface resistance on the interior surface is reduced, resulting in 1/25 of the temperature drop taking place before reaching the interior surface. As the main share of the thermal resistance is in the thermal insulation, the main temperature drop will also take place here, resulting in a wall with temperatures mainly influenced by the indoor temperature.

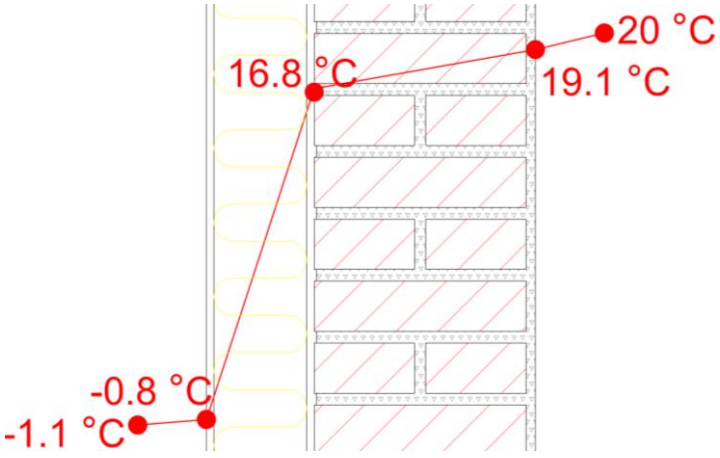


*Figure 6 Temperature distribution in 1 brick (238 mm) solid masonry spandrel with exterior thermal insulation.*

The third case concerns the same spandrel as illustrated in Figure 5, retrofitted with 100 mm thermal insulation on the interior masonry surface, illustrated in Figure 7. As the total thermal transmittance is identical to the spandrel with thermal insulation applied on the exterior masonry surface illustrated in Figure 6, a similar effect occurs regarding interior surface temperature and main temperature drop in insulation layer. The location of the insulation does however result in temperatures in the spandrel mainly influenced by the outside temperature.

The temperatures observed in the spandrel retrofitted with thermal insulation to the interior surface are discussed further in Section 2.1.3, considering moisture in a simplified example on why the application of thermal insulation to the interior surface results in risk of moisture-induced damage.

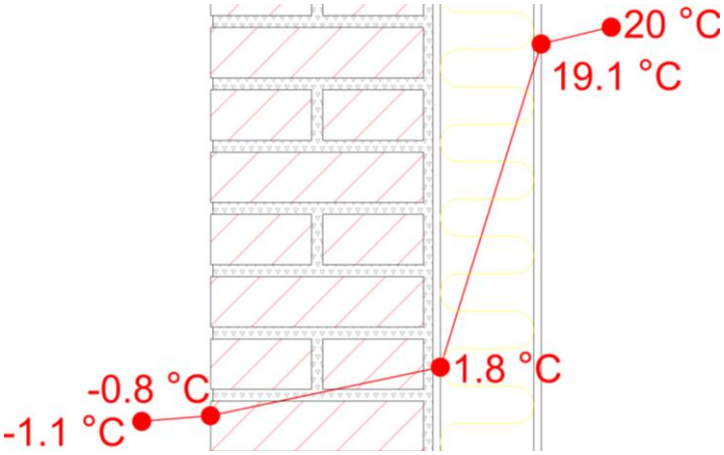


*Figure 7 Temperature distribution in 1 brick (238 mm) solid masonry spandrel with interior thermal insulation.*

### *2.1.3* Risk of condensation in solid masonry spandrel with interior thermal insulation

This section concern basic theoretical explanations to the building physics occurring in a solid masonry spandrel retrofitted with interior thermal insulation, illustrated in Figure 7, described in the end of Section 2.1.2. This section explains why the application of thermal insulation to solid masonry walls in cold climates is troublesome, considering diffusion (and convection in untight systems) from the indoor environment towards the cold masonry surface behind the thermal insulation. Besides the natural diffusion/convection from indoor, it must be remembered that the masonry is also exposed to other external effects presented in Section 2.1.1 that will further worsen the hygrothermal conditions.

The thermal insulation system in question is diffusion open materials, but the physics are also valid for moisture-tight systems if the vapour barrier has been perforated, thereby allowing moisture transport from indoor towards the masonry surface behind the thermal insulation.

Using the temperature profile previously illustrated in Figure 7 as a point of interest, a temperature of 1.8 °C can be seen behind the insulation board. The humidity by volume in the indoor environment has been determined based on a normal humidity classes 2 "*Offices, dwellings with normal occupancy and ventilation*" and 3 " *Buildings with unknown occupancy*" (Brandt et al., 2013; DS/EN ISO 13788:2013, 2013) as approximately v = 6-10 g/m³ in February (Brandt et al., 2013, fig. 31). The temperature and indoor humidity by volume have been plotted into the water vapour diagram in Figure 8, showing that this combination will result in condensation behind the thermal insulation.

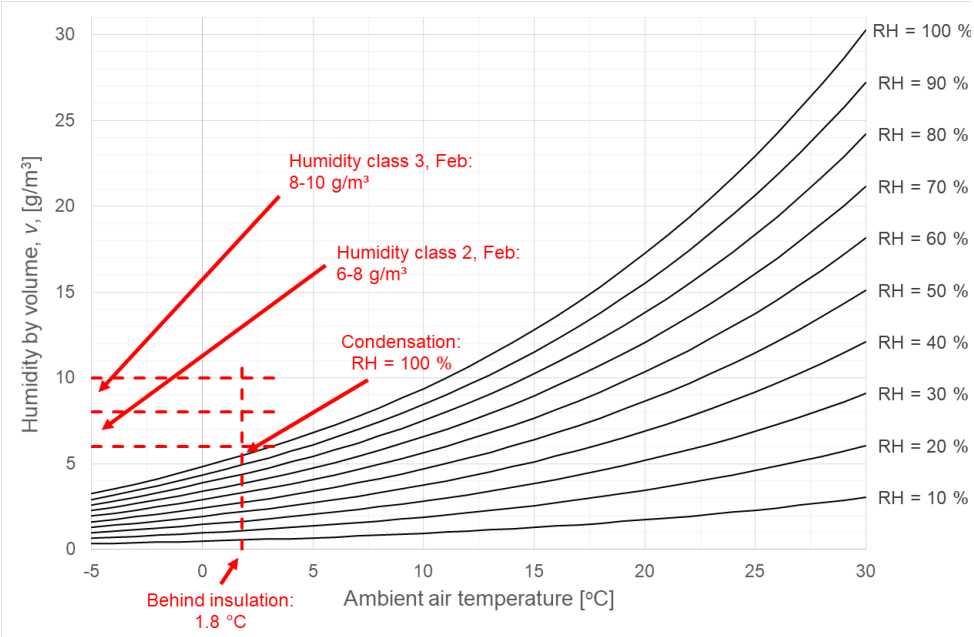


*Figure 8 Water vapour diagram. Calculations based on (DS/EN ISO 13788:2013, 2013), diagram composition inspired by similar diagram in* (Brandt et al., 2013)*. Temperature behind insulation based on steady state calculation in Figure 7.*

It must be noted that this is a very simplistic approach, not taking vapour permeability of the materials into account and calculating the situation as steady state, but also removing all outdoor moisture additions.

The simple calculation shows that there is a moisture transport towards the insulation/masonry interface from the indoor environment during cold periods. The insulation system needs to be able to cope with transport, as a substantial share of the year in the northern cold climate have low outdoor temperatures.

## 2.2 *Effect of boundary conditions on hygrothermal conditions*

The hygrothermal conditions within constructions are influenced by a range of boundary conditions, originating from the in- and outdoor environment. This section is split into a section treating the boundary conditions from the indoor environment in Section 2.2.2 and the outdoor environment in Section 2.2.3. The first Section 2.2.1 concerns the calculation of humidity by volume, *v*. This unit of measurement expresses the amount of humidity per m³ of ambient air, and while it is still slightly influenced by temperature with the expansion of air volume with temperature, it is not nearly as influenced as the commonly used relative humidity. The intermediated resulting vapour pressure, *p*, is used to define the direction of diffusion, from highest to lowest vapour pressure. This unit is an optimal unit of measure, but the definition of pressure in Pascal [Pa] is not an intuitive magnitude.

Rising damp have not been investigated, nor described in the present PhD study, as the process of capillary suction in rising damp results in a magnitude of moisture transport that must be taken care of before considering the application of thermal insulation. Danish literature exist, describing the cause and effect of rising damp, together with various solutions (Simonsen et al., 2012).

### *2.2.1* Method: Calculation of humidity by volume

Different methods exist for the calculation of saturated vapour pressure, being the vapour pressure at *RH*=100 %. I have chosen to rely in the ISO standard (DS/EN ISO 13788:2013, 2013), allowing for determination of vapour pressure and humidity by volume mathematically. The units are calculated with the empirical expressions presented in Equation (1), (2) & (3).

$$p_{sat}[Pa] = \begin{cases} 610.5\ Pa \cdot \exp\left(\frac{17.269 \cdot \theta\ [^oC]}{237.5 + \theta\ [^oC]}\right)\ if\ \theta\ [^oC] \geq 0 \\ 610.5\ Pa \cdot \exp\left(\frac{21.875 \cdot \theta\ [^oC]}{265.5 + \theta\ [^oC]}\right)\ if\ \theta\ [^oC] < 0 \end{cases} \text{ (DS/EN ISO 13788:2013, 2013)} \quad (1)$$

$$p[Pa] = p_{sat}\ [Pa] \cdot \left(\frac{\text{RH}\ [\%]}{100}\right) \text{ (DS/EN ISO 13788:2013, 2013)} \quad (2)$$

$$v\ \left[\frac{kg}{m^3}\right] = \frac{p\ [Pa]}{R_v\left[\frac{Pa \cdot m^3}{K \cdot kg}\right] \cdot T[K]} \text{ (DS/EN ISO 13788:2013, 2013)} \quad (3)$$

Where:

$\theta$ = Celsius temperature [°C].

$T$ = Absolute temperature [K].

$RH$= relative humidity [%].

$p_{sat}$ = saturated vapour pressure [Pa].

$p$ = vapour pressure [Pa].

$v$ = humidity by volume $\left[\frac{kg}{m^3}\right]$.

$R_v$ = gas constant for water vapour = $462\ \left[\frac{Pa \cdot m^3}{K \cdot kg}\right]$.

### *2.2.2* Boundary conditions from the indoor environment

The conditions of the indoor environment can be described as ambient air temperature and relative humidity.

Based on the outdoor ambient air temperature, the indoor ambient air temperature will have an addition/subtraction of heating or cooling supplied in the indoor environment. The same accounts for the indoor humidity by volume, which will be based on the outdoor humidity by volume and a state of equilibrium based on the ventilation rate and the moisture production by occupants/activities in the indoor environment.

The indoor conditions can be expressed as the indoor excess of moisture, an expression defined as the outdoor humidity by volume subtracted from the indoor humidity by volume, as described earlier in Section 2.2.1. The characteristic size of the indoor excess of moisture is defined in standards (DS/EN ISO 13788:2013, 2013) and guidelines (Brandt et al., 2013), but have been shown to vary within building style (Hansen and Møller, 2017) and occupant behaviour and room type (Møller and Hansen, 2017). Based on this, an interior thermal insulation system must be able to cope with large variations of indoor excess of moisture, and not only what is defined from the climate classes.

### *2.2.3* Boundary conditions from the outdoor environment

The conditions in the outdoor environment are more complex. It includes the ambient air temperature and relative humidity (combined into an outdoor humidity by volume), but also wind, rain, sun and rising damp.

As mentioned previously, the rising damp is not further described, as this type of moisture transport must be avoided with interior insulation.

Solar radiation on the exterior surface will increase the surface temperature. This will increase the evaporation towards the outside, but will especially in case of wet masonry (after rain events) result in a high vapour pressure at the exterior surface that can result in a solar driven moisture transport towards the interior.

The combination of wind towards the façade and simultaneous rain events are defined as wind driven rain (WDR). WDR have been shown to have a large influence on the average moisture level in masonry retrofitted with thermal insulation on the interior surface (Morelli and Svendsen, 2012; Nielsen et al., 2012), with increasing amount of water entering the façade as cracks and deficiencies of the exterior masonry surface appear (Calle and Bossche, 2017).

Based on this, further studies of the theoretical models and comparison with physical measurements have been done.

A comparison of theoretical WDR models has been done by Blocken and Carmeliet, in which the strengths and weaknesses of three presented models have been investigated (Blocken and Carmeliet, 2010). The choice of model has been based on applicability and ease of use, combined with normally available parameters from climate stations. From this, I have chosen to model WDR using the semi-empirical model originally developed by Lacy (Lacy, 1965), later extended by Straube (Straube, 2010, 1998).

The methodology of (Straube, 2010) has been followed, describing a model for calculating rain deposited on a vertical building surface, $r_{vb}$, where $r_{vb}$ consists of two main parts:

1. A variable defining the rain moving towards a vertical surface, $r_v$, based on raindrop fall speed, wind speed and wind direction in undisturbed wind at height of interest.

2. A constant, $Factor_b$, defined from a range of factors, adjusting $r_v$ from undisturbed wind to building location by specific factors defined from building style and surrounding environment.

The constant building/environment factors ($Factor_b$) for the experiment have been determined through an iterative approach, fitting calculated theoretical WDR to physically measured WDR values at the Technical University of Denmark (DTU).

The variable $r_v$ has been integrated as defined by Straube, resulting in Equation (4).

$$r_{vb} = Factor_b \cdot r_v = Factor_b \cdot DRF \cdot V(z) \cdot cos(\theta) \cdot r_h \qquad (4)$$

Where:

- V(z) is wind speed at height of interest [m/s], defined as $V(z) = V_{10} * \left(\frac{z}{10}\right)^{\alpha_V}$.
- $V_{10}$ is standard undisturbed wind speed from weather station [m/s].
- $z$ = height of interest [m] (WDR gauge = 1.75 m).
- $\alpha_V$ = exposure coefficient [-] (0.25 for suburban area (Straube, 2010)).
- $\theta$ = angle between wind direction and wall surface [°].
- $r_h$ = horizontal rain [mm or l/m²].

> The Driving Rain Factor (DRF) defines the wind speed/raindrop fall speed interaction.

The DRF is used in many WDR models, were it tends to be a fixed standard parameter defined from average conditions, varying from 0.20 to 0.25. But as raindrop fall speed changes with drop size, this factor can be in the range 0.15 to 0.50 for drizzles or cloudbursts (Straube, 2010). The DRF can be calculated based on the methodology described in Straubes PhD Thesis (Straube, 1998). The median relative frequency of raindrop size is determined from the rain intensity in Equation (5), simplified as a median raindrop diameter in Equation (6).

$$F(Ø) = 1 - Exp\left(-\left(\frac{Ø}{\left(A * r_{h,intensity}^{p}\right)}\right)^{n}\right) \qquad \text{(Best, 1950)} \qquad (5)$$

$$\overline{Ø} = 1.105 \cdot r_{h,intensity}^{0.232} \qquad \text{(Blocken and Carmeliet, 2010)} \qquad (6)$$

Where:

- $r_{h,intensity}$ = horizontal rainfall intensity [l/(m²·h) | mm/h].
- $Ø$ = raindrop diameter [mm].
- $\overline{Ø}$ = median raindrop diameter [mm].

The median raindrop size is used to determine the raindrop terminal fall speed in Equation (7).

$$V_t(Ø) = (10^{-2} * (-16.6033 + 491.8441 * Ø - 88.8016 * Ø^2 + 5.4888 * Ø^3)\ for\ Ø \leq 5.8mm \qquad \text{(Dingle and Lee, 1972)} \qquad (7)$$

Where:

- $V_t$ = terminal fall speed of raindrop [m/s].

The DRF can then be determined as the reciprocal of the fall speed in Equation (8), resulting in the varying DRF over rain intensity illustrated in Figure 9, plotted against measured and calculated DRF's (Straube, 1998).

$$DRF = \frac{1}{V_t} \qquad \text{(Straube, 2010, 1998)} \qquad (8)$$

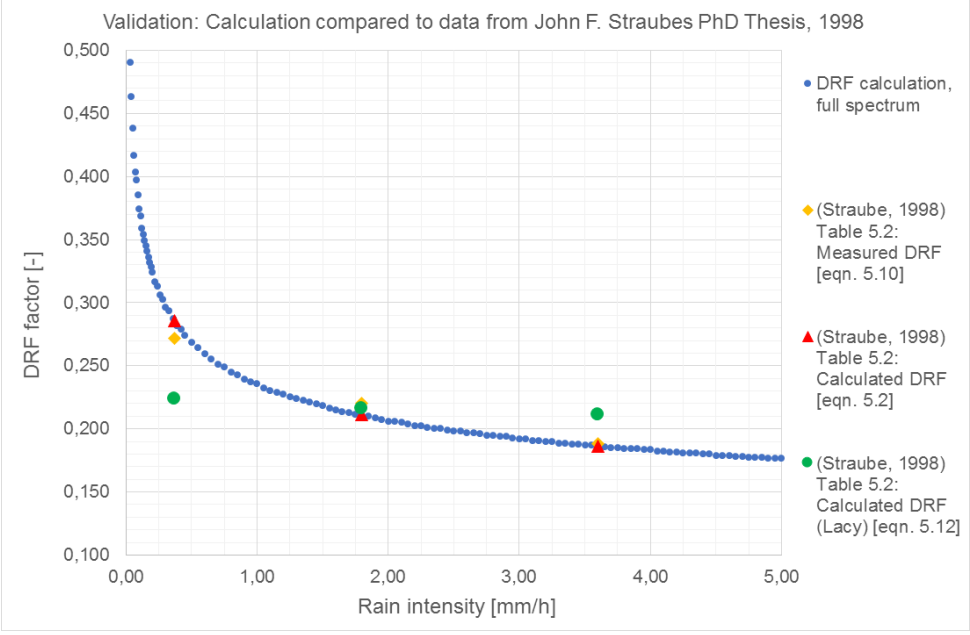


*Figure 9 Calculation of varying DRF with rain intensity, compared with table values from Straubes PhD Thesis* (Straube, 1998).

## 2.3 Method: Evaluating risk of moisture-induced damage

The combination of undesirable temperature and moisture in constructions can result in risk of moisture-induced damage. The development of undesirable hygrothermal conditions can be caused by alterations of an otherwise healthy construction by the application of an unsuitable insulation strategy, but also when the boundary conditions of the building changes, with examples being change of occupants or demolishing/erection of buildings nearby. Moisture-induced damages investigated in this PhD project include risks with relation to application of thermal insulation on the interior surface of masonry constructions. The risks involve evaluation of mould growth and decay of wood occurring, governed by (Viitanen et al., 2010b): temperature, relative humidity, exposure time and material. Another, is the risk of frost damage, governed by 3 criteria occurring at the same time (Van Aarle et al., 2015): Temperature below freezing, saturated masonry (Kuenzel, 1998) and material sensitivity to frost.

The overall methods for evaluating risks of mould growth, decay of wood and development of frost are presented in the following sections. Further moisture-induced damages exist, including attack of insects.

### *2.3.1* Evaluating risk of mould growth

Various methods exist for the prediction/risk analysis of mould growth in buildings. One must remember that mould is naturally present in the outdoor environment, therefore it is not feasible to aim for mould free buildings. The limits for when the amount of mould in the indoor environment is acceptable or unacceptable have been defined in a cooperation between two research teams:

- Sedlbauer created the bio-hygrothermal model, expressed in "growth-in-mm" (Sedlbauer, 2002, 2001). This model is used in the hygrothermal simulation software WUFI.

- Viitanen and the team from VTT Technical Research centre of Finland (VTT) and Tampere University of Technology (TUT) developed the mould index model (Hukka and Viitanen, 1999; Ojanen et al., 2010). This model is used in the hygrothermal simulation software Delphin.

- The two research teams worked together in 2015, and defined mould limits for various locations in the interior environment, based on the mould index definition (Viitanen et al., 2015).

The limits in the joint paper (Viitanen et al., 2015) are defined based on the location in the building.

- For interior surfaces in direct contact with the indoor air, Viitanen et al. accessed growth until initial stages of mould growth (MI < 1) as acceptable. Further growth still invisible to the naked eye (MI < 2) can be accepted depending on the occupant, and visible growth (MI > 2) cannot be accepted.

- For interior areas not in direct contact with the indoor air (i.e. interfaces between interior thermal insulation and solid masonry walls), Viitanen et al. accessed that slightly higher limits can be accepted. This means that growth invisible to the naked eye (MI < 2) is acceptable, some visual findings of mould can be accepted depending on the occupant (MI < 3) and severe visual findings with > 10 % coverage (MI > 3) cannot be accepted.

- Exterior areas of the construction were evaluated to not need limits, based on no contact with the indoor air/occupant side.

For the prediction of mould growth, different methods exist. Equal for all methods, (Møller et al., 2017) showed that liquid water was needed for growth to initiate, with the least growth on inorganic materials with inorganic surface treatment, increasing with the amount of organic material in the system.

Guidelines for mould germination/growth in Denmark tend to be defined based on magnitude of relative humidity, i.e. a level of relative humidity which should not be exceeded in the indoor air, independent of temperature. This type of limit is very easy to apply, but also tend to be very conservative.

The initial work of Sedlbauer defined mould (not species specific) isopleths, taking relative humidity, temperature and time into consideration, with different isopleths based on different surfaces/substrate types and their resistance to overall mould growth (Sedlbauer, 2002). This type of limit considers more parameters, but is also harder to interpret, especially as data jumps between limit lines. The isopleths are good for evaluating short time periods of data, to access if combined conditions of temperature and relative humidity can result in risk of mould growth. I have good experience with the use of this type of mould models especially for presentation of results to non-technicians. Examples of isopleths for mould germination and growth can be seen on page 142 in Figure 109 and Figure 110 respectively.

More advanced, and widely used in research, include mathematical models based on the same parameters as those for mould isopleths for prediction of overall mould germination/growth. Many different models exist in literature, and review/comparison of the different models have been done for wood (Gradeci et al., 2017a, 2017b) and other materials (Vereecken and Roels, 2012). Gradeci et al. have identified and evaluated the following mathematical models based which can calculate mould growth over time: ESP-r; Max days-model; VTT model; Biohygrothermal; Mould Germination Graph; Johansson et al Indices; MRD model; Gobakken et al model; m-model. From the amount of different mould models available, it is evident that the field of mould prediction receives big attention. The mathematical models need a long dataset, as the mould growth develops over time. The mathematical models are good for evaluating the increase or decrease of mould growth over one or more seasons. We have good experience with the use of this type of mould models for comparative analyses of long-term experimental data and hygrothermal simulations.

The general conclusion from previous reviews of mould models is that the output of the different models differs, and none of the models are able to precisely predict exact mould growth based on inputs (Gradeci et al., 2017b). This result is emphasised by the results of Møller et al., showing that no mould germination or growth occurred during a 40 week laboratory experiment with constant critical conditions for mould growth: RH = 90 % and temperature = 20 °C (Møller et al., 2017). This result differs from:

- Predictions by isopleth models presented in the paper of Møller et al.
- Visible mould criteria presented in (Tsongas et al., 2016): Relative humidity > 85 % for a 30 day running average of a sensitive material (paper-coated products).

From this finding, this must mean that mould in cementitious materials will not initiate before a second period with condensation after initial dry-out, as Viitanen et al. states that the alkaline conditions prohibit mould formation on new surfaces during the initial dry-out period (Viitanen et al., 2015).

Even though it is evident that mould models cannot be used to precisely predict mould growth or germination, the models are still believed to be valuable tools to assess the influence of the combined hygrothermal conditions, exposure time and material, compared to assessing only the development of the hygrothermal conditions. The mould growth occurring in the construction can be detected afterwards, where a range of different approaches for on-site measurements

exists, depending on the need to identify specific mould species or mould growth in general (Krause, 2003; Miller and Reeslev, 2003; Reeslev and Miller, 2002).



During the PhD study, the mathematical mould model from VTT and TUT has been used as a method to determine the influence of changed hygrothermal conditions when installing interior insulation, especially used in the appended Paper #3 for comparative analyses of different insulation strategies. The model does not distinguish between the specific mould species, but as no mould species have a positive effect on the indoor environment, this is a reasonable simplification.

A minor change was proposed to the VTT model presented in (Hukka and Viitanen, 1999; Ojanen et al., 2010). The original and proposed curve for a resistant material can be seen in Figure 10. This curve is based on a combined temperature and relative humidity limit for mould growth when using a "very sensitive" and "sensitive" material defined in (Ojanen et al., 2010), by a limit of 80 % RH with a curve in the temperature range $\theta = 0\,^{o}C \rightarrow 20\,^{o}C$ as illustrated with label "*sensitive" in Figure 10. For a medium resistant material, a limit of 85 % RH was defined (Ojanen et al., 2010), but only from 20°C and above. To cover the temperature range $\theta = 0\,^{o}C \rightarrow 20\,^{o}C$, I suggest a 3rd degree polynomial curve fit to the following defined points: $(\theta, \mathrm{RH})$ = (0, 100; 20, 85; 25, 85; 30, 85). This resulted in the following equation: $\mathrm{RH}(\theta) = -0.001 \cdot \theta^3 + 0.075 \cdot \theta^2 - 1.85 \cdot \theta + 100$. Points and resulting fit can be seen in Figure 10 with the label "*resistant". There will be no mould growth for temperatures below 0°C.

The VTT model with the proposed curve for resistant materials have been used for comparative analyses throughout this PhD project. The difference between the mathematical mould models and reality is acknowledged, and the output from the models have solely been used for comparative analyses to evaluate if different insulation strategies performs better or worse than a reference case and other insulation strategies.

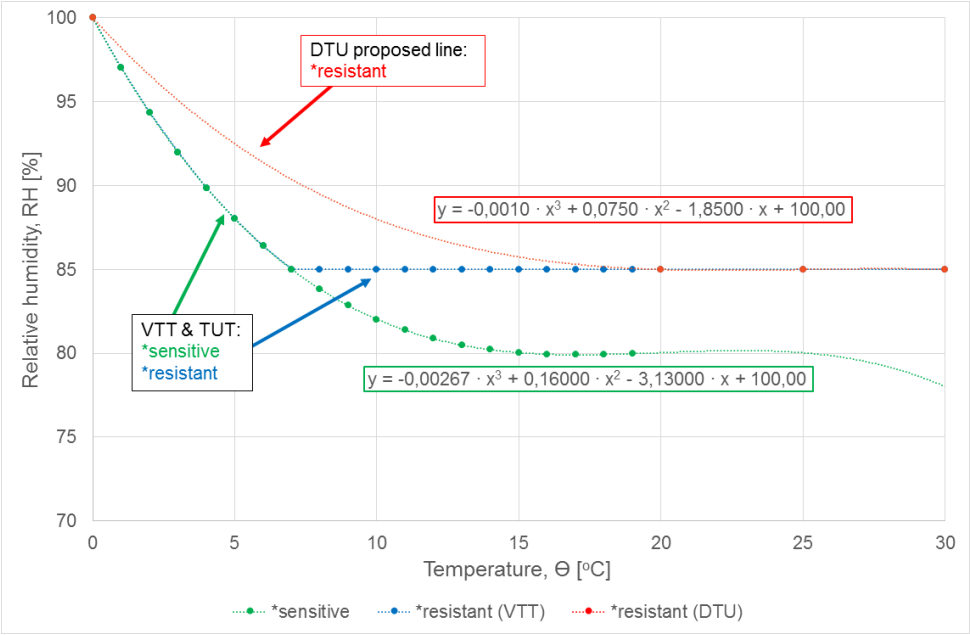


*Figure 10 RHmin limits for mould growth, *sensitive and *resistant (VTT) defined in* (Ojanen et al., 2010)*. We propose the alternative *resistant (DTU) graph, presented in the appended Paper #2.*

### *2.3.2* Evaluating risk of wooden decay



The evaluation of risk for wooden decay in wooden structural components, as illustrated in Figure 11, can be performed on basis of two major strategies.

The very simple approach is that wooden moisture should not exceed 20 weight-% in prolonged periods, as this will result in increased risk of wood decaying fungi (Koch, 2013). The German WTA guidelines define a maximum boundary based on relative humidity within the pores in the wooden medium, with a long-range maximum value of 85 % RH and a daily maximum average of 95 % RH at 0 °C up to 86 % RH at 30 °C (Scheffler et al., 2014). These overall simple approaches concern fungi in general, where the individual types of fungi with growth conditions and decay form differ and have been further described and illustrated by Koch et al. (Koch et al., 2006, 2003).


*Figure 11 Example of wooden decay/rot of wooden beam end in lower storeys of facade wall. Photo courtesy of J. Engelmark.*

Approaches that are more complex include mathematical models, able to calculate the theoretical development of wooden decay over long periods, based on datasets with temperature and relative humidity over time. Different mathematical wooden decay models exist, and a review with focus on wooden constructions exposed to outdoor conditions has been published (Brischke and Thelandersson, 2014). There have been discussions on if the models are appropriate for embedded and accessible wood on the interior side of the thermal envelope, but as the models are based on temperature, relative humidity and exposure time, the models must also be appropriate for evaluating risk of wooden decay in other positions where oxygen is available. Brischke and Thelandersson

defined a range of parameters that should be included in an appropriate model for the evaluating of risk of wooden decay, including:

- The importance of appropriate wood types.
- The need for inclusion of lag/activation process as dose-response functions for evaluating development of damage in the biological field.

The wooden decay risk evaluation in this PhD Thesis has been based on the mathematical model of H. Viitanen et al. (Viitanen et al., 2010a), evaluating overall decay caused by different species of fungi. The activation process is included in the model, defined as an index "*a*", increasing from 0 to 1 during favourable conditions for wooden decay, and decreasing linearly when conditions for wooden decay are not present with a rate of 1.0 over 2 years. Irreversible wooden decay will develop when $\alpha = 1$. The Pine Sapwood used for the development of the mathematical model was deemed appropriate, as the structural lumber in historic Danish multi-storey buildings traditionally consist of Pomeranian Pinewood, a mix of heartwood in the lower storeys and sapwood at the upper storeys (Engelmark, 2013, 1983).

In-situ investigations for wooden decay have shown that the mathematical models seem conservative when evaluating decay of embedded wooden elements. The mathematical models to evaluate wooden decay are however still believed to have a strength like that of the mould models. The decay model has therefore been used solely for comparative analyses throughout the PhD study to evaluate the difference between insulation strategies. A comparative analysis strategy similar to the use of mathematical mould growth models, without focus on the individually calculated decay values.

### *2.3.3* Evaluating risk from frost and wetting of bricks

As presented in Section 2.1.1 on page 24, the masonry becomes wetter when applying thermal insulation to the interior masonry surface. This increase of moisture content in the masonry can cause deterioration of mortar joints and softening of the bricks (Hamid and Orphy, 2012). Hamid and Orphy state that the softening of bricks especially affects less fired bricks, which are traditionally found on the interior side of the historic Danish multi-storey buildings (Engelmark, 1983).

The risk of frost damage will increase when retrofitting the interior surface with thermal insulation (Zhou et al., 2017), as the moisture content in masonry increases, and the temperature of the masonry decreases in the cold climate of

Denmark. This relate to 2 of the previous 3 defined frost-criteria which need to occur at the same time (Van Aarle et al., 2015): Temperature below freezing; wet masonry (Kuenzel, 1998); and material sensitivity to frost. Simple methods have previously consisted of evaluating the amount of freeze-thaw cycles in the outer leaf of the façade, compared to the frost resistance of the specific material. WTA guidelines define a maximum pore volume saturation of 30 % for non-frost resistant materials at 95 % RH, allowing for higher saturation degree if the relative humidity within the pores is lower than 95 % (Scheffler et al., 2014). Zhou et al. proposed a freeze-thaw damage risk (FTDR) index for evaluating freeze-that damage, based on material tests of brick for determining the critical FTDR index value, compared to calculated FTDR index based on measured/simulated hygrothermal conditions (Zhou et al., 2017).

All the methods depend on material characterisation, which have not been included in this PhD study. A simple evaluation for frost damage based on visual inspections in a case study has been included in Section 6 and Paper #2.

## 2.4 *Method: Monitoring hygrothermal conditions with wooden dowels*

The use of wooden dowels to monitor hygrothermal conditions in constructions is well-known and has proven a stable methodology for long-term measurements. The use of dowels has been described in Danish literature (Brandt et al., 1999; Brandt and Hjorslev Hansen, 2005; Christensen et al., 1999), with examples of sensors working for more than 20 years (Christensen, 2001). Wooden dowels are further mentioned in international literature, stating the applicability of wooden dowels for slow and long term-measurements of relative humidity (Ueno and Straube, 2008), up to a wooden moisture weight-% of 15 %, from where the level of moisture is underestimated and can only be used to indicate changes in relative wetness (Walker et al., 2016).

The method of monitoring the wooden moisture weight-% by DC electrical wooden resistance includes a wide range of error sources, resulting that accuracy below +/- 1 weight-% can only be achieved in well-equipped laboratories (Munch-Petersen, 1990). Munch-Petersen however state that this accuracy is sufficient to illustrate the conditions in construction components.

The measurements are traditionally performed manually with an instrument capable of measuring high values of DC electrical resistance, a T301.COW instrument (BMT Instruments ApS, 2017; Bygge og Miljøteknik, 2008). As the wooden dowel is polarised during measurement, it is important to perform the measurements after the same procedure each time to follow the development of the measurements. This study have followed the methodology of Munch-Petersen, consistently having a measurement period of 20 seconds before noting the value (Munch-Petersen, 1990). Monitoring of the development of DC electrical resistance automatically has been attempted in the experimental setup described in Section 5 on page 103, but was not yet fully functional at the time of finishing the PhD Thesis.

### *2.4.1* Conversion from DC electrical wooden resistance to wooden moisture weight percent

The conversion of DC electrical resistance and temperature measurements in wooden dowels to wood moisture weight-% is described thoroughly in Danish literature (Brandt et al., 1998; Hansen, 1996; Lohse, 1986; Munch-Petersen, 1990), with literature up to 1990 being covered by Munch-Petersen, supported by his own experiments. A range of graphs and mathematical expressions from the previously mentioned Danish literature can be seen in Figure 12. The figure is

based on temperature adjusted DC electrical resistances, while the influence of temperature has been elaborated in (Brandt et al., 1998).



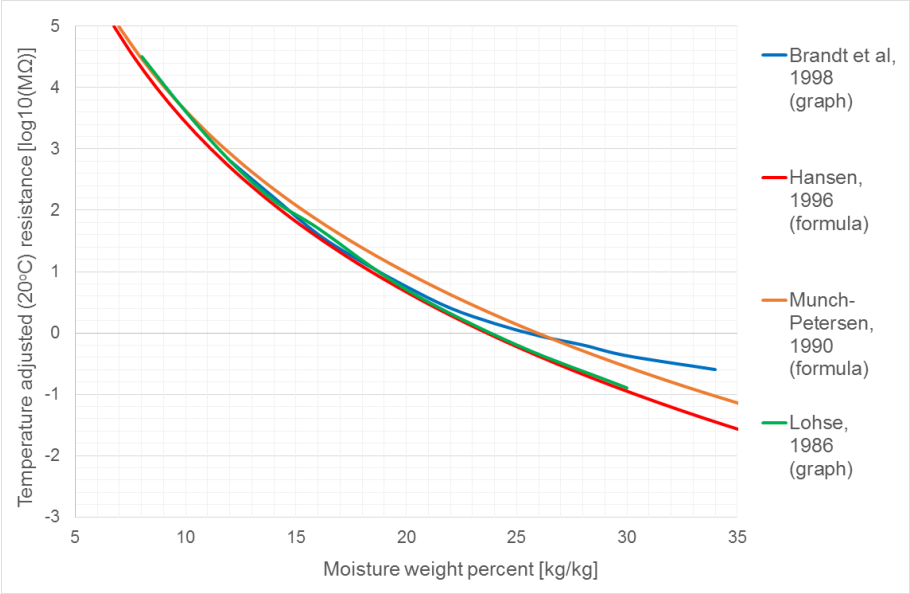


*Figure 12 Different conversions from temperature adjusted log10(MOhm) DC electrical wooden resistance to wooden moisture weight-%* (Brandt et al., 1998; Hansen, 1996; Lohse, 1986; Munch-Petersen, 1990)

First the resistances are adjusted to a temperature of 20°C by using the temperature correction method illustrated in Equation (9).

$$R_{adjusted}[log10M\Omega] = R[log10M\Omega] - (0.029 + 0.005 * R[log10M\Omega]) * (20 - \theta[^oC])$$

(Hansen, 1996) (9)

Where:

- $R$ = measured DC electrical resistance $[log10M\Omega]$.
- $R_{adjusted}$ = DC electrical resistance adjusted to 20°C $[log10M\Omega]$.

The temperature-adjusted DC electrical resistance are then converted to wooden moisture content in Equation (10).

$$u\left[\frac{kg}{kg}\right] = 10\hat{}\left(\frac{12.63 - R_{adjusted}[log10M\Omega]}{9.196}\right)$$

(Hansen, 1996) (10)

Where:

- $u$ = wooden moisture weight percent [kg/kg].

### *2.4.2* Conversion from wooden moisture weight percent to relative humidity in wooden pores

As the mathematical models for mould growth and wooden decay described earlier under Section 2.3 are based on temperature in degrees Celsius and relative humidity in percent, a conversion from wooden weight-% to relative humidity is needed.

Arguments exist against a direct relative humidity/wooden weight-% relation, as a complete state of equilibrium between the two moisture conditions can take 5-6 weeks before occurring (Munch-Petersen, 1990). This lag occurs due to hysteresis and unstable moisture conditions, while "close to equilibrium" occurs after 1-2 days, and small changes based on transient conditions are observable as well. As the changes in moisture in masonry construction occur slowly with small transient changes in the moisture and temperature conditions throughout the year, the conversion is believed possible. The conversion into relative humidity is based on the adsorption and desorption isotherm illustrated in Figure 13. As it was not possible to know the current state of hysteresis of the wooden dowel, the relative humidity was determined from 50% of the adsorption curve, and 50% of the desorption curve. This conversion means that during adsorption, the relative humidity in the material will be overestimated, and during desorption, the relative humidity will be underestimated, as illustrated later in Figure 116 on page 150.

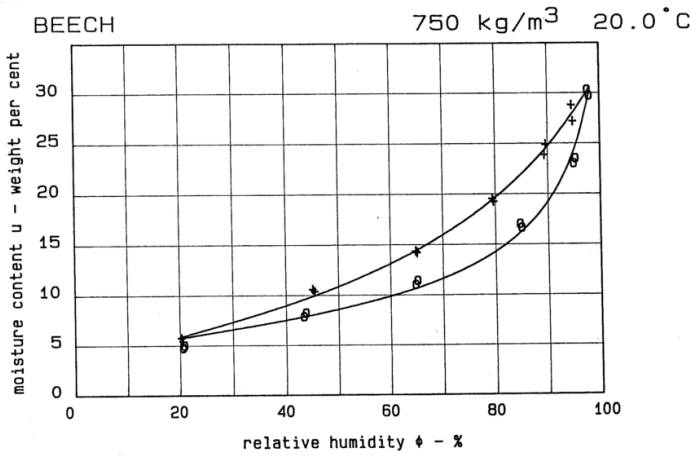


*Figure 13 Sorption isotherm for beech wood (Ahlgren, 1972; Hansen, 1986), which the wooden dowels consist off. Original measurements performed by Ahlgren. Illustration courtesy of K. K. Hansen.*

The mathematical process of converting wooden moisture weight-% to relative humidity was based on curve fitting to the ad- and desorption isotherm for beech wood illustrated in Figure 13 (Ahlgren, 1972; Hansen, 1986). The relative humidity was determined as via the general model presented in Equation (11) and the following ad- and desorption factors:

$$\mathrm{RH}(u)\ [\%] = 0.5 \cdot \left( \begin{array}{l} \left( C_{adsorption} \cdot \exp\left( 1 - \left( \frac{u\left[\frac{kg}{kg}\right]}{A_{adsorption}} \right)^{B_{adsorption}} \right) \right) + \\ \left( C_{desorption} \cdot \exp\left( 1 - \left( \frac{u\left[\frac{kg}{kg}\right]}{A_{desorption}} \right)^{B_{desorption}} \right) \right) \end{array} \right) \qquad (11)$$

Where:

A, B & C [-] being the following factors for ad- and desorption:

- $A_{adsorption}$=7.608, $B_{adsorption}$=-1.353, $C_{adsorption}$=42.960.
- $A_{desorption}$=12.690, $B_{desorption}$=-0.8945, $C_{desorption}$=57.440.

# 3 CHARACTERISTICS, AMOUNT AND DISTRIBUTION OF MULTI-STOREY BUILDINGS FROM 1850-1930

Section 3 concern Sub-hypothesis #1 and Sub-hypothesis #2. **SH1** is addressed first, investigating and describing the characteristics of the traditional Danish multi-storey buildings in Section 3.2, based on literature, drawings and photographs. The investigations in Section 3.2 limit the period of erection for multi-storey buildings with solid masonry facades and wooden elements to 1850-1930, why this period is used throughout the Thesis. **SH1** form the foundation to answer **SH2**, describing the amount and distribution of multi-storey buildings and apartments built in the period 1850-1930 in Section 3.3.

## *3.1* ***Summary of papers related to Section 3***

The following text will describe the correlation between the content of the papers and this section, and address how the sub-hypotheses were treated in the papers. This section only describes the content, the discussion and conclusion of the individual sub-hypothesis are done in the sub-discussion and sub-conclusion, Section 3.4 and 3.5 respectively.

Section 3 is based on some of the content in the appended Paper #1: "Interior insulation – Characterisation of the historic, solid masonry building segment and analysis of the heat saving potential by 1d, 2d, and 3d simulation" and a conference paper not appended in present thesis (Odgaard et al., 2015).

Regarding **SH1**, the characteristics of Danish multi-storey buildings, the content in Section 3.2.1 are similar to that of the appended Paper #1 (Sec. 2), extended with more descriptive text and especially a large degree of photographs illustrating the characteristic composition of the segment. The floorplan investigations in Section 3.2.2 contain a shortened edition of the methodology and registrations presented in the appended Paper #1 (Section Sec. 3.2, Sec. 4.2 & Sec. 5.2), as the focus in this Thesis is solely on the horizontal distribution of window width over the width of thermal envelope and floor area. These numbers are used to validate the characteristics found in Section 3.2.1, ultimately creating figures for assessing the areas available for retrofitting the interior surface with thermal insulation. For further information regarding the floorplan analysis, see the appended Paper #1.

The investigations in Section 3.3 regarding **SH2**, the size and distribution of multi-storey buildings and apartments, are an extended version of that used in the appended Paper #1, why the content in the paper will not be presented further.

The content in the appended Paper #1 related to Section 3 of this Thesis contain a further investigation of the later period 1930-1950. In this later period, the building style of solid masonry facades with embedded wooden elements became less frequent, and this period have not been included in this Thesis.

## *3.2* ***Characteristics of traditional Danish multi-storey buildings, year 1850-1930***

Section 3.2 is based on Sub-hypothesis #1, regarding the characteristics of traditional Danish multi-storey buildings with solid masonry walls and embedded wooden elements. The sub-hypothesis has been investigated by different approaches, as presented in the following sub-sub-sections:

- Section 3.2.1 is based on literature, discussions with Associate Professor Engelmark and his unpublished extensive database of photographs documenting buildings undergoing demolitions and renovations.
- Section 3.2.2 concern an investigation of floorplans from buildings in Copenhagen, aiming to determine a common ratio of window length over length of thermal envelope and floor area.
- Section 3.2.3 take a point of departure in Section 3.2.2, the ratio of windows over length of thermal envelope. This distribution is used for selecting an exterior façade, hatch areas unavailable for retrofitting interior thermal insulation and calculate the share of areas.

### *3.2.1* Investigation based on literature, discussions with experts and photographs

The buildings from the period 1850-1930 were generally built after the same principles. This consistence in building style within the segment, relates to the introduction of strict building legislation in 1856 (Engelmark, 2013; Nielsen, 1919), defining consistent general dimensions and construction techniques until the 1930's. Initially, the legislation applied to construction in Copenhagen, but the regional boroughs of Denmark quickly adopted the regulations.

The multi-storey buildings were designed by architects to the limit of regulations, only involving engineers if special details were needed. Because of this, the majority of buildings constructed in the period share specific and well-documented

characteristics, resulting in a structure as illustrated in Figure 14. The building style of the Danish multi-storey buildings in the period 1850-1900 has been extensively researched by J. Engelmark during his period as a postgraduate fellow and documented in Danish (Engelmark, 1983), providing detailed documentation about the composition of this type of buildings. Engelmark continued his work with further research covering the period 1850-2000, documented in Danish in book form (Engelmark, 2013). The work of Engelmark has led to two webpages, one with literature regarding Danish building style and legislation from 1850-2000 (Danskbyggeskik.dk et al., 2017), the second one with 3-dimensional examples of details as illustrated in Figure 15 (Danskebygningsmodeller.dk et al., 2017). During my PhD study I have worked in an adjacent office to Associate Professor Engelmark, and have had the delightful opportunity to discuss details concerning the building styles and receive a large amount of unpublished pictorial material.

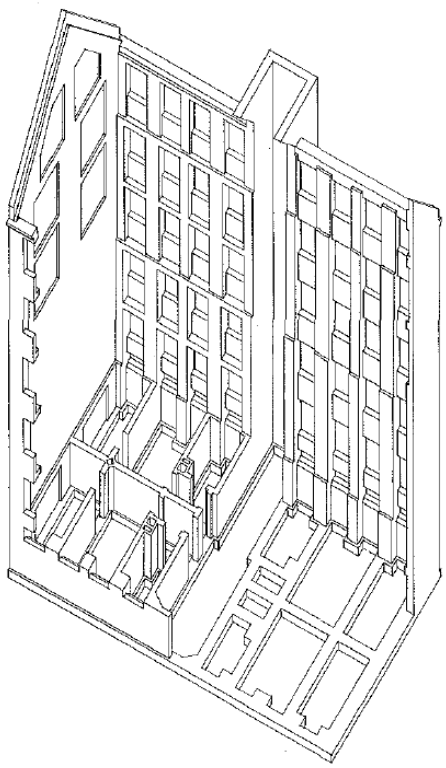

*Figure 14 Maximum perforation of outer leaf.*

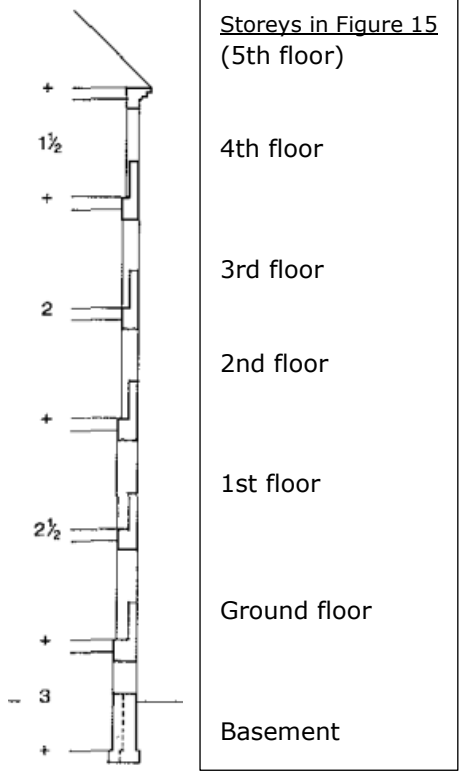


*Figure 15 Thickness of masonry columns in bricks, defined from top (1 brick ≈ 0.24 m).*

*Illustrations in Figure 14 and Figure 15 courtesy of J. Engelmark, both extracts from (Engelmark, 1983).*

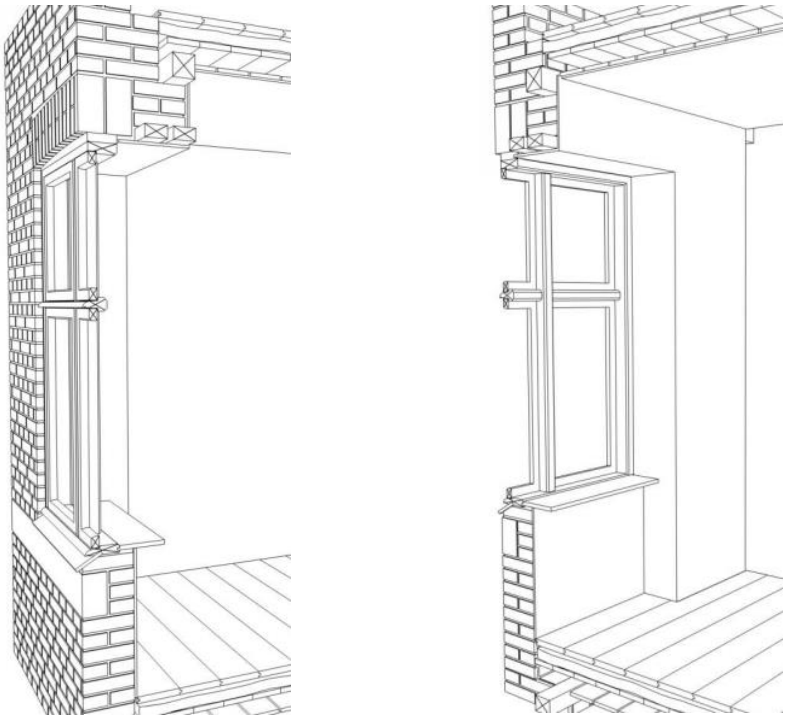

*Figure 16 Illustration of characteristic multi-storey facade, cut through spandrel. Illustration from in- and outside. Screen dumps from facade 3d-models* (Danskebygningsmodeller.dk et al., 2017)*, with permission from J. Engelmark.*

The façade of the multi-storey buildings built in the period 1850-1930 is typically constructed with masonry, with or without exterior render or sandstone cladding, and with a wall plate along the facade as support for the wooden beams (floor joists).

A building from 1890 has been opened from the courtyard for the implementation of modern bathrooms as shown in Figure 17 and Figure 18, revealing many of the characteristic constructional details.

The floor structure consists of wooden beams, with wooden floorboards on top, clay pugging placed on wooden pugging boards between the beams and wooden furring strips below as underlay for a rendered ceiling, as seen in Figure 23 and Figure 24. The wooden beam is supported by the masonry columns as seen in Figure 19, Figure 20, Figure 21, Figure 22 and Figure 29. In between the masonry columns, the wooden beam is supported by a wall plate, running along the façade, as seen in Figure 25, Figure 26, Figure 27, Figure 28 and Figure 30.


*Figure 17 Opening of courtyard facade, photo showing ground until 3rd floor.*

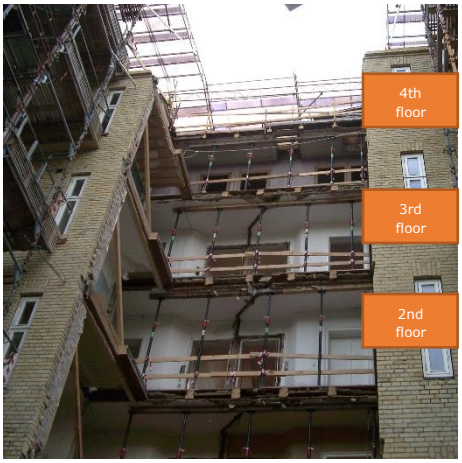


*Figure 18 Opening of courtyard facade, photo showing 1st until 4th floor. 4th floor is under the roof.*

*Multi-storey building built in 1890. Details of facade/wooden beam interaction in Figure 19, Figure 20, Figure 21 and Figure 22, details in the pugging layer in Figure 23 and Figure 24.*

*Photos in Figure 17 and Figure 18 courtesy of J. Engelmark.*

The building regulations defined the composition of the façade. It must be understood that Danish masonry is constructed after modular dimensions revolving around brick dimensions (228 x 108 x 54) mm with mortar joints in the horizontal direction of 12 mm and in the vertical direction of (3 bricks + 3 mortar layers) = 200 mm. The thickness of the load bearing masonry columns in the façade was defined by the amount of bricks, increasing downwards from 1½ bricks' thickness (348mm) at the top storey, as illustrated in Figure 15. The changing thickness of masonry columns can further be seen in Figure 19, Figure 20, Figure 21 and Figure 22.

*Figure 19 Facade/wooden beam interaction, ground floor (2½ bricks) --> 1st floor (2 bricks).*


*Figure 20 Facade/wooden beam interaction, 1st floor (2 bricks) --> 2nd floor (2 bricks).*

*Multi-storey building built in 1890. Photos in Figure 19 and Figure 20 courtesy of J. Engelmark.*

*Figure 21 Facade/wooden beam interaction, 2nd floor (2 bricks) --> 3rd floor (1½ bricks).*

*Figure 22 Facade/wooden beam interaction, 3rd floor (1½ bricks) --> 4th floor (roof).*

*Multi-storey building built in 1890. Photos in Figure 21 and Figure 22 courtesy of J. Engelmark.*

*Figure 23 Wooden floor structure with wooden beam and pugging layer.*

*Figure 24 Wooden floor structure, note the recess in the wooden beam for pugging boards.*

*Multi-storey building built in 1890. Photos in Figure 23 and Figure 24 courtesy of J. Engelmark.*

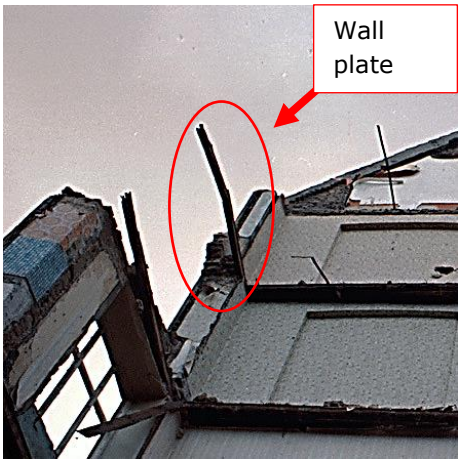


*Figure 25 Wall plates in façade uncovered during demolition of building.*

*Figure 26 Wall plates and beams uncovered during demolition of building.*

*Photos in Figure 25 and Figure 26 courtesy of J. Engelmark.*

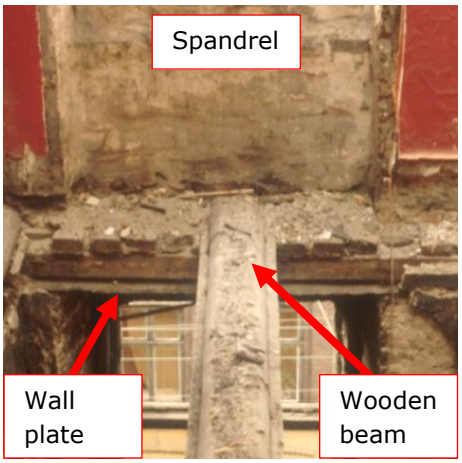


*Figure 27 Wooden beam supported by a wall plate in between masonry columns, seen from top.*

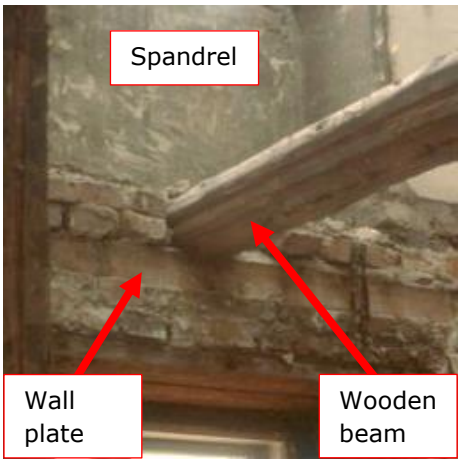


*Figure 28 Wooden beam supported by a wall plate in between masonry columns, seen from below.*

*Photos in Figure 27 and Figure 28 courtesy of J. Engelmark.*


*Figure 29 Cleaned up construction: Wooden beam end in masonry column, supported by a wall plate.*


*Figure 30 Cleaned up construction: Wooden beam supported by a wall plate in between masonry columns.*

*The constructions illustrated in Figure 29 and Figure 30 were cleaned up before taking the photograph by removing bricks, gravel and dirt by hand and brush. The original before cleaning would look similar to constructions illustrated in Figure 27 and Figure 28.*

*Photos in Figure 29 and Figure 30 courtesy of J. Engelmark.*

Windows were placed between the masonry columns, with spandrels completing the façade in the vertical areas between the windows and the floor decks with a constant thickness of 1 brick (240 mm), regardless of the floor number. A picture of a window section between two masonry columns can be seen in Figure 31 and Figure 32, with and without finishing towards the inside.

*Figure 31 Interior facade wall, window section. Before dismantling finishing.*

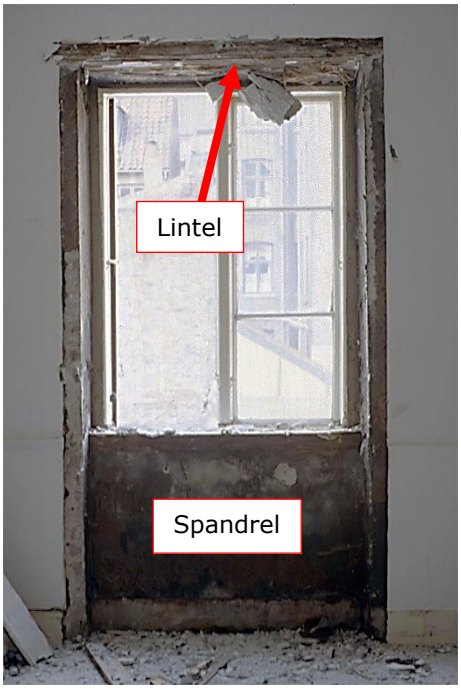


*Figure 32 Interior facade wall, window section. After dismantling finishing into masonry surface. A lintel over a window can be seen in Figure 35.*

*Photos in Figure 31 and Figure 32 courtesy of J. Engelmark.*

A picture of the finishing in front of a masonry spandrel can be seen in Figure 33, in this case with retrofitted mineral wool between the masonry and finishing. A picture showing a 1 brick thin masonry spandrel next to a 2 brick thick masonry column can be seen in Figure 34. The wall above the window had a thickness corresponding to the masonry column thickness at the given floor, with masonry resting on a lintel constructed from wood, as seen in Figure 35.

*Figure 33 Timber finishing in front of spandrel. In some cases retrofitted with thermal insulation.*

*Figure 34 Interior masonry surface of window section. Removed finishing.*

*Photos in Figure 33 and Figure 34 courtesy of J. Engelmark.*

Figure 35 Lintel over window in façade. Photo courtesy of J. Engelmark

### *3.2.2* Floorplan investigation to validate horizontal characteristics

The complete methodology and registrations from the investigation is described in depth in the appended Paper #1, while the content of this section focus on the resulting horizontal distribution of window width over width of thermal envelope and floor area. The investigation involved registration of parameters on 43 apartment floorplans distributed over nine buildings. The period of erection for the nine buildings spanned from the earliest erected in 1874, to the latest erected in 1920. The investigation included registration of parameters on an apartment level: Amount of rooms, registration of individual window widths, floor area including walls, perimeter length of thermal envelope and perimeter length of gable.

The results from the investigation showed that the majority of individual window sizes are 1.0, 1.1 and 1.2 m wide, accounting for 50 % of the registered windows, as can be seen in Figure 36.

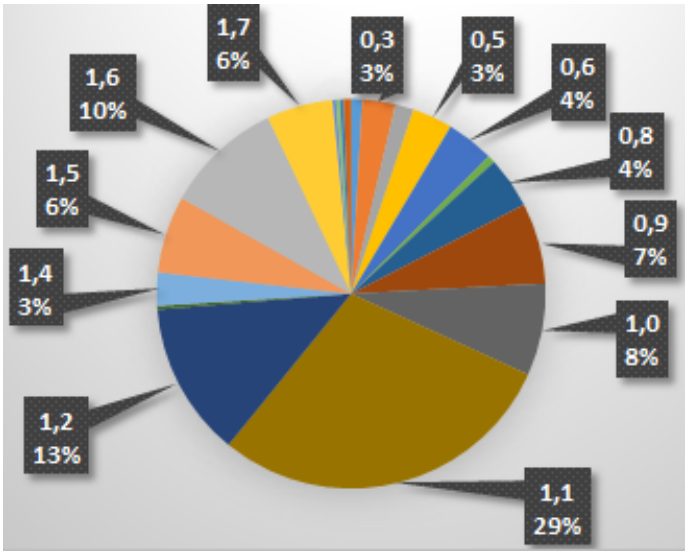


*Figure 36 Registered windows in 43 apartments/9 buildings.*
*Label when sum < 3 % have been removed from graph.*

The registered values, presented in Table 2, were tested for correlation in the appended Paper #1. The paper documented a correlation between the apartment's sum of window widths and both the perimeter length of thermal envelope excl. gable and the apartment's sum of window widths and floor area, as seen in Figure 37 and Figure 38 respectively.

| Parameters available in the Danish Building and Dwelling Register (BBR) | Window parameters affecting available area for interior insulation |
|---|---|
| * Amount of rooms.<br>* Apartment floor area, incl. walls.<br>* Perimeter length of thermal envelope. | * Total amount of windows in apartment.<br>* Sum of window widths in apartment. |

*Table 2 Tested correlation between parameters.*

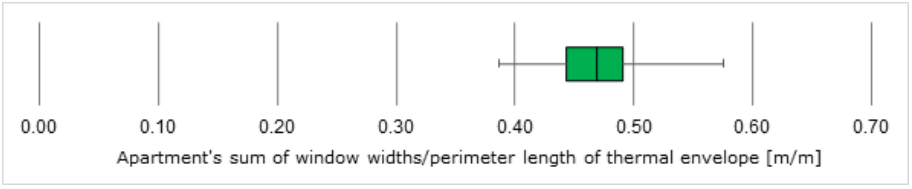


*Figure 37 Box plot of correlation between the apartment's sum of window widths and perimeter length of thermal envelope, excl. perimeter length of gable. Whiskers defined as min- and maximum registered values.*

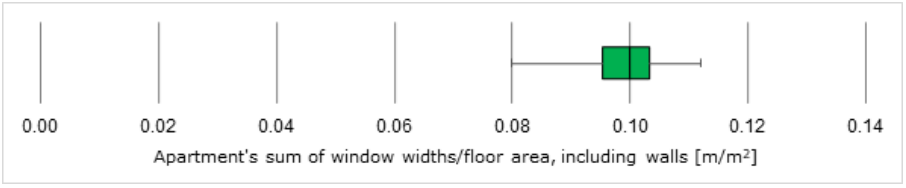


*Figure 38 Box plot of correlation between the apartment's sum of window widths and individual floor area. Whiskers defined as min- and maximum registered values.*

### *3.2.3* Available areas for application of interior thermal insulation

When considering the application of thermal insulation to the interior surface, it must be acknowledged that a smaller extent is possible, compared to the application of exterior insulation. This difference originates from areas in which interior insulation is not possible, such as floor structure and solid partitions, as illustrated with photographs in Section 3.2.1.

The available area for installation of interior insulation was clarified based on the floorplan analysis performed in the appended Paper #1 and Section 3.2.2. It was found that the ratio of windows over thermal envelope, illustrated in Figure 37, was below the maximum permissible degree of perforation allowed in the building regulations in force in the period 1850-1930. The building regulations in force stated a maximum degree of perforation for windows and door of 2/3's of the surface in the horizontal direction, and 1/2 of the surface in the vertical direction.

The 25 % quartile of the box plot in Figure 37 define 0.44 meter window per meter thermal envelope. This share was used to identify a floorplan with an equivalent share of windows. A building constructed in 1927 has been illustrated in Figure 39, where the façade has a window/thermal envelope ratio of 0.43 m/m. The apartment's floorplan was used to mark areas where interior insulation was not directly applicable, showing that the areas for interior insulation is limited:

- Yellow hatches mark windows.
- Red hatches show the position of solid partitions, separating fire cells from neighbour apartments/staircases.
- Blue hatches show the position of partitions, which could be either timber or solid masonry walls.
- Green hatches show the position of the floor structure.

The hatched areas were used to calculate the facades share of windows and the total unavailable area for interior insulation, both stated in the caption of the figure.

It is possible to insulate the volume in the floor structure within the wooden beams and the ceiling/floor boards, but based on interviews with major Danish contractors it is found that this is not usually done, as it significantly increases the cost and complexity of the refurbishment.

An additional typical façade has been illustrated in Figure 40, showing a façade with a comparable high degree of perforations and very limited areas available for the application of interior insulation.

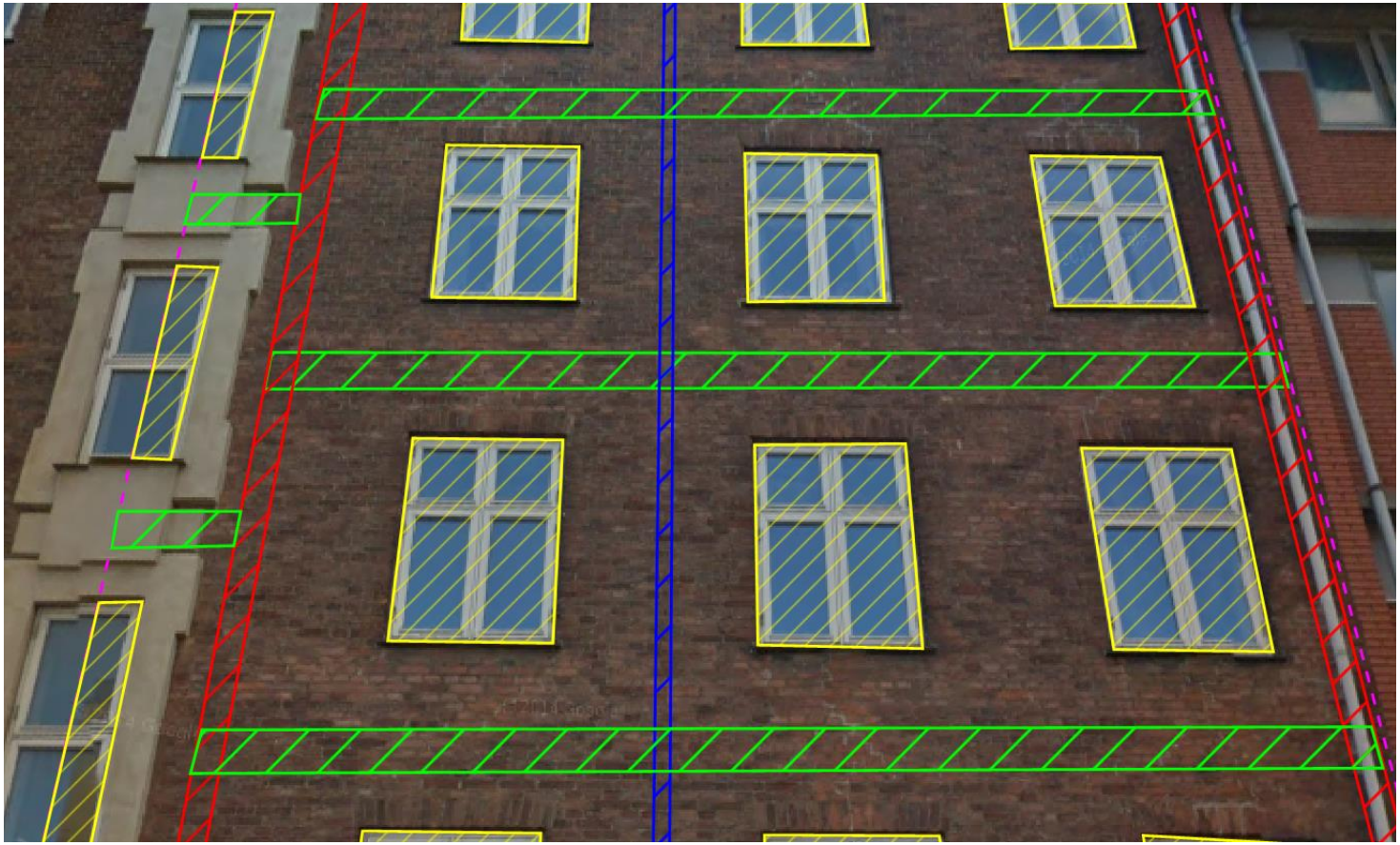

*Figure 39 Exterior surface of a 1927 multi-storey building with a horizontal window/thermal envelope ratio of 43.0 % within the pink dashed lines. Hatches were defined as follows: Yellow = windows, blue = light/solid partitions, red = solid/fire walls, green = floor structure. Hatches were based on actual floorplan. Share of areas between pink dashed lines and top/bottom edges of picture: Window & door area = 20 %, area unavailable for retrofitting interior insulation: 38 %. Original photo by Google street view.*

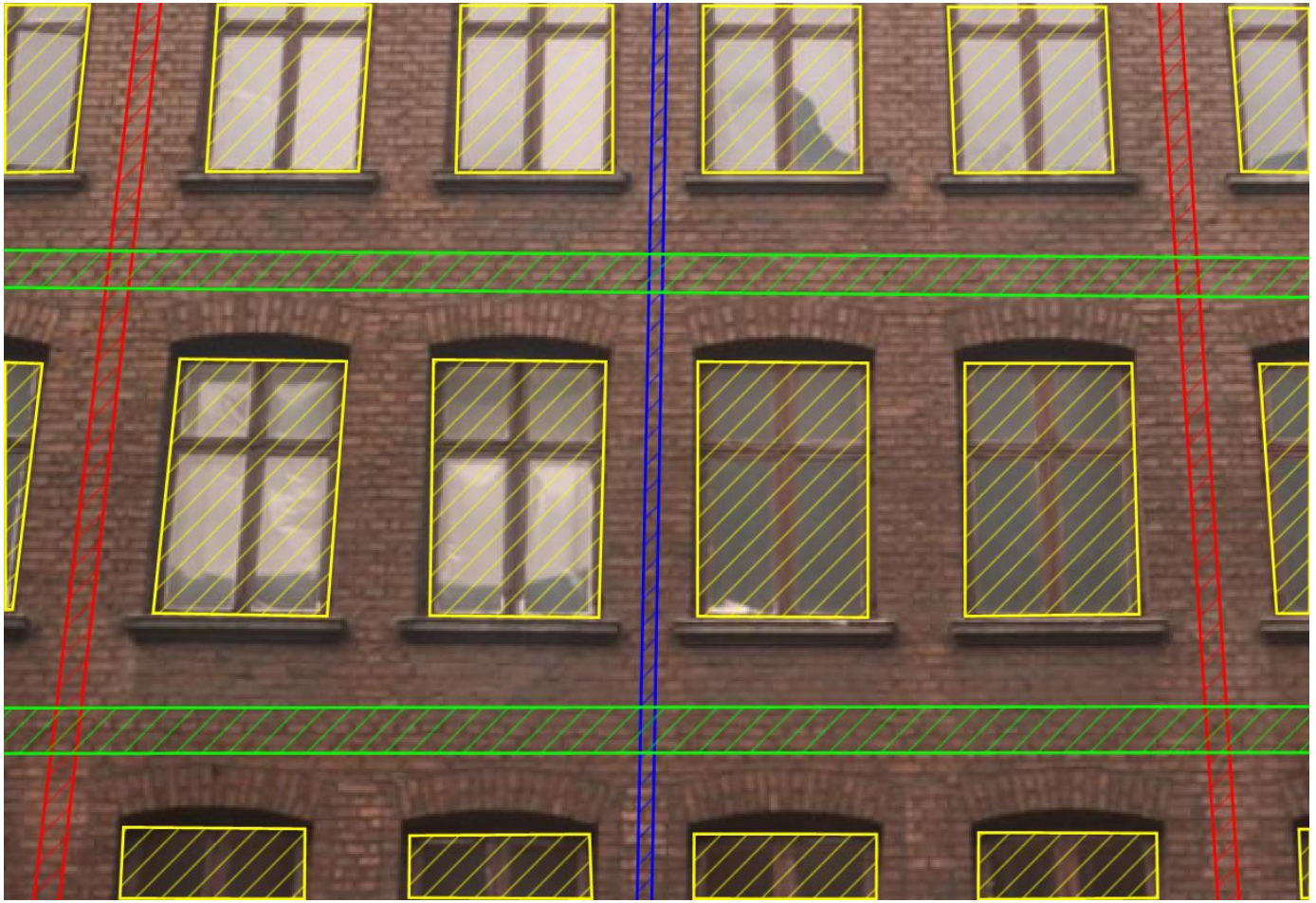

*Figure 40 Exterior masonry surface of typical Danish historic multi-storey building. Hatch definition similar to Figure 39. Hatches were based on expert discussions with professor Engelmark. Share of areas within edges of picture: Window & door area = 31 %, area unavailable for retrofitting interior insulation: 45 %. Original photo courtesy of J. Engelmark.*

## *3.3* ***Size and distribution of multi-storey buildings and apartments***

Section 3.3 is based on Sub-hypothesis #2, regarding the distribution of traditional Danish multi-storey buildings with solid masonry walls and embedded wooden elements. Section 3.3 contains an extended version of the database-based investigation presented in the appended Paper #1, with focus solely on the erection period 1851-1930.

A similar investigation is currently performed under the RIBuild project (RIBuild.eu et al., 2017), with participation from 10 research partners aiming to determine similar segment analysis, but on an European scale.

### *3.3.1* Method to analyse segment

The national amount and nationwide distribution of multi-storey buildings in Denmark has been investigated via a unique database: the Danish Building and Dwelling Register, shortened "BBR".

The BBR is administered at a governmental/ministry level, containing information on all buildings in Denmark down to apartment/unit level (SKAT et al., 2012). The register was established in 1977 based on questionnaires to all owners in Denmark, but has continuously been updated and extended so it now includes data regarding physical properties of the units, usage, rent, building services etc. The data is used by all levels of authorities and private companies, including banks and utility companies. This wide usage of the register and the extensive feedback and contributions it gets from the many users is assumed to minimize the risk of errors in the database.

The register is used to investigate the segment size of relevant multi-storey dwellings in Denmark, where the application of exterior thermal insulation is often not a possible solution for enhancing occupant comfort and reduce energy consumption.

The data from BBR can be sorted based on many different parameters, for example construction material, areas and technical services. The following sorting parameters have been applied to emphasise different aspects of the building segment:



1. Apartment or building level:
Buildings and apartments have unique ID numbers in the data. This sorting mechanism isolate either unique building or apartment numbers, resulting in data on either of the two levels.

2. Demolished buildings:
The possibility of including buildings that have been demolished exists. In this study, only non-demolished buildings have been included.

3. Type of building:
The data is sorted into a wide range of buildings or type of use, for example day cares. In this study, only residential multi-storey buildings have been included.

4. Façade material:
The BBR include data on the façade material, masonry, wood etc.

5. Apartments on basement and/or attic level:
In some buildings, rooms situated at the original attic or basement level have been converted into apartments. The new apartments can be included, or focus can be kept on the original apartments from the time of erection. Only original apartments are included in this investigation.

6. Year of construction:
The data is sorted based on the construction year of the individual building. Data was drawn on January 25th, 2017.

7. Number of storeys in building:
This parameter defines the number of storeys of the building. There is a similar possibility to sort individual apartment units based on the storey they are situated at (not included in this study).

8. Regional location:
The position of each building is defined based on municipality number (addresses and coordinates are possible, but not included in this study). Denmark was split into 98 municipalities, comprising 5 regions, at the time of the study. Neither the municipalities, nor the regions were equivalent in size

or population. Only municipalities with high amounts of buildings/apartments were extracted and documented separately, why other units are summed under the region. An example of regions and the separate extracted municipality values can be seen in Figure 43.

The combination of sorting parameters that have been applied to the BBR data can be seen in Table 3.

| | Sorting number | | | | | |
|---|---|---|---|---|---|---|
| | 1 | 2 | 3 | 4 | 5 | 6 |
| Apartment or building? | Apartment | Building | Apartment | Building | Apartment | Building |
| Demolished buildings: | No | No | No | No | No | No |
| Bulding type: | Multi-storey | Multi-storey | Multi-storey | Multi-storey | Multi-storey | Multi-storey |
| Façade material: | All | All | Brick facade & all | Brick facade & all | Brick facade | Brick facade |
| Apartments on basement and/or attic level: | No | Not applicable | No | Not applicable | No | Not applicable |
| Year of construction: | Sectiona-lised | Sectiona-lised | 1851-1930 & all | 1851-1930 & all | 1851-1930 | 1851-1930 |
| Number of storeys in building: | Sectiona-lised | Sectiona-lised | 2 < | 2 < | 2 < | 2 < |
| Regional location: | All | All | All | All | Sectiona-lised | Sectiona-lised |

*Table 3 Combination of sorting parameters applied to data from BBR in PhD Thesis.*

### *3.3.2* Results from database-based analysis

The distribution of multi-storey buildings and apartments in different time steps, have been investigated by applying sorting number 1 and 2 of Table 3, illustrated in Figure 41 and Figure 42. The used time periods represent shifts in building style, inspired by Kragh, Wittchen & Engelmark (Engelmark, 2013; Kragh and Wittchen, 2014). Multi-storey buildings with 1 storey consist of original 1-storey buildings where the attic space have been utilised for another household.

As illustrated in Figure 41, a large amount of the current multi-storey apartment stock was constructed in the period 1851-1930. When isolating the buildings in Figure 42, it is clear that a large amount of the current multi-storey building stock consists of 1 and 2 storey buildings from the period 1851-1930. This segment of small 1-2 storey buildings and apartments have been removed in later sorting, as this type of buildings are minor town houses and not what are normally characterised as multi-storey houses.

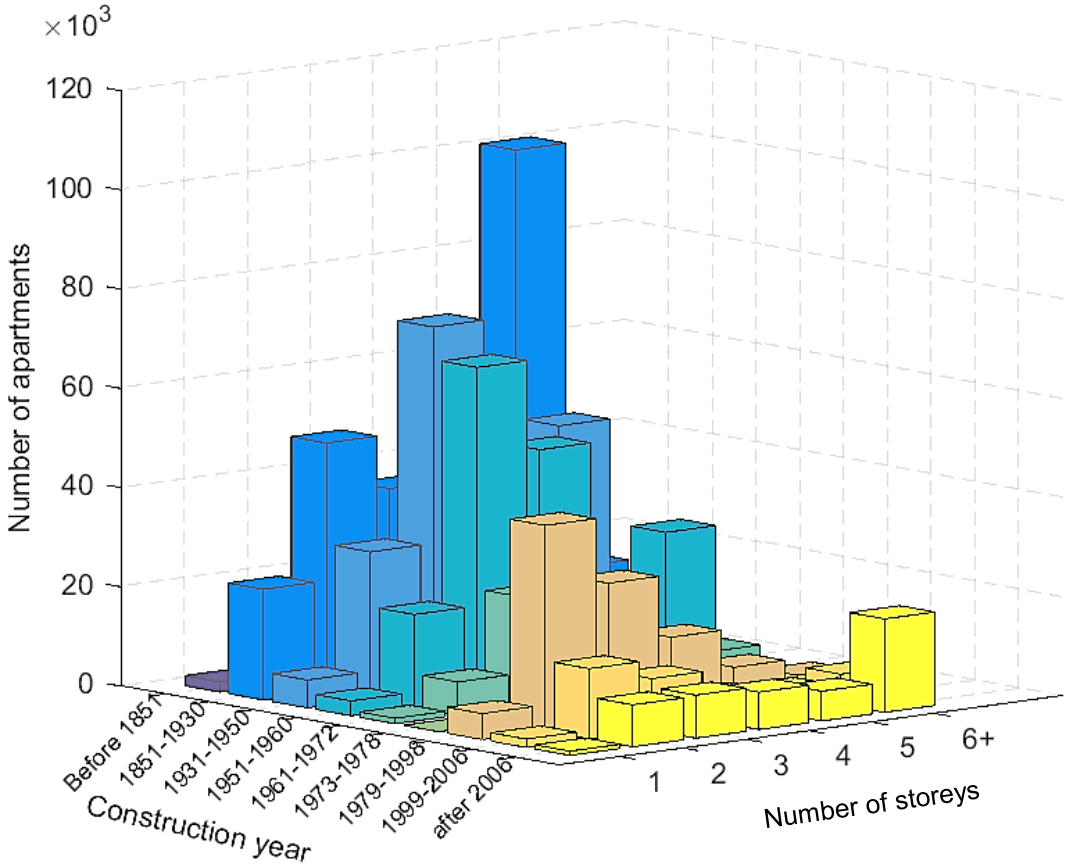


*Figure 41 Apartment units, sorted after construction year and number of storeys. Based on sorting number 1 in Table 3. Time steps represent shifts in building style, inspired by Wittchen & Engelmark (Engelmark, 2013; Kragh and Wittchen, 2014)*

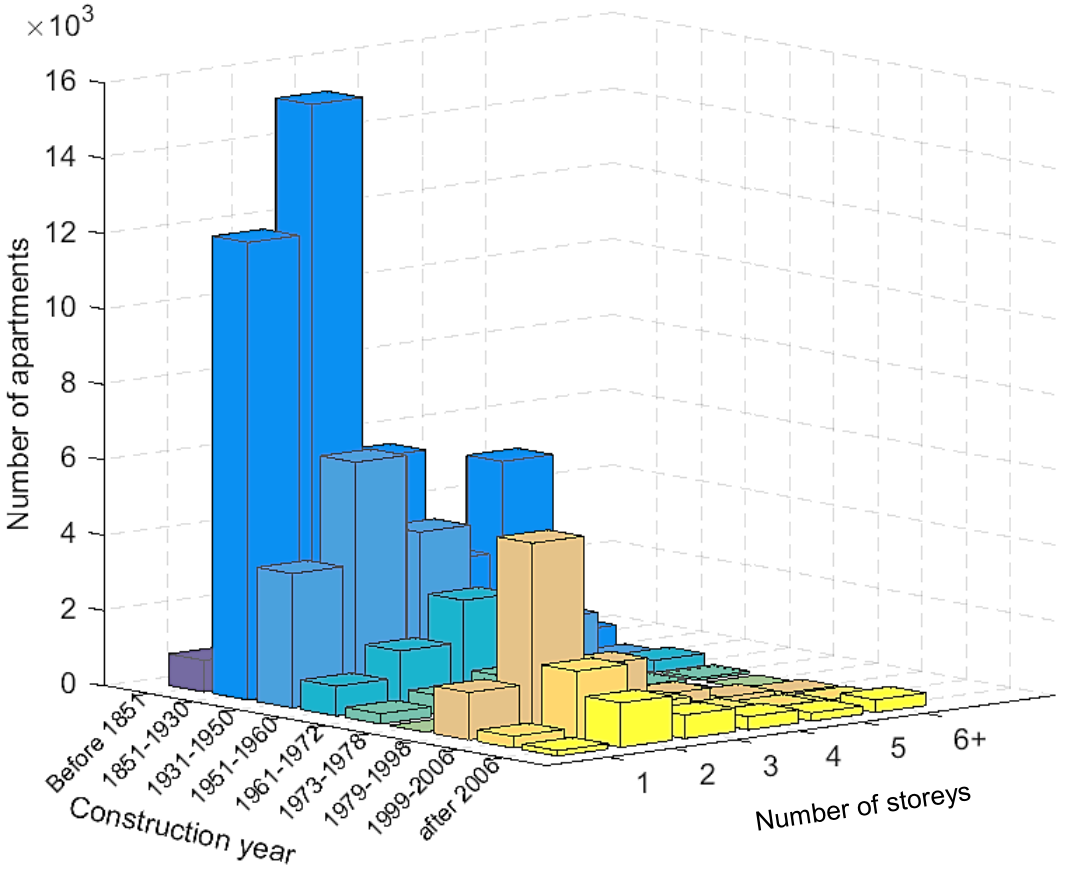


*Figure 42 Building units, sorted after construction year and number of storeys. Based on sorting number 2 in Table 3. Time steps represent shifts in building style, inspired by Wittchen & Engelmark (Engelmark, 2013; Kragh and Wittchen, 2014)*

Sorting mechanism 3 and 4 of Table 3 have been applied to analyse the amount of multi-storey buildings constructed in the period 1851-1930, compared to all Danish multi-storey buildings in Table 4. From the data in Table 4, it can be concluded that of the current Danish multi-storey building stock over 2 storeys, 25.2% of the apartments and 41.1% of the buildings have masonry facades and originates from the period 1851-1930.

| | | | | Number of storeys in building | | | | |
|---|---|---|---|---|---|---|---|---|
| Sorting number (Table 3) | Façade material | Year of construction | Apartment or building level | 3 storeys | 4 storeys | 5 storeys | 6+ storeys | 3+ storeys (sum) |
| 4 | Masonry façade | 1851 to 1930 | Buildings | 5,962 | 2,994 | 5,381 | 640 | 14,977 |
| 3 | | | Apartments | 38,961 | 31,118 | 103,414 | 18,004 | 191,497 |
| 4 | All façade types incl. masonry | - ∞ to 2017.01.25 | Buildings | 18,836 | 7,534 | 8,044 | 2,004 | 36,418 |
| 3 | | | Apartments | 299,175 | 159,593 | 196,572 | 105,725 | 761,065 |

*Table 4 Segment analysis, number of multi-storey buildings and apartments. Based on sorting number 3 and 4 in Table 3.*

The regional distribution clarified via sorting number 5 of Table 3 can be seen for apartments in Figure 43 and Table 5, and number 6 on a building level in Figure 44. Most of the apartments constructed in the years 1851-1930 are situated in the larger cities of Denmark: Copenhagen/Frederiksberg; Aarhus; Aalborg; Odense; and Gentofte. The Danish capital, Copenhagen/Frederiksberg, accounted for the largest proportion of all, with 71 % of the apartment units accounted for in the figure.

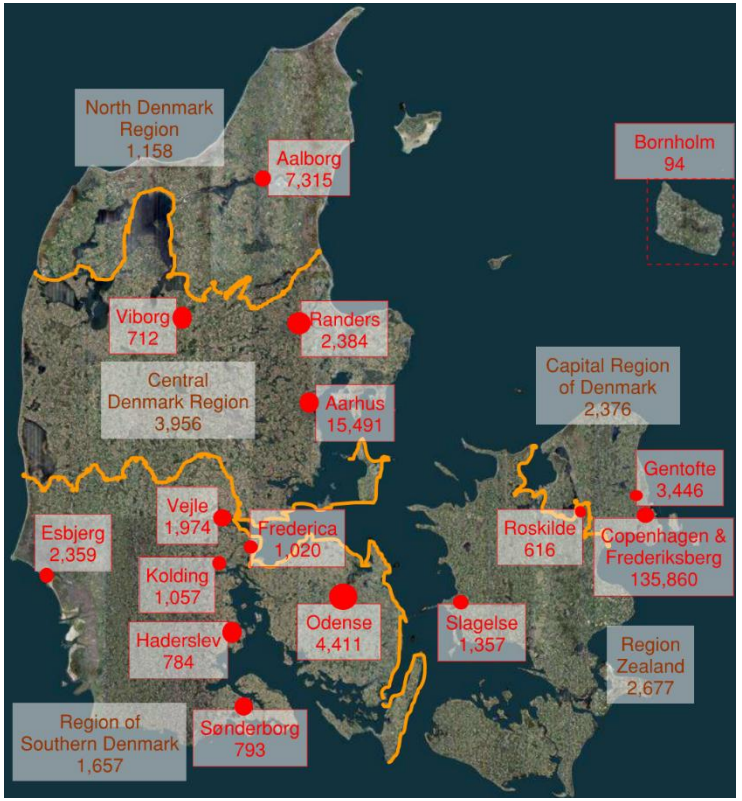


*Figure 43 Regional distribution of apartments, as defined in sorting number 5 in Table 3. Same numbers presented with percentiles in Table 5. Orange lines illustrate borders of regions, orange text in box contain apartments not included in highlighted cities of region.*


*Figure 44 Regional distribution of buildings, as defined in sorting number 6 in Table 3. Orange lines illustrate borders of regions, orange text in box contain buildings not included in highlighted cities of region.*

| Municipality | Amount of apartments | Percentage of sum |
|---|---|---|
| Copenhagen & Frederiksberg | 135,860 | 70.9% |
| Aarhus | 15,996 | 8.4% |

| Denmark | Amount of apartments | Percentage of sum |
|---|---|---|
| Sum | 191,497 | 100.0% |

| Region | Amount of apartments | Percentage of sum |
|---|---|---|
| Capital Region of Denmark | 141,776 | 74.0% |
| Region Zealand | 4,650 | 2.4% |
| North Denmark Region | 8,473 | 4.4% |
| Central Denmark Region | 22,543 | 11.8% |
| Region of Southern Denmark | 14,055 | 7.3% |

*Table 5 Amount and percentile of apartments in municipalities and regions. Based on sorting number 5 in Table 3.*

## *3.4* ***Sub-discussion of hypotheses***

The section will discuss the goals of the sub-hypotheses, previously presented in Section 1.3.1 and Table 1. The structure of the section is comprised of a repetition of the sub-hypothesis goals, following an individual discussion of each goal.

**Sub-hypothesis #1, goal 1** is defined as: "*A period of erection for characteristic Danish multi-storey buildings with solid masonry walls and embedded wooden elements can be determined based on a literature* study".

The period of erection of multi-storey buildings with solid masonry facades and embedded wooden elements was clarified from literature to be the period 1850-1930, as described in Sec. 3.1.1 of the appended Paper #1 and Section 3.2.2 of this Thesis. The incentive for action have been shed light on in Section 1.1.1 and 1.2, illustrating that 3 % of the total Danish energy use for space heating and domestic hot water is used in multi-storey buildings from this specific period. Looking into the specific energy use in the total Danish multi-storey building stock, then buildings from this period account for 38 % of this energy use.

✓ Goal 1 of Sub-hypothesis #1 is assessed as fulfilled based on the above.

**Sub-hypothesis #1, goal 2** is defined as: "*Multi-storey buildings constructed within the period of erection share a characteristic composition, which can be determined based on a literature study and validated against existing* constructions".

The work is documented in Section 3.2.1, where a large amount of Danish literature, mostly authored by Associate professor Jesper Engelmark, have been used as a point of origin for further discussions with the professor. Associate Professor Engelmark further possessed a large amount of photographs

documenting the buildings in different stages of demolition or refurbishment. Some of the photographic material have been picked out and presented in Section 3.2.1 of this Thesis to validate the typical characteristics of the buildings in real life. It can be concluded from the investigation that the buildings share a strict and characteristic composition.



✓ Goal 2 of Sub-hypothesis #1 is assessed as fulfilled based on the above.

**Sub-hypothesis #1, goal 3** is defined as: "*More than 33 % of the total exterior leaf for a typical façade wall from the period are unavailable for retrofitting interior thermal insulation*".

The ratio of 33 % in the goal originate from the strict legislation in force during the erection period of interest. The legislation stated a maximum degree of perforation for multi-storey buildings of 2/3 in horizontal direction, and 1/2 in the vertical direction, resulting in maximum perforation degree of: 2/3 x 1/2 =1/3 = 33 %. Floor structures and partition walls further add to the unavailable area when considering retrofitting of thermal insulation to the interior side, why this ratio was deemed plausible.

Investigation of the goal is divided into 2 minor investigations:

1. Investigation of horizontal building composition, using a range of floorplans.
2. Assessment of exterior façade areas to clarify potential for retrofitting thermal insulation.

The investigation of the horizontal building composition in existing constructions, presented in Section 3.2.2 showed a maximum registered value of 58 %, and thereby no floorplans exceeding the maximum allowed horizontal perforation degree. The 25 % quartile showed a ratio of 44 %.

The found 44 % horizontal perforation degree in the floorplan analysis was used to assess areas where retrofitting thermal insulation to the interior surface is possible. This was done by identifying a building with a horizontal perforation degree close to the 25 % quartile from the investigation and assess the areas relative to each other in Figure 39. The investigation of the share of façade areas showed that the window & door area made up 20 % of the overall area, with 38 % total area unavailable for retrofitting interior insulation. A building with a higher perforation degree close to the maximum permissible was investigated in Figure 40, showing an exterior façade with a window/door area of 31 % and an area unavailable for retrofitting interior insulation of 45 %.

✓ Goal 3 of Sub-hypothesis #1 is assessed as fulfilled based on the above.

**Sub-hypothesis #2, goal 1** is defined as: "*The share of the investigated multi-storey dwellings and buildings are substantial if more than 20 % share a characteristic composition,* originating from a specific period of erection".

The specific erection period for investigated multi-storey dwellings have been defined as 1850-1930 in Sub-hypothesis #1, goal 1. The buildings were found to share similar characteristics, which were described and illustrated in Section 3.2. The size and distribution of the segment was described in Sec. 5.1 of the appended Paper #1 and in Section 3.3 of this Thesis, concluding that as of January 2017: 25 % of the apartments and 41 % of the buildings in the Danish stock of buildings with more than 2 storeys share a characteristic building composition.

✓ Goal 1 of Sub-hypothesis #2 is assessed as fulfilled based on the above.

**Sub-hypothesis #2, goal 2** is defined as: "*A large degree of the investigated multi-storey dwellings is situated in the capitol of Denmark. A large degree is for this goal defined as more than 60%*".

The national distribution of the investigated multi-storey buildings in Denmark was documented in Sec. 5.1 of the appended Paper #1 and in Table 5 of Section 3.3 in this Thesis. The investigation showed that as of January 2017, 71 % of the apartment units in multi-storey buildings over 2 stories erected in the period 1850-1930 were situated in the Danish capital, Copenhagen/Frederiksberg.

The large share of apartments originating from this specific period, sharing similar building characteristics, are characteristic for the inner city of Copenhagen. An inclined aerial photo towards the inner city of Copenhagen have been presented in Figure 45 to illustrate this.

✓ Goal 2 of Sub-hypothesis #2 is assessed as fulfilled based on the above.

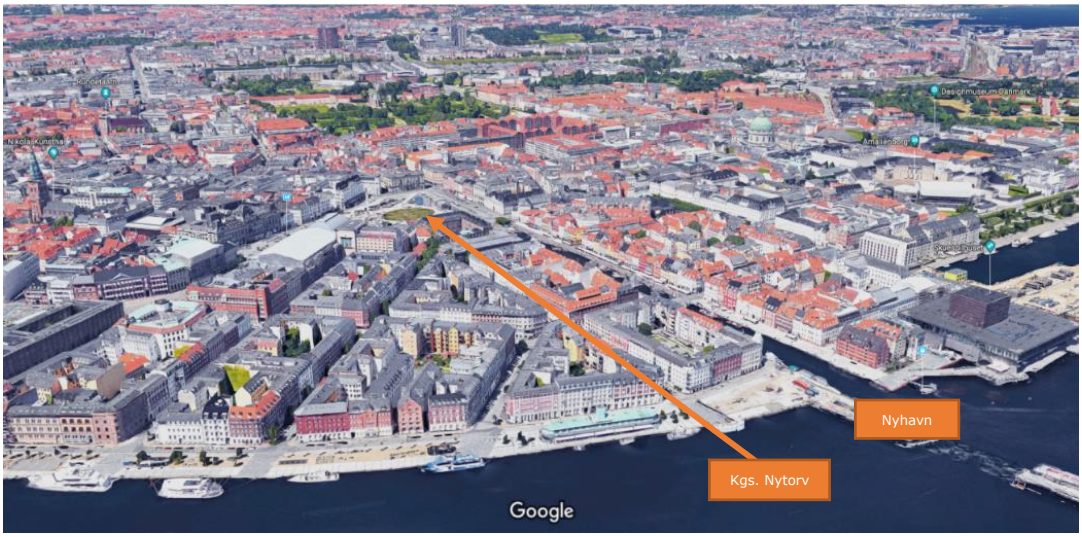


*Figure 45 Inclined aerial photo towards the city centre of Copenhagen, courtesy of Google maps.*

## *3.5* ***Sub-conclusion of hypotheses***

The section will conclude on the sub-hypotheses, previously presented in Section 1.3.1 and Table 1, based on the sub-discussion in Section 3.4. The structure of the section is comprised of a repetition of the individual sub-hypotheses treated in this section, following a conclusion if the sub-hypothesis can be rejected.

**Sub-hypothesis #1:** "*A characteristic composition and period of erection can be determined for Danish multi-storey buildings with solid masonry walls and embedded wooden elements, illustrating that the areas available for retrofitting interior insulation is limited*".

✓ Sub-hypothesis #1 cannot be rejected, as goal 1, 2 & 3 of the sub-hypothesis was assessed as fulfilled.

**Sub-hypothesis #2:** "*The share of Danish multi-storey dwellings with solid masonry walls and embedded wooden elements is substantial compared to the total Danish multi-storey building stock, with a nationwide distribution showing a large degree of dwellings situated in major cities at the time* of erection".

✓ Sub-hypothesis #2 cannot be rejected, as goal 1 & 2 of the sub-hypothesis was assessed as fulfilled.

### *3.5.1* Outcome of new knowledge obtained in study

The part of the industrial PhD study documented in Section 3 and the appended Paper #1 have provided new knowledge, including:

- 41 % of Danish multi-storey buildings with more than 2 storeys was erected in the period 1850-1930 and share a characteristic building composition.
- 71 % of the apartments in multi-storey buildings with more than 2 storeys, erected in the period 1850-1930, are situated in the capitol of Denmark.
- More than 33 % of the thermal envelope in buildings/apartments from the period 1850-1930 are unavailable for retrofitting thermal insulation.

# 4 POTENTIAL FOR REDUCING THERMAL TRANSMITTANCE IN MULTI-STOREY BUILDINGS FROM 1850-1930

Section 4 concern Sub-hypothesis #3, investigating the potential for reducing the heat loss of facades in historic multi-storey solid masonry buildings constructed in the period 1850 until 1930. The section includes the theoretical potential for heat savings when considering the application of interior thermal insulation, investigated via modelling in a multi-dimensional simulation tool. The approach is based on a 3-dimensional investigation, including a range of variations to find the theoretical reduction in heat loss with different insulation strategies.

## *4.1* ***Summary of paper related to Section 4***

The following text will describe the correlation between the content of the papers and this section, and address how the sub-hypotheses were treated in the papers. This section only describes the content, the discussion and conclusion of the individual sub-hypothesis are done in the sub-discussion and sub-conclusion, Section 4.3 and 4.4 respectively.

Section 4 is based on some of the content of the appended Paper #1: "Interior insulation – Characterisation of the historic, solid masonry building segment and analysis of the heat saving potential by 1d, 2d, and 3d simulation".

The appended Paper #1 included a comparative analysis of the differences in output when performing 1-, 2- and 3-dimensional thermal simulations. A large focus in the appended paper was on the error when simplifying a 3-dimensional problem, such as the window section of a multi-storey building, as a 1- or 2-dimensional model. It was found in the paper that 3-dimensional analysis was needed to obtain realistic results of such constructions, as 2-dimensional simulation underestimated the heat loss when applying interior insulation by up to 57 % with 100mm insulation. This part of the paper has not been further included in this Thesis.

The appended Paper #1 included 3-dimensional parametric simulations of two different insulation strategies related to **SH3**, comparing the difference in potential reduction in average thermal transmittance:

- Full coverage of the interior masonry surface, presented in Fig. 3(f) of the appended Paper #1.
- Reduced strategy, only retrofitting the spandrel with thermal insulation, presented in Fig. 3(c) of the appended Paper #1.

The two insulation strategies have been presented in Figure 49 and Figure 50 of this Thesis respectively, along with additional models further concerning implementation of offsets from floor/loft, simulating a partition wall and influence of thickness of masonry column. The investigation concerning the 3-dimensional thermal model in this Thesis is thereby an extension of the original investigation in the appended paper, why this part of the appended paper will not be addressed further.

## *4.2 Theoretical study of the effect from installing interior thermal insulation*

The 3-dimensional thermal simulation model presented in this section is identical to the one thoroughly described in the appended Paper #1, but with additional variations in the 3-dimensional model which were not included in the original paper.

### *4.2.1* Method used in study

A typical façade section has been built in the simulation software COMSOL Multiphysics® (COMSOL, 2015). The dimensions for the model have been based on the characteristics for a multi-storey building built in 1850-1930, described in Section 3.2 and Section 3.2.3, and illustrated in Figure 46.

The model was used to perform a thermal investigation and to calculate the relative reduction in average thermal transmittance (U-value) for the masonry part of the model, achieved by applying interior insulation that varied in extent and thickness. The model consisted of a wall section, with vertical delimitation in the middle of masonry columns on the left and right side of a spandrel. The horizontal delimitation was underneath the wooden pugging board in the floor structure.

The 3-dimensional model was designed as a parametric model, with a base model as illustrated in Figure 46. The base model in this study had a masonry column depth of 2 bricks (478 mm), corresponding to the traditional construction at the second and third floor from the top. The model has an exterior masonry area of 3.83 $m^2$ after subtracting the window area (as described later in this section). The vertical composition of the model is based on the illustration on page 84 of (Engelmark, 2013). This construction has a total height of 2.985 m, with an interior surface height of 2.75 m. The window has a height of 1.70 m, with 0.70 m of spandrel below and 0.35 m of interior wall above. The horizontal composition of the model was based on conversations with J. Engelmark, on his thesis (Engelmark, 1983) and on the floorplan investigation described in Section 3.2.2. The width of the construction consists of two half masonry columns of 0.30 m on each side of 4½ bricks (1.092 m) of spandrel or window structure, resulting in a total width for one wall section of 1.692 m.

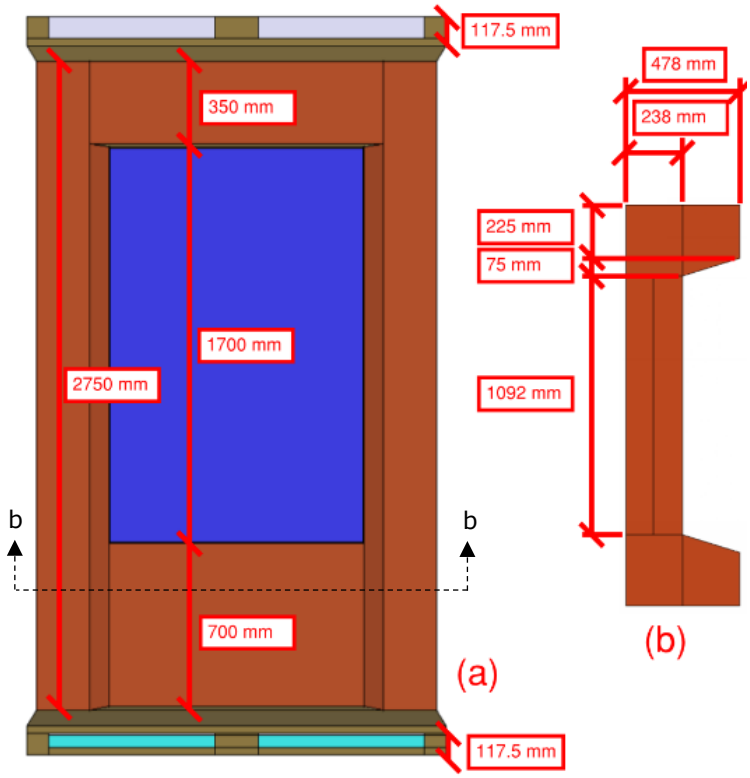


*Figure 46 Dimensions of COMSOL model. (a) side view of 3-dimensional model, (b) horizontal cross-section through spandrel.*

The thermal conductivity values of the materials in the model were mainly obtained from the Delphin material database (Nicolai et al., 2017, 2008):

- Masonry (brick + mortar), $\lambda$=0.8 W/(m·K), coloured red in the models.
- Thermal insulation, $\lambda$=0.045 W/(m·K), coloured yellow in the models.
- Wood (longitudinal), $\lambda$=0.194 W/(m·K), coloured brown in the models.
- Sandy clay, used as pugging, $\lambda$=1.76 W/(m·K), coloured green in models.
- AAC, density=390 kg/m³, replaces insulation at floor and ceiling in selected models, $\lambda$=0.095 W/(m·K), coloured dark grey in models.

The properties of air were defined in COMSOL Multiphysics® (COMSOL, 2015). The heat transfer through the air was thereby not limited to conduction, but also included radiation and convection, depending on the dimensions of the object. The air was coloured light grey in models.

The window, coloured dark blue in models, was modelled as a thin wall of 115 mm with an average thermal transmittance of $U_{window}$= 0.60 W/(m²·K). The defined thermal transmittance was transformed to a thermal conductivity coefficient using the equation: $\lambda = d / R$, resulting in Equation (12):

$$\lambda_{window} = \frac{d_{window}}{\frac{1}{U_{window}} - R_{si} - R_{se}} = \frac{0.115m}{\frac{1}{0.60\frac{W}{m^2 \cdot K}} - 0.13\frac{m^2 \cdot K}{W} - 0.04\frac{m^2 \cdot K}{W}} = 0.077\frac{W}{m \cdot K} \qquad (12)$$

Where:

- $d$ = Thickness [m].
- $R$ = Thermal resistance [m²K/W].
- $R_s$ = Convective heat transfer resistance [m²K/W].
- subscript $i$ = interior.
- subscript $e$ = exterior.

The thermal conductance induced from the window was subtracted from the simulation results, as focus was on the potential reduction in average thermal transmittance of the masonry area. This was done by transferring the heat flow to a resulting thermal conductance, defining the heat loss of the window based on a temperature gradient. The thermal conductance was calculated by using the demand in linear thermal transmittance for windows during refurbishment in Denmark: $\Psi_{window}$ = 0.06 W/(m·K) (The Danish Transport and Construction Agency, 2015). This yielded a total reduction from the simulation results as seen in Equation (13) and (14):

$$C_{th,window} = U_{window} \cdot (h_{window} \cdot w_{window}) + \Psi_{window} \cdot \left(2 \cdot (h_{window} + w_{window})\right) \quad (13)$$

$$C_{th,window} = 0.60 \frac{W}{m^2 \cdot K} \cdot (1{,}1175m \cdot 1{,}092m) + 0.06 \frac{W}{m * K} \cdot \left(2 \cdot (1{,}1175m + 1{,}092m)\right) = 1.00 \frac{W}{K} \quad (14)$$

Where:

- $C_{th}$ =Thermal conductance [W/K].
- $h$ = Height [m].
- $w$ = Width [m].
- $\Psi$ = Linear thermal transmittance [W/(m·K)].
- $U$ = Thermal transmittance [W/(m²·K)].

It was not possible to omit the window from the model, as the reduced dimensions of the masonry in the embrasure around the window is of key interest when considering the application of interior insulation.

A 3-dimensional illustration of the base model can be seen in Figure 47. One variation of the model included a solid masonry partition, as illustrated in Figure 48.

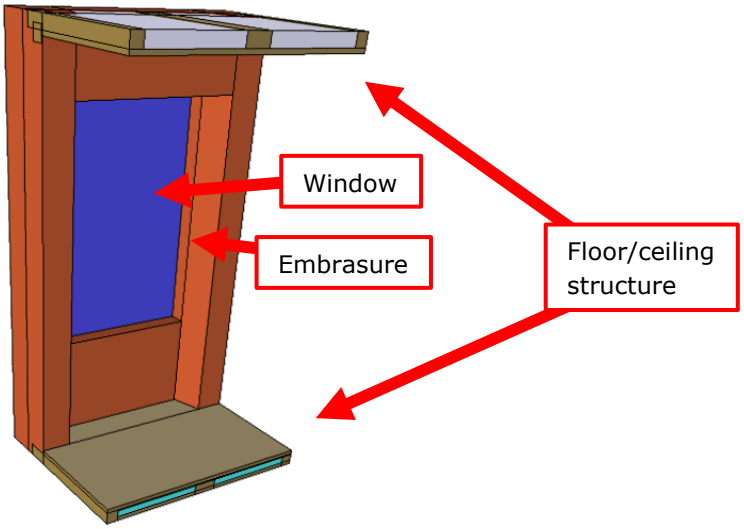


*Figure 47 Base model without insulation.*

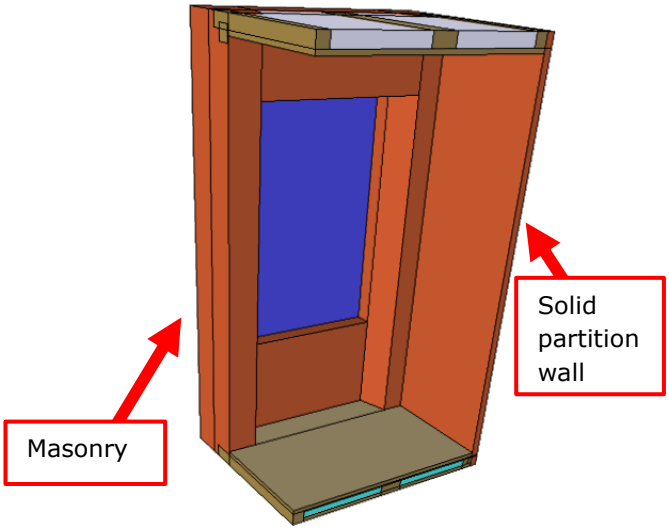


*Figure 48 Base model with partition at one side, without insulation. Thickness of partition wall = 1 brick (108mm).*

Different insulation strategies for the base wall with no partition wall, illustrated in Figure 47, have been investigated:

- A full insulation strategy, retrofitting entire interior masonry surfaces with thermal insulation, illustrated in Figure 49.
- A partly insulation strategy, only retrofitting the interior masonry surface of the spandrel, illustrated in Figure 50.
- A full insulation strategy similar to the one illustrated in Figure 49, but replacing the 200 mm of insulation at the top and/or bottom with air, illustrated in Figure 51.
- A full insulation strategy similar to the one illustrated in Figure 49, but replacing the 200 mm of insulation at the top and/or bottom with AAC, illustrated in Figure 52.



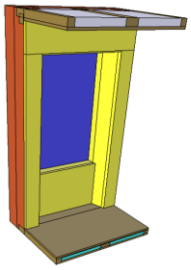

*Figure 49 Full insulation strategy covering spandrel, sides and front of masonry columns.*

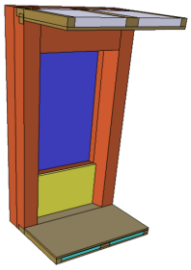

*Figure 50 Partly insulation strategy covering spandrel.*

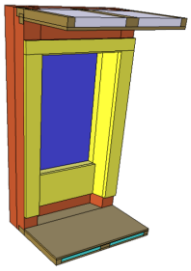

*Figure 51 Full insulation strategy, without insulation at the top and bottom 200 mm. Possible to include air offset at either floor or ceiling individually.*

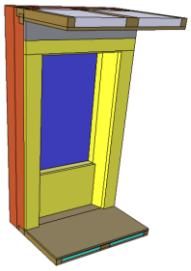

*Figure 52 Top 200 mm insulation replaced with AAC. Also possible at floor or combined.*

Two different insulation strategies have been investigated for the base model with a partition wall, illustrated in Figure 48:

> No insulation on the partition wall, illustrated in Figure 53.

> Wedge insulation on the partition wall, illustrated in Figure 54.

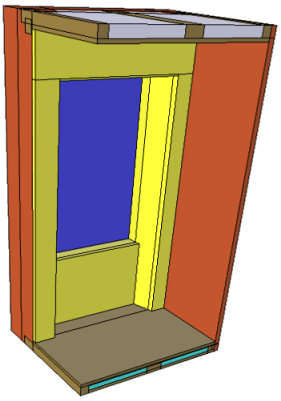

*Figure 53 Model with partition wall, full insulation strategy and no insulation on partition.*

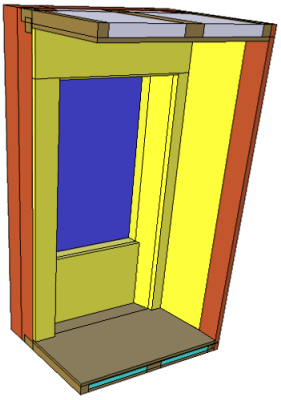

*Figure 54 Model with partition wall, full insulation strategy and wedge along partition. Thickness of insulation at masonry column = 50 mm, depth into room = 600mm.*

The simulation was run with two different methods, depending on the base wall in the model. For both models, an identical model was applied to the top and bottom of the analysed section to ensure the boundary conditions, as illustrated in Figure 55 and Figure 56.

> For base walls without a partition wall: The model was cut at the symmetry line in the middle of the window to reduce computational time, as illustrated in Figure 55.

> For base walls with a partition wall: The model was kept at the full width to see the effect of the partition, as illustrated in Figure 56.



*Figure 55 Simulation setup for models without partition wall: Model cut at symmetry line with identical models on top/bottom for boundary conditions.*

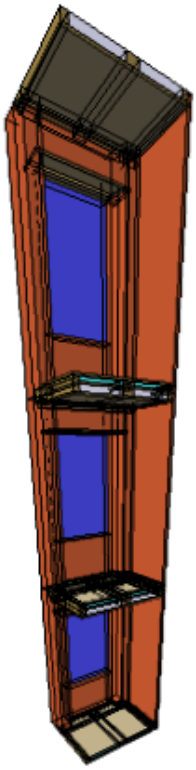

*Figure 56 Simulation setup for models with partition wall: No symmetry line, identical models on top/bottom for boundary conditions.*

### *4.2.2* Results and discussion of thermal simulation variations

All investigated cases have a point of reference defined as the model illustrated in Figure 49, a full insulation strategy in a model with 2 bricks thick masonry columns (478 mm).

#### 4.2.2.1 Full insulation strategy versus partial spandrel insulation

The aim of this variation is a comparison between the full insulation strategy (Figure 49) and a partly insulation strategy (Figure 50) only covering the thinnest part of the thermal envelope: The spandrel underneath the window.

The area needed to insulate the spandrel is 17 % of the fully covering insulation strategy, with 0.77 m² compared to 4.65 m². The outcome from the investigation has been illustrated in Figure 57, summed up with focus on comparing the reduction from the different insulation strategies in Table 6.

The investigation showed that 33-40 % of the reduction in thermal transmittance from covering the entire interior masonry surface with thermal insulation could be achieved by just applying thermal insulation to the spandrel underneath the window.

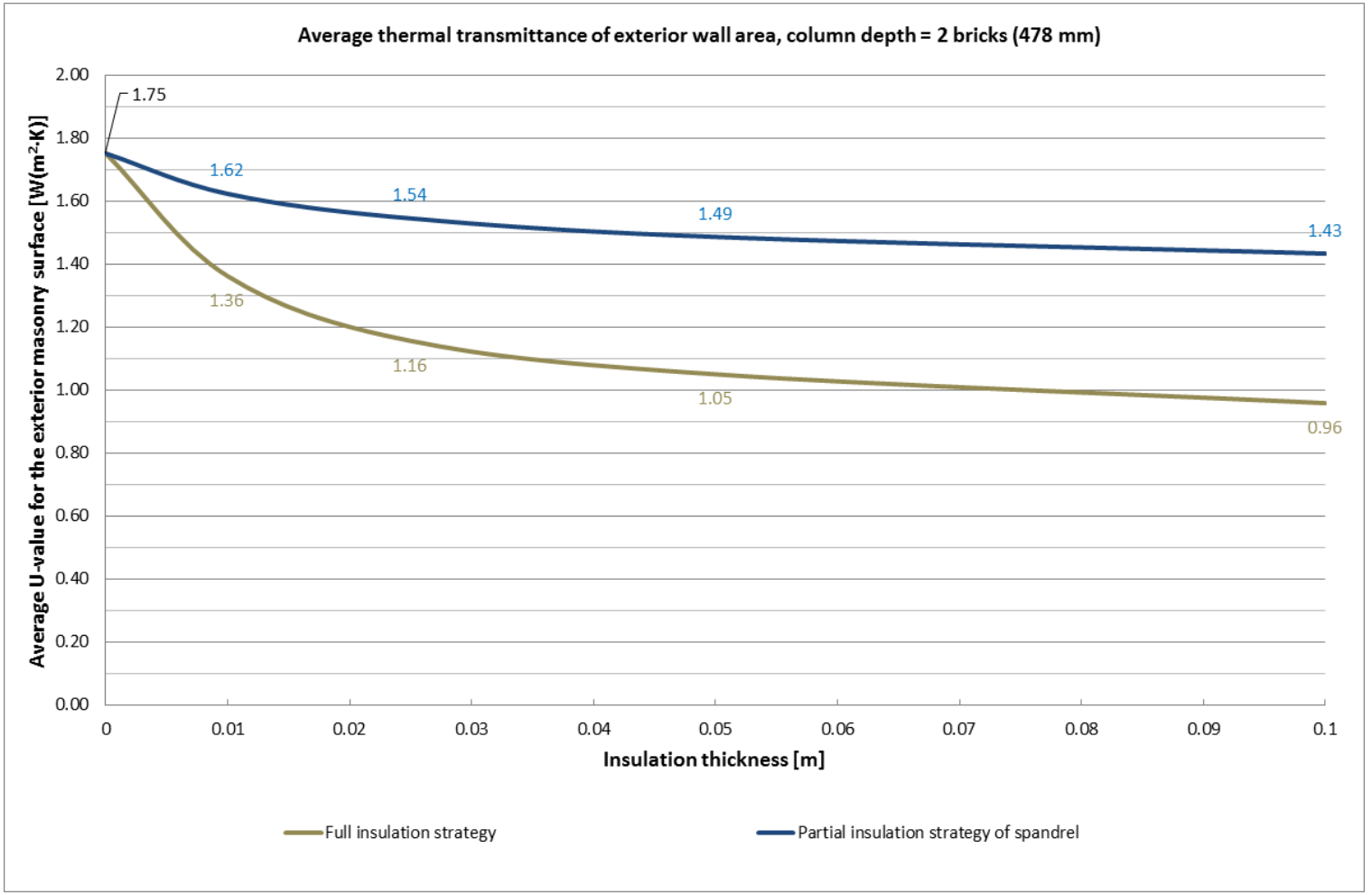


*Figure 57 Outcome from theoretical model expressed in thermal transmittance (U-value). The simulated base model with thermal insulation fully covering the masonry surface is illustrated in Figure 49, compared to only spandrel insulation illustrated in Figure 50.*

| | | Insulation thickness [mm] | | | | |
|---|---|---|---|---|---|---|
| | | 0 | 10 | 25 | 50 | 100 |
| Application of thermal insulation to the entire masonry surface | Thermal transmittance $\left[\frac{W}{m^2K}\right]$ | 1.75 | 1.36 | 1.16 | 1.05 | 0.96 |
| | Reduction of thermal transmittance $\left[\frac{W}{m^2K}\right]$ | - | 0.39 | 0.59 | 0.70 | 0.79 |
| | Savings compared to un-insulated construction | - | 22 % | 34 % | 40 % | 45 % |
| Application of thermal insulation to spandrel | Thermal transmittance $\left[\frac{W}{m^2K}\right]$ | 1.75 | 1.62 | 1.54 | 1.49 | 1.43 |
| | Reduction of thermal transmittance $\left[\frac{W}{m^2K}\right]$ | - | 0.13 | 0.21 | 0.27 | 0.32 |
| | Savings compared to un-insulated construction | - | 7 % | 12 % | 15 % | 18 % |
| | **Achieved by spandrel vs. full insulation** | **-** | **33 %** | **35 %** | **38 %** | **40 %** |

*Table 6 Thermal transmittance of the models illustrated in Figure 49 and Figure 50, the reduction from thermal insulation and the possible percentage achievable from partly insulating the spandrel, compared to a full covering insulation strategy.*

#### 4.2.2.2 Partly replacing insulation with air or AAC, as a moisture safety precaution for embedded wooden elements

The aim of this variation concerns the insulation strategies proposed in previous researches (Harrestrup and Svendsen, 2016, 2015; Morelli et al., 2010; Morelli and Svendsen, 2012). The variation included an insulation offset from the floor and ceiling to decrease the worsening of the hygrothermal conditions when applying thermal insulation to the interior surface, thereby protecting the wooden beam in the wall. This insulation strategy has been investigated with a thermal perspective to see the effect of the reduced extent of insulation. With an approximate width of 1.7 m in the model, and an offset of 0.2 meters, an offset reduces the extent of insulated masonry surface by 0.34 m². An offset at the floor and ceiling in the model illustrated in Figure 51 thereby reduce the extent of insulation from 4.65 m² to 3.97 m².

Compared to the full insulation strategy in Figure 58, the replacement of 200 mm insulation with air at the floor and ceiling reduce the relative reduction of thermal transmittance from 45 % to 30 % with 100 mm insulation in Figure 59. The main influence is seen when replacing insulation with air near the floor, as the lack of insulation at floor level expose the masonry surface of the thin spandrel. Instead of replacing insulation with air, which need to be secured for damp air, we have instead proposed to replace part of the insulation with AAC, resulting in a thermal transmittance close to that of the full insulation strategy. The change in hygrothermal conditions from replacing the top 200 mm of thermal insulation with AAC have been investigated in the field experiment at DTU and documented in the appended Paper #3.

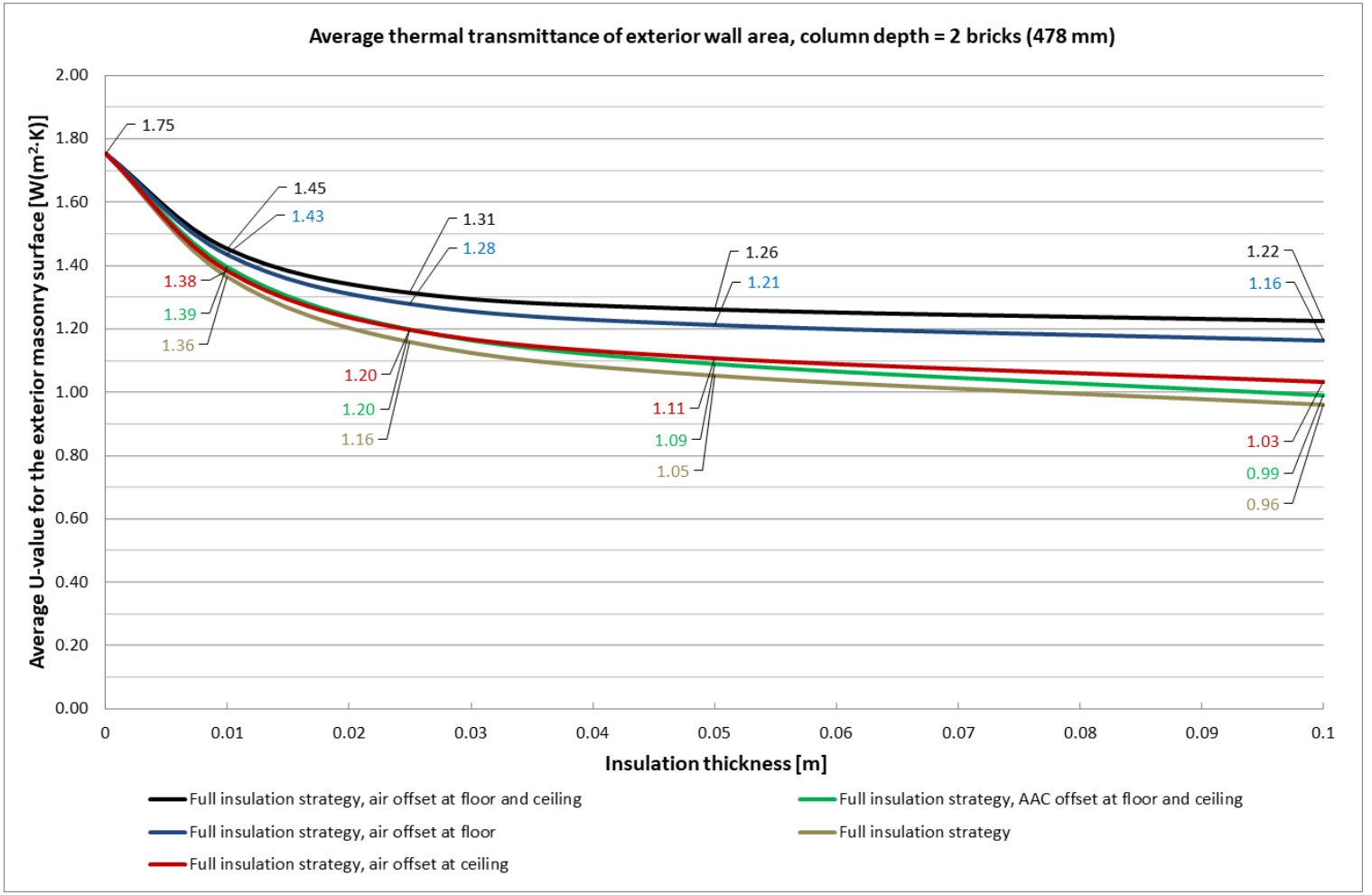


*Figure 58 Outcome from theoretical model expressed in thermal transmittance (U-value). The simulated base model is illustrated in Figure 49, compared to the variations illustrated in Figure 51 and Figure 52.*

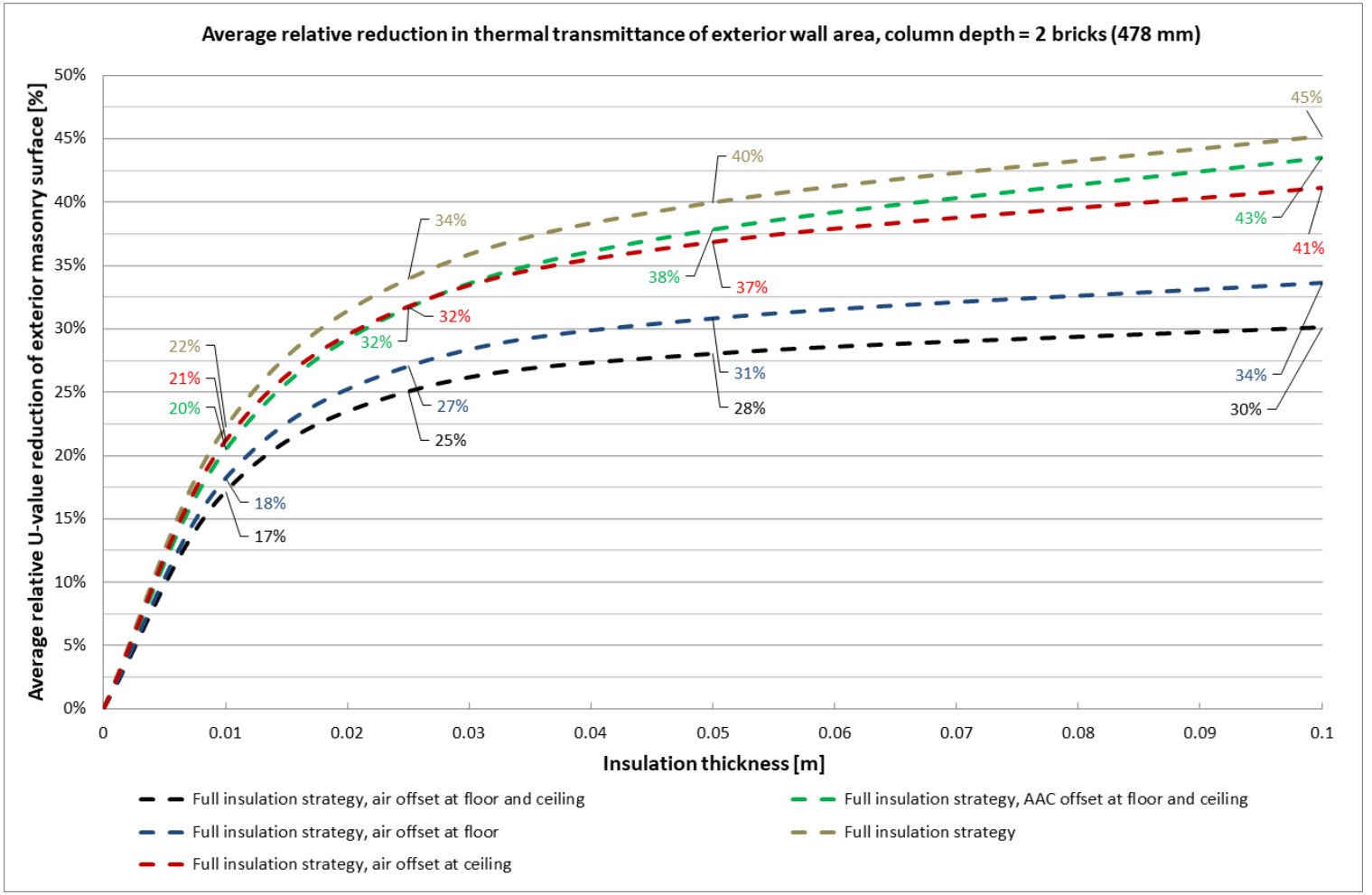


*Figure 59 Outcome from theoretical model expressed as relative reduction in thermal transmittance compared to the un-insulated wall. The simulated base model is illustrated in Figure 49, compared to the variations illustrated in Figure 51 and Figure 52.*

#### 4.2.2.3 Influence on thermal transmittance by intersecting interior partition walls between window sections

The aim of this variation concerns the interaction between a full covering insulation strategy and a solid interior partition wall. These walls are characteristic in historic multi-storey buildings, dividing the building into apartments and staircases as fire cells or as partitions within the apartment. The walls are traditionally 1 brick wide with rendering on both sides (128 mm).

The results illustrated in Figure 60 indicate that solid partition walls do not significantly change the average thermal transmittance of the façade section. This indicate that the purpose of wedge-cut insulation is to decrease thermal discomfort introduced by cold surfaces and reduce risk of moisture-induced damage caused by condensate at cold surfaces.

The hygrothermal conditions at the interface between interior thermal insulation on a solid masonry wall and a solid partition wall are currently being investigated in the field experiment at DTU, presented in Section 5.

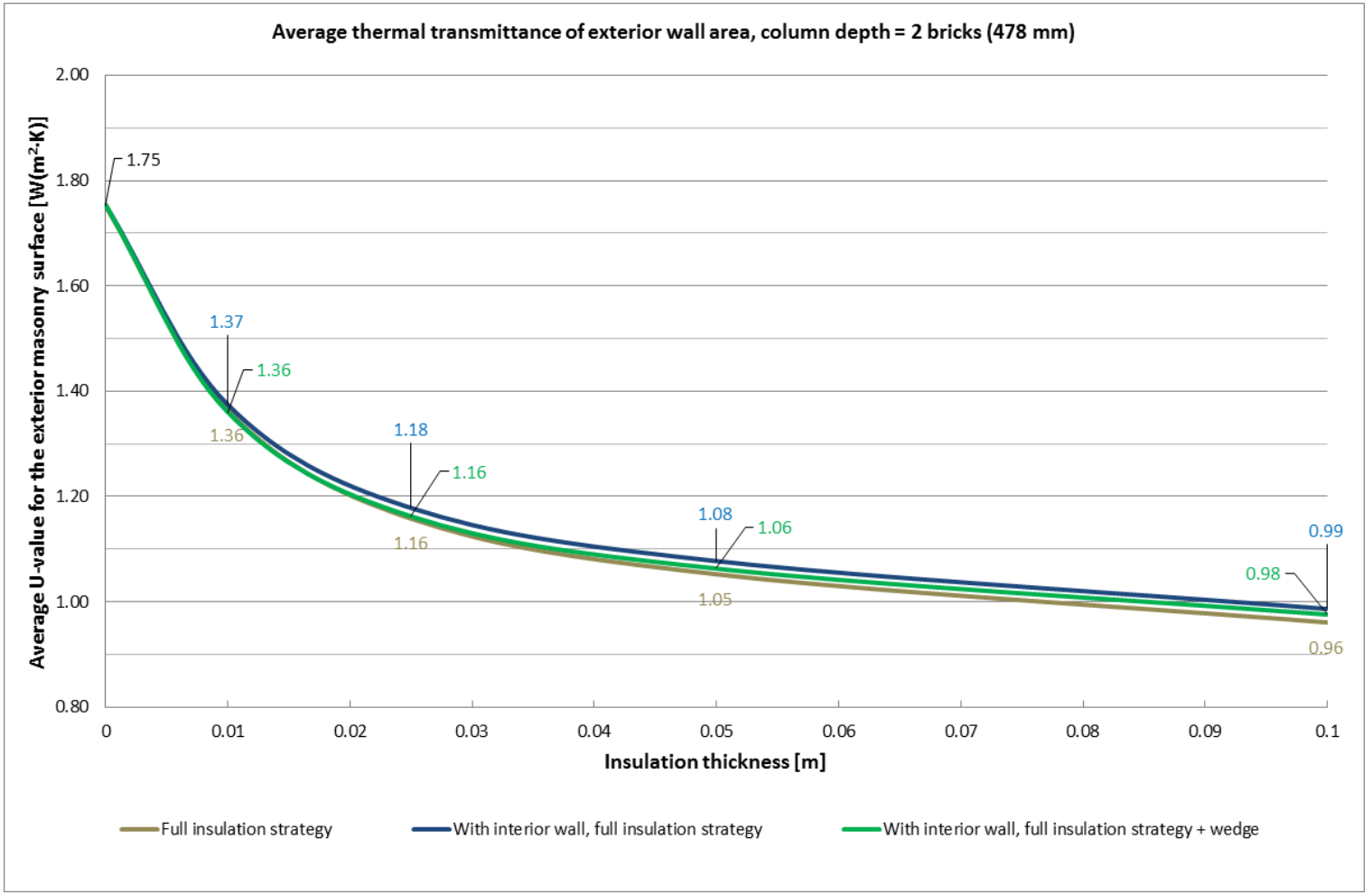


*Figure 60 Outcome from theoretical model expressed in thermal transmittance (U-value). The simulated base model is illustrated in Figure 49, compared to the variations illustrated in Figure 53 and Figure 54.*

#### 4.2.2.4 Influence of masonry column thickness

The aim of this variation concerns the difference induced by changing the investigated storey, and thereby varying the thickness of the masonry column. As illustrated in Figure 15 on page 51, the masonry columns increase in size down through the multi-storey buildings, with 1½ bricks on the top floor, 2 bricks on the 2nd and 3rd highest floor, 2½ on the next 2 floors and so forth.

The results of the investigation in Figure 61 and Figure 62 show larger potential for reduction of thermal transmittance at the highest storeys (smallest masonry columns), decreasing as the masonry column thickness increases.

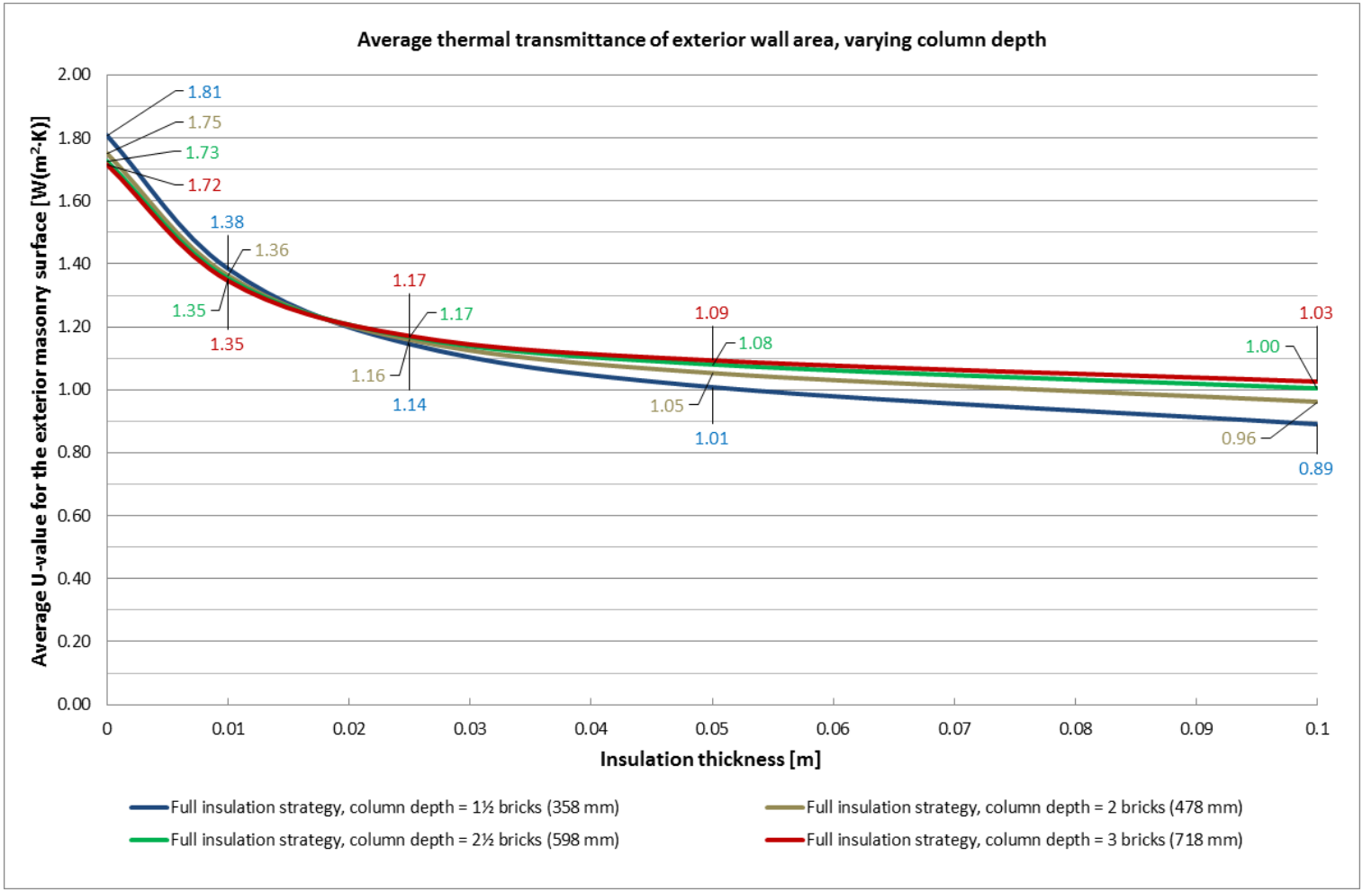


*Figure 61 Outcome from theoretical model expressed in thermal transmittance (U-value). The simulated base model is illustrated in Figure 49, with varying thickness of masonry column.*

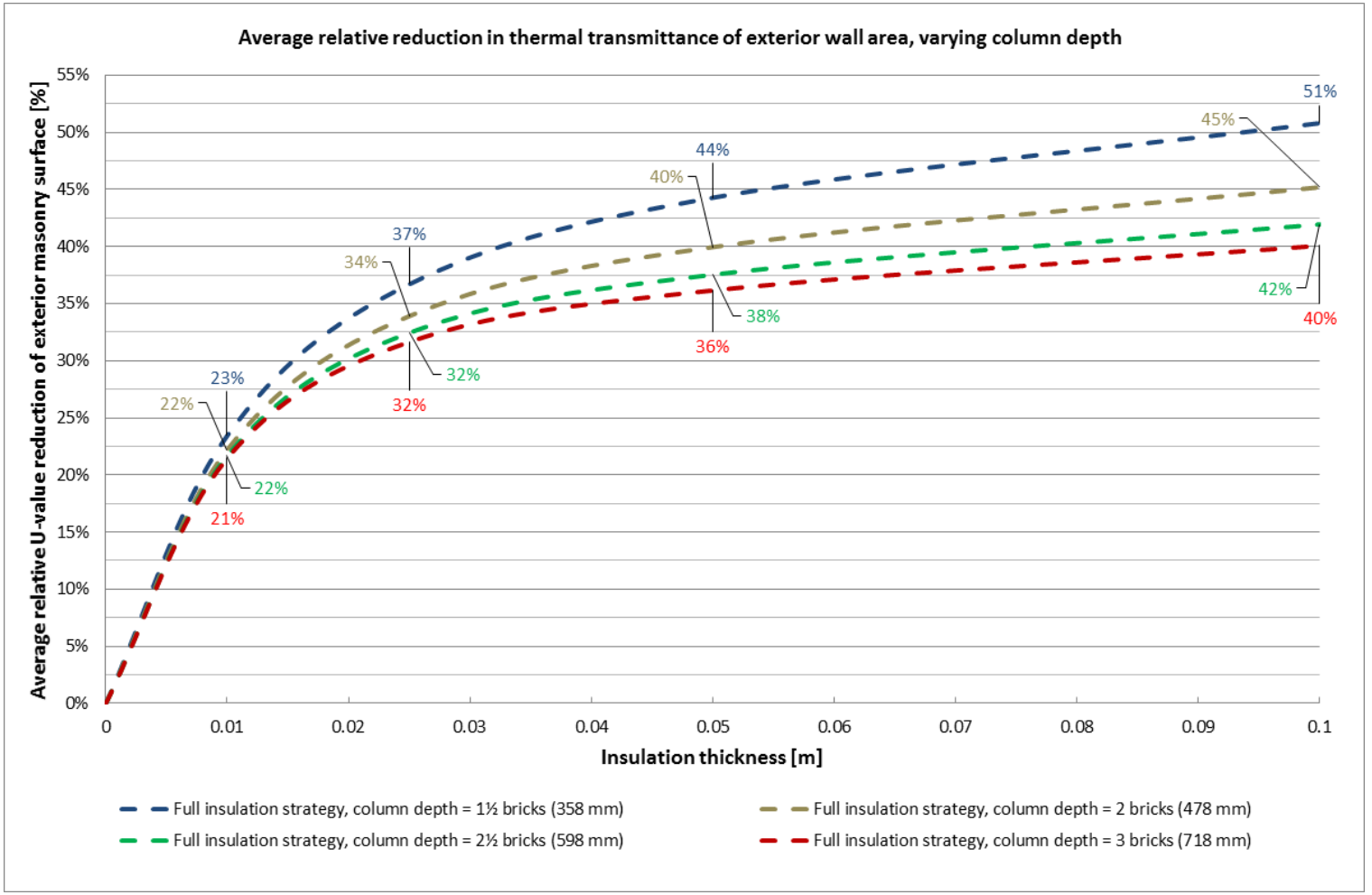


*Figure 62 Outcome from theoretical model expressed as relative reduction in thermal transmittance compared to the un-insulated wall. The simulated base model is illustrated in Figure 49, with varying thickness of masonry column.*

## *4.3* ***Sub-discussion of hypothesis***

The section will discuss the goals of the sub-hypotheses, previously presented in Section 1.3.1 and Table 1. The structure of the section is comprised of a general discussion of the results from the thermal simulation, repetition of the sub-hypothesis goals and an individual discussion of each goal.

**Generally, regarding results from the thermal simulations**

It should be emphasised that the heat flux analysis in this section focus on a potential decrease in thermal transmittance. The different thermal insulation strategies will result in different heat flow patterns, which could introduce occupant discomfort due to cold surfaces. The application of thermal insulation will change the hygrothermal balance in the original structure, especially by changing the position of the dewpoint, why this should be further investigated.

The heat flux analysis is based on a steady heat flow with boundary conditions covering the complete interior and exterior surface area. In real life, radiators might be installed at the spandrel, as illustrated in Figure 63, increasing surface temperature/boundary condition of the interior surface of the spandrel, thereby resulting in an increased heat flow through the spandrel.

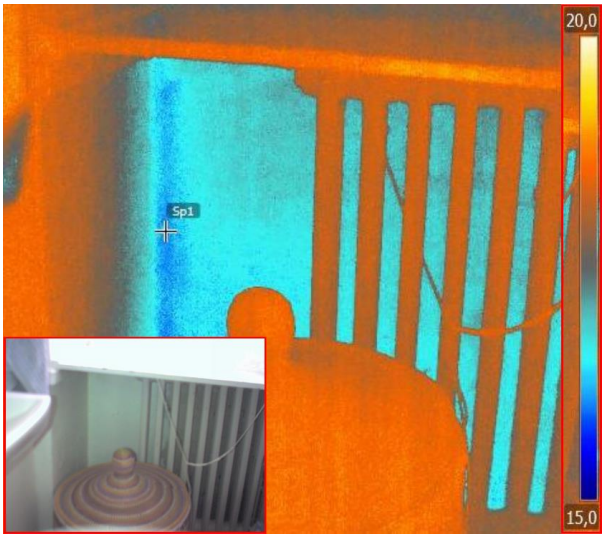


*Figure 63 Thermal image towards spandrel behind radiator. Bottom left: Photograph of thermal image area. Emissivity set to painted rendering = 0.93, temperature reading from metallic surface of radiator thereby not true: ϴSp1 = 15.7 °C. Outdoor temperature at time of investigation: ϴout = 13.7 °C. Material by courtesy of ISOLINK and Erik Møller Arkitekter.*

**Sub-hypothesis #3, goal 1** is defined as: "*A 3-dimensional parametric thermal simulation model show that: More than 25 % of the potential reduction in average thermal transmittance from full coverage thermal insulation of the interior masonry surface can be achieved by only* insulating the spandrel".

The resulting average thermal transmittance from a model of a typical multi-storey façade, retrofitted with interior insulation covering the entire interior surface, and a reduced variation only retrofitted to the spandrel, has been treated in Section 4.2.2.1 and shown in Figure 57. The results from the two insulation strategies have been compared in Table 6, illustrating the individual saving obtained from retrofitting insulation, and a comparison of the two different strategies. As it can be seen from the comparison of the two strategies, a large share of the average thermal transmittance derives from the thin masonry spandrel, why 33-40 % of the potential reduction of fully covering the interior surface can be achieved from just insulating the spandrel.

The cold surface on the interior side of an un-insulated spandrel has been illustrated in Figure 63 to illustrate the potential for reducing the thermal transmittance. Figure 64 show the exterior masonry surface of a multi-storey building, the figure clearly shows the position of hot radiators, resulting in heated spandrels due to the high heat flow under some of the windows.

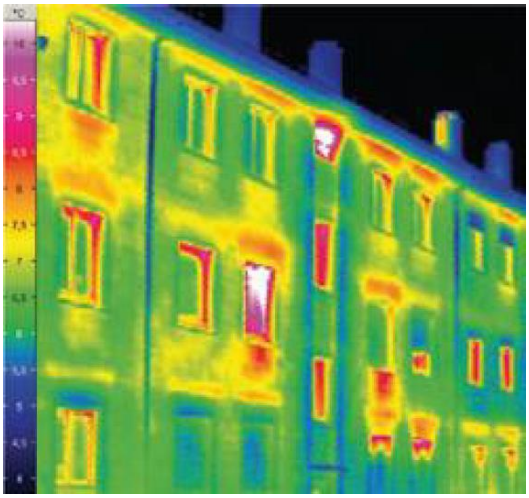

*Figure 64 Thermal image of a masonry façade. Material by courtesy of Associate Professor Bjarløv.*

✓ Goal 1 of Sub-hypothesis #3 is assessed as fulfilled based on the above.

**Sub-hypothesis #3, goal 2** is defined as: "*A 3-dimensional parametric thermal simulation model show that: Creating a deliberate thermal bridge with AAC next to the wall plate will decrease the reduction in average thermal transmittance obtained from full coverage interior thermal insulation by less* than 5 %".

The resulting average thermal transmittance from a model of a typical multi-storey façade, retrofitted with insulation with varying types of offset from the floor and ceiling, has been treated in Section 4.2.2.2 and shown in Figure 58. The average thermal transmittances have been calculated into reductions from the un-insulated case, as illustrated in Figure 59. This figure shows a large decrease in thermal transmittance when offsetting insulation vertically, where the offset at floor and ceiling level accounts for a reduction of 11 % and 4 % respectively. To decrease this reduction, while still implementing a deliberate thermal bridge, a model using AAC have been simulated. This model showed that when replacing 200 mm of insulation at both floor and ceiling level, this resulted in a reduction in average thermal transmittance of only 4 %.

✓ Goal 2 of Sub-hypothesis #3 is assessed as fulfilled based on the above, but it must be noted that this investigation is only based on a thermal simulation model. The hygrothermal conditions when replacing insulation with AAC have been investigated as part of Sub-hypothesis #5, in Section 5 and the appended Paper #3.

**Sub-hypothesis #3, goal 3** is defined as: "*A 3-dimensional parametric thermal simulation model show that: The thermal bridge introduced by an intersecting wall is a comfort issue and do only influence the average thermal transmittance of an interior insulated wall section insignificantly. Insignificantly is for this goal defined as a decrease of the reduction by less than 2.5* %".

The resulting average thermal transmittance from a model of a typical multi-storey façade, with or without an interior partition wall, retrofitted with insulation has been treated in Section 4.2.2.3 and shown in Figure 60. The hypothesis concerned if an intersecting wall had an influence on the average thermal transmittance of the facade, or if the intersecting wall solely was an issue regarding cold surface discomfort and risk of condensate. The investigation showed that the influence of the intersecting wall only decreased the reduction in thermal transmittance by 1 %, and it was thereby concluded that the introduction of a wedge is not based on the thermal transmittance.

✓ Goal 3 of Sub-hypothesis #3 is assessed as fulfilled based on the above.

## *4.4* ***Sub-conclusion of hypothesis***

The section will conclude on the sub-hypothesis, previously presented in Section 1.3.1 and Table 1, based on the sub-discussion in Section 4.3. The structure of the section is comprised of a repetition of the sub-hypothesis treated in this section, following a conclusion if the sub-hypothesis can be rejected.



**Sub-hypothesis #3:** "*The potential reduction in average thermal transmittance by various interior thermal insulation strategies, retrofitted to Danish multi-storey buildings with solid masonry walls and embedded wooden elements, can be determined by thermal simulation*".

✓ Sub-hypothesis #3 cannot be rejected, as goal 1, 2 & 3 of the sub-hypothesis was assessed as fulfilled.

### *4.4.1* Outcome of new knowledge obtained in study

The part of the industrial PhD study documented in Section 4 and the appended Paper #1 have provided new knowledge, including:

> Document the saving potential for insulation strategies: Full covering of interior masonry surface or only the spandrel, illustrating that large reductions in average thermal transmittance can be obtained from just retrofitting the spandrels with insulation.

> Document how simplified simulation in 1 and 2 dimensions significantly overestimates heat saving potential.

> Illustrate that insulation material can be replaced with AAC to create a deliberate thermal bridge, without significantly decreasing the potential reduction in thermal transmittance.

> Wedged insulation retrofitted to an intersecting partition wall in the façade is not an issue with thermal transmittance, but a comfort/hygrothermal issue.

# 5 LARGE SCALE FIELD EXPERIMENT: 24 SOLID MASONRY WALLS WITH VARIOUS INSULATION SOLUTIONS

Section 5 concern Sub-hypothesis #4, Sub-hypothesis #5 and Independent-hypothesis #1, treating and documenting measurements from 6 walls and 9 measurement points of a large scale field experiment, developed and built at the Technical University of Denmark in Kgs. Lyngby. The section further documents the construction of the experiment:

- The construction of 24 solid masonry walls, resembling multi-storey buildings from 1850-1930.
- The climatic conditions in the experiment, exposing the masonry walls to a natural outdoor climate and a high, but realistic, interior moisture load
- Description of the used sensor types and the position of measurement points, built into and on the surface of masonry walls, embedded wood and thermal insulation systems.
- The application of various types and variations of moisture-open and -tight interior thermal insulation systems.

The appended Paper #3 presented a part of the field experiment, treating and documenting measurements from 4 walls of the smallest part of the field experiment, a container with 8 experimental walls facing southwest. Section 5 will include presentation of measurements from 2 southwest facing walls of the largest part of the field experiment, a container comprising a total of 16 solid masonry walls, facing southwest and northeast.

## *5.1* ***Summary of paper related to Section 5***

The following paragraphs will describe the correlation between the content of the appended Paper #3: "Influence of hydrophobation and deliberate thermal bridge on hygrothermal conditions of internally insulated historic solid masonry walls with built-in wood" and this section, and address how the sub-hypotheses were investigated in the paper. A discussion and conclusion of the individual sub-hypothesis are done based on the paper and section content in Section 5.4 and 5.5, the sub-discussion and sub-conclusion respectively.

The content of Section 5 and the appended Paper #3 are both based on the field experiment at the Technical university of Denmark, but with different focus areas.

The content of Section 5 has focus on a moisture-tight thermal insulation systems, where the content documented in the appended Paper #3 had focus on variations of a moisture-open systems. The comparison of measurements from moisture-open and -tight thermal insulation systems are one of the goals of **SH4**.

The appended Paper #3 include a short description of the experimental setup for one of the containers. The setup is more thoroughly described in Section 5.2 of this Thesis, why this part of the paper is not described further.

The variations of a moisture-open thermal insulation system, documented in the appended Paper #3, are related to **SH5** and one of the goals of **SH4**. The two sub-hypotheses concern the influence of exterior surface treatments and variations of one type of thermal insulation system, retrofitted to a solid masonry construction with embedded wooden elements.

The investigated exterior surfaces were:

- Traditional bare brick masonry wall.
- Hydrophobized bare brick masonry wall.

The variations of the thermal insulation system were:

- Standard moisture-open thermal insulation system.
- Replacement of 200 mm thermal insulation with AAC.

The goal of **SH4** regarding the length of the stabilization period, the period from initiation of field experiment until measurements could be used for a comparative analysis, was assessed in the appended Paper #3. The assessment was divided between thermal and relative humidity measurements, finding that the RH measurements took 1 year to stabilize, while the thermal measurements stabilized in 3 months.

The goal of **SH4** regarding observation of wind driven rain in relative humidity measurements was also documented in the appended Paper #3. The findings in the paper observed minor short-term increases in relative humidity in the wooden elements a long time after large wind driven rain events had occurred.

The work with **IH1**, regarding resistance measurements, was mainly treated in Section 5, presenting the method in Section 5.2.4.1 and discussing the results in Section 5.3.1. The content of the appended Paper #3 regarding this sub-hypothesis was limited, presenting the calculated relative humidity from DC electrical resistance measurements in 4 measurement points and comparing these results to digital RH measurements.

## 5.2 **Method: Experimental design**

The objective of the experiment presented in Section 5 was to investigate the changing hygrothermal conditions in a large range of sensor points, when combining various combinations of interior thermal insulation systems with exterior surface treatments.

To fulfil this objective, an experimental setup was developed and constructed with a large amount of measurement points within solid masonry walls, embedded wooden elements and interior thermal insulation systems. I have planned the experiment with my main supervisor, Associate Professor Søren Peter Bjarløv, followed the construction of it and thereafter supervised the monitoring for 2 years after applying desired boundary conditions.



The data collection system was designed in such a way that the same methods are applied to all measurements. This means that the measurements presented during this PhD study: Combinations of 6 walls and 9 measurement points (a total of 33 unique measurement point), and all 24 walls and 18 measurement points (a total of 228 unique measurement points) are treated the same way. For consistency, the following sections describing the design and construction of the field experiment will mention all walls and measurement points.

### *5.2.1* Design of experiment and investigated thermal insulation systems

The 24 identical base walls were designed to resemble the construction detail illustrated in Figure 65: The intersection of a masonry column at the highest floor with a solid interior partition and a floor structure, including a wooden beam. This design is characteristic for the Danish multi-storey building. Illustrations of the experimental design can be seen in Figure 66(a-c). The horizontal design of the base walls had a width of 948 mm, equal to 4 bricks, and a thickness of 358 mm, equal to 1½ bricks, with a layer of rendering on the inside. The rendering and mortar joints were made of the same material: Lime mortar. The masonry walls were constructed by professional masons as solid masonry walls in a characteristic cross bond with lime mortar joints. The partition wall was built with a thickness of 128 mm, ½ brick with a layer of rendering on both sides. The vertical design of the base walls had a height of 1987 mm, 30 courses, complete with a floor structure having a top point at the vertical middle of the wall. The floor structure consisted of a 100 x 100 mm wall plate along the masonry wall with a 175 x 175 mm wooden beam resting on top. 15 mm OSB boards on all sides except towards the partition encapsulated the wooden beam. 100 mm of mineral wool were placed in the OSB board enclosure to emulate a pugging layer. The floor structure was

constructed to the left of the partition, while the space on the right side was kept empty, also for walls where insulation systems were applied.

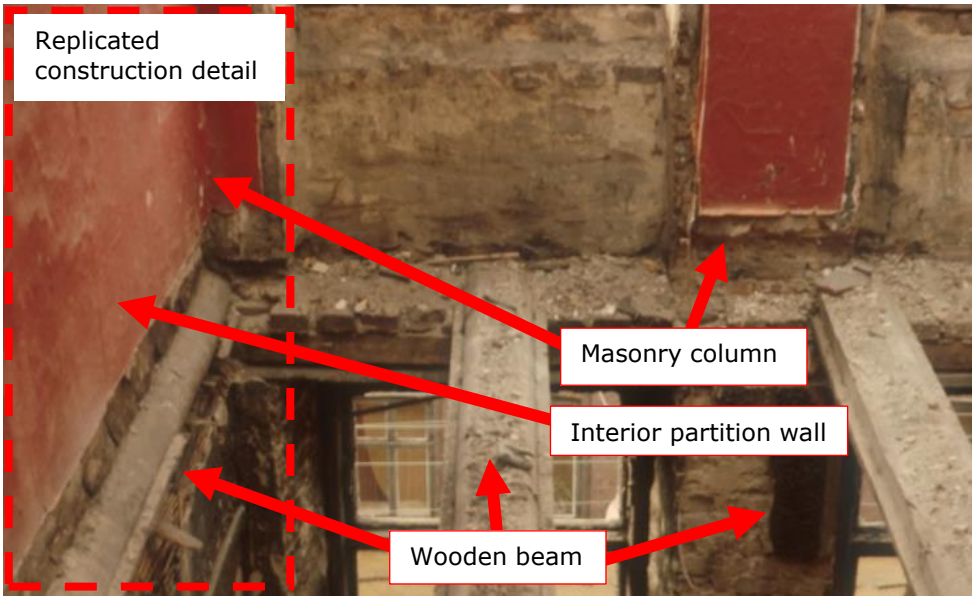


*Figure 65 Replicated construction detail in experimental setup. Original photo courtesy of J. Engelmark.*

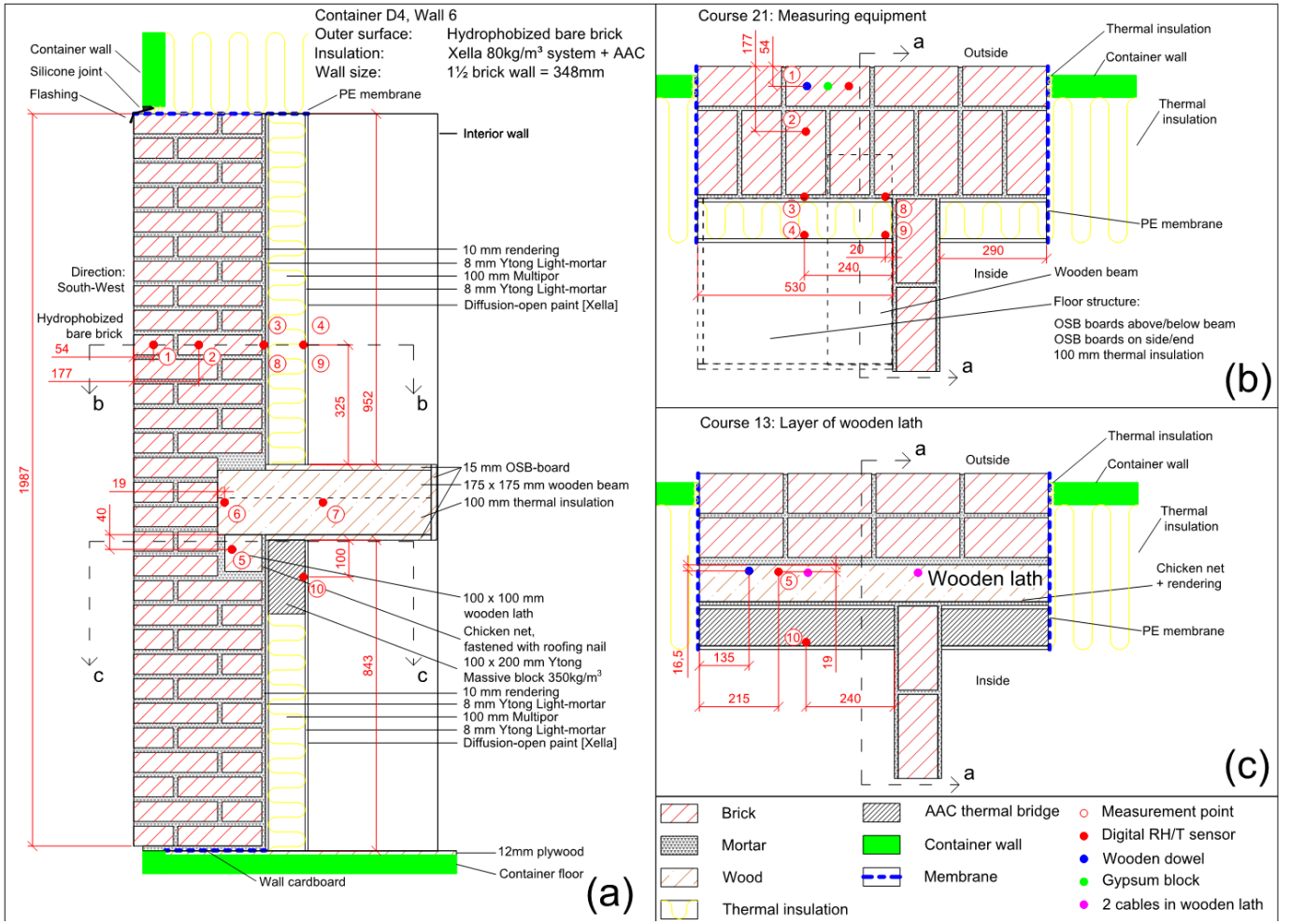


*Figure 66 Illustration of the wall compositions and placement of measurements. (a) show a vertical cut in the wooden beam of Wall 6, (b) & (c) show courses with measuring equipment.*

The experimental design deviated from the real characteristic construction, thoroughly described in Danish literature (Engelmark, 1983). The wall thickness was kept constant above/below the floor structure, where a column thickness of 1½ bricks characteristically would have had a column thickness of 2 bricks (478 mm) below, with a spandrel next to the column above the floor structure. The wooden beam end had a small overlap of the wall plate, where the wooden beam would normally have an overlap equivalent to the wooden beam height. The pugging layer between the ceiling/floor boards were simplified to 100 mm mineral wool, while the characteristic construction would consist of wooden boards with a layer of approximately 50 mm clay.

As part of a collaboration between TUD and DTU, all construction and thermal insulation materials used in the experiment have undergone material characterization at the material laboratory of TUD as preparatory work for later simulation in hygrothermal simulation software, Delphin. The basic materials used in the experiment were:

> Yellow soft-moulded brick from Helligsø Teglværk. Selected with technical assistance from the Danish Technological Institute (TI) as the modern brick with the closest resemblance to historic bricks from the period 1850-1930.

> 7.7 % lime adjusted mortar (air lime), grain size 0-4mm from Wewers A/S designed to resemble the one used in historic buildings.

> Wall plates and wooden beams (floor joists) of Pomeranian pine wood.

> OSB board.

The 24 base walls had various thermal insulation systems applied to the interior masonry surface and in some walls variations within the systems. An overview of the installed insulations systems in the two containers can be seen in Figure 70 and Figure 71, where the notation next to each wall describe the installed interior insulation system and internal/external surface. The used notations in Figure 70 and Figure 71 is explained in the following pages:

> First line: Description of installed thermal insulation system.

- Reference wall: No insulation installed, identical to base walls.
- Mineral wool with vapour barrier: The traditional moisture-tight interior thermal insulation system in Denmark, described in Danish guidelines (Brandt et al., 2013). The system consists of a wooden frame, with 100 mm mineral wool in between. The interior surface is finished with a tight vapour barrier and a gypsum board.
- Remmers IQ-therm: A polyurethane foam with perforations of surface-active calcium silicate and air for capillary water transport and diffusion. Installed with IQ-Fix as adhesive, IQ-Top and IQ-Fill as topcoat.
- Skamol SkamoPlus: Capillary active Calcium silicate board also sold under the name "CasiPlus". Installed with Weber Multi 292 as adhesive and topcoat.
- DTU Foam concrete: Moisture-open thermal insulation system based on a recipe of a protein based foam (luca-industries.com et al., 2018) and cement paste developed at DTU by (Dysted and Sandholdt, 2015). Installed with same adhesive and topcoat as "Ytong Multipor int. system".
- TI Insulating mortar: Moisture-open thermal insulation system based on an insulating lime mortar, designed by the Danish Technological Institute for use in protected buildings. Installed in-situ.
- Ytong Multipor int. system: Diffusion open thermal insulation system based on Ytong Multipor Interior Mineral Insulation Boards with a density of 85-95 kg/m³. Installed with Ytong Multipor Light Mortar as adhesive and topcoat.
- Ytong Multipor int. system + therm. bridge: The same system as described under "Ytong Multipor int. system", supplemented with a 100 x 200 mm Ytong massive block with a density of 340 kg/m³ in the top 200 mm underneath the floor structure. This block was implemented to create an intentional thermal bridge, meant to protect the wooden components embedded in the wall. A detail drawing of the system can be seen in Figure 66(a).

> Second line: Description of the interior surface.

  - Rendering: Rendered surface of the base wall, with the same lime mortar used for the mortar joints in the masonry wall.
  - Diffusion-open paint: The paint approved by the respective producers for use with their thermal insulation systems, being:
    - Ytong: Ytong Multipor Silicate Interior Paint.
    - Remmers: IQ-Paint.
    - SkamoPlus: Weber Ton top 411.
  - Airlime rendering mortar: A traditional whitewash of the interior surface.
  - Gypsum board: Gypsum board, untreated.
  - Gypsum + regular paint: Gypsum board painted with regular paint (described in the following bullet point).
  - Regular paint: Painted with Flügger Flutex 5, a commonly used paint in Denmark (Dysted and Sandholdt, 2015).

> Third line: Description of the exterior surface.

- Bare brick (illustrated in Figure 68): Bare brick masonry surface, identical to the base wall.
- Hydrophobized bare brick (illustrated in Figure 69): Hydrophobic facade treatment of the bare brick masonry surface with Remmers Funcosil FC (Concentration = ~40 % w/w). The hydrophobic façade treatment was applied after drying out the walls, but before exposing them to the natural environment, retaining the salts on the surface extracted during the initial dry-out (consequently keeping the white expression of the wall as a left-over from brushing the façade with a wire brush).
- Rendering (illustrated in Figure 67): Rendered with the same lime mortar used for the mortar joints in the masonry wall.



*Figure 67 Rendered exterior surface.*
*Container D4, Wall 1.*

*Figure 68 Bare brick exterior surface.*
*Container D4, Wall 2*

*Figure 69 Hydrophobized bare brick exterior surface.*
*Container D4, Wall 3.*

Results from the wall configurations 2, 3, 5 & 6 in container D4, measurement Points 1-2 for Wall 2 and 3, Points 3-6 for all wall combinations and Point 10 for Wall 6, was presented in the appended Paper #3. Results from the wall configurations 1 & 3 in container C3, measurement Points 3-6, is presented in Section 5.3.

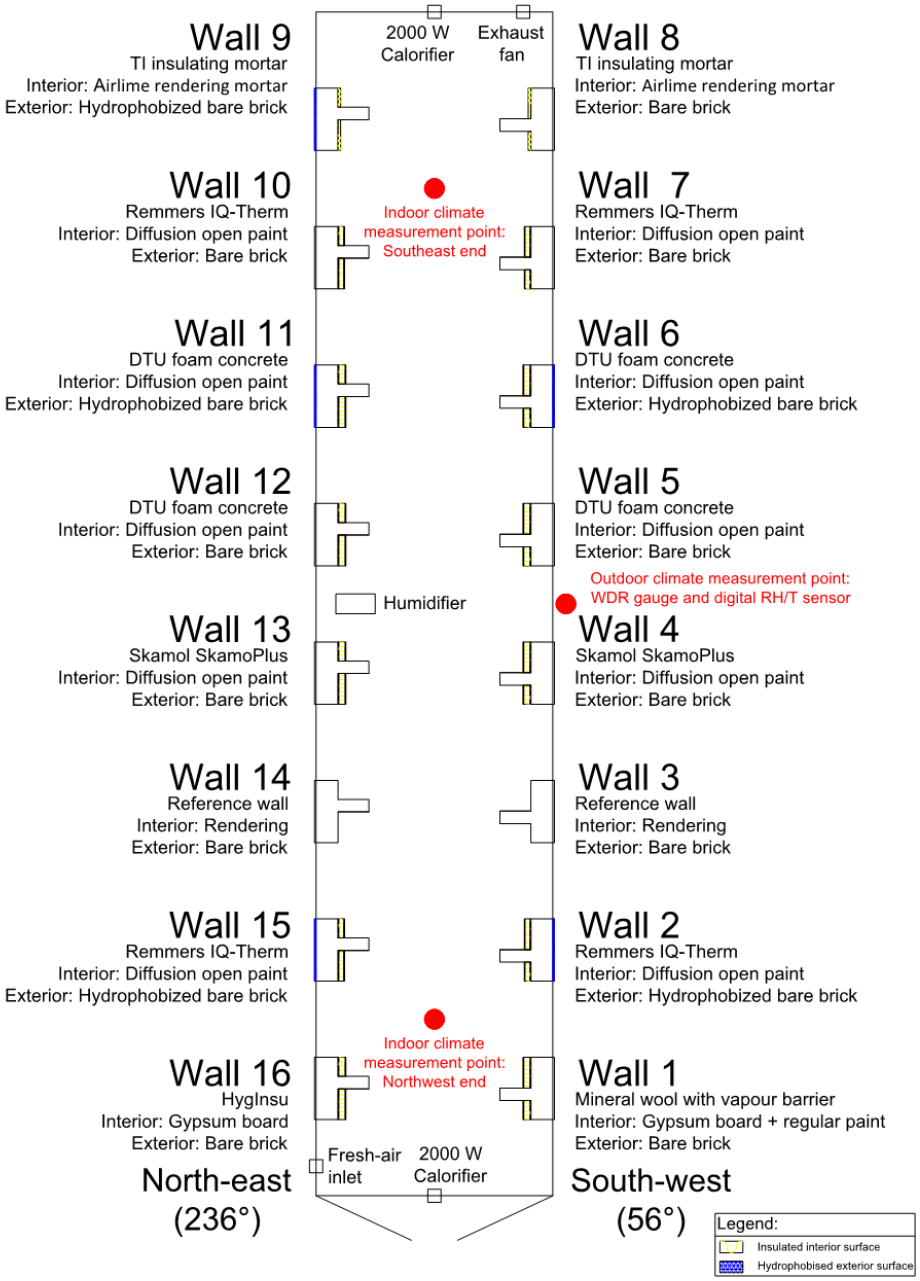


*Figure 70 Overview of installed interior thermal insulation systems and interior/exterior surfaces in container C3 (Funded by Grundejernes Investeringsfond).*

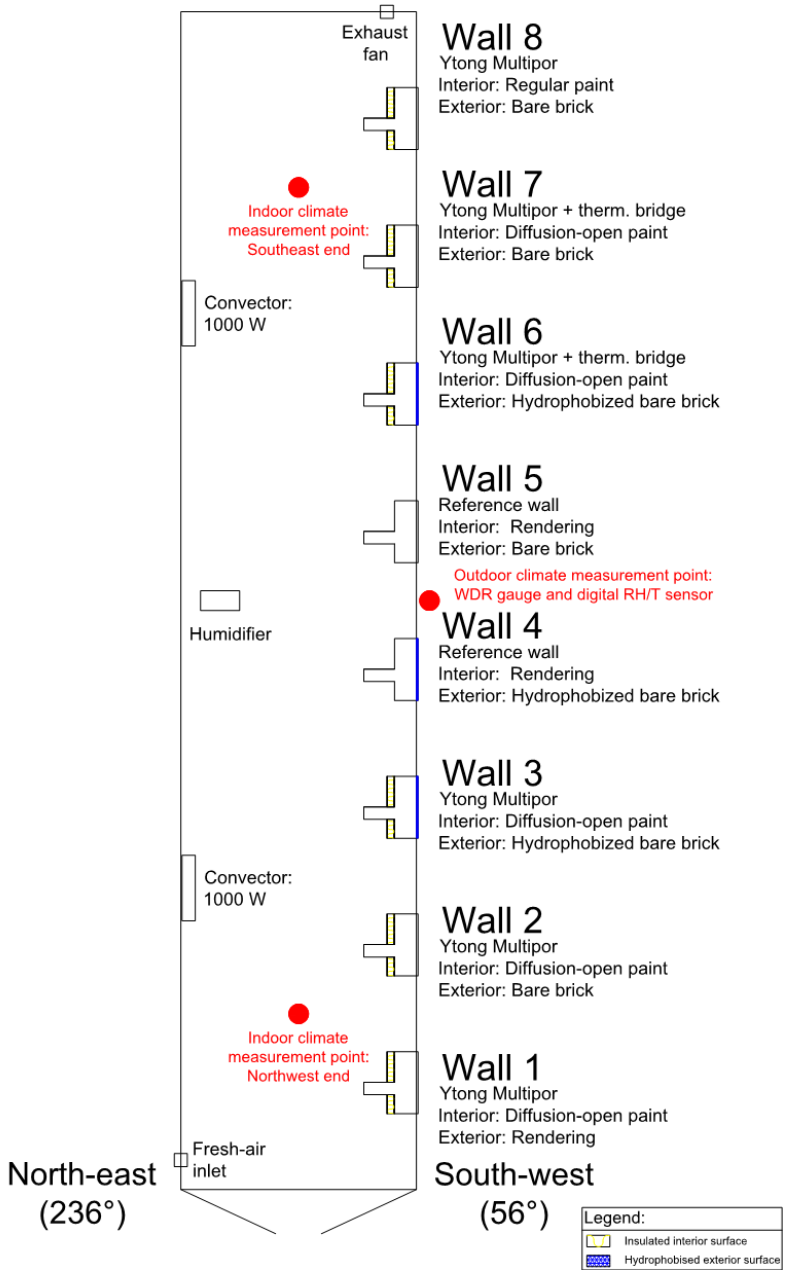


*Figure 71 Overview of installed interior thermal insulation systems and interior/exterior surfaces in container D4 (Funded by RealDania).*

### *5.2.2* Construction of experiment

The planning of the experiment started in December 2013, Container C3 and D4 were delivered in July 2014. The state of the experimental area in the start and end of this current PhD study can be seen in Figure 72 and Figure 73 respectively, with orientation of walls illustrated in Figure 74. The construction of the masonry walls started in August 2014. First, the containers were perforated (Figure 75), then the masonry walls were constructed by professional masons (Figure 76). The measurements points were pre-installed into bricks and wooden elements beforehand, which were then installed by the masons (Figure 77). The wooden beam was installed, and rendering was applied to all interior surfaces (Figure 78). Construction of the walls with installation of vapour barriers and thermal insulation to reduce the walls influencing each other were finished in November 2014. In the period from November 2014 until April 2015, forced dry-out of the walls were done. The walls were protected against rain with a canopy on the outside, and high temperatures and low relative humidity were applied on both sides of the walls to force a dry-out. The dry-out was followed by regular Troxler measurements.

*Figure 72 DTU test site in year 2013, before setting up experiment. Photo courtesy of Maps from COWI.*

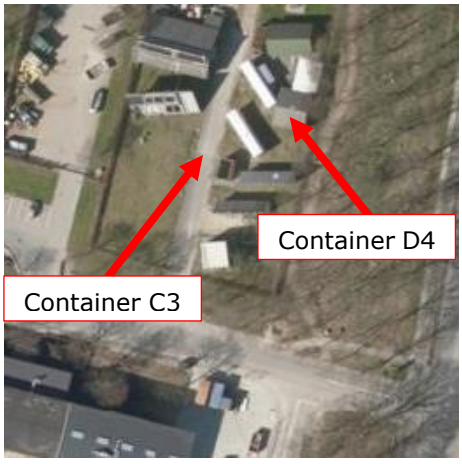


*Figure 73 DTU test site in year 2017, experiment in place. Photo courtesy of Maps from COWI.*

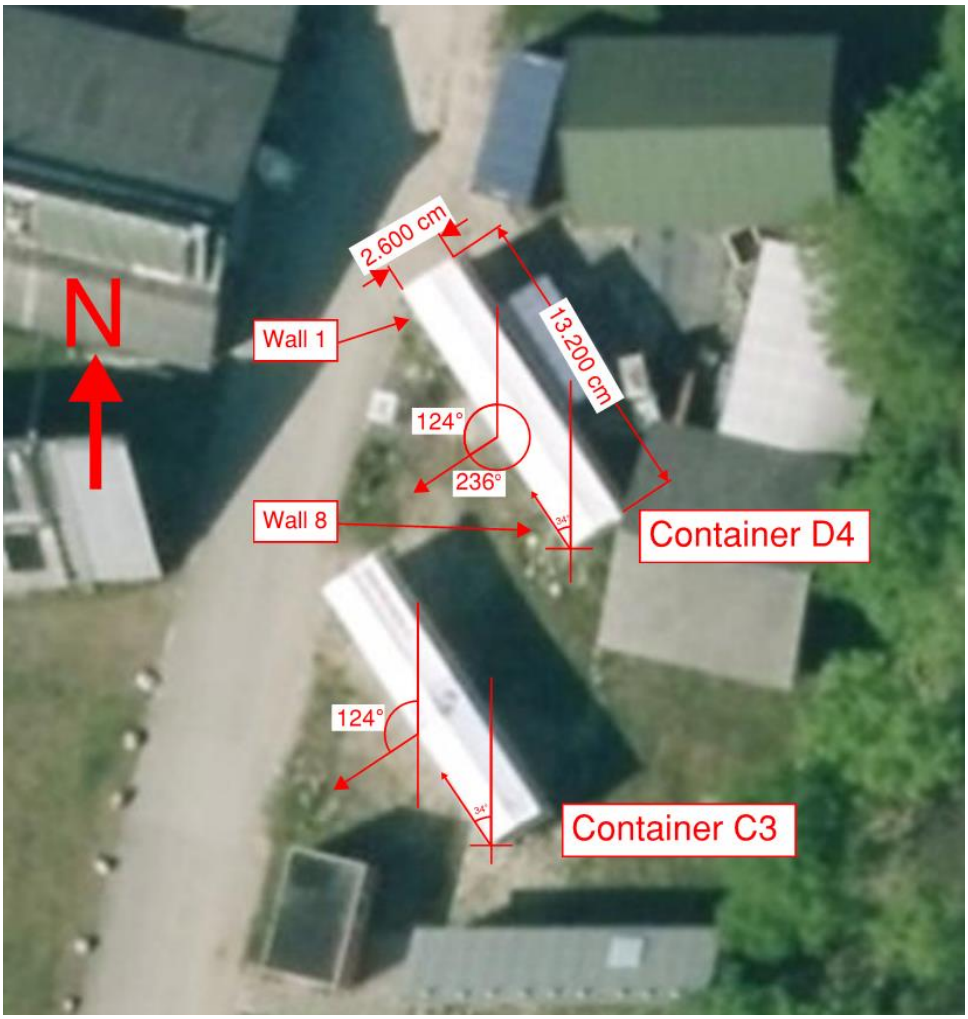


*Figure 74 Orthophoto of experimental containers, including orientation. Photo courtesy of Maps from COWI.*

*Figure 75 Perforated container C3.*

*Figure 76 Construction of solid masonry walls with embedded wooden elements.*

*Figure 77 Mason installing brick with pre-installed sensors at measurement point 1.*

*Figure 78 Finished solid masonry wall with wooden beam, before installing vapour barrier and thermal insulation at the boundaries of the wall.*

The various insulation systems were installed when the masonry walls had dried out sufficiently. The insulations systems were installed by the producers, following normal guidelines including reinforcement, as seen in Figure 80. The different systems and surface treatments were installed at the following times:

- Primo February: Remmers IQ-Therm.
- Primo February: Skamol SkamoPlus.
- Medio February: Ytong Multipor.
- Ultimo March: DTU Foam Concrete.
- Ultimo March: Apply hydrophobic façade treatment to exterior surfaces.
- Medio April: Mineral wool with vapour barrier.
- Ultimo April: TI Insulating mortar.

The outside protecting canopy was removed in April 2015.

*Figure 79 Thermal insulation is installed by the producers following system guidelines.*

*Figure 80 Thermal insulation is installed by the producers following system guidelines.*

### *5.2.3* Boundary conditions in experiment

The indoor boundary conditions in the experiment was controlled by installing heaters and a humidifier, ensuring a controlled minimum level of indoor relative humidity and temperature. Cooling and dehumidification were not carried out, leading to periods in the summer with uncontrollable high temperature and relative humidity. The indoor set points were a temperature of 20 °C and relative humidity of 60 % (70 % in the first 3 months due to initial adjustments).

The outdoor wall surfaces were uncontrolled, exposed to the local climate, a similar procedure used in other European projects at BBRI, Belgium (Mets et al., 2017) and UCEEB, Czech Republic (Kopecký et al., 2017).

The indoor and outdoor boundary conditions were monitored throughout the experiment, where Wind Driven Rain (WDR) is described in Section 5.2.3.1.

The in- and outdoor temperature and relative humidity were used to evaluate the moisture load in the container, based on humidity classes (Brandt et al., 2013; DS/EN ISO 13788:2013, 2013). The calculated monthly average indoor excess of humidity by volume over the monthly average outdoor temperature can be seen in Figure 81. As the period outside the heating season is not of interest, the humidity class in the experiment within the heating season is defined as class 3 "Buildings with unknown occupancy", in periods up to 4 "Sports halls, kitchens, canteens." (DS/EN ISO 13788:2013, 2013).

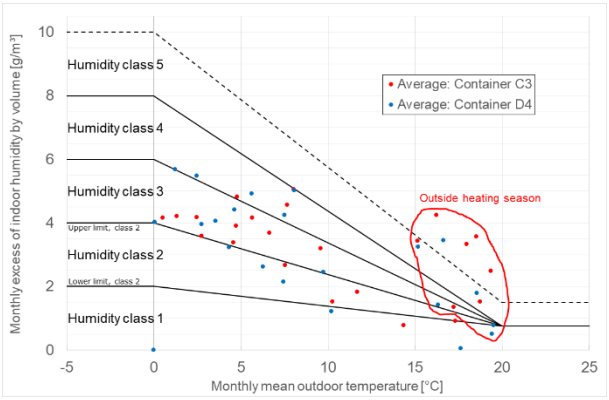


*Figure 81 Assessment of moisture excess in relation to the humidity classes* (Brandt et al., 2013; DS/EN ISO 13788:2013, 2013).
*Enlarged version in Figure 151 on page 212.*

#### 5.2.3.1 Wind driven rain (WDR)

The WDR load on the exterior wall surfaces was both measured with WDR gauges and calculated from rain and wind measurements at the climate station at DTU (Andersen et al., 2014).

The construction of the WDR gauges have been described in the appended Paper #3, and can be seen in Figure 82. The gauges were installed between Wall 4 and 5 on container C3 and D4 and between 12 and 13 on container C3, as seen in Figure 70 and Figure 71.



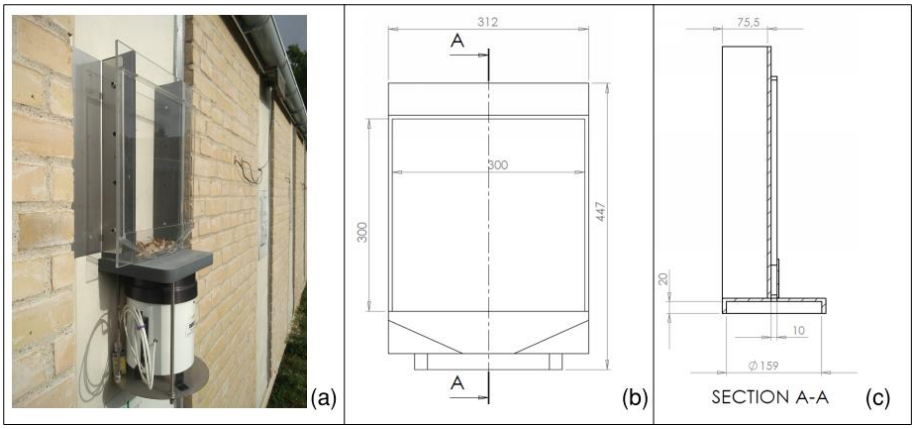


*Figure 82 Picture (a) and drawings (b) & (c) of WDR sensor. Drawings produced by Linatex A/S.*

The WDR was calculated by the method described in Section 2.2.3 on page 32, including scaling of DRF based on rainfall intensity. The factor for fitting WDR in free wind ($r_v$) to the exterior surface of the experiment ($r_{vb}$) was determined through an iterative process, resulting in:

- Southeast direction: $Factor_b$ = 0.49.
- Northeast direction: $Factor_b$ = 0.64.

The resulting fit between WDR gauge measurement and calculations can be seen in Figure 83, where the gaps in measured data occur due to malfunction in the WDR data logger.

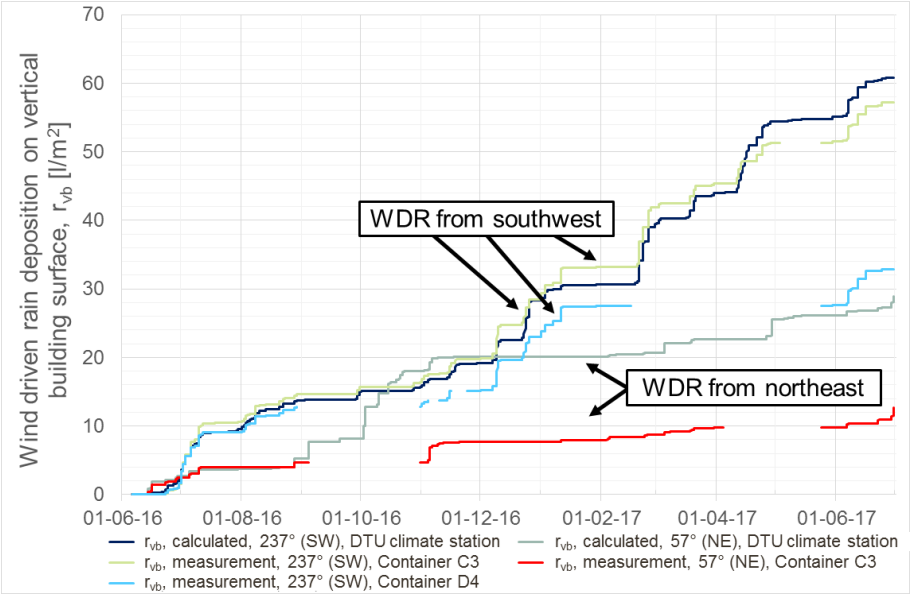


*Figure 83 Fitted calculated to measured $r_{vb}$. Gaps and displacement are caused by periods with fault on sensors. Enlarged version in Figure 152 on page 213.*

### *5.2.4* Measurement system

I have in the start of the PhD study investigated the market and identified the sensors used in the experiment, resulting in that the hygrothermal conditions in the measurement points were monitored via two systems, described in the following two sections. A more detailed description of the Matlab script I have developed to treat the data from the two measurements systems have been described in Appendix B on page 231, including flowcharts describing the data collection setup in Figure 169 on page 234 and the process of the Matlab script in Figure 170 on page 235.

The physical data logging systems were developed by technician in metrology at DTU, Lars Kokholm Andersen. This work is illustrated as black arrows from the "field experiments", to the "PC's in containers" in Figure 169 on page 234.

#### 5.2.4.1 DC electrical resistance measurement system

A DC electrical resistance system was developed, measuring in three different mediums: Measurements in wooden dowels, directly in the wall plate and in gypsum blocks. These resistance-based measurements were only performed in a limited amount of measurement points, mainly as reference values to the values

measured by the digital measurements. The choice of limiting the extent of the resistance-based system was based on high cost of the individual points, mainly due to the price of cobber-constantan wires and data logging system.

The measurement of DC electrical resistance in a wooden dowel and temperature based on a soldering between a cobber and a constantan wire are a well-known and referenced method, as described in Section 2.4 on page 44. The DC electrical resistance and temperature was measured by the automatic logging system every 1 hour. Further manual measurements of the DC electrical resistance were performed with a T301.COW instrument (BMT Instruments ApS, 2017; Bygge og Miljøteknik, 2008) at various intervals from August 2015 and forward.



The measurement of DC electrical resistance directly in a wall plate is similar to that of measuring in the wooden dowels. The method and measurement points are further described in the last bullet point of Section 5.2.4.3 and in Figure 103. The measurements in the wall plate were measured manually with a T301.COW instrument (BMT Instruments ApS, 2017; Bygge og Miljøteknik, 2008) at various intervals from August 2015 and forward.

The measurement of DC electrical resistance in gypsum blocks are a method traditionally used for monitoring soil water content. The method is similar to that of DC electrical measurement in wooden dowels, but can only be used to monitor conditions when brick is saturated, based on the high magnitude of the DC electrical resistance in dry state. The DC electrical resistance was measured by the automatic logging system every 1 hour. Further manual measurements of the DC electrical resistance were performed with a T301.COW instrument (BMT Instruments ApS, 2017; Bygge og Miljøteknik, 2008) at various intervals from August 2015 and forward.

The wires from wooden dowels and gypsum blocks in each wall were installed in a cabinet in the middle of the container, plugged into a multiplexer system. The setup was designed as an automatic system, with the possibility to measure with a manual handheld instrument. At the time of handing in this PhD Thesis, some of the manual measurements in the walls described in Section 5.3.1 have been used, with the temperature from the digital system at the nearest time step. The automatic system still lacked calibration.

#### 5.2.4.2 Digital measurement system

A system able to log measurements from a large amount of digital RH/T sensors was developed. The system was developed based on Arduino boards, serving as an interface between a computer and the sensors via the software LabVIEW. The used "HYT 221" sensor from Innovative Sensor Technology IST AG (IST) communicate over the I2C protocol. The I2C protocol made it possible to build a system connecting multiple sensors via patch panels to a single cable towards an Arduino, as illustrated in Figure 84, with up to 127 sensors on a single Arduino. The system was split into three separate groups, one per 8 walls. Up until April 2016, the setup included one Arduino board per group, which was changed to one Arduino per wall for a more robust system, as a malfunctioning sensor would short circuit the entire connected group until removed.

A total of 44 sensors have malfunctioned and have been replaced from the period of the first sensor activation in December 2014, up until July 2017. In the case of a malfunctioning sensor in the masonry wall, the sensor has been disconnected and a new have been installed in the course above the original, as seen in Figure 85, where after the hole have been filled with a silicone sealant. There has been a total of 4 instances of malfunctioning sensors in the wooden beam, wall plate or rendering layer, and 9 instances where a replaced sensor in the exterior surface have had to be changed again. Remaining malfunctioning sensors was in masonry.

*Figure 84 Patch panel connecting multiple sensors to 1 cable.*

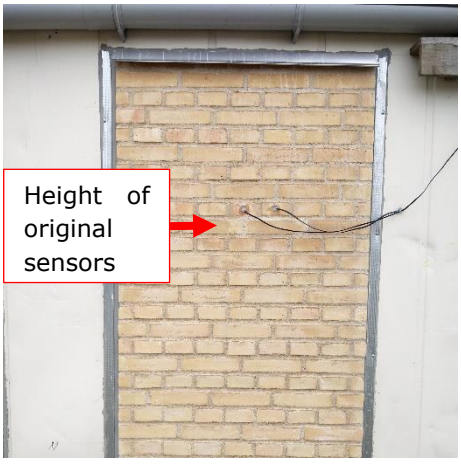


*Figure 85 Container D4, Wall 5. 2 changed sensors, drilled in from exterior surface in the course above the original sensors.*

As of July 2017, a total of 228 unique digital RH/T sensors were installed in the experiment.

#### 5.2.4.2.1 Protection of digital sensors against moisture

The digital RH/T "HYT 221" sensor module from IST are delivered as print boards, as illustrated in Figure 86. The connection from the sensor module to the patch panel was done via a "sensorcable for EK-H3/H4" from Sensirion. The two products was connected and covered with adhesive lined shrink tubing for protection, as illustrated in Figure 87, Figure 88 and Figure 89. The finished protected sensor can be seen in Figure 89, where only the yellow net covering the sensor area is uncovered.



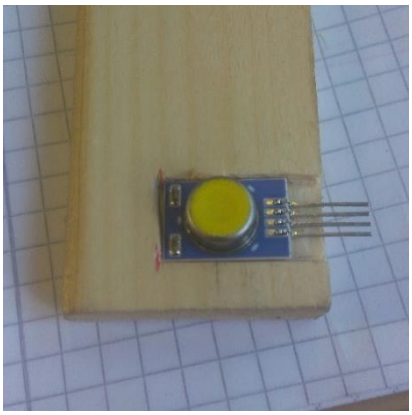

*Figure 86 Original sensor before attaching cable and protecting with adhesive lined shrink tubing.*

*Figure 87 Sensor connected to cable, before covering and applying heat to adhesive lined shrink tubing.*

*Figure 88 Applying light pressure to mold after heating up adhesive lined shrink tubing, to ensure a protective layer of glue and shrink tubing on the print board.*

*Figure 89 Finished protected sensor and cable connection. Yellow net was covered with cardboard during heating, to avoid glue covering the sensor area.*

#### 5.2.4.2.2 Calibration of digital sensors

After protecting the sensor and cable as described in Section 5.2.4.2.1, the measured relative humidity for each individual sensor was calibrated over known saturated salt solutions. This calibration was done in a moisture-tight box with an internal fan, as illustrated in Figure 90, in a room with stationary temperature conditions. The measured relative humidity for each sensor was calibrated in the following ad- and desorption steps, where each step was validated using a Rotronic Hygrometer A2, calibrated prior to the process over certified Rotronic ampoules:

1. Potassium Carbonate $K_2CO_3$ (44 %)
2. Sodium Chloride NaCl (75 %)
3. Potassium Nitrate $KNO_3$ (93 %)
4. Potassium Sulfate $K_2SO_4$ (97 %)
5. Potassium Nitrate $KNO_3$ (93 %)
6. Sodium Chloride NaCl (75 %)
7. Potassium Carbonate $K_2CO_3$ (44 %)

The focus when choosing salt solutions for the calibration were in the range 75 – 97 % RH, the range in which conditions amenable to mould growth and decay conditions would be met (Viitanen, 2007; Viitanen et al., 2015, 2010a).

The sensors were exposed to the saturated salt solution until steady conditions were achieved, as illustrated in Figure 91. After the calibration process, unique linear trend lines were fitted to the individual measurements, resulting in an equation for converting the measured relative humidity to validated relative humidity. The sensor was discarded if values from the individual sensor and the certified Rotronic Hygrometer A2 showed large differences, or the sensor had outliers.

The resulting unique calibration equations had the form presented in Equation (15). An example of some calibration values can be seen in Table 7.

$$RH_{calibrated} = RH_{measured} \cdot a_{calibration} + b_{calibration} \quad (15)$$

*Figure 90 Set-up for calibration: Isolated box with various know salt solutions.*

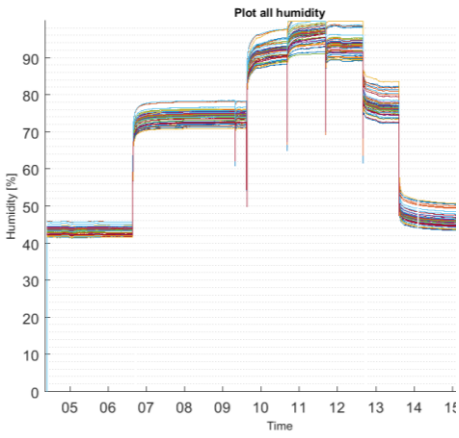


*Figure 91 Output from 7th calibration. Real RH is measured before step-change.*

| Container | Wall | Point | $a_{calibration}$ | $b_{calibration}$ |
|---|---|---|---|---|
| D4 | 2 | 3 | 1.020 | -0.568 |
| D4 | 3 | 3 | 1.018 | -0.891 |
| D4 | 6 | 3 | 1.011 | -2.779 |
| D4 | 2 | 6 | 1.043 | 1.815 |
| D4 | 3 | 6 | 1.034 | 0.569 |
| D4 | 5 | 6 | 0.998 | -2.323 |
| D4 | 6 | 6 | 1.066 | -1.504 |
| D4 | 2 | 5 | 0.980 | 0.282 |
| D4 | 3 | 5 | 0.978 | -0.044 |
| D4 | 5 | 5 | 1.029 | 0.636 |
| D4 | 6 | 5 | 0.955 | 1.914 |
| D4 | 6 | 10 | 1.008 | 0.201 |
| D4 | Internal | NW | 0.995 | 1.739 |
| D4 | Internal | SE | 0.986 | 1.177 |
| D4 | External | SW | 0.989 | 0.079 |

*Table 7 Examples of calibration values for sensors in container D4.*

#### 5.2.4.2.3 Post processing of digital measurements

The individual calibration values of each sensor were applied, and results were truncated to be between 0.00 and 99.99 % RH. This truncation was done by applying the following procedure to each measured value throughout the experiment:

- If the measured relative humidity by the sensor was above 99.98, the value was kept. Else the individual calibration equation was applied:
    - If the resulting value exceeded 99.99, then the value was adjusted to 99.99.
    - If the resulting value was under 0.00, then the value was adjusted to 0.00.

Failing or defective sensors and power cuts can result in logging of wrong values. The wrong values included temperatures of +120 °C or -40 °C, relative humidity of >100 % or =<0 % or outliers significantly different from recently measured values. These values were removed with the following procedure:

- As the following extreme values did not occur in Denmark, they were filtered away. Values outside the following boundaries:
    - Temperature: $-35 < \theta\ [°C] < 50$.
    - Relative Humidity: $5 < RH\ [\%] < 100$.
- The outliers were defined as values with sudden significant difference from previously measured values. The significance of the difference was defined based on Grubbs test, with a significance level of 5 %.

#### 5.2.4.3 Sensor placement

The points and types of measurements are described in the following bullet list with positions illustrated in Figure 66(a-c) and Figure 102.

- Point 1 (illustrated in Figure 92): Digital RH/T sensor, wooden dowel and gypsum dowel, mounted in brick. The digital RH/T sensor and wooden dowel was installed from opposite ends of the brick, 1/3 into the brick length. The gypsum dowel was installed from the top of the brick. All sensors were installed in the middle of the brick width, resulting in 54 mm from exterior façade surface.
- Point 2 (illustrated in Figure 92): Digital RH/T sensor, mounted 57 mm from brick end pointing towards the exterior surface, in middle of masonry wall, 177 mm from exterior surface.
- Point 3 & 8 (illustrated in Figure 93 and Figure 94): Digital RH/T sensors, mounted on interior masonry surface, covered by rendering. Point 3 had a horizontal measurement point 240 mm from the partition, point 8 was placed against the partition.

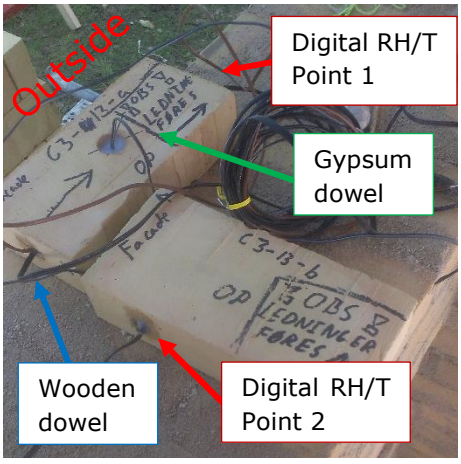


*Figure 92 Sensor Point 1 and 2: Measurement point closest to the exterior surface and in the middle of the masonry wall.*

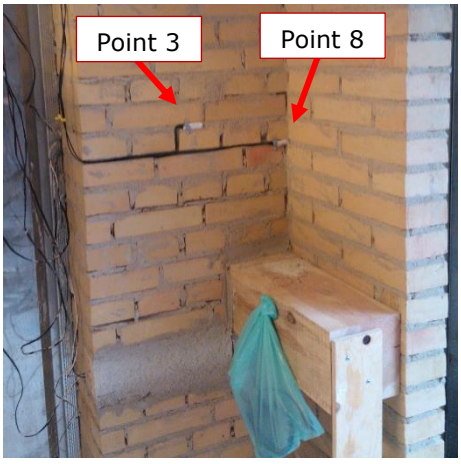


*Figure 93 Sensor Point 3 and 8: Measurement point closest to the original interior surface of the masonry wall. Photo courtesy of Søren Peter Bjarløv.*

- Point 4 & 9 (illustrated in Figure 95): Digital RH/T sensors, mounted in 10 mm deep cut channel in the interior insulation, covered with the mortar of the insulation system. Vertical and horizontal position can be seen in Figure 95.


*Figure 94 Sensor Point 3 and 8: Measurement point closest to the original interior surface of the masonry wall, sensing area facing mortar. Photo courtesy of Søren Peter Bjarløv.*

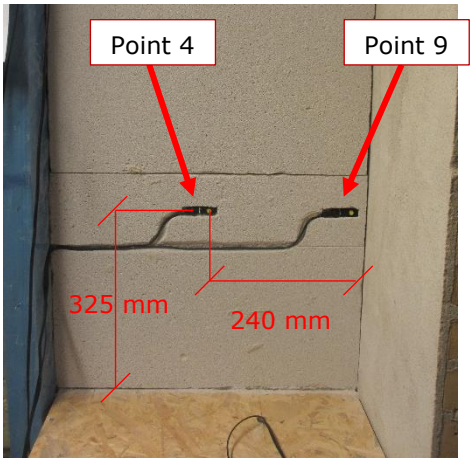


*Figure 95 Sensor Point 4 and 9: Measurement point closest to the interior surface of insulation system.*

- Point 5 (illustrated in Figure 96 and Figure 97): Digital RH/T sensor and wooden dowel, mounted in wall plate from the bottom and sealed with silicone. The middle of the sensor points was vertically 40 mm from the top of the wall plate. The digital sensor was placed horizontally 215 mm from the left vapour barrier and 19 mm from the front facing towards the façade. The wooden dowel was placed horizontally 135 mm from the left vapour barrier and 16.5 mm from the front facing towards the facade.

- Point 6 & 7 (illustrated in Figure 98): Digital RH/T sensor, mounted in wooden beam and sealed with silicone. Hole drilled horizontally from side opposite of the partition, with measurement point in the beam centre. Sensor 6 had a distance of 19 mm from the beam end, sensor 7 had a distance of 286 mm from the beam end.

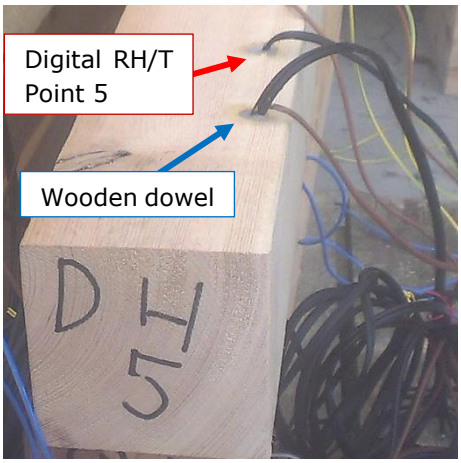


*Figure 96 Sensor Point 5: Measurement points in wall plate.*

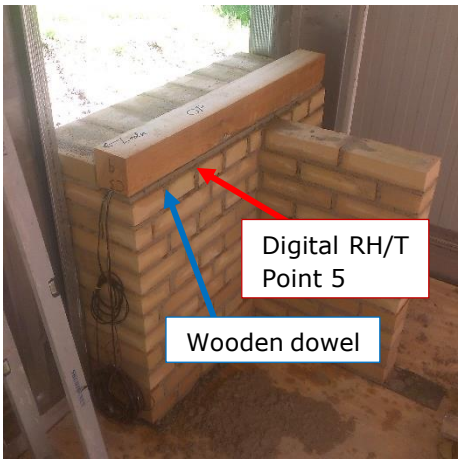


*Figure 97 Sensor Point 5: Measurement points in wall plate.*

- Point 10 (illustrated in Figure 99): Digital RH/T sensor. Mounted in 10 mm deep cut channel in the AAC deliberate thermal bridge, covered with the mortar belonging to the insulation system. The sensor was placed horizontally 240 mm from the partition, and vertically 100 mm beneath the floor structure, in the middle of the AAC block. This sensor point was exclusively installed in Wall 6 and 7 in container D4.

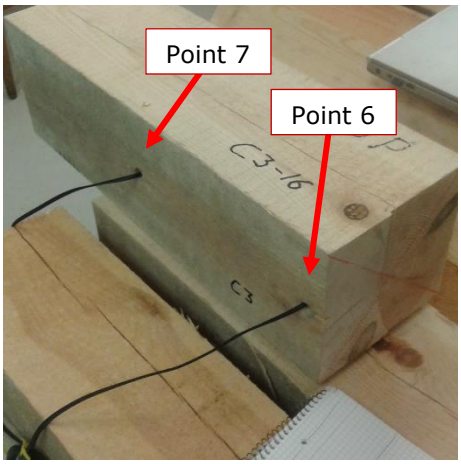


*Figure 98 Sensor Point 6 and 7: Measurement points close to the wooden beam end and 286 mm from the beam end.*

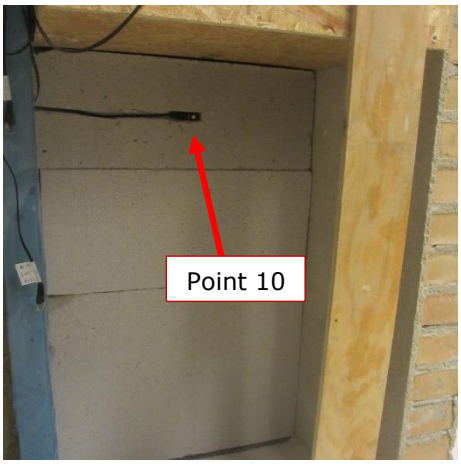


*Figure 99 Sensor Point 10: Measurement point in deliberate thermal bridge in front of wall plate.*

- Point 18 (illustrated in Figure 100): Digital RH/T sensor mounted as part of student project *(Jacobsen and Dabelsteen, 2016)* behind a 250 mm x 250 mm Plexiglas plate. The plate was installed to mimic the microclimate behind a painting on a façade wall. This sensor point was exclusively installed on Wall 2, 4 and 7 in container C3, and Wall 1, 2, 3, 4 and 5 in container D4.

- Point 19 (illustrated in Figure 101): Digital RH/T sensor mounted as part of student project *(Jacobsen and Dabelsteen, 2016)* behind a 250 mm x 250 mm leather strip. The leather strip was installed to mimic the microclimate behind a sofa, in contact with a façade wall. This sensor point was exclusively installed on Wall 2 and 3 in container D4.

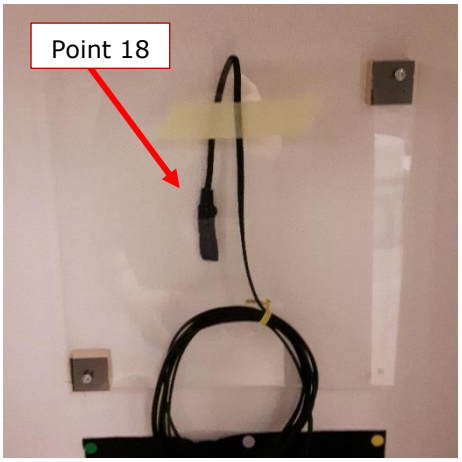


*Figure 100 Sensor Point 18: Plexiglas on interior surface. Photo from* (Jacobsen and Dabelsteen, 2016)*. Position on wall further in Figure 102.*

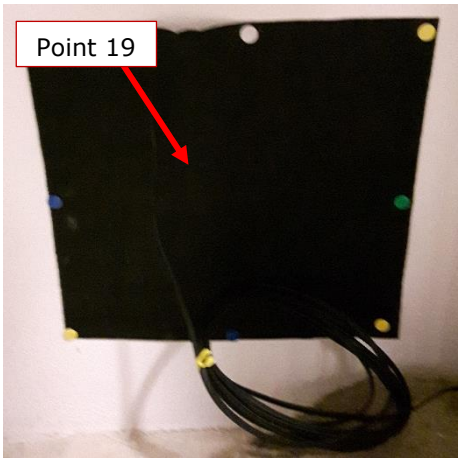


*Figure 101 Sensor Point 19: Leather strip on interior surface. Photo from* (Jacobsen and Dabelsteen, 2016)*. Position on wall illustrated in Figure 102.*

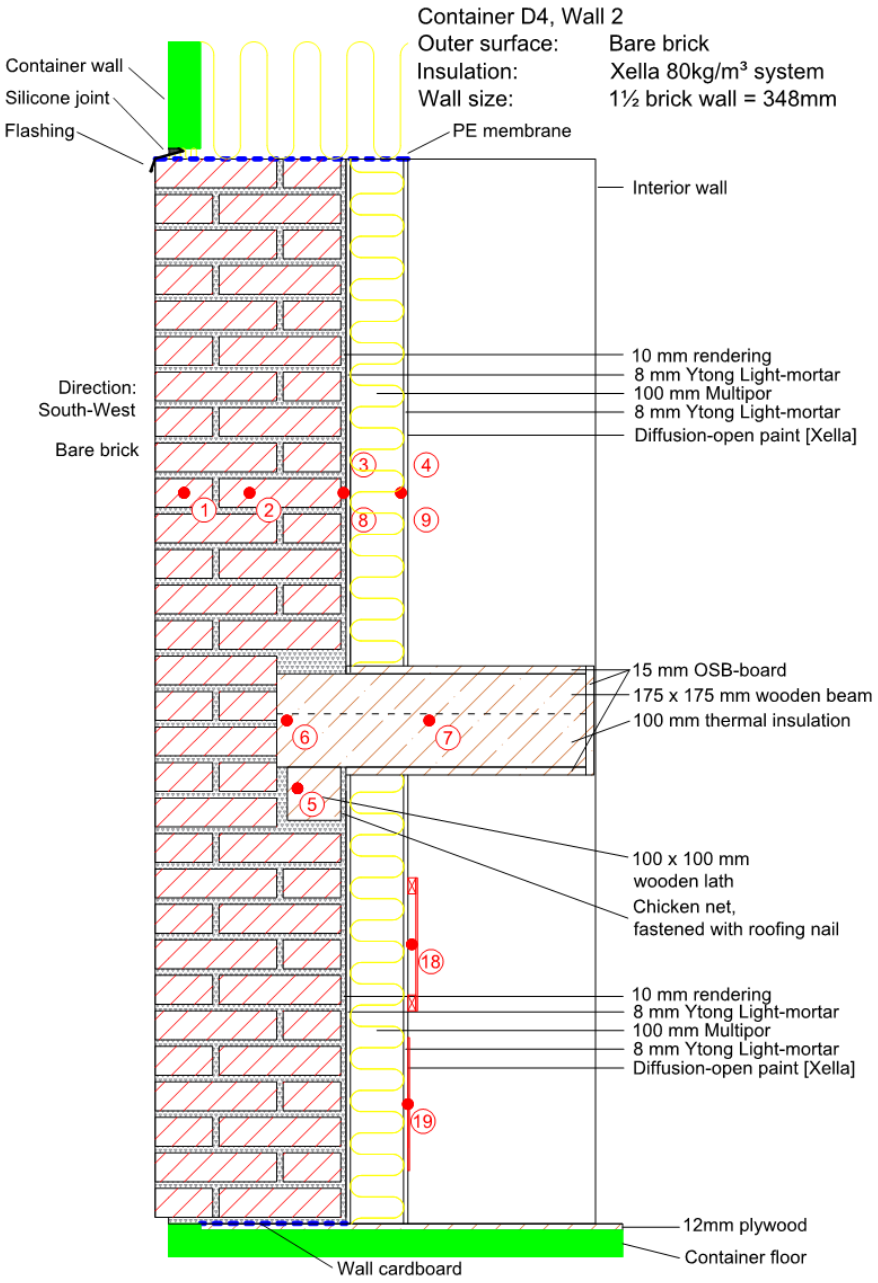


*Figure 102 Drawing of Wall 2 in container D4 to illustrate placement of sensor Point 18 & 19. Specific location described in (Jacobsen and Dabelsteen, 2016).*

- Point 23-26: Four digital RH/T sensors. These sensor points were exclusively installed in Wall 16 in container C3 (HygInsu thermal insulation system).

- Additional DC electrical resistance measurement points (illustrated in Figure 103): Three additional measurement points, based on normal metal screws, connected to 1-mm² wires and protected with silicone on the surface against direct influence from surface moisture. Installed to measure DC electrical resistance manually and monitor the moisture content in the wall plate at three different points: Blue wire = top of wall plate, close to digital RH/T sensor Point 5; brown = bottom of wall plate, close to digital RH/T sensor Point 5; yellow/green = bottom of wall plate, at intersection with partition. These sensor points were exclusively installed in Wall 4 and 5 in container D4.

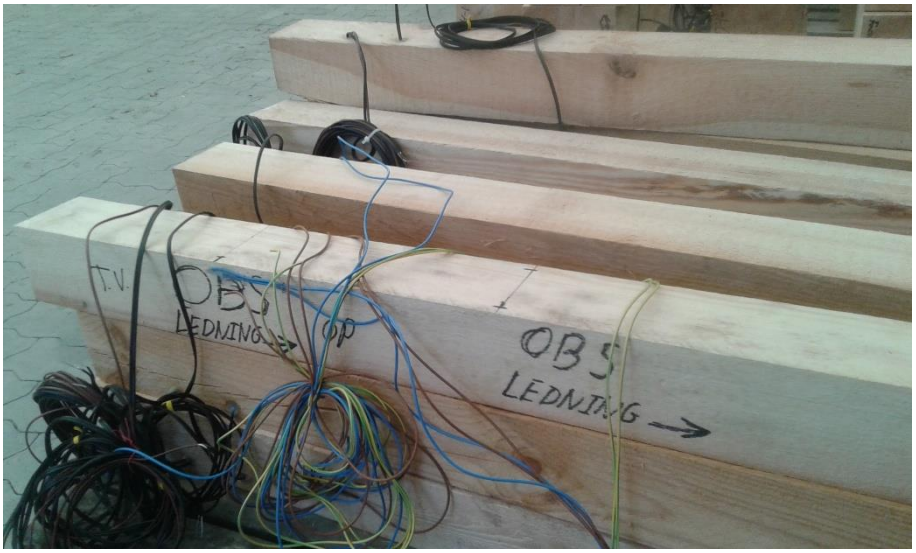


*Figure 103 Additional DC electrical resistance measurement points connected to blue, brown and yellow/green wire.*

## 5.3 *Discussion of results from field experiments*

The focus of the analysis performed in Section 5 of this PhD Thesis is on a comparative analysis of the hygrothermal performance of a moisture-tight thermal insulation system, retrofitted to a solid masonry wall with embedded wooden elements. Further results from the field experiment were presented in the appended Paper #3, with focus on variations of a moisture-open thermal insulation system in container D4.



The comparative analysis in Section 5 was performed based on the following wall setups:

- Wall 1 in container C3, illustrated in Figure 105. This system consists of a moisture-tight system, applied to the interior masonry surface. The system was installed following current Danish guidelines (Brandt et al., 2013), based on mineral wool placed within a wooden frame, finished with a vapour barrier and a Gypsum board on top. Sensor Point 3, 4, 8 & 9 were placed between the interior masonry surface and the vapour barrier, on the cold and hot side respectively of the mineral wool. The placement of sensor Point 4 & 9 is illustrated in Figure 104.
- Wall 3 in container C3, illustrated in Figure 106. This system consists of a reference wall facing the same direction as Wall 1.

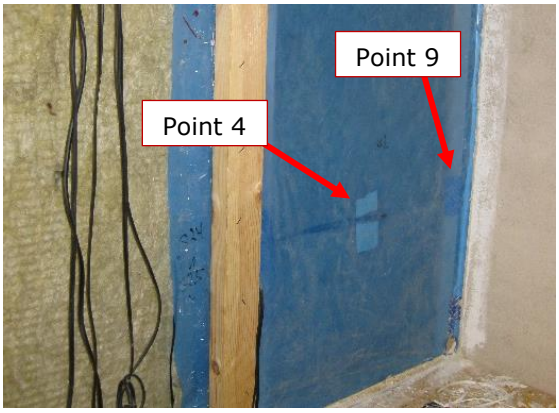


*Figure 104 Container C3, Wall 1: Gypsum board removed to expose vapour barrier during mould investigation in February 2017. Gypsum board reinstalled afterwards.*

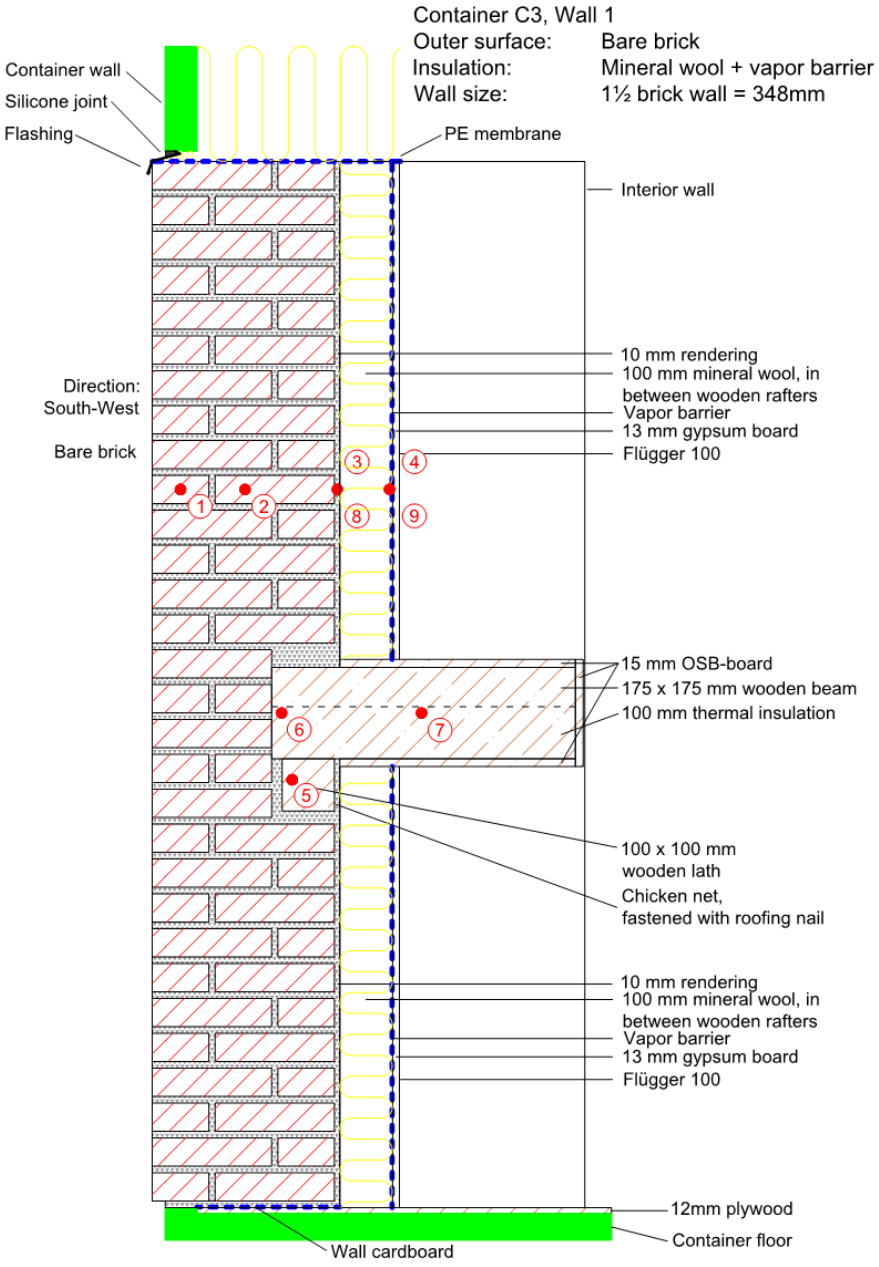


*Figure 105 Drawing of Wall 1 in container C3. Location within container illustrated in Figure 70.*

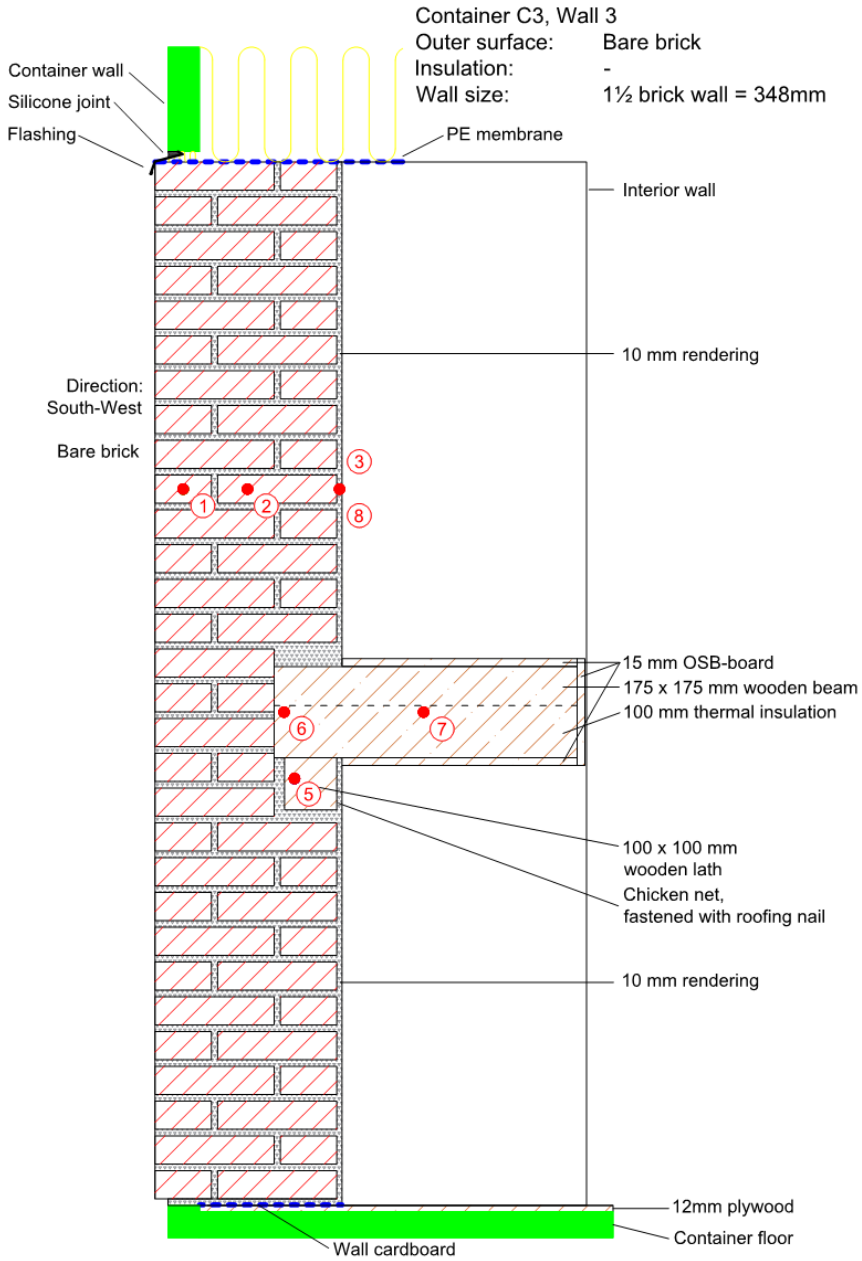


*Figure 106 Drawing of Wall 3 in container C3. Location within container illustrated in Figure 70.*

The indoor conditions in container C3 and D4 vary despite identical set points of the containers individual heating and humidifier systems. The in- and outdoor conditions for container C3 have been illustrated in Figure 107, where the WDR have been calculated as described in general in Section 2.2.3 on page 32 and specifically for the containers in Section 5.2.3.1 on page 119. The measured WDR values follow the calculated values from the DTU climate station in the period before the gauges were installed and during periods with faults in logging of the WDR measurements.

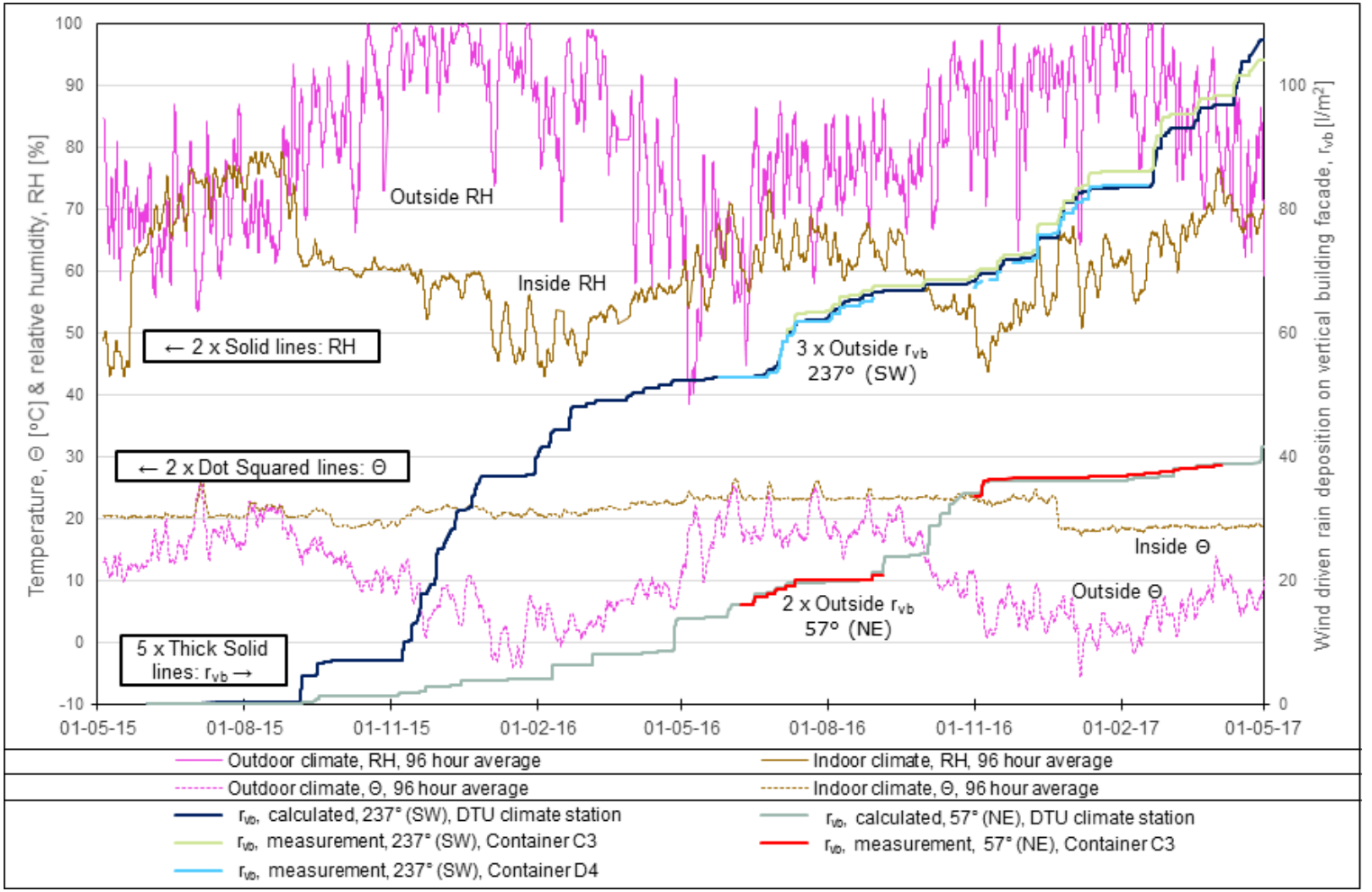


*Figure 107 96-hour averages of indoor and outdoor boundary conditions in container C3. $r_{vb}$ values in period with missing data follow calculated $r_{vb}$ values from DTU's climate station.*

The 96-hour averages of measurements in sensor Point 3 and 4 in Wall 1 and 3 of container C3 have been plotted in Figure 108. The study in the appended Paper #3 found that the thermal conditions in the walls took 3 months to stabilize, while the moisture conditions in the walls took 1 year. The starting point of all plots in Section 5 have been defined as after moisture conditions stabilized. The mould index has been calculated from mathematical models previously presented in Section 2.3.1, based on non-smoothened measurement data, with starting point after the moisture conditions have stabilized.

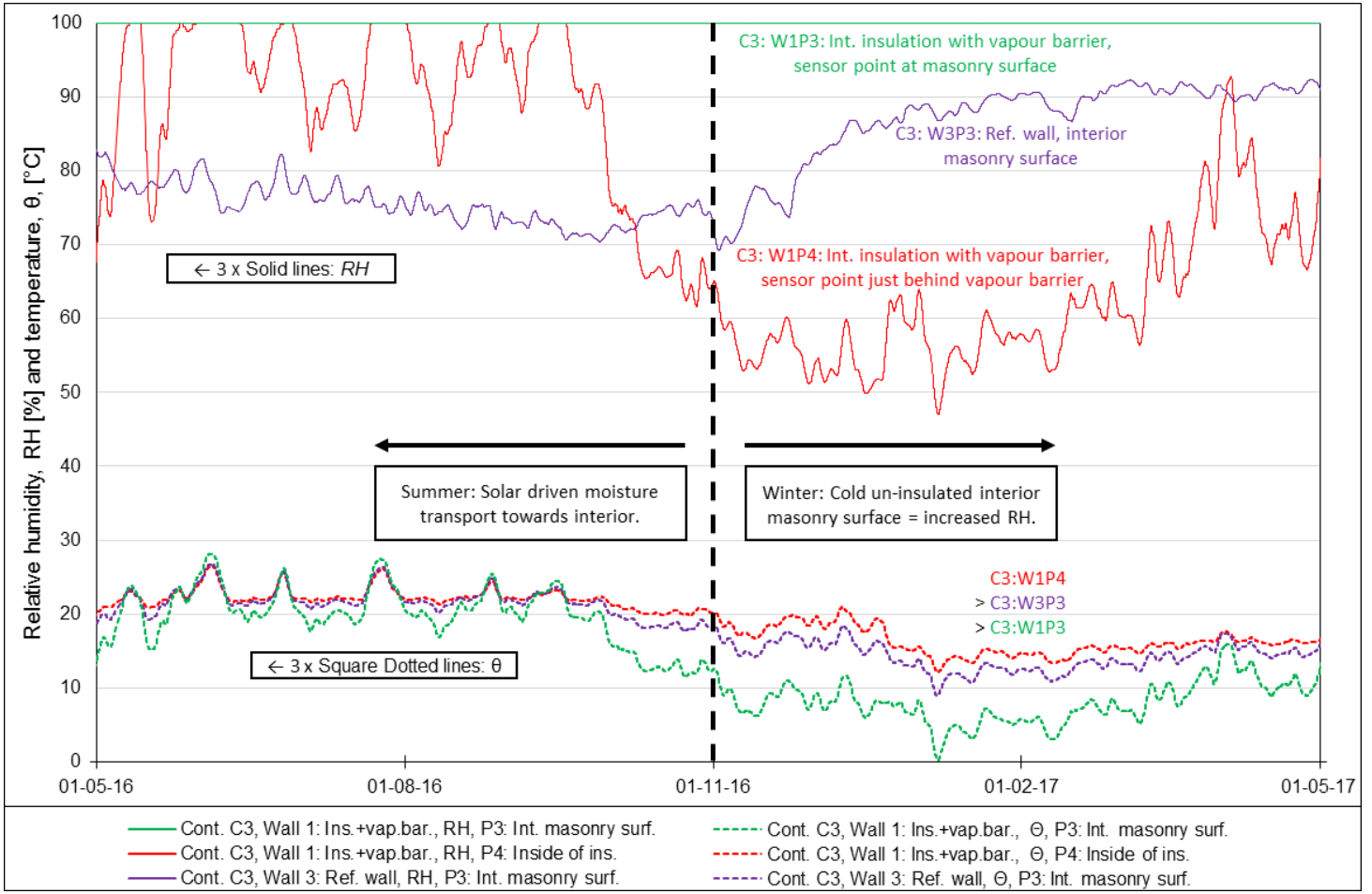


*Figure 108 96-hour average of measured temperature and relative humidity. Mould index is calculated based on non-smoothened values. Results from Wall 1 (illustrated in Figure 105) and Wall 3 (illustrated in Figure 106), measurement Point 3 (illustrated in Figure 93) and Point 4 (Figure 95), locations of both further illustrated in Figure 66.*

Using the reference Wall 1 as point of reference, the expected effect of applying thermal insulation to the interior masonry surface are observed: The temperature in Point 3 on the interior surface of the masonry wall are reduced. The reduction relates to the decreased contribution of heat from the indoor environment. The combination of the changed thermal conditions and the lack of possibility for evaporation to the indoor environment result in constant relative humidity at level equivalent to saturated vapour pressure at the masonry surface.

Comparing the surface measurements in the reference wall with measurements from the insulated wall in sensor Point 4, behind the vapour barrier, a similar tendency is seen:

- High/increasing observed relative humidity during the summer period May until September 2016.

- Low /decreasing relative humidity during the winter period October 2016 until March 2017.

The increasing and decreasing tendencies are opposite to that of the reference wall, with relative humidity increasing when entering the winter period, resulting in high indoor relative humidity in the ambient air reaching the cold interior surface.

Summarizing: The hygrothermal conditions when applying interior thermal insulation to the interior solid masonry surface based on a moisture-tight system are:

- Improved during winter periods.

- Worsened during summer periods.

The measured non-smoothened hygrothermal conditions have been used as input in mathematical models for calculating mould germination and growth (Hukka and Viitanen, 1999; Ojanen et al., 2010), with the materials defined as resistant and a decline factor of 0.1. The results show:

- Wall 1, Point 3 (Interior insulation applied, at interior masonry surface):
  - The mould index increases constantly during the period, reaching M = 1.6 after 1 year of calculation.

- Wall 1, Point 4 (Interior insulation applied, behind vapour barrier):
  - The mould index only increases in the summer period, reaching M = 0.5 after one year of calculation.

- Wall 3, Point 3 (Reference wall, at interior masonry surface):
  - The mould index only increases during the winter period, reaching M = 0.2 after one year of calculation.

The mould germination and growth rate are further illustrated visually based on isopleths for resistant materials. As previously presented in Section 2.3.1 on page 36, the isopleths are inaccurate, but very strong visual tools for illustrating how the combination of temperature and relative humidity in periods can result in mould germination/growth. The force of the used mathematical models is the possibility to take the duration of combined conditions within each limit into account and calculate the resulting increase. The plotted values are based on measurements in 5 days in August 2016 and 5 days in January 2017, being periods with combined conditions favourable for mould germination/growth in the measurement point closest to the interior surface in Wall 1 or 3. The mould germination and growth isopleths can be seen in Figure 109 and Figure 110 respectively for the interior surface of insulated Wall 1, and Figure 111 and Figure 112 respectively for the interior surface of reference Wall 3.

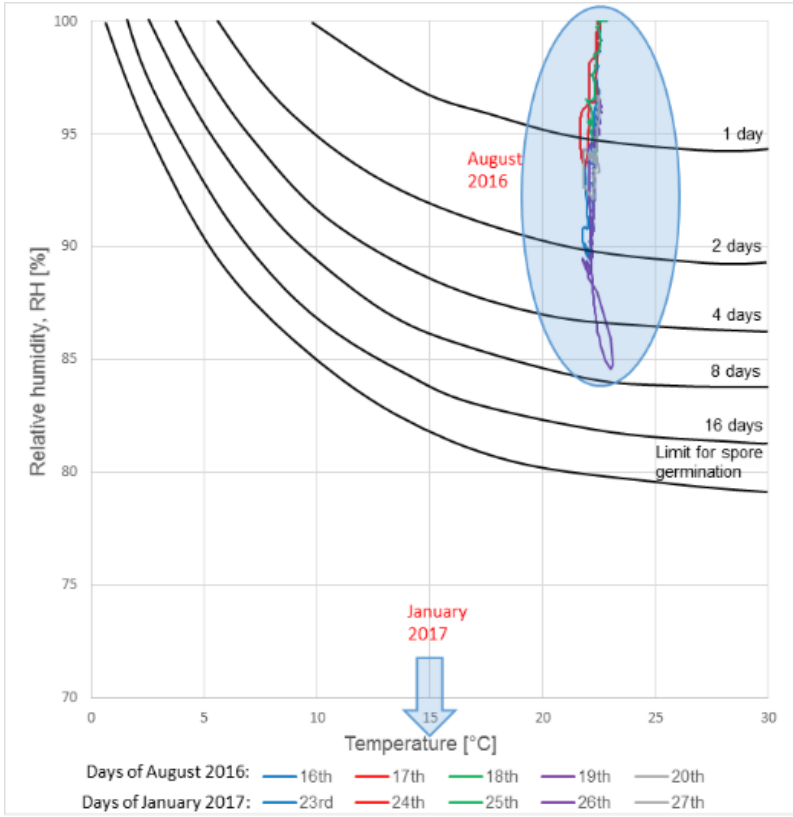


*Figure 109 Measurements plotted in scatter plot against isopleth for spore germination.*

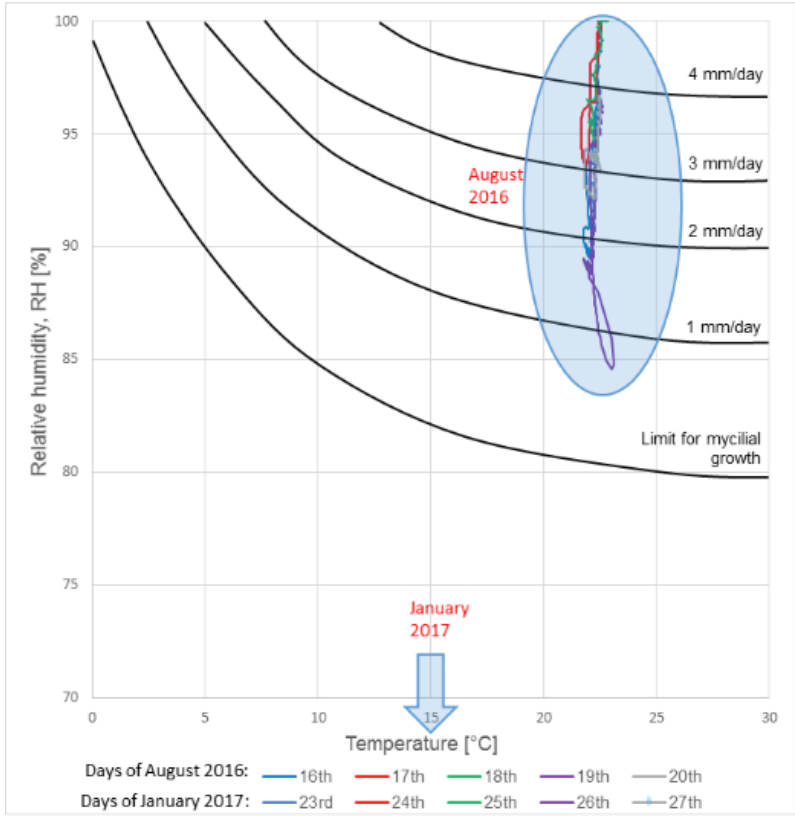


*Figure 110 Measurements plotted in scatter plot against isopleth for mycelia growth, after spore germination.*

*Figure 109 and Figure 110 are based on measured non-smoothened temperature and relative humidity in August 2016 and January 2017, coloured for each day, from Wall 1 (illustrated in Figure 105), Point 4 (illustrated in Figure 95, Figure 66).*

*The used germination and growth isopleths have been defined by Sedlbauer, from a large group of different mould types (Sedlbauer, 2002). The used isopleths are for substrate group II (renderings and non-biological insulation materials.*

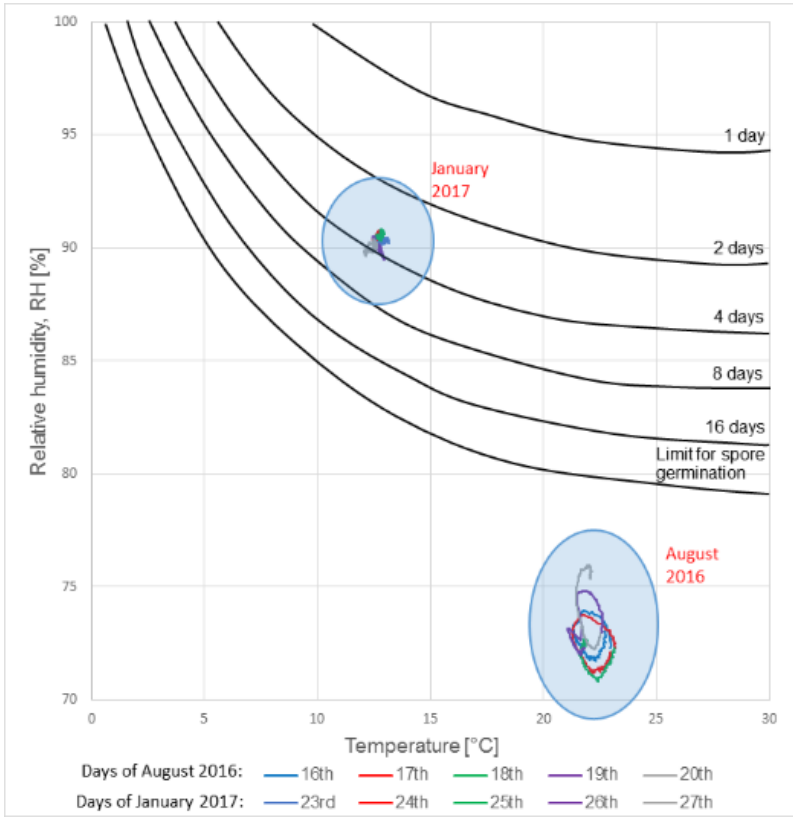


*Figure 111 Measurements plotted in scatter plot against isopleth for spore germination.*

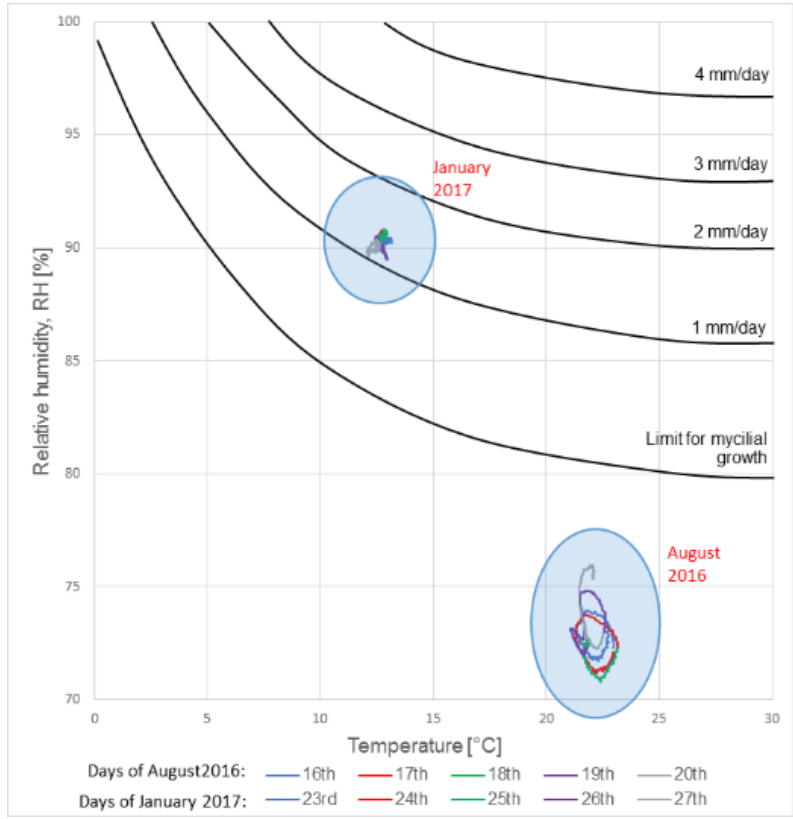


*Figure 112 Measurements plotted in scatter plot against isopleth for mycelia growth, after spore germination.*

*Figure 111 and Figure 112 are based on measured non-smoothened temperature and relative humidity in August 2016 and January 2017, coloured for each day, from Wall 3 (illustrated in Figure 106), Point 3 (illustrated in Figure 93, Figure 66).*

*The used germination and growth isopleths have been defined by Sedlbauer, from a large group of different mould types (Sedlbauer, 2002). The used isopleths are for substrate group II (renderings and non-biological insulation materials.*

The 96-hour averages of the temperature and relative humidity measurements in Point 5 and 6 in Wall 1 and 3 have been plotted in Figure 113 and Figure 114 respectively. The measured temperature in the summer period, May until October, is close to identical, while differences are observable outside these periods, where it is clear that the application of interior insulation reduces the 96-hour average temperatures in the wall plate and wooden beam end by approximately 2.5 °C. For both walls, the highest temperature in the two points are observed in the wooden beam end, with larger difference between the temperatures of the wall plate and wooden beam end in the insulated case.

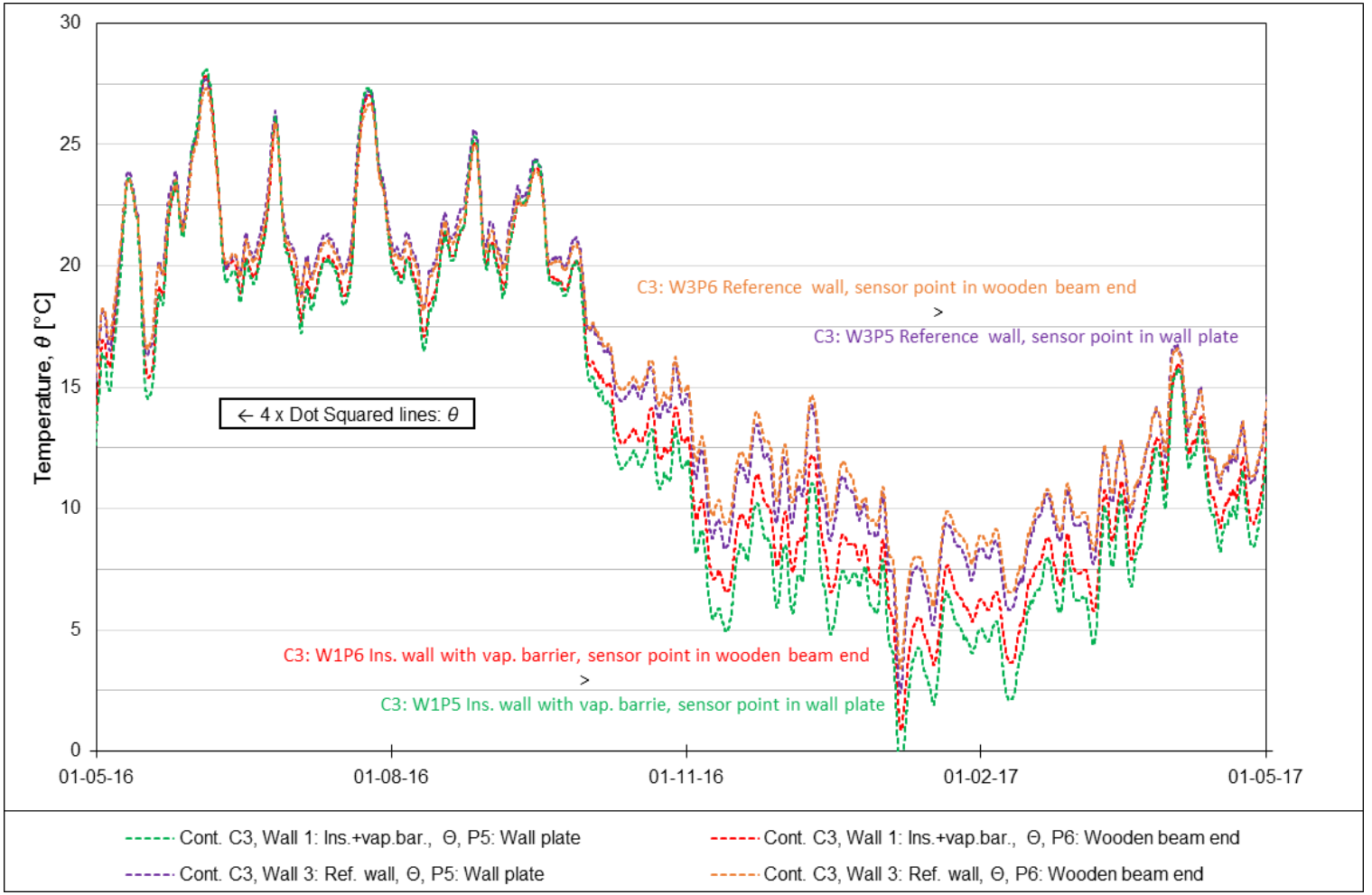


*Figure 113 96-hour average of measured temperature. Results from Wall 1 (illustrated in Figure 105) and Wall 3 (illustrated in Figure 106), measurement Point 5 (illustrated in Figure 96 and Figure 97) and Point 6 (Figure 98), locations of both further illustrated in Figure 66.*

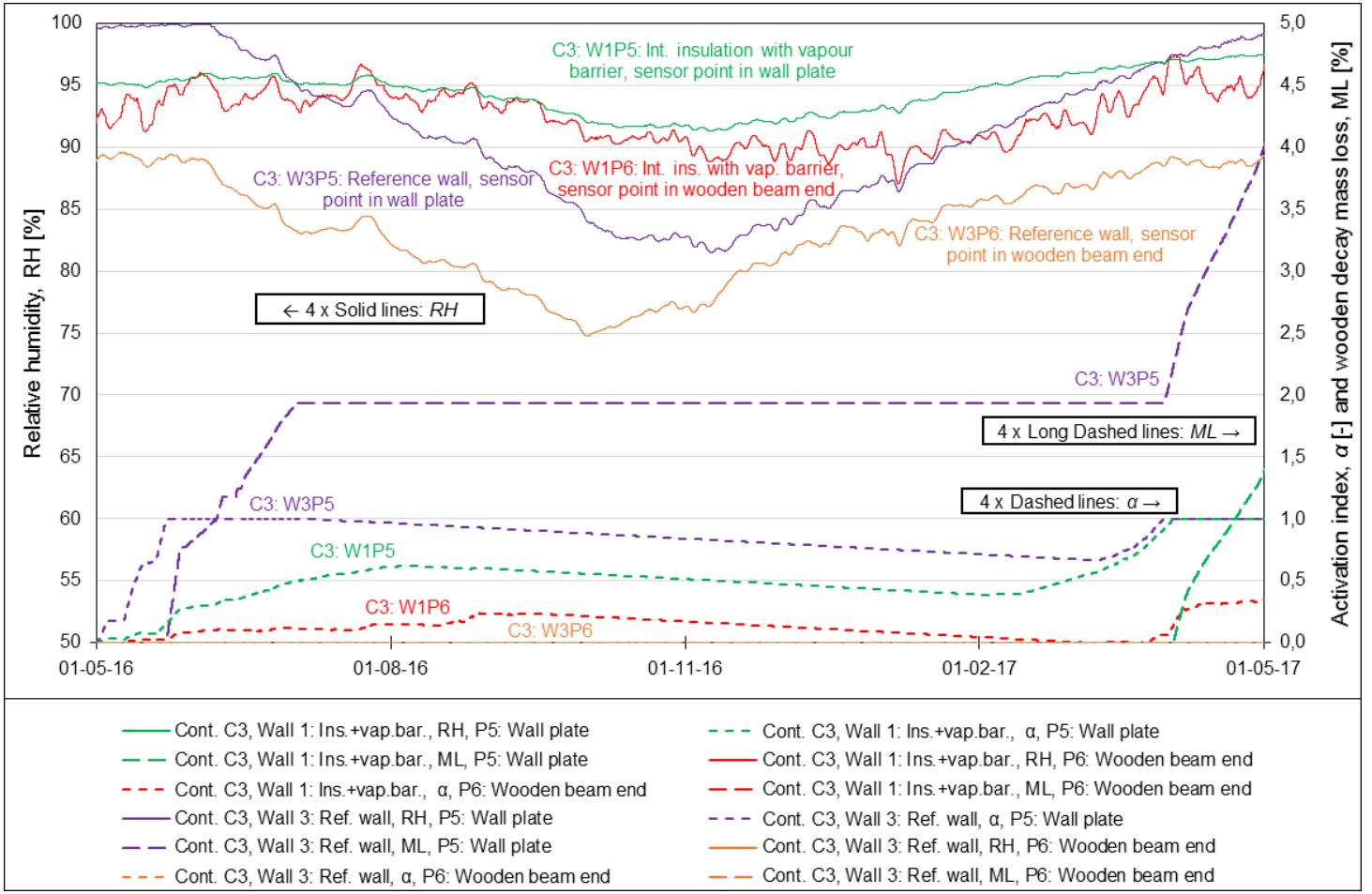


*Figure 114 96-hour average of measured relative humidity. Activation index and wooden decay mass loss is calculated based on non-smoothened temperature and relative humidity values. Results from Wall 1 (illustrated in Figure 105) and Wall 3 (illustrated in Figure 106), measurement Point 5 (illustrated in Figure 96 and Figure 97) and Point 6 (Figure 98), locations of both further illustrated in Figure 66.*

Looking onto the 96-hour average values of measured relative humidity in Figure 114, a clear difference between the values from the reference Wall 1 and insulated Wall 3 can be seen. While the values for the un-insulated wall vary with approximately 15 % RH over the course of the year, the insulated wall have a steadier level, vary with approximately 7.5 % RH over the course of the year. The influence of the difference in relative humidity for the wooden elements are evaluated by mathematical wooden decay models previously presented in Section 2.3.2, based on non-smoothened measurement data. The resulting activation index and wooden decay mass loss have been plotted in Figure 114. The following is found in a comparative analysis of the theoretical calculated wooden decay mass loss, where the activation index and next the irreversible wooden decay mass loss increase as relative humidity levels > 95 % RH and temperature > 0 °C, with speed depending on the magnitude of the conditions:



- Wall 3, Point 5 (Reference wall, in wall plate):
  - The wall plate in its original state is troubled, when stressed with a constant high indoor relative humidity of 60 % RH, which in May 2016 and 2017 result in activation index $\alpha = 1$ and thereby development of theoretical irreversible wooden decay mass loss. This emphasise the need to ventilate and limit the indoor excess of moisture in historic multi-storey buildings.
- Wall 3, Point 6 (Reference wall, in wooden beam end):
  - As the activation index stay at $\alpha = 0.0$, no calculated risk of wooden decay is predicted.
- Wall 1, Point 5 (Interior insulation applied, in wall plate):
  - The activation index increases to $\alpha = 0.6$ in May-August 2016, further developing to $\alpha = 1.0$ in February 2017, resulting in starting irreversible wooden decay mass loss. Results from comparative analysis show less theoretical wooden decay mass loss than the reference case.
- Wall 1, Point 6 (Interior insulation applied, in wooden beam end):
  - Minor activity is seen in the activation process, with highest registered $\alpha = 0.4$ in May 2017. Irreversible wooden decay mass loss has not started, but comparative analysis show that the situation is worsened compared to the reference wall.

### *5.3.1* Reference measurements with DC electrical resistance measurements in wooden dowel in wall plate

The measurements from the digital RH/T sensors in Point 5, the wall plate, was tested by referencing the monitored values with the manual DC electrical wooden resistance measurements in the same medium, calculated into relative humidity.

The following measurements are included in Figure 115:

- Measured DC electrical wooden resistance.
- Temperature in the digital sensor at the time of investigation.
- The relative humidity calculated from the resistance measurement.
- The relative humidity measured by the digital RH/T sensors.

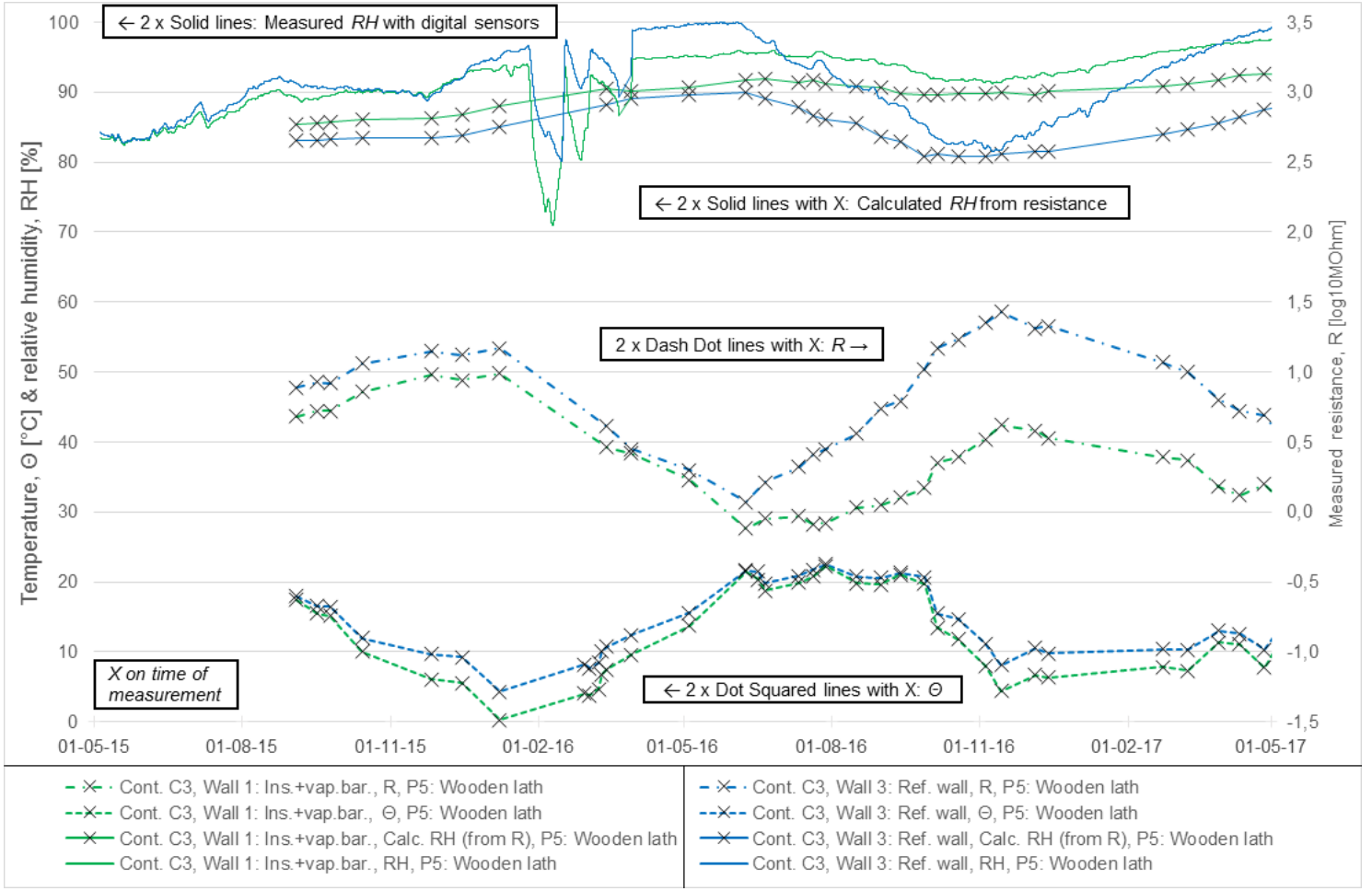


*Figure 115 Manual measured DC electrical wooden resistance, temperature from digital measurement at same time step, calculated relative humidity and relative humidity from digital sensors in wall plate: Point 5.*

The relative humidity from the wooden dowel and digital sensors do not show similar results. The reasoning for this had to be investigated.

It has been assumed that the method described in Section 2.4.1 on page 44, converting DC electrical wooden resistance and temperature to wooden weight-%, is correct since the method follows the procedure from the producer of the dowels. The investigation instead focused on the method described in Section 2.4.2 on page 46, converting wooden weight-% to relative humidity, via sorption isotherms for beech wood.

Every calculated wooden weight-% and relative humidity measured in the period May 1st 2016 until May 1st 2017 has been plotted in Figure 116, along with the used ad- and desorption isotherms for beech wood at 20 °C. As described in Section 2.4.2, the conversion from wooden weight-% to relative humidity is based on average ad- and desorption RH values, and thereby with no concern to hysteresis/scanning curves. This simplification to average values, leaves a wide uncertainty range, marked with transparent fill in Figure 116.

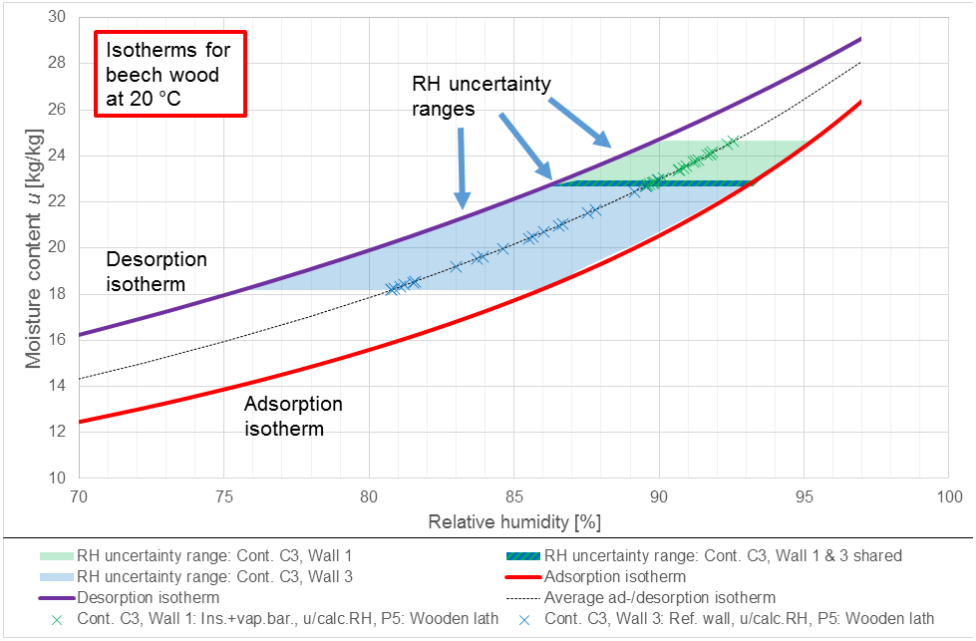


*Figure 116 Calculated wooden moisture mass percent and calculated equivalent relative humidity based on average of ad- and desorption isotherm after stabilization of measurements. Areas with transparent fill illustrate possible real RH due to hysteresis/scanning curves. Further error from transient temperature ≠ 20 °C not included. Enlarged version in Figure 153 on page 214.*

The uncertainty range for each measurement in wooden dowels has been marked in Figure 117 as areas with transparent fill, showing the range of possible relative humidity for each point. The amplitude of the RH-values can be expected to be larger when scanning is considered, which corresponds well with the amplitude of the digital sensors. If scanning is considered, the result should tend towards the lower parts of the interval marked by the areas with transparent fill in periods of drying (summer and early fall) and tend towards the upper parts in periods of wetting (winter and early spring). The relative humidity measured by the digital RH/T measurements is only inside these uncertainty ranges in the limited period, October-December 2016, and outside the areas with transparent fill in the remaining months. The inclusion of hysteresis/scanning curves will thereby not improve the correspondence between digital RH/T sensors and DC electrical wooden resistance.



The difference in hygrothermal mass between the two sensor types will result in a time difference for the measurements, as the wooden dowels hygroscopic ability to store water is larger than for the digital sensor. Based on this, calculated relative humidity from the DC electrical resistance measurements in the wooden dowels will be slower than for the digital RH/T sensor. This time difference can however neither explain the lack of correspondence between digital RH/T sensors and DC electrical wooden resistance measurements.

The lack of correspondence between digital RH/T sensors and DC electrical wooden resistance is instead determined to relate to the magnitude of the wooden moisture content. At moisture content above 15 %, the wooden dowel underestimate the level of moisture, and can only be used to indicate changes in relative wetness (Walker et al., 2016). As the moisture content in both wooden dowels in Wall 1 & 3, Point 5 are above 15 % throughout the year (corresponding to 66-72 % RH, depending on state of hysteresis), the dowels can thereby only show changes in relative wetness in this actual case. The increase and decrease of relative wetness do follow the measurements from the digital RH/T sensors in Figure 117.

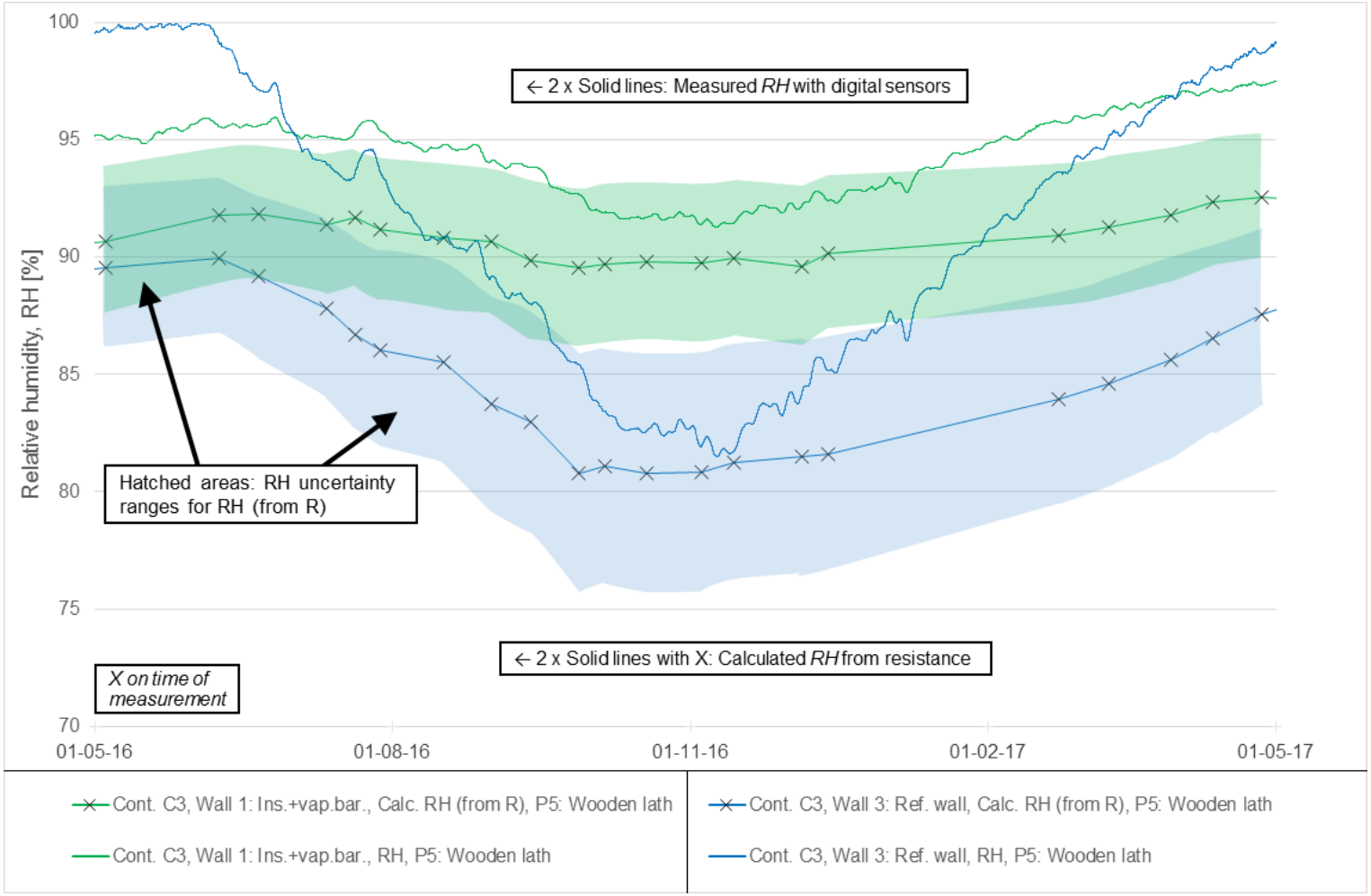


*Figure 117 Calculated RH from DC electrical resistance measurements including uncertainty ranges due to hysteresis/scanning curves, compared to measured RH from digital sensors. Further error relating to transient temperature ≠ 20 °C not included. Enlarged version in Figure 154 on page 215.*

## 5.4 *Sub-discussion of hypotheses*

The section will discuss the goals of the sub-hypotheses, previously presented in Section 1.3.1 and Table 1. The structure of the section is comprised of a repetition of the sub-hypothesis goals, following an individual discussion of each goal.

Based on the current state of the field experiment, the measurements have so far only been used for comparative analyses. This means that the measurements and calculated mould index and wooden decay have been used to show how various walls, with or without an interior insulation system, perform and thereby if the individual system perform better/worse than each other and uninsulated walls.



**Sub-hypothesis #4, goal 1** is defined as: "*A clear difference between the initial stabilization period and stabilized measurements can be identified for relative humidity and temperature measurements*".

The stabilization period was identified in Sec. 3 of the appended Paper #3. The evaluation of the stabilization period was based on the course of the measurements, identifying when recurrence of comparable yearly measurements developed. It was found that the length of the stabilization period differed for temperature and relative humidity measurements, noting that even though moisture conditions do have an influence on the thermal properties, this influence was assessed as minimal.

It was concluded that the period from application of transient boundary conditions, until stabilized measurements could be used for a comparative analysis, was:

- 3 months for thermal measurements.
- 1 year for relative humidity measurements.

✓ Goal 1 of Sub-hypothesis #4 is assessed as fulfilled based on the above.

**Sub-hypothesis #4, goal 2** is defined as: "*Comparative analyses show clear and explainable differences for measurements obtained from variations of an interior thermal insulation system*".

As the investigation of variations of an interior thermal insulation system was documented in the appended Paper #3, this goal will be based solely on content of the paper. All figure references within this goal are thereby referring to the appended Paper #3.

The differences in thermal measurements from different sensor points within a wall setup can be seen in Fig. 6, showing uniform low temperatures in the wooden elements and at the interior masonry surface behind the thermal insulation, with

increasing temperature at the interior surface of the deliberate thermal bridge (sensor Point 10) until the highest registered temperatures at the interior surface of the thermal insulation. Thermal measurements from the same sensor Point 5 (wall plate) have been compared in Fig. 7, showing uniform low temperatures in wall plates with insulation applied on the interior surface, increasing when replacing thermal insulation with a deliberate thermal bridge until the highest registered temperature in an un-insulated construction.

- ✓ Based on the above, it is concluded that temperature measurements from different measurement points are clear and explainable.

Relative humidity measurements at the interior masonry surface, behind internal thermal insulation, can be seen in Fig. 9. A clear difference between the measurements from the Wall 2 and Wall 3/6 are identified, with construction details differing with a bare brick surface of Wall 2, and hydrophobized bare brick for the other walls. The measurements in the equivalent constructions at the measurement point of Wall 3 and 6 (red and black line respectively) do as expected show similar measurements.

Relative humidity measurements and calculated relative humidity from DC electrical resistance measurements in the wall plate for 3 variations of a thermal insulation system and a reference wall can be seen in Fig. 11. The measurements are illustrated without marking of the stabilization period, and it can be seen how the relative humidity and the calculated relative humidity follow the same tendency with a distinct difference between the different measurements. Note that the DC electrical resistance measurements are further treated in Independent-hypothesis #1.

- ✓ Based on the above, it is concluded that relative humidity measurements from different measurement points are clear and explainable.

✓ As it is concluded that the temperature and relative humidity measurements are clear and explainable, goal 2 of Sub-hypothesis #4 is assessed as fulfilled.

**Sub-hypothesis #4, goal 3** is defined as: "*There is a clear and explainable difference in hygrothermal behaviour for moisture-tight and moisture-open insulation systems when retrofitted to an interior masonry surface*".

This goal is based on measurements documented in Section 5.3 and the appended Paper #3. The measurements have been joined into Figure 118 and Figure 119, showing similar measurement points in walls retrofitted with moisture-tight or moisture-open thermal insulation systems, with an exterior bare brick surface and no variations from the standard insulation system. The most distinguished difference between measurements from the two systems can be seen for measurement Point 4 in Figure 118, showing:

- During the summer period: Solar driven moisture transport towards the interior, resulting in a build-up of moisture behind the vapour barrier in the moisture-tight system. The moisture-open system for the moisture diffusion to continue towards the interior climate.
- During the winter period: The interior moisture load result in a build-up of moisture in the moisture-open insulation system. The vapour barrier of the moisture-tight system isolates against the interior moisture load, while moisture transport towards the exterior allows for emission of moisture build-up during the summer period.
    - ✓ It is concluded that there is a clear and explainable difference for measurements behind the vapour barrier/in the surface of the insulation material for moisture-tight and moisture-open systems.



Comparative analysis of measurements at Point 3 in the interior masonry surface show relative humidity condensation values for both types of thermal insulation systems, with only a small decline for the moisture-open system in the end of the summer. This indicates that the masonry behind the moisture-tight system is wetter than the masonry behind the moisture-open system.

- ✓ The measurements from Point 3 must be evaluated with the measurements from the wooden beam end, showing similar higher degrees of moisture in the wooden beam end behind the moisture-tight system. Based on results from the two measurement points, it is concluded that there is a clear and explainable difference for measurements in the interior masonry surface for moisture-tight and moisture-open systems.

The measurements in the embedded wooden elements illustrated in Figure 119 show the following:

- Measurements in Point 5, the wall plate, show high relative humidity values throughout the year, with values from the moisture-tight system generally a little higher than for the moisture-open systems. The combination of RH and temperature have been calculated into activation index, α, illustrating activation of wooden decay with α = 1.0. The calculated activation index shows similar conditions favourable for wooden decay in both constructions.
    - ✓ It is concluded that no clear difference can be found between measurements in the wall plate for moisture-tight and moisture-open systems.

- Measurements in Point 6, the wooden beam end, show overall significantly less moisture in the moisture-open system, than with the moisture-tight

system. The measurements in the moisture-tight system is more favourable for wooden decay.

- ✓ The measurements from Point 6 must be evaluated with the measurements from the interior masonry surface, showing similar higher degrees of moisture in the masonry behind the moisture-tight system. Based on the two measurement points, it is concluded that there is a clear and explainable difference for measurements in the wooden beam end for moisture-tight and moisture-open systems.

✓ Goal 3 of Sub-hypothesis #4 is assessed as fulfilled based on the above.

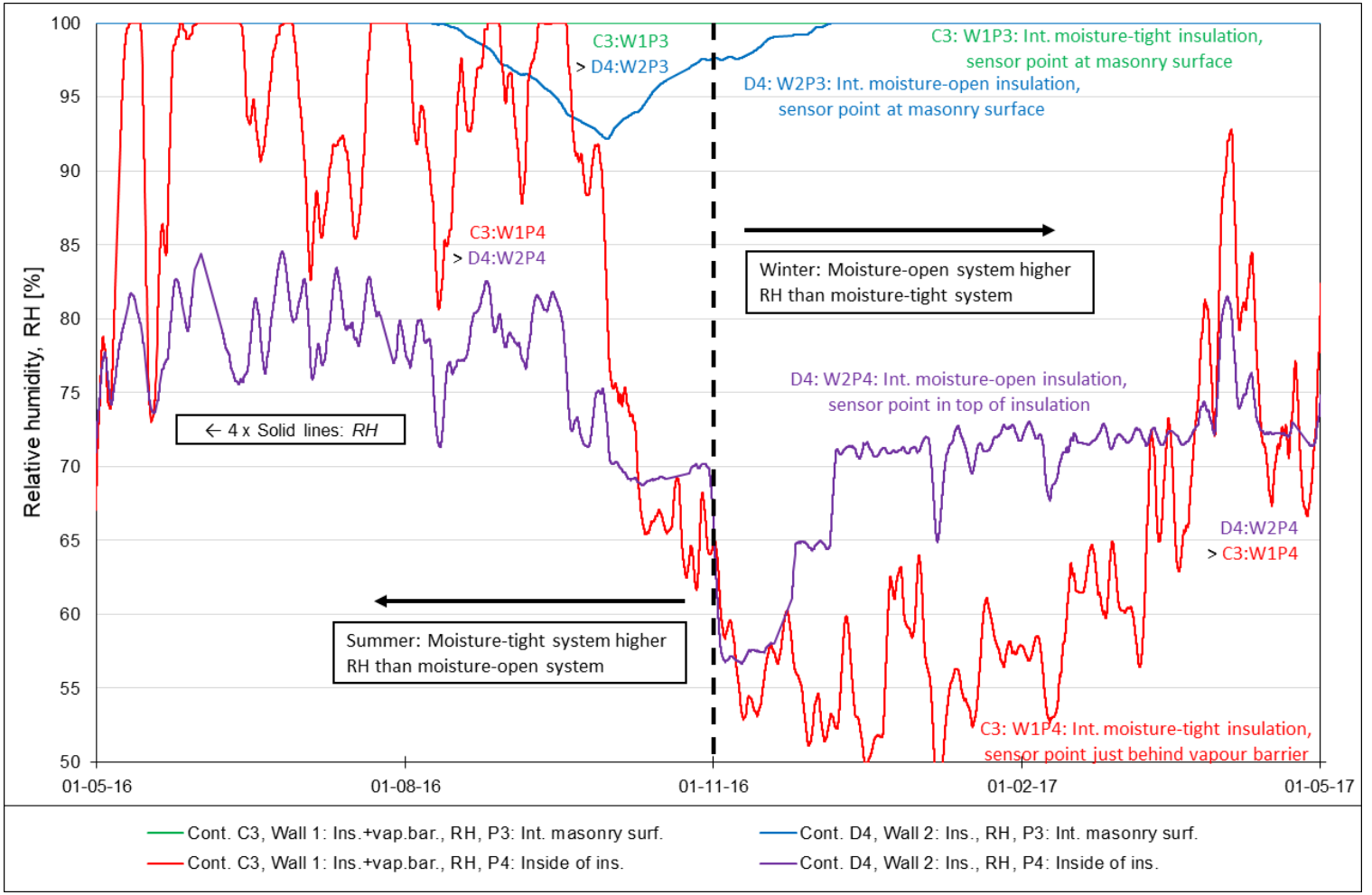


*Figure 118 Measurements at masonry and insulation surface. Figure is a compilation of Figure 108 of this Thesis and Fig. 8 and Fig. 9 and of the appended Paper #3*

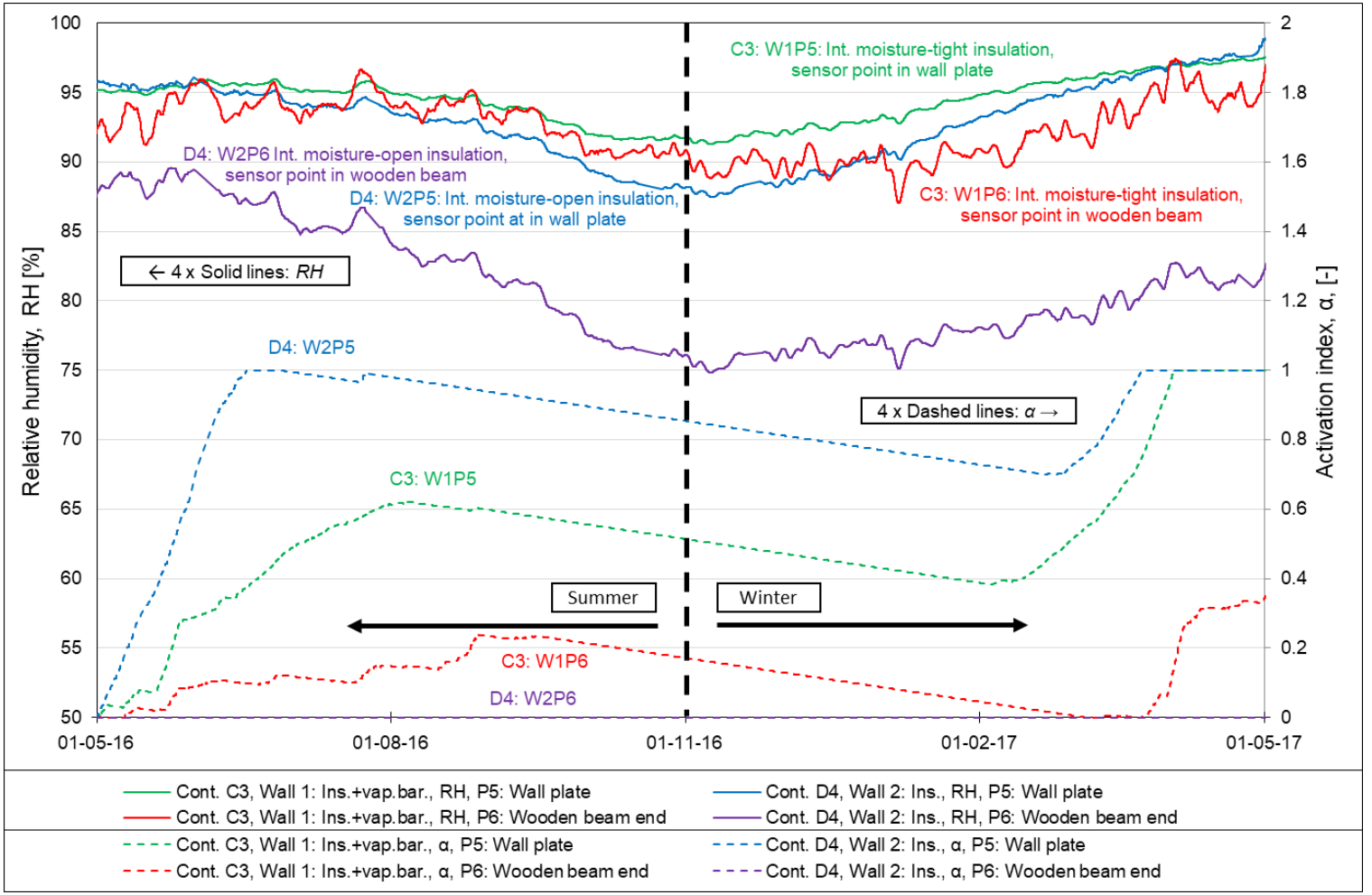


*Figure 119 Measurements in wooden beam end and wall plate. Figure is a compilation of Figure 114 of this Thesis and Fig. 10 and Fig. 12 of the appended Paper #3*

**Sub-hypothesis #4, goal 4** is defined as: "*The effect of wind driven rain can be observed by relative humidity measurements in the embedded wooden elements*".

As Sub-hypothesis #4, goal 4, was investigated in Sec. 3.4 of the appended Paper #3, this goal will be based solely on content of the paper. All section and figure references within this goal are thereby referring to the appended Paper #3.

It was documented in Sec. 3.4 in Fig. 14 that, based on non-smoothened measurements from moisture-open systems in the embedded wooden elements during the summer period:

- Depositing 7.3 l/m² of wind driven rain over 10 days resulted in a short-term increase in relative humidity 9 days after the end of this rain event.
- A less intense, but longer rain event, in August 2016 resulted in a similar, but smaller increase measured in relative humidity.

Similar measurements during a winter period in Fig. 15 showed that rain events did not result in similar short-term increases comparable to those seen in the summer period, but that a more general increase in relative humidity characterised the period.

✓ Goal 4 of Sub-hypothesis #4 is assessed as fulfilled based on the above.

**Sub-hypothesis #5, goal 1** is defined as: "*The introduction of a deliberate thermal bridge, replacing insulation material next to the wall plate and wooden beam end, reduce the worsening of the hygrothermal conditions from retrofitting with interior thermal insulation*".

As the investigation of replacing insulation material with AAC was documented in the appended Paper #3, this goal will be based solely on content of the paper. All figure references within this goal are thereby referring to the appended Paper #3. It should be noted that the implementation of a thermal bridge in the paper was only investigated in combination with hydrophobation.

Thermal measurements in the wall plate, sensor Point 5, have been compared in Fig. 7. The measurements in the figure illustrate how the lowering of the temperature in the wall plate during winter, induced from retrofitted insulation, can be reduced by replacing thermal insulation material with a deliberate thermal bridge. The thermal bridge did further reduce the measured relative humidity in the wall plate, as illustrated in Fig. 10, resulting in reduced risk of wooden decay from the combination of higher temperature and lower RH.

The conditions in the wooden beam end was documented in Fig. 12. The figure shows how hydrophobation of the exterior surface induced a positive reduction of the relative humidity during the summer period, but a negative increase during

the winter period. This hygrothermal behaviour during the winter period was shown able to change by replacing insulation material with a deliberate thermal bridge, reducing the exterior hydrophobation induced increase in RH in the wooden beam end, to that observed in the reference and insulated wall.

✓ Goal 1 of Sub-hypothesis #5 is assessed as fulfilled based on the above.

**Sub-hypothesis #5, goal 2** is defined as: "*Hydrophobation of the exterior masonry surface reduce the worsening of the hygrothermal conditions introduced from retrofitting with interior thermal insulation*".



As hydrophobation was summed up in Sec. 3.3.7 and Sec. 4 of the appended Paper #3, this goal will be based solely on content of the paper. All section and figure references within this goal are thereby referring to the appended Paper #3.

The effect of hydrophobizing the exterior bare brick masonry surface can be seen in Fig. 12 and Fig. 13. The hydrophobizing agent was found to have a varying seasonal effect on the measured conditions in the walls. The changed seasonal hygrothermal balances of the hydrophobized walls can be summarized as:

- During winter: The hydrophobation limits the transport of moisture towards the exterior surface, thereby reducing the evaporation to the cold and dry Danish climate. The result of the hydrophobic façade treatment can be seen as a rapid increase in RH in hydrophobized walls during the winter period, especially for the wooden beam end in Fig. 12. The RH measurements in the wooden beam end illustrate that hydrophobation is not un-problematic, and this could potentially develop into a risk of wooden decay if the RH do not decrease rapidly before temperatures occur which are favourable for wooden decay.
- During summer: Hydrophobation reduce the solar driven moisture transport towards the interior, thereby reducing the measured RH in the measurement points. Reduction of RH during the summer is positive, as the high temperatures during this period are favourable for development of mould and wooden decay.

Hydrophobation of the exterior masonry surface do in overall reduce the measured yearly relative humidity in the measurement points, thereby overall reducing the worsening of the hygrothermal conditions introduced by retrofitting interior insulation.

✓ Goal 2 of Sub-hypothesis #5 is assessed as fulfilled based on the above, but a combination with a deliberate thermal bridge seem promising and should be considered.

**Independent-hypothesis #1, goal 1** is defined as: "*Calculated relative humidity from DC electrical resistance measurements in wooden dowels and digital relative humidity sensors, installed in the same wooden element, show similar results during a transient experiment. In this goal, similar is defined as +/5 %-points in relative humidity*".

This goal was treated in Section 5.3.1, after finding that the outcome from digital and DC electrical resistance-based measurements, expressed in relative humidity, did not show similar results. Comparison of DC electrical resistance measurements converted into RH, with marked uncertainty ranges from hysteresis, and digital RH measurements were done in Figure 117. The figure showed that DC electrical based measurements could not be used in such wet conditions as those observed during the field experiment.

It was found in Section 5.3.1, based on literature, that DC electrical resistance based measurements were only able to show if the construction is in a wetting or drying phase when the wooden weight-% is above 15 %, corresponding to 66 - 72 % RH (depending on the state of hysteresis).

Fig. 11 of the appended Paper #3 show similar results, with digital and DC electrical resistance-based measurements, expressed as relative humidity, not showing corresponding values. The results did however show similar tendencies, with DC electrical resistance-based measurements illustrating if the moisture conditions in the individual measurement point was in a wetting or drying phase.

/ The goal of Independent-hypothesis #1 is assessed as not fulfilled based on the above, as it was found that DC electrical resistance measurements in the wet constructions of the field experiment can only be used to indicate if the construction is in a wetting or drying phase.

## 5.5 Sub-conclusion of hypotheses

The section will conclude on the sub-hypotheses, previously presented in Section 1.3.1 and Table 1, based on the sub-discussion in Section 5.4. The structure of the section is comprised of a repetition of the sub-hypotheses treated in this section, following a conclusion if the individual sub-hypothesis can be rejected.



**Sub-hypothesis #4:** "*The hygrothermal balance in solid masonry walls with embedded wooden elements, combined with various types of interior thermal insulation systems and exterior surface treatments, can be evaluated in controlled field experiments exposed to real weather* conditions".

✓ Sub-hypothesis #4 cannot be rejected, as goal 1, 2, 3 and 4 of the sub-hypothesis was assessed as fulfilled.

**Sub-hypothesis #5:** "*The worsening of the hygrothermal balance when retrofitting the interior masonry surface with thermal insulation can be reduced by introducing a hydrophobic treatment to the exterior surface or a deliberate thermal* bridge on the interior side".

✓ Sub-hypothesis #5 cannot be rejected, as goal 1 & 2 of the sub-hypothesis was assessed as fulfilled.

**Independent-hypothesis #1:** "*DC electrical resistance measurements in wooden dowels can be used to monitor the development of relative humidity during a* transient experiment".

/ Independent-hypothesis #1 is rejected, as the goal of the independent-hypothesis could not be fulfilled. The independent-hypothesis showed that when exposed to the conditions in the field experiment, then DC electrical resistance measurements could only be used to indicate if the monitored part of the construction was in a wetting or a drying phase.

### *5.5.1* Outcome of new knowledge obtained in study

The part of the industrial PhD study documented in Section 5 and the appended Paper #3 have provided new knowledge, including:

> Document the setup of a large scale field experiment, designed and constructed at the Technical University of Denmark as basis for research within interior thermal insulation. This work included comparative

analyses of measurements, illustrating that it is possible to differentiate measurements from various measurement points.

> Identify the length of the stabilization period for an experiment with solid masonry walls constructed with lime adjusted mortar (air lime).

> Visualize the differences in hygrothermal behaviour from a moisture-tight and moisture-open interior thermal insulation system.

> Illustrate different variations of a thermal insulation system, able to decrease the worsening of the hygrothermal conditions in the masonry wall, thermal insulation and built-in wood:

  - Hydrophobation of the exterior bare brick surface.
    - Including the specific effect in a cold tempered climate, showing how hydrophobation reduced the relative humidity in the summer, but increased in the winter period.
  - Exchanging part of the thermal insulation material with a material with a higher thermal conductivity.

> Example of fit between wind driven rain model and measurements.

> Identify the effect from wind driven rain in embedded wooden elements of solid masonry constructions.

> Evaluating the use of DC electrical resistance measurements in wooden dowels, to measure the hygrothermal balance in a transient experiment with solid masonry walls and embedded wooden elements.

# 6 EXPERIMENTAL CASE STUDY: RETROFITTING EXISTING SPANDREL WITH THERMAL INSULATION

Section 6 concern Sub-hypothesis #6, an investigation of the hygrothermal response and risk of moisture-induced damage in a case study where an existing solid masonry spandrel in a multi-storey building have been retrofitted with interior thermal insulation.

The investigation includes clarifying the reason for retrofitting interior thermal insulation, based on a preservation and comfort point of view. It includes an extensive damage evaluation of the monitored values, based on mathematical models and physical tests for mould, wooden decay and frost.

## 6.1 *Summary of paper related to Section 6*

The section is based on the appended Paper #2: "Interior insulation - Experimental investigation of hygrothermal conditions and damage evaluation of solid masonry façades in a listed building".

The content of the paper have generally been included in an extended version throughout Section 6 and as part of the theory presented in Section 2, with an exception of the physical on-site test for active mould growth via the Mycometer®-test. The Mycometer®-test results are included in Section 6.3.3, while the theory are included in Sec. 2.6 of the appended Paper #2.

## 6.2 *Method: Description of the case study*

The experiment was performed in a historic and listed multi-storey building, Borchs dormitory, built in 1823 and located in the centre of the Danish capital. The investigated façade area was facing northwest and situated at the 1st floor (2nd in American terms), with a construction consisting of solid masonry walls with masonry columns and thin spandrels, rendered and painted on the interior and exterior surface as illustrated in Figure 120. A floorplan of the investigated rooms can be seen in Figure 121.

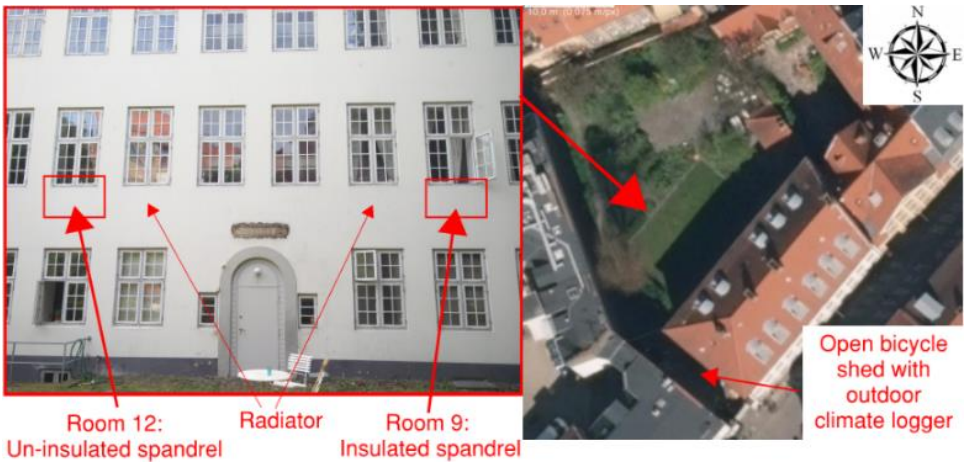


*Figure 120 Façade used in experiment. Overview courtesy of Maps from COWI.*

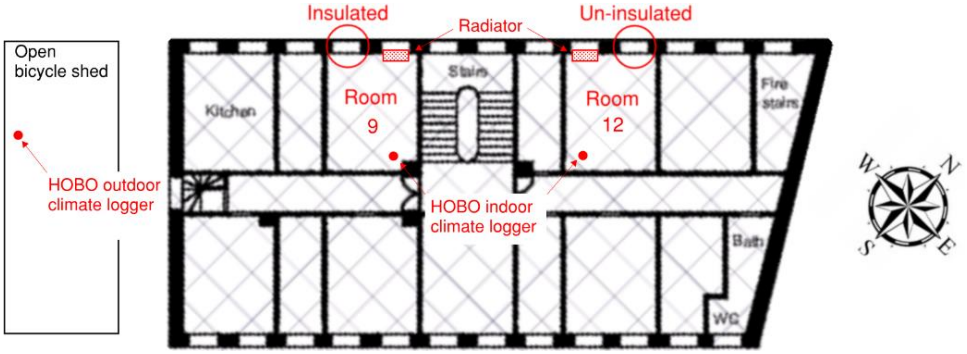


*Figure 121 Floorplan of the 1st floor (2nd in American terms) in Borchs dormitory.*

The building used in the case was at the time of investigation defined as "Listed" (Agency for Culture and Palaces, 1995). This class of preservation make demands for the interior and exterior expression of the building, with considerations about the material use and the possibility for re-establishment at a later stage. Any changes to listed building in Denmark requires permission from the Ministry of Culture (Ministry of Culture Denmark and Tarp, 2014). In this case, a dispensation was given for applying thermal insulation to the interior surface of one spandrel.

Two similar spandrels in each their room were monitored in this study, over a period of 2 years and 8 months. One spandrel was kept as a reference, illustrated in Figure 122, and the other was retrofitted with thermal insulation on the interior masonry surface, illustrated in Figure 123. 2-dimensional drawings of the insulated wall can be seen in Figure 124.

*Figure 122 Interior surface of un-insulated spandrel in room 12.*

*Figure 123 Interior surface of insulated spandrel in room 09.*

The hygrothermal conditions in the masonry wall and thermal insulation were monitored, via DC electrical resistance and temperature measurements in wooden dowels. The measurement points, with locations, are in Figure 125. There are three points installed in the masonry wall, and one point in the insulation layer.

The use of DC electrical wooden resistance and temperature measurements to monitor development in hygrothermal balances has been presented and discussed in Section 2.4, Section 5.3.1 and Independent-hypothesis #1. It was found in the hypothesis that values over 15 wooden weight-% merely show if the dowel is in a wetting or a drying phase.

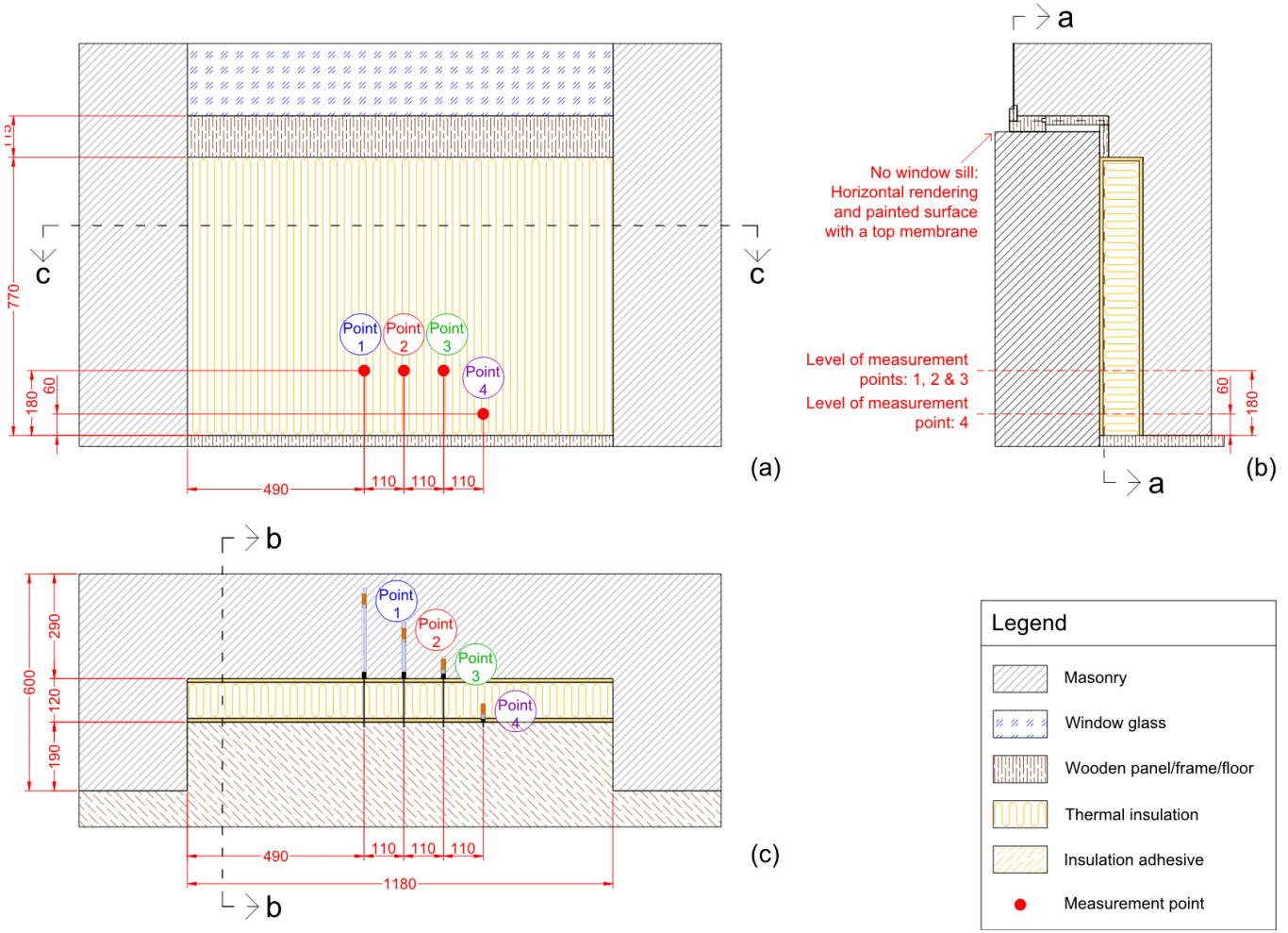


*Figure 124 2-dimensional drawings of the construction: Insulated spandrel in between masonry columns of 2½ bricks thickness. Depth of measurements points illustrated in Figure 125.*

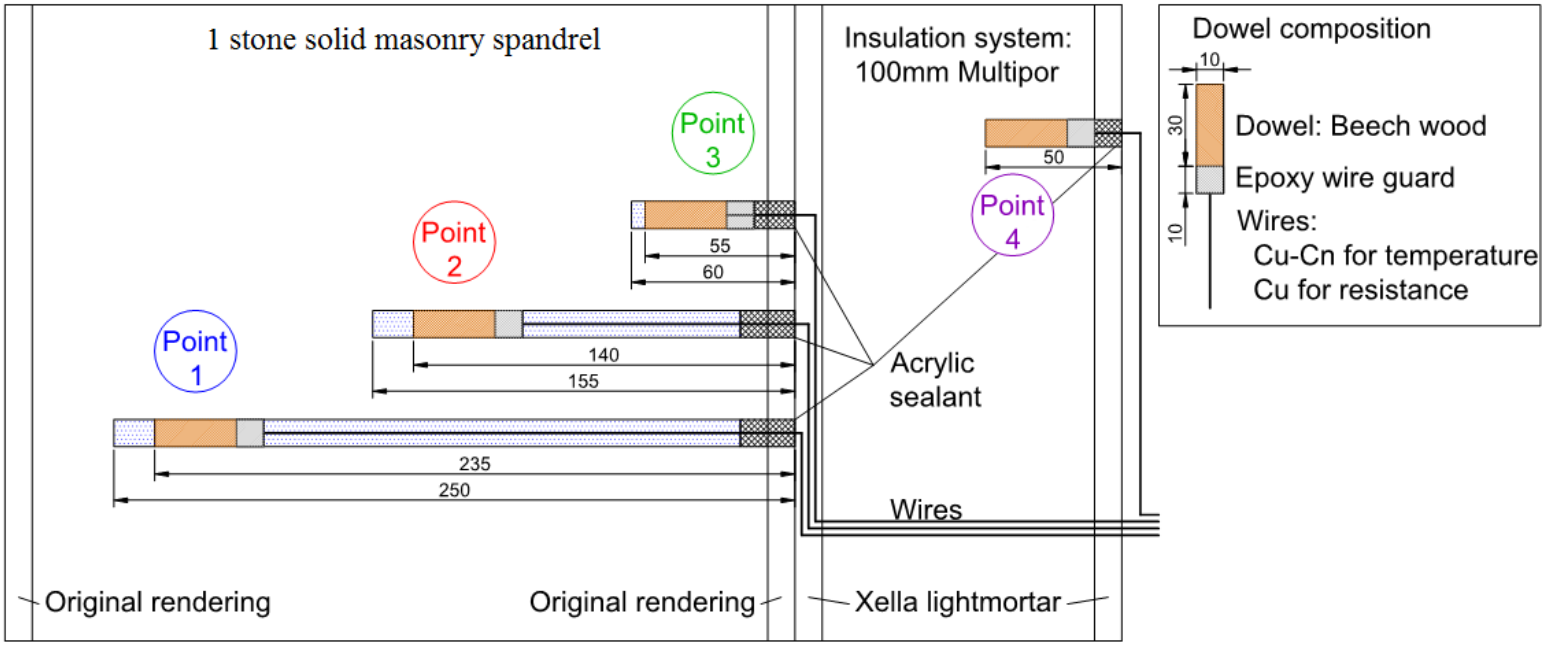


*Figure 125 Illustration of dowel placement. DC electrical resistance is measured in the wooden dowel; temperature is measured within the epoxy wire guard.*

## 6.3 **Results and discussion of measurements**

This section will present the measurements from the case study and discuss the individual measurements. The section is divided into boundary conditions, measurements calculated into relative humidity and ultimately the results from the applied damage models of on-site measurements/registrations.

### *6.3.1* Mild boundary conditions

The boundary conditions affecting the walls were monitored indoors with two RH/T data loggers and outdoors with one RH/T data logger, as illustrated in Figure 120 and Figure 121. The outdoor climate was further measured by two climate stations, located outside the centre of Copenhagen, as illustrated in Figure 126.

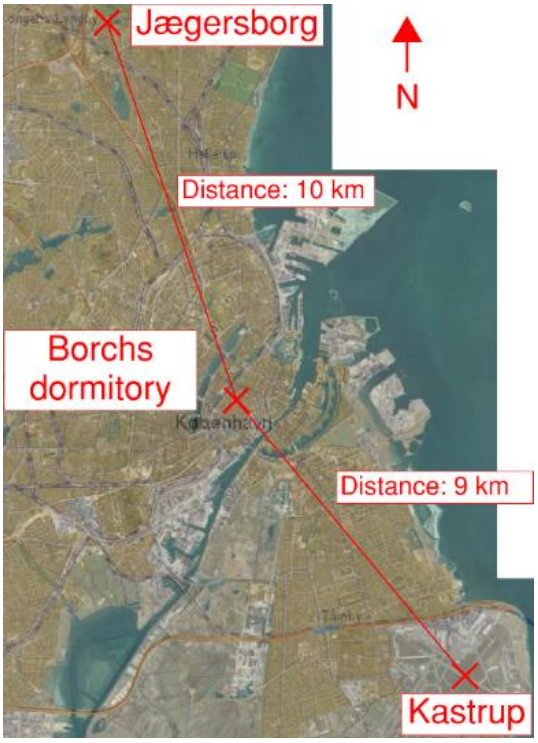


*Figure 126 Location of climate stations in Jægersborg and Kastrup* (NCEI GIS Agile Team et al., 2017)*, compared to Borchs dormitory. Courtesy of Maps from COWI.*

The measured temperature in the two rooms can be seen in Figure 127, with the corresponding relative humidity in Figure 128.

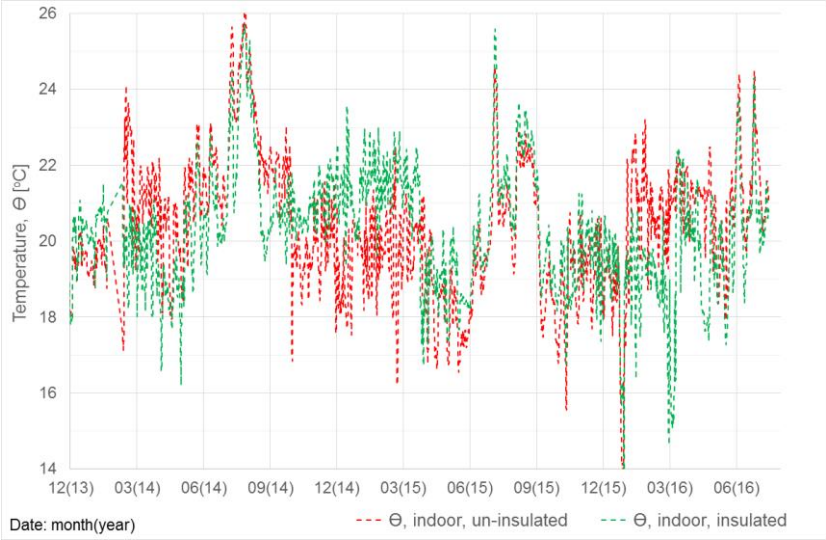


*Figure 127 2-day averages of measured indoor temperatures in both rooms.*

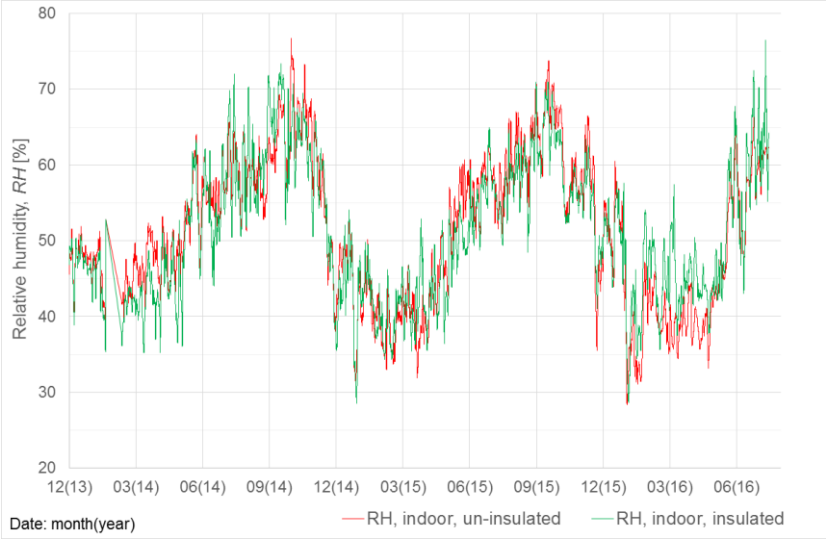


*Figure 128 2-day averages of measured indoor relative humidity in both rooms.*

The measured temperature from the local outdoor RH/T data logger next to the dormitory and the two climate stations can be seen in Figure 129, with the corresponding relative humidity in Figure 130.

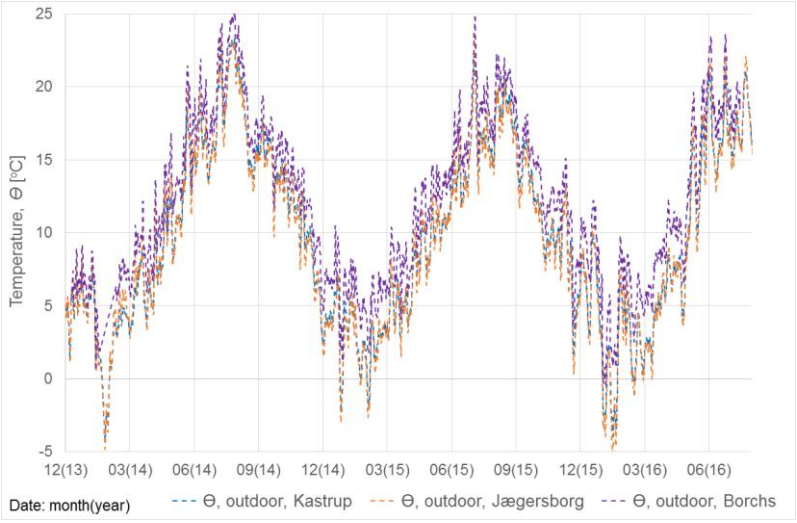


*Figure 129 2-day averages of measured outdoor temperatures.*

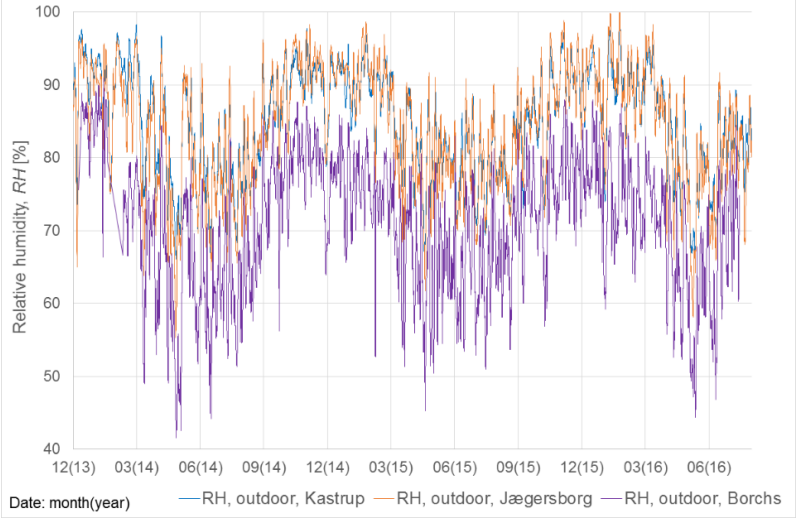


*Figure 130 2-day averages of measured outdoor relative humidity.*

As it might be noticed, higher outdoor temperatures and lower relative humidity have been measured locally next to the dormitory, compared to the two climate stations situated outside the city centre of Copenhagen. A comparison of the un-smoothened temperatures can be seen in Figure 131 and Figure 132 for the 2nd and the 3rd winter in the monitoring period. The figures show that the measured local temperatures in the Copenhagen city centre are higher than the measurements at the climate stations situated outside the city centre. The local temperature rarely drops below freezing point, even when the temperature drops below -6 °C at the climate stations.



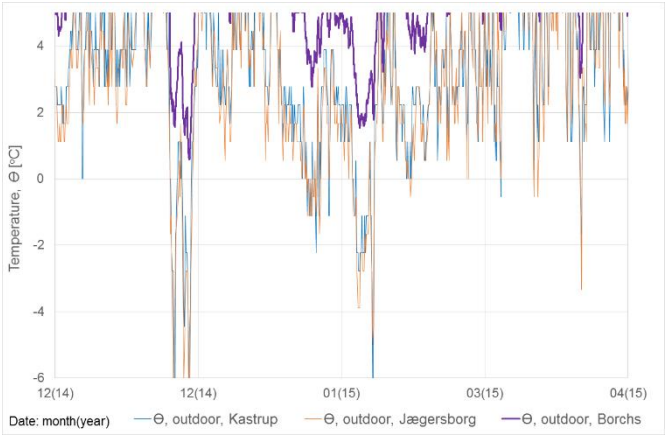


*Figure 131 Un-smoothened outdoor temperatures, winter of 2014/2015. Enlarged version in Figure 155 on page 216.*

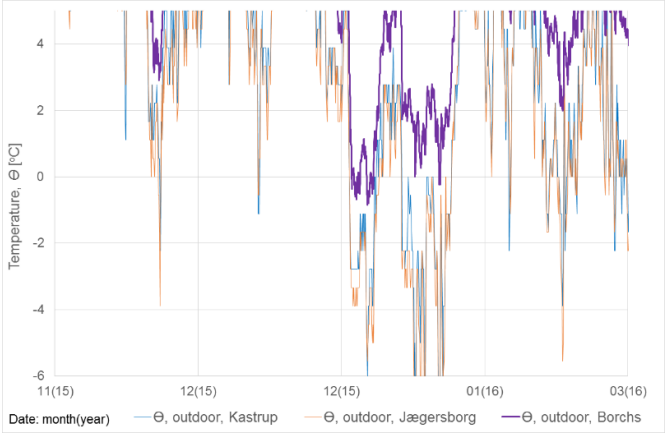


*Figure 132 Un-smoothened outdoor temperatures, winter of 2015/2016. Enlarged version in Figure 156 on page 217.*

The measured in- and outdoor temperatures and relative humidity have been converted to humidity by volume using the method previously described in Section 2.2.1. The resulting humidity by volume for all measurements in- and outdoor can be seen in Figure 133. The local outdoor measurements and at the two climate stations show similar humidity by volume values, meaning that the outdoor airs humidity by volume to some degree is constant within the 10 km from the dormitory.

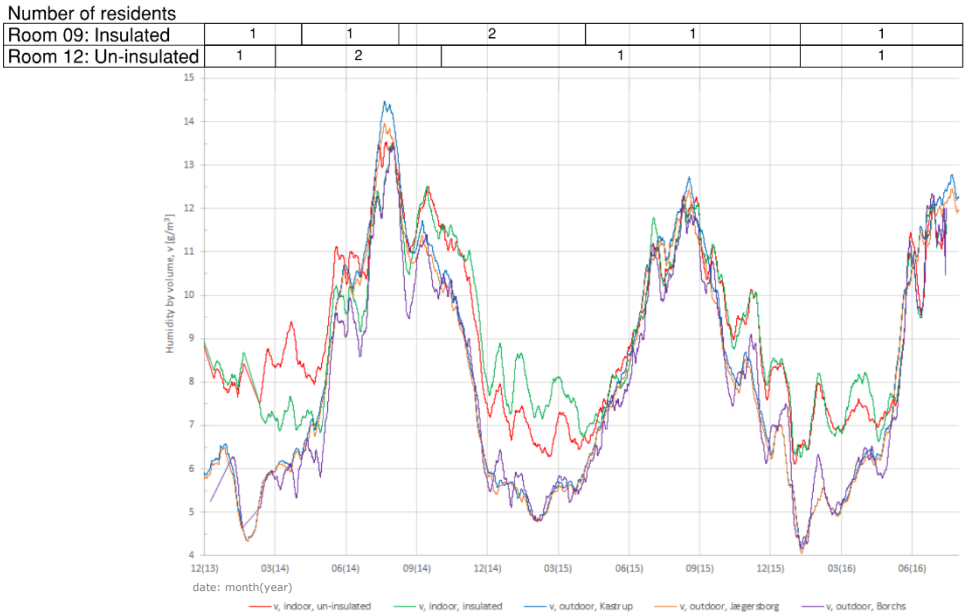


*Figure 133 28-day average of calculated humidity by volume for the indoor and outdoor climates. Note the similarity between outdoor humidity by volume, despite differences in measurements of temperature in Figure 129 and relative humidity in Figure 130. Enlarged version in Figure 157 on page 218.*

Looking into the indoor measurements, some differences between the humidity by volume in the two rooms are observed from the beginning of 2014 until the beginning of 2015, with the highest moisture load in the un-insulated room in 2014 and in the insulated room in 2015. The differences originate from the number of residents inhabiting the rooms, as stated in the top of the graph in Figure 133, with residents changing several times during the monitoring period.

The indoor humidity by volume of the two rooms, Figure 133, shows values following the outdoor climate, with a moisture excess to the indoor air caused by the occupant activity. The calculated monthly average indoor excess of humidity by volume over the monthly average outdoor temperature for both rooms can be

seen in Figure 134, where the room with an insulated spandrel has an excess of indoor humidity by volume in the coldest months within humidity class 2. The room does not exceed humidity class 2, defined as *"Offices, dwellings with normal occupancy and ventilation"* (DS/EN ISO 13788:2013, 2013). The airtightness of the dormitory was investigated at the start of the experiment by ISOLINK, finding leakage/air changes at double the recommended values, based on the age and type of building. The floor of interest had 5.3 air changes per hour at a pressure difference of 50 Pa (Due, 2013).



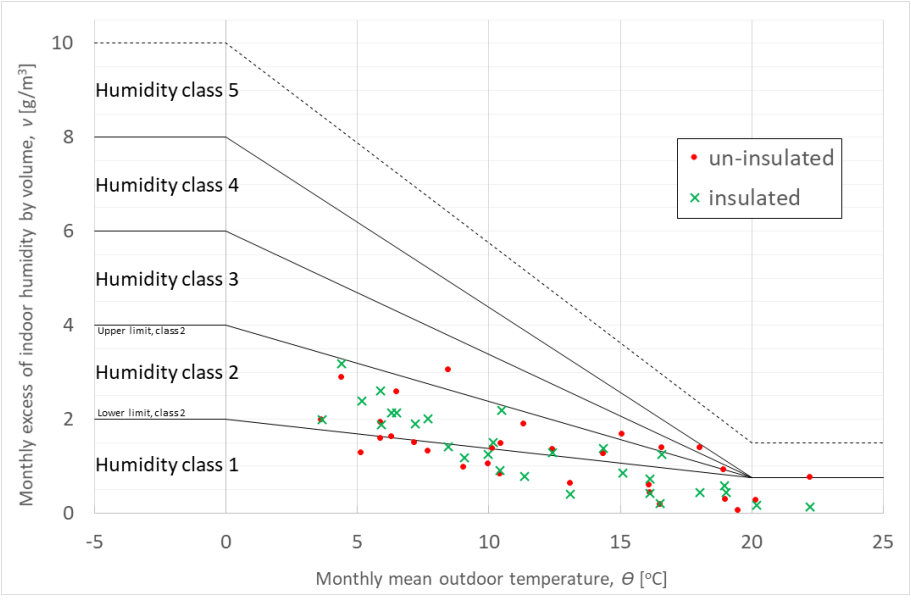


*Figure 134 Monthly average excess of indoor humidity by volume compared to outdoor ambient air temperature. Plotted against climate classes, inspired by* (Brandt et al., 2013; DS/EN ISO 13788:2013, 2013).

### *6.3.2* Outcome of monitoring

The hygrothermal conditions in the walls were monitored in the period November 2013 until July 2016. The insulation was installed in December 2013. The measurement of wooden DC electrical resistance and temperature in the wooden dowels were performed at the following intensity:

- 2013-11-25 → 2014-01-23: Every ~3-5 days.
- 2014-01-23 → 2014-06-04 every ~14 days.

> 2014-06-04 → 2016-07-15 every ~1-2 months.

The measured DC electrical wooden resistance and temperature in the insulated and un-insulated wall can be seen in Figure 135, Figure 136, Figure 137 and Figure 138, where the time of measurements have been marked with "X".

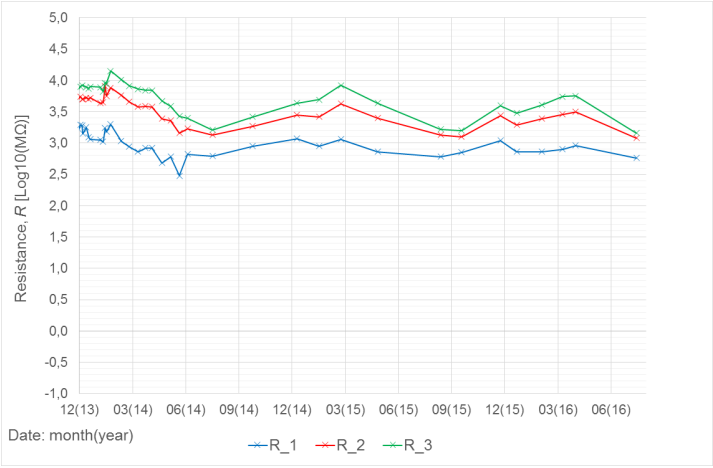


*Figure 135 Measurements of DC electrical wooden resistance, R, in un-insulated spandrel in Room 12. Enlarged version in Figure 158 on page 219.*

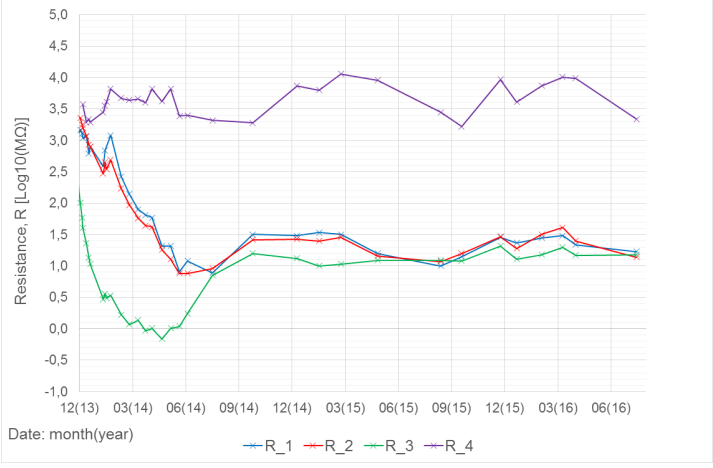


*Figure 136 Measurements of DC electrical wooden resistance, R, in insulated spandrel in Room 9. Enlarged version in Figure 159 on page 220.*

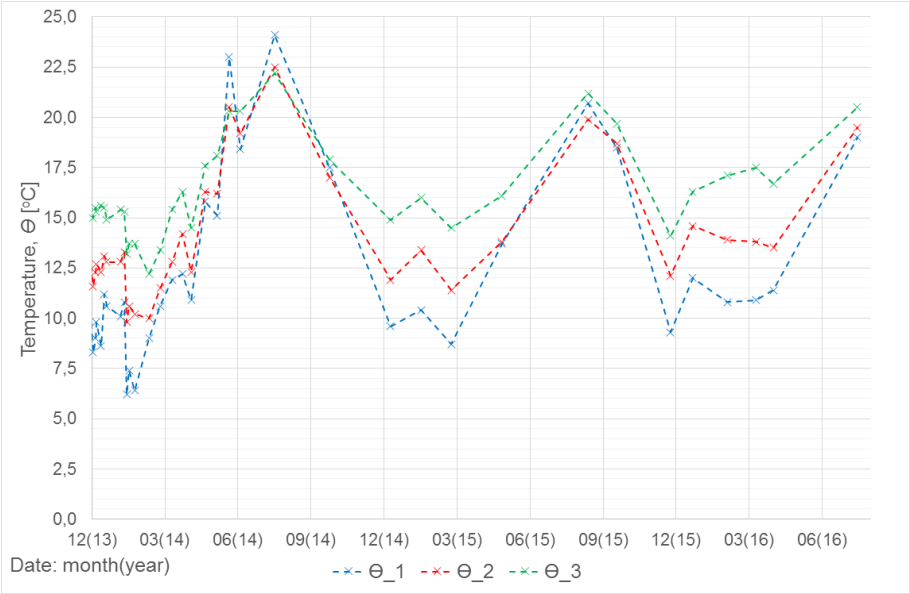


*Figure 137 Measurements of temperature, θ, in un-insulated spandrel in Room 12. Enlarged version in Figure 160 on page 221.*

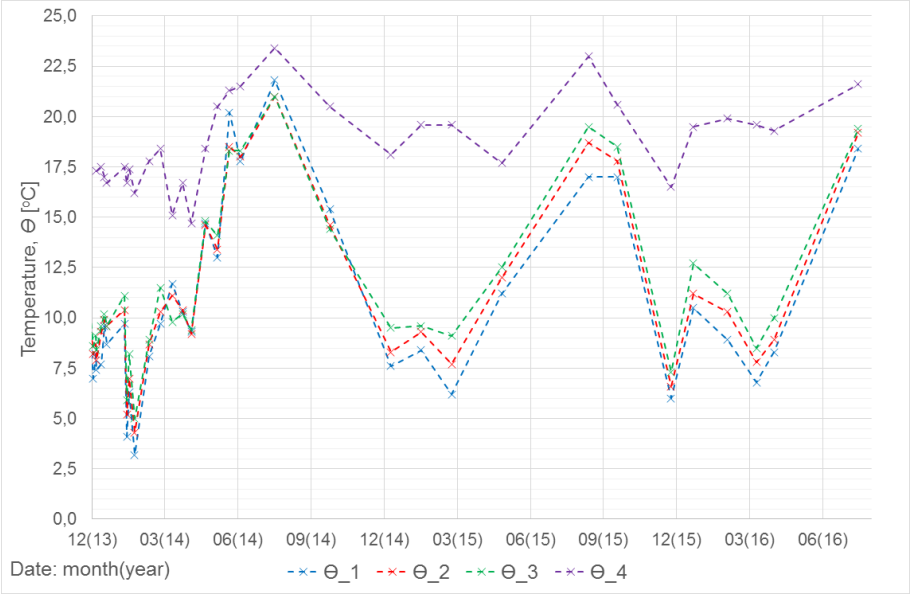


*Figure 138 Measurements of temperature, θ, in insulated spandrel in Room 9. Enlarged version in Figure 161 on page 222.*

The measured DC electrical resistance and temperature in the wooden dowels are converted into wooden moisture content, expressed as wooden weight-%. The found wooden weight-% is an expression for the moisture in the air surrounding the wooden dowel, together with the moisture transferred via capillary suction from contact between wood and masonry. The calculation from DC electrical wooden resistance and temperature to wooden moisture content has been described in Section 2.4.1 on page 44, resulting in the values illustrated in Figure 139 and Figure 140. Please note that according to Independent-hypothesis #1, values over 15 wooden weight-% merely show if the dowel is in a wetting or a drying phase.

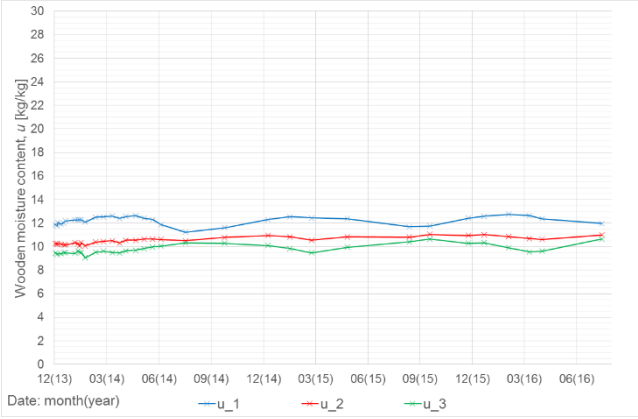


*Figure 139 Calculated wooden moisture weight-%, u, for un-insulated spandrel in Room 12. Enlarged version in Figure 162 on page 223.*

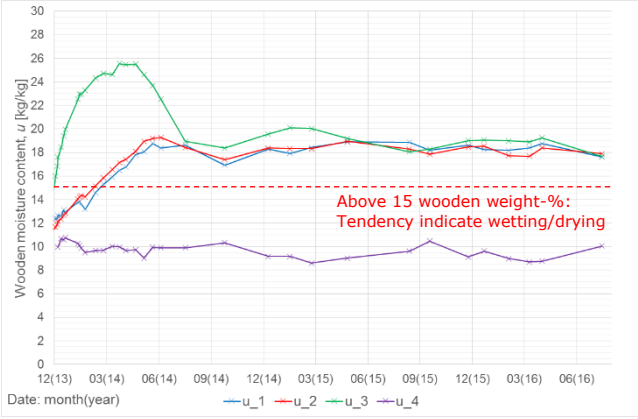


*Figure 140 Calculated wooden moisture weight-%, u, for insulated spandrel in Room 09. Enlarged version in Figure 163 on page 224.*

The approximated relative humidity in the wooden dowel, serving as an approximation for the relative humidity in the air/masonry surrounding the wooden dowel, is calculated based on the measured temperature in the wooden dowels and the calculated wooden moisture weight-%. The calculation is described in Section 2.4.2 on page 46, resulting in the approximated relative humidity illustrated in Figure 141 and Figure 142. All relative humidity calculations in the masonry behind the insulation over 66 - 72 % RH (depending on the state of hysteresis) merely show if the dowel is in a wetting or a drying phase, as described in the discussion of Independent-hypothesis #1. As the amplitude of yearly changes are small, high increases of relative humidity are not expected.



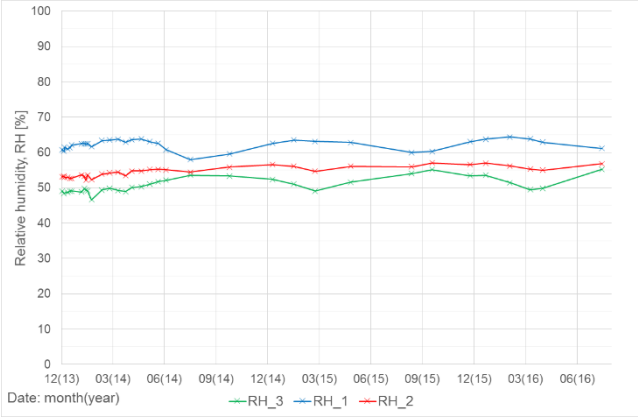


*Figure 141 Calculated relative humidity, RH, for un-insulated spandrel in Room 12. Enlarged version in Figure 164 on page 225.*

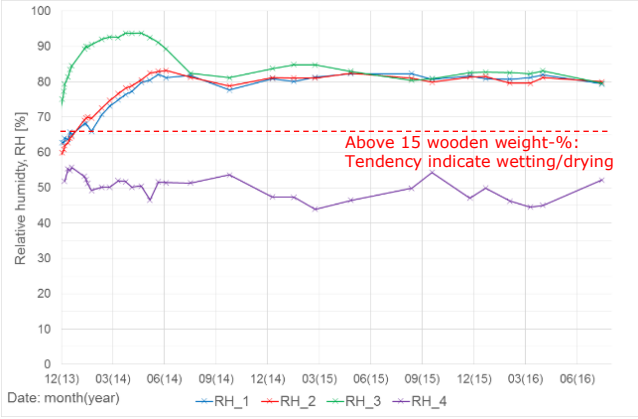


*Figure 142 Calculated relative humidity, RH, for insulated spandrel in Room 09. Enlarged version in Figure 165 on page 226.*

### *6.3.3* Damage models: Mould and wooden decay

The temperatures illustrated in Figure 137 and Figure 138, and the calculated relative humidity illustrated in Figure 141 and Figure 142, have been used to calculate the risk of moisture-induced damage: mould and wooden decay. It must be noted that the calculated relative humidity is used as calculated, acknowledging that the real relative humidity might be higher. The risk of damage have been evaluated using the mathematical models from VTT for both mould germination/growth (Hukka and Viitanen, 1999; Ojanen et al., 2010) and wooden decay (Viitanen et al., 2010a), as previously described in Section 2.3 on page 36. The resulting calculated risk of mould growth and wooden decay can be seen in Figure 143, where it must be noted that as the adhesive for the insulation board is categorized as a cementitious material, the alkaline conditions will prohibit mould formation during the initial dry-out period, resulting in no risk of mould growth in this case. Had the adhesive not been a cementitious material, then the initial high amount of moisture in the insulation/masonry interface would result in a mould index of 0.3, a mould index indicating acceptable microscopic mould growth. The calculated risks was verified with physical in situ Mycometer tests, confirming no mould growth in the insulation/masonry interface, with 6 tests showing results below background level for mould spores, and 2 tests near the floor showing above background level (most likely due to improper cleaning/old dust containing mould spores before mounting insulation).

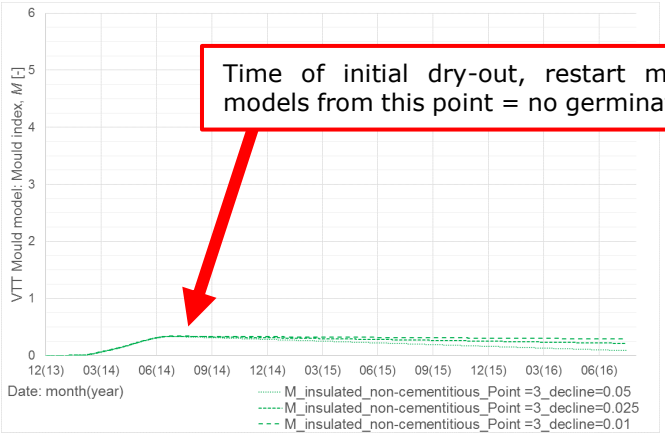


*Figure 143 Results from calculated VTT mould and decay models > 0, if adhesive layer had been non-cementitious. Calculations based on values for un-insulated and insulated spandrel. As the alkaline conditions prohibit mould germination on new surfaces* (Viitanen et al., 2015)*, a new starting point for mould germination was defined at the date of initial drying: 2014-07-17. The mould models with this new starting point did not show risk of mould growth. Enlarged version in Figure 166 on page 227.*

### *6.3.4* Damage models: Increased moisture content and frost

The moisture content in the spandrel increase when interior thermal insulation is applied. The increase is clear when inspecting the change in wooden moisture content in Figure 139/Figure 140.

Considering the risk of frost damage of the exterior façade, it is clear that the changed hygrothermal conditions with colder and wetter masonry walls results in a worse state than the initial. The case in Borchs dormitory was investigated visually for frost risk during the experiment, showing no damage at the exterior surface from June 2014 (illustrated in Figure 144), to 1 year after the end of the monitoring period in July 2017 (illustrated in Figure 145).



It must be noted that the outdoor conditions in the city centre environment were observed to be milder than the climate outside the city, as illustrated in Figure 131 and Figure 132, with only short periods of outdoor temperatures below freezing in the range 0-1 °C. Based on this, it is clear that buildings situated in the city centres are less subject to frost damage.

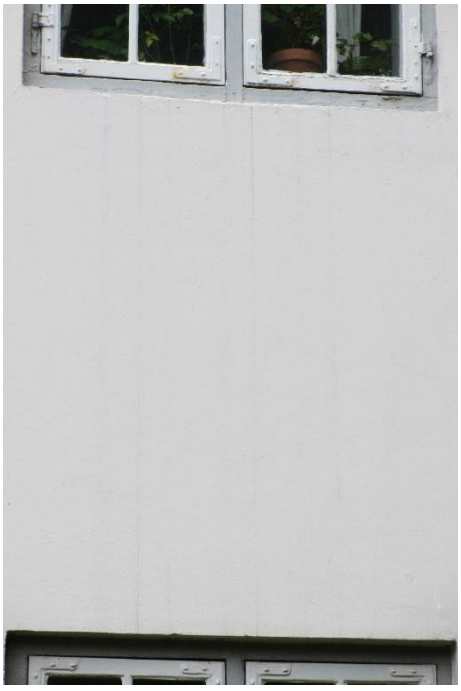

*Figure 144 Exterior surface of the insulated spandrel, June 2014.*

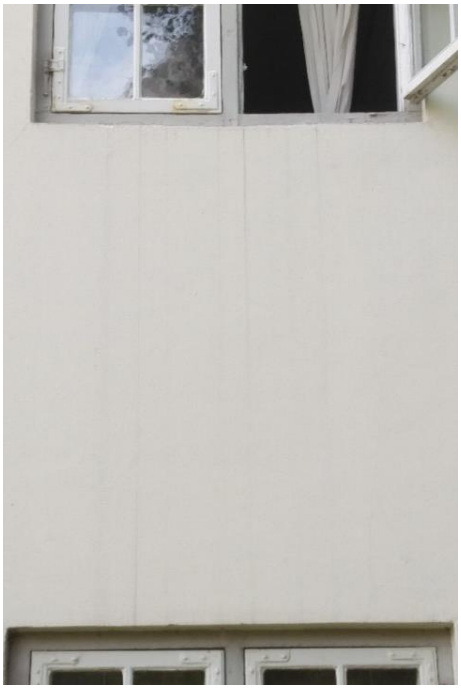

*Figure 145 Exterior surface of the insulated spandrel, July 2017.*

## 6.4 **Sub-discussion of hypothesis**

The incentive to initiate the study presented in Section 6 and the appended Paper #2, was the occupant (dis-)comfort from cold surfaces when living in old multi-storey buildings with thin solid masonry spandrels. One aim of the dissemination was to break from focusing on energy savings when considering the application of interior thermal insulation. The initial conditions registered via thermal imaging showed very cold interior surfaces in spandrels, influencing the floor far into the building, as illustrated in Figure 146, Figure 147 and Figure 148.

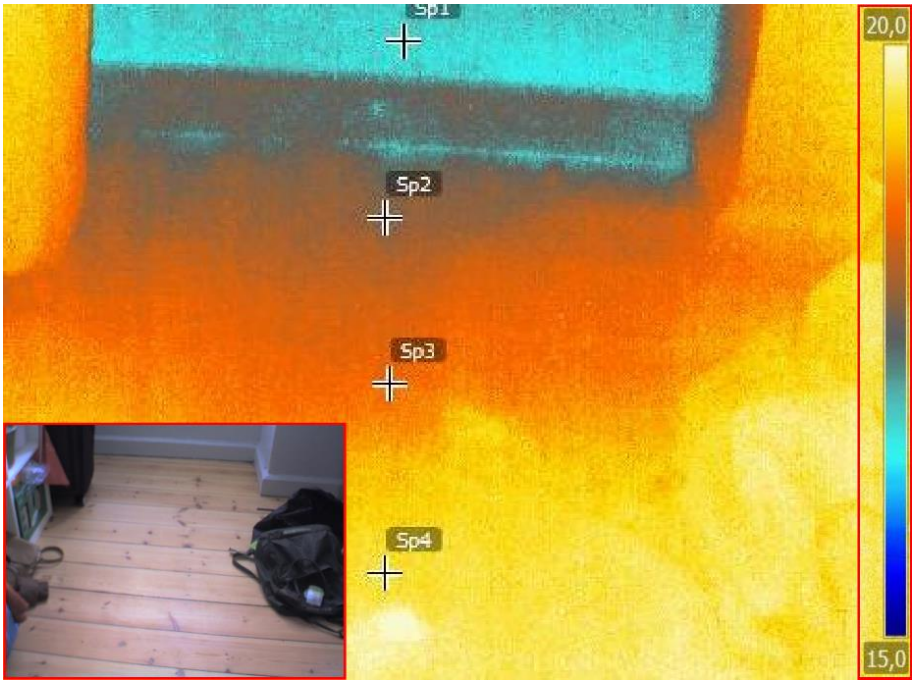


*Figure 146 Thermal image in Room 9. Bottom left: Photograph of thermal image area: Floor towards facade. Emissivity = 0.93: $\theta_{Sp1}$ = 16.7 °C, $\theta_{Sp2}$ = 17.8 °C, $\theta_{Sp3}$ = 18.5 °C, $\theta_{Sp4}$ = 19.5 °C. Outdoor temperature at time of investigation: $\theta_{out}$ = 13.7 °C. Material by courtesy of ISOLINK and Erik Møller Arkitekter.*

To reduce the influence of the cold surfaces, this study was initiated with focus on the changes in hygrothermal conditions when retrofitting thermal insulation to the interior surface of a spandrel. Spandrel retrofitted with thermal insulation has shown theoretically possible to reduce the average thermal transmittance through the masonry wall by up to 40 % in Section 4.2.2.1 on page 86.

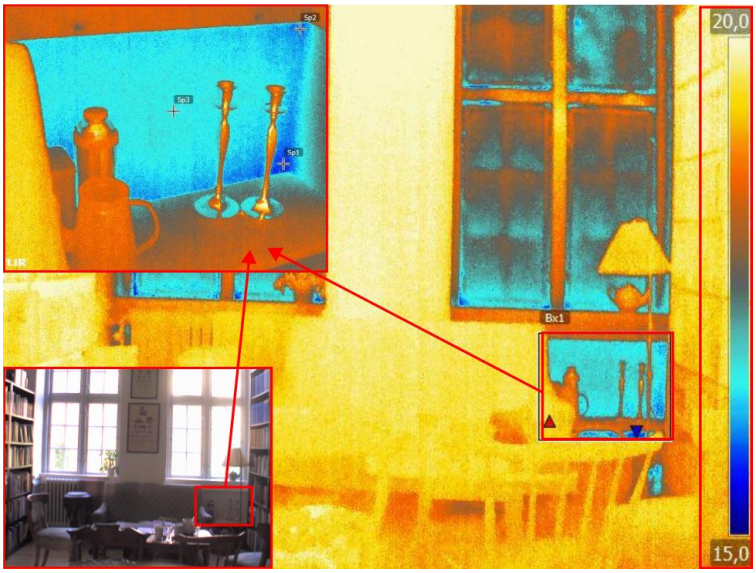


*Figure 147 Thermal image in Room 12. Bottom left: Photograph of thermal image area: Interior surface of facade. Top left: Thermal image of red square noted Bx1. Emissivity = 0.93: $\theta_{Sp1}$ = 15.6 °C, $\theta_{Sp2}$ = 15.8 °C, $\theta_{Sp3}$ = 16.7 °C. Outdoor temperature at time of investigation: $\theta_{out}$ = 13.7 °C. Material by courtesy of ISOLINK and Erik Møller Arkitekter.*

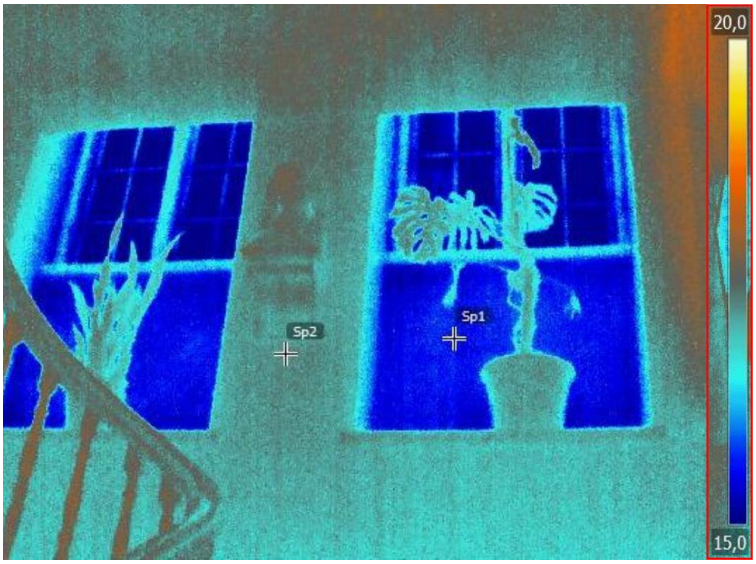


*Figure 148 Thermal image of interior surface of facade at stairs. Emissivity = 0.93: θSp1 = 15.6 °C, θSp2 = 17.3 °C. Outdoor temperature at time of investigation: θout = 13.7 °C. Material by courtesy of ISOLINK and Erik Møller Arkitekter.*

**Sub-hypothesis #6, goal 1** is defined as: "*Reliable measurements from a case study can be obtained, despite the many uncertainties in such an experiment, showing clear and explainable hygrothermal distinctions between a reference and an internally insulated spandrel*".

The study showed that the application of 100 mm thermal insulation to the spandrel resulted in reduced temperatures and increased moisture content within the masonry wall. Comparing the insulation-induced change in temperature, the main temperature drop takes place in the insulation layer, as expected. This result in notable lower temperatures throughout the masonry, with a low difference between inside and outside measurements. A similar change can be seen for the moisture content in the construction, with insulation resulting in a high moisture content throughout the wall and a low difference between inside and outside measurements. The changed hygrothermal conditions are especially seen during the winter periods, where the moisture-open insulation system allows for diffusion of moisture from the interior climate towards the cold masonry wall behind the thermal insulation, corresponding to what was previously described in Sub-hypothesis #4**, goal 3**, on page 154. It must be noted that uncertainties regarding wooden moisture weight-% and relative humidity based on DC electrical resistance measurements have been treated in Independent-hypothesis #1, goal 1, on page 162: Concluding that measurements in wet masonry with wooden dowel weight-% above 15 % could only show if construction was in a wetting or drying phase. Comparing measurements from the insulated and un-insulation construction, it can still be concluded that the insulated construction is wetter, as the measurements in the un-insulated construction is below this limit, while measurements in the insulated construction is above.

Looking into the interior surface temperatures, a plot has been produced showing the measured in- and outdoor ambient air temperature at the time of measurements in Figure 149, with the difference between indoor ambient temperature and the measurement point closest to the surface illustrated in Figure 150. It is clear from the figures that retrofitting interior thermal insulation did as expected reduce the difference between the surface temperature and the ambient air temperature, resulting in decreased risk of occupant discomfort from cold surfaces.

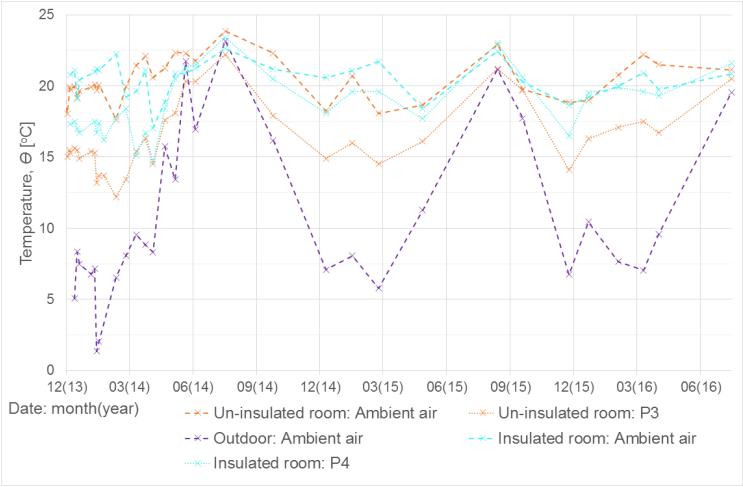


*Figure 149 In- and outdoor ambient air and surface temperatures at time of measurements, both rooms. Enlarged version in Figure 167 on page 228.*

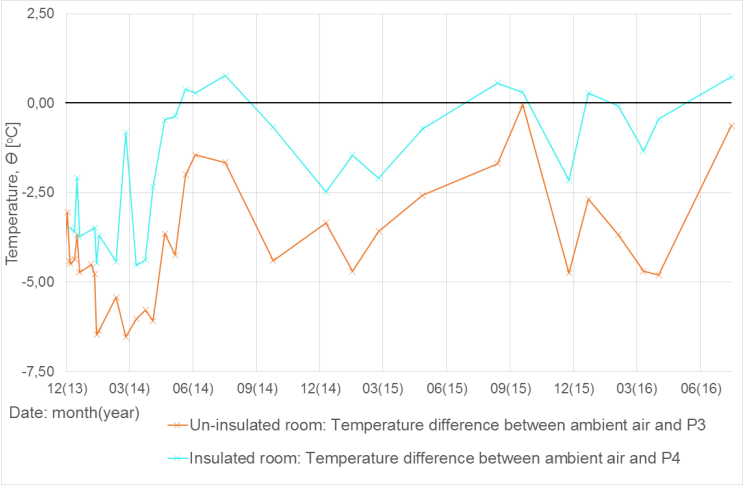


*Figure 150 Difference between indoor ambient air temperature and surface temperature at time of measurements, both rooms. Enlarged version in Figure 168 on page 229.*

✓ It is concluded that the insulation-induced changes are clear and explainable, and further follow the observations from the field experiment in Section 5. Goal 1 of Sub-hypothesis #6 is thereby assessed as fulfilled.

**Sub-hypothesis #6, goal 2** is defined as: "*Clear distinction can be made, separating the initial hygrothermal response and the long-term effect on the hygrothermal balance when retrofitting an interior masonry surface with thermal insulation*".

The immediate hygrothermal response from retrofitting thermal insulation to the existing interior masonry surface is clear when observing the calculated wooden moisture weight-% for the insulated spandrel in Figure 140. All measurement points in the masonry increase from steady measurements of 9-13 wooden moisture weight-%, to steady long-term measurements of 16-20 wooden moisture weight-%. The measurement point closest to the existing interior masonry surface show a distinct initial hygrothermal response to the application of insulation with a wet mortar, with a rapid increase to a high moisture content over a long period.

✓ Goal 2 of Sub-hypothesis #6 is assessed as fulfilled based on the above.

**Sub-hypothesis #6, goal 3** is defined as: "*Retrofitting the existing interior surface of a solid masonry spandrel with a thermal insulation system must not result in moisture-induced damage. The risk of moisture-induced damage is evaluated* by: *Mould growth is evaluated mathematically and by in-situ measurements. The results must be within acceptable boundaries defined by the respective methods*".

The VTT mould model described in Section 2.3.1 was applied to the measured values of Point 3 and 4 for the insulated spandrel in Figure 142, and Point 3 for the un-insulated spandrel in Figure 141. The outcomes with mould index > 0 can be seen in Figure 143, with a maximum mould index of $M$=0.3 obtained at Point 3 for the insulated wall during the initial dry-out period. It must be noted that the calculated relative humidity is used as calculated, acknowledging that the real relative humidity might be higher based on the discussion of Independent-hypothesis #1. Using the evaluation scheme described in Section 2.3.1 for the interface layer, it becomes clear that even if the installed insulation system had not been based on cementitious material, then the calculated mould index would still resulted in the category 0 < M < 2 = "acceptable". As the Xella Multipor insulation board were mounted with light mortar, which contain more than 20 weight-% Portland cement, the glue can be categorized as a cementitious material. Ojanen et al. found that during construction with cementitious materials, the alkaline conditions prohibit mould formation on new surfaces. Based on this, a new starting point for mould growth was defined after the date of initial dry-out: 2014-07-17. The mould models with this new starting point did not show risk of mould growth. Evaluation of mould for the un-insulated wall indicated no risk.

In situ investigation of mould growth of the insulated wall using Mycometer®-tests in Sec. 2.6 of the appended Paper #2 showed 6 of 8 samples within category A: below background level. The two samples taken behind the insulation, close to the floor, had results within category B: above background level. Thereby, no physical mould growth was found on or behind the insulation board.

✓ Goal 3 of Sub-hypothesis #6 is assessed as fulfilled based on the mathematical and on-site investigation for mould growth.



**Sub-hypothesis #6, goal 4** is defined as: "*Retrofitting the existing interior surface of a solid masonry spandrel with a thermal insulation system must not result in moisture-induced damage. The risk of moisture-induced damage is evaluated* by: *Wooden decay is evaluated mathematically, the results must show no occurrence of irreversible decay*".

It is important to emphasise that the traditional solid masonry spandrels did not contain wooden elements. Evaluating the risk of irreversible mass loss from wooden decay was based on the hypothesis that the increase of moisture in the masonry could influence nearby wooden components, being the wooden floor and the load bearing structure underneath the insulated spandrel. The load bearing structure of the historic multi-storey buildings consisted of wooden beams, supported in the solid masonry façade columns or on a wooden exchange running parallel to the façade.

The model to calculate decay of wood, described in Section 2.3.2, was applied to the measured values of the un-insulated and the insulated spandrel. The model showed an activation process not exceeding 0 during the monitoring period at either of the sensor Points 1, 2 or 3. As the activation process did not reach a value of 1, this indicate no calculated risk of decay of wood at either point in the solid masonry wall.

As the open floor structure will be subject to better hygrothermal conditions than the masonry/interior insulation interface, there appears to be no risk of decay of the wooden components. The better hygrothermal conditions derive from the natural ability of wood to distribute moisture along the fibres, as described in Section 2.1 and Figure 3. The distribution of moisture will result in a larger surface area for evaporation of excess moisture to the air volume within the floor structure.

✓ Goal 4 of Sub-hypothesis #6 is assessed as fulfilled based on the above.

**Sub-hypothesis #6, goal 5** is defined as: "*Retrofitting the existing interior surface of a solid masonry spandrel with a thermal insulation system must not result in moisture-induced damage. The risk of moisture-induced damage is evaluated* by: *Frost is evaluated based on measurements and visual observations, observation must show no frost* damage of the exterior surface".

As stated in Section 2.3.3, frost damage can be evaluated by 3 criteria occurring at the same time. Two of these criteria have been evaluated based on measurements in this investigation: Temperature of masonry below freezing and wet masonry. The insulated spandrel become wetter than the un-insulated spandrel, but as the maximum calculated relative humidity in the exterior masonry measurement is stable at 82% RH, it is concluded that the masonry does not reach a wet state (RH > 98 %). Considering the conclusion of Independent-hypothesis #1 regarding uncertainty of high calculated relative humidity, it is still presumed that the masonry does not reach a wet state based on the stability/low amplitude of the calculated relative humidity throughout the year.

The temperature conditions in the masonry in the time between the manual measurements have been evaluated by plotting the raw data for locally measured temperature in the nearby bicycle shed in Figure 131 and Figure 132 (enlarged in Figure 155 and Figure 156 respectively). While the climate stations show periods with temperature down to -10 °C over consecutive days, the local temperatures only go below freezing 2 times during the 3 monitored winters, to a minimum temperature of -2 °C. As the masonry will have a significant contribution of heat from the inside, the temperature in the outer layer of the masonry will not drop below the freezing point in the time between the manual measurements.

Based on the observation that the outdoor conditions in the city centre environment were milder than the climate outside the city, it can further be concluded that buildings situated in the city centres are less subject to frost.

The case in Borchs dormitory was investigated visually for frost risk during the experiment, not observing any frost damage of the exterior surface from June 2014 (illustrated in Figure 144), to the final visual inspection one year after ending the monitoring in the masonry, in July 2017 (illustrated in Figure 145).

✓ Goal 5 of Sub-hypothesis #6 is assessed as fulfilled based on the above.

## 6.5 **Sub-conclusion of hypothesis**

The section will conclude on the sub-hypothesis, previously presented in Section 1.3.1 and Table 1, based on the sub-discussion in Section 6.4. The structure of the section is comprised of a repetition of the sub-hypothesis treated in this section, following a conclusion if the sub-hypothesis can be rejected.

**Sub-hypothesis #6:** "*The thin solid masonry spandrel in existing multi-storey dwellings can be retrofitted with interior thermal insulation without risking moisture-induced damage from neither the initial response, nor the long-term changed hygrothermal balance*".



✓ Sub-hypothesis #6 cannot be rejected, as goal 1, 2, 3, 4 and 5 of the sub-hypothesis was assessed as fulfilled. It can thereby be concluded that retrofitting the spandrel of a historic and listed multi-storey building with interior thermal insulation, exposed to the boundary conditions registered during the 2 years and 8 months monitoring period, can increase occupant comfort without resulting in moisture-induced damage.

### *6.5.1* Outcome of new knowledge obtained in study

The part of the industrial PhD study documented in Section 6 and the appended Paper #2 have provided new knowledge, including:

> Documentation that thin solid masonry spandrels in existing multi-storey dwellings can be retrofitted with interior thermal insulation, without resulting in moisture-induced damage from neither the initial response, nor the long-term changed hygrothermal balance.

> A transfer of focus from energy savings towards occupant comfort considerations, based on thermal images illustrating the cold interior surfaces of existing thin masonry spandrels in historic buildings.

> Illustrate how thermal insulation can reduce the discomfort by increasing the interior surface temperature.

> Illustrate how retrofitting of insulation result in colder and wetter masonry walls, with uniform measurements throughout the wall.

> Document how the outside temperatures are higher, while humidity by volume is similar, within a major city compared to locations outside the city.

# 7 DISCUSSION: A CROSS SECTION ANALYSIS OF THE RESEARCH CONDUCTED IN THE INDUSTRIAL PHD STUDY

The outcome of the PhD study, in relation to the main hypothesis, show that techniques exist, able to address and improve the building physical challenges regarding interior thermal insulation. The use of such techniques show that it is possible, with various means, to decrease the negative hygrothermal impact when retrofitting solid masonry multi-storey building facades with thermal insulation on the interior side.

The comparative analyses of measurements from 9 measurement points in 6 walls in the field experiments, presented in the appended Paper #3, showed that the hygrothermal response could be altered by hydrophobation of the façade and the introduction of a thermal bridge. Correlating with the results presented in Section 5 further showed the difference between a moisture-tight and a moisture-open interior insulation system, retrofitted to an entire interior surface area. While the change in hygrothermal balance was identifiable, comparative analyses based on measurements from the walls showed an increased risk of calculated mould growth behind the installed thermal insulation, compared to the reference wall. The comparative analyses showed that while calculations showed irreversible wooden decay in the embedded wall plate and the wooden beam end for the moisture-tight system, moisture-open systems only showed calculated wooden decay in the embedded wall plate, further reduced in insulation systems where hydrophobation or a deliberate thermal bridge have been added.

The case study presented in Section 6 and the appended Paper #2 can be defined as a variation of the moisture-open interior insulation system presented in the appended Paper #3, exposed to milder boundary conditions. The case study showed that it was possible to retrofit a moisture-open interior insulation system to a spandrel in a room with low interior moisture excess, without resulting in moisture-induced damage.

A comparative analysis of the experimental outcome from monitoring hygrothermal conditions in different solid masonry walls and interior thermal insulation systems throughout the PhD study can be summed up to:

1. Retrofitting the interior masonry surface of a solid masonry spandrel with thermal insulation has not resulted in moisture-induced damage (Section 6 and the appended Paper #2).

2. Retrofitting the entire interior masonry surface of a solid masonry construction with a moisture-tight or moisture-open thermal insulation system worsened the observed hygrothermal condition, expressed as calculated moisture-induced damage (Section 5 and the appended Paper #3).

3. Different variations have been successfully tested, showing able to reduce the worsening of the hygrothermal conditions from retrofitting the entire interior masonry surface with thermal insulation (appended Paper #3).

Based on the listed three experimental outcomes from this PhD study, it is clear that the hygrothermal conditions observed in the solid masonry and embedded wooden elements in the experiments go from acceptable to un-acceptable somewhere between the following situations:

> Acceptable: Retrofitting a solid masonry spandrel with interior thermal insulation, combined with the expected excess of moisture up to humidity class 2 in a building located in an urban area.

> Un-acceptable: Retrofitting the entire interior masonry surface of a solid masonry construction with interior thermal insulation, combined with a high excess of moisture up to humidity class 4 in a construction located in a rural area.

As presented in Section 6, low temperatures can be detected on the interior surfaces of especially the solid masonry spandrels in historic multi-storey buildings. This illustrate a need to increase the interior surface temperature to ensure occupant comfort. The segment analysis presented in Section 3.3 show a large segment of buildings which share this challenge and have a common and well defined building composition, as described in Section 3.2. The results presented in the appended Paper #1 and Section 4 showed that when considering reduction of heat loss, then application of thermal insulation to the interior surface can only give a low overall energy reduction, due to areas where insulation is not applicable. Based on the need to increase the interior surface temperature, a

proposition could be to apply insulation only to the coldest areas of the thermal envelope, namely the thin spandrels. As shown in the appended Paper #1 and in Section 4.2.2.1, by insulating the spandrel it is possible to achieve up to 40 % of the maximum possible reduction in overall thermal transmittance from interior insulation.

# 8 CONCLUSION

The section will conclude on the main hypothesis, based on the sub-conclusions in Section 3.5, Section 4.4, Section 5.5 and Section 6.5.

The main hypothesis of the industrial PhD study reads:

**Main hypothesis:** "Techniques to solve the building physical challenges when retrofitting the high share of solid masonry facade walls in Denmark with interior thermal insulation can be found by comparative evaluation, based on reliable quality measurement data from long-term laboratory experiments and a case study. Retrofitting of interior insulation to a representative selection of such walls can increase occupant comfort and reduce the thermal transmittance, without the risk of moisture-induced damage occurring in the construction".

None of the sub-hypotheses presented in Section 1.3.1 have been rejected. Independent-hypothesis #1 have been rejected. Independent-hypothesis #1 reads:

**Independent-hypothesis #1:** "*DC electrical resistance measurements in wooden dowels can be used to monitor the development of relative humidity during a* transient experiment".

This independent-hypothesis concerns a metrological part of the study, used in the case study and as a 2nd measurement system in the field experiments. The work related to the independent-hypothesis clarified the uncertainty when using DC electrical resistance measurements to monitor moisture in wet constructions, demonstrating that these measurements cannot be used to evaluate the moisture content at more than 15 wooden weight-%. The use of DC electrical resistance measurements in the case study was used to demonstrate the change in hygrothermal balance when retrofitting a solid masonry spandrel with interior thermal insulation, showing clearly that the masonry becomes wetter and colder.

- ✓ It is concluded that the main hypothesis cannot be rejected. But the use of relative humidity calculated from DC electrical resistance measurements in wet masonry should be used with care: It does show wetting/drying tendencies, but cannot be transferred directly to percentage of relative humidity.

## *8.1* ***Future research***

The research field regarding retrofitting the interior surfaces of historic buildings with thermal insulation is currently receiving large public and scientific interest.

During my PhD study I have participated in a seminar and several discussions under the European Research and Innovation funded topic "Energy strategies and solutions for deep renovation of historic buildings", a cross-border research project, with eight research institutions and two companies under the popular name "RIBuild". The objective of the research project is to produce a number of guidelines with descriptions of whether it is possible, and how to retrofit the interior surface with thermal insulation.

Other projects regarding retrofitting the interior surface of masonry with thermal insulation to are underway. One is a laboratory-based project at DTU concerning control and prevention of mould growth in relation to interior thermal insulation, funded by Grundejernes Investeringsfond. Another one is a knowledge-based project at the Danish Building Research Institute SBi and DTU concerning moisture safe energy refurbishment of worth-to-preserve masonry buildings, funded by Grundejernes Investeringsfond, Landsbyggefonden and Realdania.

The future work with the results from the field experiments with 24 solid masonry walls at DTU is planned to include analysis of remaining hygrothermal measurements in masonry, wood and insulation materials. Currently measurements from 85 % of the measurement points collected in this PhD project are still unpublished, leaving a large amount of data for further analyse. Based on the total of 228 active digital RH/T sensors/measurement points, results from the following sensors have been presented:

- Appended Paper #3: 2 years of measurements from 23 digital RH/T sensors, including boundary conditions.
- Section 5 of this Thesis: 1 years of measurements from 10 digital RH/T sensors after stabilization, including boundary conditions.

The initial presentations of results from the experimental setup have been based on the measured result, where future work should include simulation of similar construction in the simulation software Delphin in collaboration with the staff at TUD, aiming to do parameter analysis. A collaboration agreement was signed between DTU and TUD in 2015, on the creation of such hygrothermal simulations over the experimental data. This collaboration has been active during this PhD study, with contact between the two universities, awaiting finished material

characterisation. The preparatory work for performing hygrothermal simulations have thereby been started. Future work is planned for TUD and the following DTU PhD student(s) to include:

- Further analyse of longer time periods and additional constructions.
- Fitting of experimental data and simulation results.
- Perform parameter variation and determine the point when going from acceptable to unacceptable hygrothermal conditions in the construction, as mentioned in the discussion, Section 7. Ideas for parameter variation include:
  - Construction
    - Thickness of applied thermal insulation to interior surface.
    - Extent of interior thermal insulation coverage.
  - Interior boundary conditions:
    - Vary the moisture load based on climate classes (Brandt et al., 2013; DS/EN ISO 13788:2013, 2013).
    - Vary the temperature.
  - Exterior boundary conditions:
    - Change geographical position to other European locations and thereby the specific outdoor conditions (temperature, relative humidity, sun, wind and rain).
    - Change the height of the construction (influence of WDR).
    - Change the WDR catch ratio of the surface.
    - Change the direction of the exterior surface.

A large part of this PhD study comprised of planning, building and maintenance of the two large scale fields experiments at DTU. I have put special care into writing a program as user-friendly as possible, able to transpose the large amount of data, stored originally in text files, into Excel ".csv" files and Delphin ".out" files. The program is based on Matlab and have been presented in Appendix B on page 231. This preparatory work was done to ease the future work of following researchers, facilitating extraction of future datasets from specific periods and sensor points with few inputs into a script, hopefully easing the dissemination of further data from the field experiments.

A study regarding the resistance of the interior thermal insulation systems was started in a Danish bachelor project (Jacobsen and Dabelsteen, 2016) under the research questions:

> Does the interior surface of the insulation systems have an impact resistance that can withstand everyday life?
> Does the insulation systems have a load-carrying capacity enabling the mounting of normal items on the wall, e.g. paintings and shelves?
> Will paintings and furniture near the interior surface of the insulation systems result in microclimates with conditions favourable for mould growth?

The bachelor project included physical tests of impact resistance and load-carrying capacity of the installed thermal insulation systems and investigation of moisture resistance by installing remedies acting as paintings and sofas placed near the wall, for testing the hygrothermal development in the microclimate behind such objects.

> The results regarding impact resistance and load-carrying capacity are available (Jacobsen and Dabelsteen, 2016), but have not been further analysed and reported in international peer-reviewed journals.

> The microclimate measurements are still running and have been described in Section 5.2.4.3, Figure 100 and Figure 101. Only a short measurement period has been presented (Jacobsen and Dabelsteen, 2016), therefore a future study should include a longer dataset, comparing surface measurements to microclimate measurements.

A second study within resistance have been started, concerning the use of inappropriate interior paint treatment under the research question:

> Can the insulation systems cope with occupants using paint treatments deviating from system specifications?

The experiment was set up at the beginning of the project on Wall 8 in container D4, but the results are yet to be analysed.

# REFERENCES


Agency for Culture and Palaces, 1995. Fredede & bevaringsværdige bygninger, Bygning: Collegium mediceum 1691 [WWW Document]. URL www.kulturarv.dk/fbb/bygningvis.pub?bygning=3180332 (accessed 3.22.17).

Ahlgren, L., 1972. Report 36: Fuktfixering i porösa byggnadsmaterial/Moisture fixation in porous building materials. Lund, Sweden.

Andersen, E., Dragsted, J., Kristensen, T. V., Andersen, L.K., 2014. Upgrade and Extension of the Climate station at DTU Byg.

Best, A.C., 1950. The size distribution of raindrops. Q. J. R. Meteorol. Soc. 76, 16–36.

Blocken, B., Carmeliet, J., 2010. Overview of three state-of-the-art wind-driven rain assessment models and comparison based on model theory. Build. Environ. 45, 691–703. https://doi.org/10.1016/j.buildenv.2009.08.007

BMT Instruments ApS, 2017. COW T301. Vedbæk.

Brandt, E., Christensen, G., Hansen, M.H., 1999. Erfaringsblad (99)141004: Fugtindhold i træ - måleudstyr, metoder og vurdering. BYG-ERFA.

Brandt, E., Hjorslev Hansen, M., 2005. Erfaringsblad (99)050505: Fugtindhold i beton og murværk - måling og fejlkilder. BYG-ERFA.

Brandt, E., Møller, E.B., Bunch-Nielsen, T., Christensen, G., Gudum, C., Hansen, M.H., 2013. SBi Anvisning 224: Fugt i bygninger, 2.0. ed. Statens Byggeforskningsinstitut, SBI.

Brandt, E., Morten Hjorslev Hansen, Hansen, O.H., Mossing, P., 1998. Måling af træfugt ved modstandsmåling. Byggeindustrien 26–30.

Brischke, C., Thelandersson, S., 2014. Modelling the outdoor performance of wood products - A review on existing approaches. Constr. Build. Mater. 66, 384–397. https://doi.org/10.1016/j.conbuildmat.2014.05.087

BYG-ERFA, 2009. Press statement: Undgå indvendig isolering [WWW Document]. URL https://byg-erfa.dk/PM-indvendig-efterisol (accessed 6.20.17).

Bygge og Miljøteknik, 2008. Fugtmåler, T 301 COW [WWW Document].

Calle, K., Bossche, N. Van Den, 2017. Towards understanding rain infiltration in historic brickwork, in: 11th Nordic Symposium on Building Physics, NSB2017. Elsevier Ltd, Trondheim, Norway, pp.

676–681. https://doi.org/10.1016/j.egypro.2017.10.005

Christensen, G., 2001. Albertslund gårdhavehuse – opfølgende målinger i trætagkonstruktioner. TOR-NYT I/2001 12–14.

Christensen, G., Koch, A.P., Møller, E.B., 2015. Erfaringsblad (31)151115: Indvendig efterisolering - ældre ydervægge af murværk. BYG-ERFA.

Christensen, G., Kolbe, J., Brandt, E., 1999. Erfaringsblad (99)141005: Langtidsmåling af fugtforhold - i bygninger og bygningskonstruktioner. BYG-ERFA.

COMSOL, 2015. COMSOL Multiphysics.

Danish Energy Agency, 2017. Tilskud til Energibesparelser [WWW Document]. URL https://sparenergi.dk/offentlig/bygninger/tilskud-til-energibesparelser

Danskbyggeskik.dk, Engelmark, J., Simonsen, G., 2017. Dansk Byggeskik [WWW Document]. URL http://danskbyggeskik.dk/ (accessed 11.30.17).

Danskebygningsmodeller.dk, Engelmark, J., Simonsen, G., 2017. Danske Bygningsmodeller [WWW Document]. URL http://www.danskebygningsmodeller.dk/ (accessed 11.30.17).

Dingle, N., Lee, Y., 1972. Terminal Fallspeeds of Raindrops. J. Appl. Meteorol. 11, 877–879. https://doi.org/10.1175/1520-0450(1972)011<0877:TFOR>2.0.CO;2

DS/EN ISO 13788:2013, 2013. Hygrothermal performance of building components and building elements — Internal surface temperature to avoid critical surface humidity and interstitial condensation — Calculation methods, 2. edition. ed. Dansk Standard/Danish Standards, Charlottenlund.

DS/EN ISO 7730:2006, 2006. Ergonomics of the thermal environment – Analytical determination and interpretation of thermal comfort using calculation of the PMV and PPD indices and local thermal comfort criteria, 3. edition. ed. Dansk Standard/Danish Standards, Charlottenlund.

DS/ISO/TS 13732-2:2011, 2011. Ergonomics of the thermal environment – Methods for the assessment of human responses to contact with surfaces – Part 2: Human contact with surfaces at moderate temperature, 1. edition. ed. Dansk Standard/Danish Standards, Charlottenlund.

DS 418:2011, 2011. Beregning af bygningers varmetab/Calculation of heat loss from buildings. Charlottenlund.

Due, L., 2013. Bygningsundersøgelseaf Borchs Kollegium, KBH. Sags. nr. 2682. Boeslunde.

Dysted, D., Sandholdt, H., 2015. Experimental and theoretical investigation of Interior insulation of solid brick walls with foam concrete and another silicate based material. Technical University of Denmark.

Engelmark, J., 2013. Dansk Byggeskik : Etagebyggeriet gennem 150 år, 1. edition. ed, Artikelsamling om dansk byggeteknik fra perioden 1850-2000. Realdania Byg.

Engelmark, J., 1983. Københavnsk etageboligbyggeri 1850-1900. En byggeteknisk undersøgelse. Statens Byggeforskningsinstitut, Hørsholm.

Fanger, P.O., Ipsern, B.M., Langkilde, G., Olesen, B.W., Christensen, N.K., Tanabe, S., 1985. Comfort Limits for Assymetric Thermal Radiation. Energy and Buildigns 8, 225–236. https://doi.org/10.1016/0378-7788(85)90006-4

Fanger, P.O., Lund, H., Hansen, H.E., Danig, P.O., Kjerulf-Jensen, P., Elbæk, B., Nielsen, P. V., Aggerholm, S., Antvorskov, F., Gustavsson, J., Stampe, O.B., Lund Madsen, T., Danig, P.O., Worsøe-Schmidt, P., 2006. Danvak Grundbog i varme- og klimateknik, 3rd ed. Danvak APs, Vojens, Denmark.

Finken, G.R., Bjarløv, S.P., Peuhkuri, R.H., 2016. Effect of facade impregnation on feasibility of capillary active thermal internal insulation for a historic dormitory - A hygrothermal simulation study. Constr. Build. Mater. 113, 202–214. https://doi.org/10.1016/j.conbuildmat.2016.03.019

Gradeci, K., Labonnote, N., Köhler, J., Time, B., 2017a. Mould Models Applicable to Wood-Based Materials – A Generic Framework, in: 11th Nordic Symposium on Building Physics, NSB2017. Elsevier Ltd, Trondheim, Norway, pp. 177–182. https://doi.org/10.1016/j.egypro.2017.09.751

Gradeci, K., Labonnote, N., Time, B., Köhler, J., 2017b. Mould Growth Criteria and Design Avoidance Approaches in Wood-Based Materials – A Systematic Review. Constr. Build. Mater. 150, 77–88. https://doi.org/10.1016/j.conbuildmat.2017.05.204

Hagentoft, C.-E., 2001. Introduction to building physics. Studentlitteratur, Lund, Sweden.

Halding, P.S., Hertz, K.D., Schmidt, J.W., 2016. Construction and Design of Post-Tensioned Pearl-Chain Bridges using SL-Technology. The Technical University of Denmark.

Hamid, A.A., Orphy, M., 2012. Durability of historic brick masonry, in: Jasieńko, J. (Ed.), 8th International Conference on Structural Analysis of Historical Constructions. Structural Analysis of Historical Constructions, Wroclaw, Poland, pp. 1836–1843.

Hamid, A.A., Wallent En, P., 2017. Hygrothermal assessment of internally added thermal insulation on external brick walls in Swedish multifamily buildings. Build. Environ. 123, 351–362. https://doi.org/10.1016/j.buildenv.2017.05.019

Hansen, E.J. de P., 1996. Supplerende undersøgelser til SBI-rapport 268 - Byggematerialers frostbestandighed. Statens byggeforskningsinstitut (SBI).

Hansen, E.J. de P., Møller, E.B., 2017. Moisture supply in Danish single-family houses – the influence of building style, in: 11th Nordic Symposium on Building Physics, NSB2017. Elsevier Ltd, Trondheim, Norway, pp. 147–152. https://doi.org/10.1016/j.egypro.2017.09.663

Hansen, K.K., 1986. Technical report 162/86 Sorption Isotherms a Catalogue. Build. Mater. Lab. Tech. Univ. Denmark.

Harrestrup, M., Svendsen, S., 2016. Internal insulation applied in heritage multi-storey buildings with wooden beams embedded in solid masonry brick façades. Build. Environ. 99, 59–72. https://doi.org/10.1016/j.buildenv.2016.01.019

Harrestrup, M., Svendsen, S., 2015. Full-scale test of an old heritage multi-storey building undergoing energy retrofitting with focus on internal insulation and moisture. Build. Environ. 85, 123–133. https://doi.org/10.1016/j.buildenv.2014.12.005

Harrestrup, M., Svendsen, S., 2014. Heat planning for fossil-fuel-free district heating areas with extensive end-use heat savings: A case study of the Copenhagen district heating area in Denmark. Energy Policy 68, 294–305. https://doi.org/10.1016/j.enpol.2014.01.031

Hens, H., 2012. Building Physics - Heat, Air and Moisture: Fundamentals and Engineering Methods with Examples and Exercises, 2nd editio. ed. Wilhelm Ernst & Sohn, Leuven, Belgium.

Høegh, B.H., 2015. Presentation: Indvendig efterisolering og Skimmel. Build. Green Conf.

Hukka, A., Viitanen, H.A., 1999. A mathematical model of mould growth on wooden material. Wood Sci. Technol. 33, 475–485.

Jacobsen, J.S., Dabelsteen, K.H., 2016. Undersøgelse af robusthed af indvendig isolering. Technical University of Denmark.

Koch, A.P., 2013. Erfaringsblad (29)131230: Forebyggelse mod trænedbrydning - råd-, svampe- og instektskader. BYG-ERFA.

Koch, A.P., Munck, O., Larsen, H.J., 2003. Erfaringsblad (29)031228: Trænedbrydende svampe - kendetegn, vækstbetingelser og nedbrydningsformer. BYG-ERFA.

Koch, A.P., Sode-Larsen, H.E., Munck, O., 2006. Erfaringsblad (99)061222: Ægte Hussvamp – identifikation og reparation af skader. BYG-ERFA.

Kopecký, P., Staněk, K., Bureš, M., Richter, J., Tywoniak, J., 2017. Experimental investigations of wooden beam ends in masonry with internal insulation, in: 11th Nordic Symposium on Building Physics, NSB2017. Elsevier Ltd, Trondheim, Norway, pp. 682–687. https://doi.org/10.1016/j.egypro.2017.10.006

Kragh, J., Wittchen, K.B.B., 2014. Development of two Danish building typologies for residential buildings. Energy Build. 68, 79–86. https://doi.org/10.1016/j.enbuild.2013.04.028

Krause, J.D., 2003. Analytical Instrument Performance Criteria Application: Application of a Fluorometric Method for the Detection of Mold in Indoor Environments. Appl. Occup. Environ. Hyg. 18, 1–5. https://doi.org/10.1080/10473220301457

Kuenzel, H.M., 1998. Effect of interior and exterior insulation on the hygrothermal behaviour of exposed walls. Mater. Struct. 31, 99–103.

Lacy, R.E., 1965. Driving-Rain maps and the onslaught of rain on buildings. Proc. RILEM/CIB Symp. Moisture Probl. Build. 29.

Lohse, U., 1986. SBI-Rapport 176: Laboratorieforsøg med fuger omkring trævinduer. Hørsholm.

luca-industries.com, Lucà, S.F., Lucà, M.H.M., 2018. Luca Industries International GmbH [WWW Document]. URL http://www.luca-industries.com (accessed 1.15.18).

Mets, T. De, Tilmans, A., Loncour, X., 2017. Hygrothermal assessment of internal insulation systems of brick walls through numerical simulation and full-scale laboratory testing, in: 11th Nordic Symposium on Building Physics, NSB2017. Elsevier Ltd, Trondheim, Norway, pp. 753–758. https://doi.org/10.1016/j.egypro.2017.10.022

Miller, M., Reeslev, M., 2003. Skimmelsporer og skimmelvækst er ikke det samme. Dansk kemi 1, 20–23.

Ministry of Culture Denmark, Tarp, K., 2014. LBK nr 970: Bekendtgørelse af lov om bygningsfredning og bevaring af bygninger og bymiljøer. Copenhagen K.

Møller, E.B., Andersen, B., Rode, C., Peuhkuri, R., 2017. Conditions for mould growth on typical interior surfaces, in: 11th Nordic Symposium on Building Physics, NSB2017. Elsevier Ltd, Trondheim, Norway, pp. 171–176. https://doi.org/10.1016/j.egypro.2017.09.680

Møller, E.B., Hansen, E.J. de P., 2017. Moisture supply in Danish single-family houses – the influence of occupant behavior and type of room, in: 11th Nordic Symposium on Building Physics, NSB2017. Elsevier Ltd, Trondheim, Norway, pp. 141–146. https://doi.org/10.1016/j.egypro.2017.09.661

Morelli, M., Nielsen, T.R., Scheffler, G.A., Svendsen, S., 2010. Internal Insulation of Masonry Walls with Wooden Floor Beams in Northern Humid Climate, in: 11th International Conference on Thermal Performance of the Exterior Envelopes of Whole Buildings, Buildings XI. American Society of Heating, Refrigeration, and Air-Conditioning Engineers (ASHRAE).

Morelli, M., Rønby, L., Mikkelsen, S.E., Minzari, M.G., Kildemoes, T., Tommerup, H.M., 2012. Energy retrofitting of a typical old Danish multi-family building to a “nearly-zero” energy building based on experiences from a test apartment. Energy Build. 54, 395–406. https://doi.org/10.1016/j.enbuild.2012.07.046

Morelli, M., Svendsen, S., 2012. Investigation of interior post-insulated masonry walls with wooden beam ends. J. Build. Phys. 36, 265–293. https://doi.org/10.1177/1744259112447928

Munch-Andersen, J., 2008. SBi-anvisning 221 - Efterisolering af etageboliger, 1.0. ed. Statens Byggeforskningsinstitut, SBI, Hørsholm.

Munch-Petersen, J.F., 1990. Fugtmåledyvler, rapport nr. 198. Lyngby.

NCEI GIS Agile Team, National Oceanic and Atmospheric Administration (NOAA), National Centers for Environmental Information, 2017. Hourly/Sub-Hourly Observational Data Map [WWW Document]. Version 1.8.2. URL https://gis.ncdc.noaa.gov/maps/ncei/cdo/hourly (accessed 2.8.17).

Nicolai, A., Grunewald, J., Fechner, H., 2017. DELPHIN: Simulation program for coupled heat, air, moisture, salt and VOC transport.

Nicolai, A., Scheffler, G.A., Grunewald, J., Plagge, R., 2008. An efficient numerical solution method and implementation for coupled heat, moisture, and salt Transport: The DELPHIN Simulation Program, Research Report on Priority Program DFG SPP 1122. https://doi.org/10.1081/E-EEE2-120046011

Nielsen, A., 1919. Samling af Bestemmelser vedrørende Københavns Kommune 1840-1863. København.

Nielsen, A., Møller, E.B., Rasmussen, T.V., Hansen, E.J. de P., 2012. Use of sensitivity analysis to evaluate hygrothermal conditions in solid brick walls with interior insulation, in: Proceedings of the 5th International Building Physics Conference (IBPC). Kyoto University, Kyoto, Japan, pp. 377–384.

Odgaard, T., 2014. Moisture transport model for anisotropic wood. Research topic for evaluation: "International PhD School: Energy and Moisture in Buildings: from the Microstructure of Porous Materials to the Building Energy Efficiency."

Odgaard, T., Bjarløv, S.P., Rode, C., 2018a. Interior insulation—Characterisation of the historic, solid masonry building segment and analysis of the heat saving potential by 1d, 2d, and 3d simulation. Energy Build. 162, 1–11. https://doi.org/10.1016/j.enbuild.2017.12.008

Odgaard, T., Bjarløv, S.P., Rode, C., 2018b. Interior insulation – Experimental investigation of hygrothermal conditions and damage evaluation of solid masonry façades in a listed building. Build. Environ. 129, 1–14. https://doi.org/10.1016/j.buildenv.2017.11.015

Odgaard, T., Bjarløv, S.P., Rode, C., 2018c. Influence of hydrophobation and deliberate thermal bridge on hygrothermal conditions of internally insulated historic solid masonry walls with built-in wood. Energy Build. 173, 530–546. https://doi.org/10.1016/J.ENBUILD.2018.05.053

Odgaard, T., Bjarløv, S.P., Rode, C., Vesterløkke, M., 2015. Building renovation with interior insulation on solid masonry walls in Denmark - a study of the building segment and possible solutions, in: 6th International Building Physics Conference, IBPC 2015. Elsevier Ltd., Torino, Italy, pp. 830–835. https://doi.org/10.1016/j.egypro.2015.11.003

Ojanen, T., Viitanen, H., Peuhkuri, R., Lähdesmäki, K., Vinha, J., Salminen, K., 2010. Mold Growth Modeling of Building Structures Using Sensitivity Classes of Materials. Therm. Perform. Exter. Envel. Build. XI 1–10.

Pavlik, Z., 2009. Hygrothermal performance study of an innovative interior thermal insulation system. Appl. Therm. Eng. 29, 1941–1946. https://doi.org/10.1016/j.applthermaleng.2008.09.013

Pedersen, C.R., 1989. Koblet fugt- og varmetransport i bygningskonstruktioner - Fugtfysik. Rapport Nr. 86-2. Danmarks Tekniske Højskole.

Reeslev, A.M., Miller, M., 2002. Måling af skimmelsvampe i bygninger – hvorfor og hvordan? Byggeindustriens Byggeforum 18–19.

RIBuild.eu, Danish Building Research Institute at Aalborg University Copenhagen, Riga Technical University, KU Leuven, Dresden University of Technology, Marche Polytechnic University, Technical University of Denmark, SP Technical Research Institute of Sweden, University of Applied Sciences Western Switzerland, INTRO FLEX ApS, Erik Møller Architects, 2017. RIBuild [WWW Document]. URL www.ribuild.eu

Rode, C., Lund, M.S.M., 2016. Combined Heat and Moisture Transfer in Building Constructions. Kgs Lyngby, Denmark.

Saïd, M.N.., Demers, R.G., McSheffrey, L.L., 2003. Hygrothermal performance of a masonry wall retrofitted with interior insulation. Res. Build. Phys. 445–454.

Scheffler, G., Worch, A., Bäumler, S., Beck-Bazlen, J., Binder, A., Borsch-Laaks, R., Burcek, K., Elbel, M., Engel, J., Epple, M., Eßmann, F., Gänßmantel, J., Hecht, C., Hildebrand, M., Hofmann, D., Kehl, D., Lenker, C., Plumanns, S., Range, A., Riggert, H., Rudolph, G., Ruisinger, U., Steiner, T., Vogt, D., Wegerer, P., Walther, W., Zirkelbach, D., 2014. WTA-Merkblatt 6-5: Interior insulation according to WTA II : Evaluation of internal insulation systems with numerical design methods.

Scheffler, G.A., 2011. Hygric performance of internal insulation with light-weight autoclaved aerated concrete. Proc. 5th Int. Conf. Autoclaved Aerated Concr. Sept. 15-16, 2011 323–335.

Sedlbauer, K., 2002. Prediction of Mould Growth by Hygrothermal Calculation. J. Build. Phys. 25, 321–336. https://doi.org/10.1177/0075424202025004093

Sedlbauer, K., 2001. Prediction of mould fungus formation on the surface of and inside building components. Frauenhofer Institute.

Simonsen, G., Vesterløkke, M., Brendstrup, J., Hansen, H., Hansen, M.H., Larsen, P.K., 2012. Standsning af grundfugt i ældre ejendomme. København, Denmark.

SKAT, KOMBIT, KL, 2012. The Building and Dwelling Register [WWW Document]. URL http://bbr.dk/bbrkort (accessed 1.19.15).

Straube, J., 2010. Simplified Prediction of Driving Rain on Buildings : ASHRAE 160P and WUFI 4.0. Build. Sci. Dig. 1–16.

Straube, J., Schumacher, C., 2007. Interior insulation retrofits of load-bearing masonry walls in cold climates. J. Green Build. 2, 42–50. https://doi.org/10.3992/jgb.2.2.42

Straube, J.F., 1998. Moisture control and enclosure systems. University of Waterloo.

The Danish Transport and Construction Agency, 2015. Danish Building Regulations 2015.

Toman, J., Vimmrova, A., Cerny, R., 2009. Long-term on-site assessment of hygrothermal performance of interior thermal insulation system without water vapour barrier. Energy Build. 41, 51–55. https://doi.org/10.1016/j.enbuild.2008.07.007

Tsongas, B.Y.G.A., Ph, D., Ashrae, M., Riordan, F., 2016. Minimum Conditions for Visible Mold Growth. ASHRAE J. 32–43.

Ueno, K., Straube, J., 2008. Laboratory Calibration and Field Results of Wood Resistance Humidity Sensors, in: Proceedings of BEST 1 Conference, June 10-12. Minneapolis.

Ueno, K., Straube, J., Straaten, R. Van, 2013. Field monitoring and simulation of a historic mass masonry building retrofitted with interior insulation, in: Thermal Performance of the Exterior Envelopes of Whole Buildings XII International Conference. ASHRAE, pp. 1–16.

Van Aarle, M., Schellen, H., Van Schijndel, J., 2015. Hygro thermal simulation to predict the risk of frost damage in masonry; effects of climate change. Energy Procedia 78, 2536–2541. https://doi.org/10.1016/j.egypro.2015.11.268

Vereecken, E., Roels, S., 2015. Capillary active interior insulation: do the advantages really offset potential disadvantages? Mater. Struct. 48, 3009–3021. https://doi.org/10.1617/s11527-014-0373-9

Vereecken, E., Roels, S., 2014. A comparison of the hygric performance of interior insulation systems: a hot box–cold box experiment. Energy Build. 80, 37–44. https://doi.org/10.1016/j.enbuild.2014.04.033

Vereecken, E., Roels, S., 2012. Review of mould prediction models and their influence on mould risk evaluation. Build. Environ. 51, 296–310. https://doi.org/10.1016/j.buildenv.2011.11.003

Viitanen, H., 2007. Improved Model to Predict Mold Growth in Building Materials, in: Buildings X. ASHRAE, pp. 1–8.

Viitanen, H., Krus, M., Ojanen, T., Eitner, V., Zirkelbach, D., 2015. Mold risk classification based on comparative evaluation of two established growth models, in: Energy Procedia. Elsevier B.V., pp. 1425–1430. https://doi.org/10.1016/j.egypro.2015.11.165

Viitanen, H., Toratti, T., Makkonen, L., Peuhkuri, R., Ojanen, T., Ruokolainen, L., Räisänen, J., 2010a. Towards modelling of decay risk of wooden materials. Eur. J. Wood Prod 68, 303–313. https://doi.org/10.1007/s00107-010-0450-x

Viitanen, H., Vinha, J., Salminen, K., Ojanen, T., Peuhkuri, R., Paajanen, L., Lahdesmaki, K., 2010b. Moisture and Bio-deterioration Risk of Building Materials and Structures. J. Build. Phys. 33, 201–224. https://doi.org/10.1177/1744259109343511

Walker, R., Pavía, S., Dalton, M., 2016. Measurement of moisture content in solid brick walls using timber dowel. Mater. Struct. 49, 2549–2561. https://doi.org/10.1617/s11527-015-0667-6

Wittchen, K.B., Kragh, J., Jensen, O.M., 2011. Energy saving potentials – A case study on the Danish building stock. ECEEE 2011 SUMMER STUDY • ENERGY Effic. FIRST Found. A LOW-CARBON Soc. 1355–1363.

Zhao, J., Grunewald, J., Ruisinger, U., Feng, S., 2017. Evaluation of capillary-active mineral insulation systems for interior retrofit solution. Build. Environ. 115, 215–227. https://doi.org/10.1016/j.buildenv.2017.01.004

Zhou, X., Derome, D., Carmeliet, J., 2017. Hygrothermal modeling and evaluation of freeze-thaw damage risk of masonry walls retrofitted with internal insulation. Build. Environ. 125, 285–298. https://doi.org/10.1016/J.BUILDENV.2017.08.001

# APPENDIX

# APPENDIX A FIGURES IN PAPER IN LARGER SCALE

The following subsections contain figures already included in present thesis. This have been done as the small format of the thesis made some figures difficult to interpret due to the size.

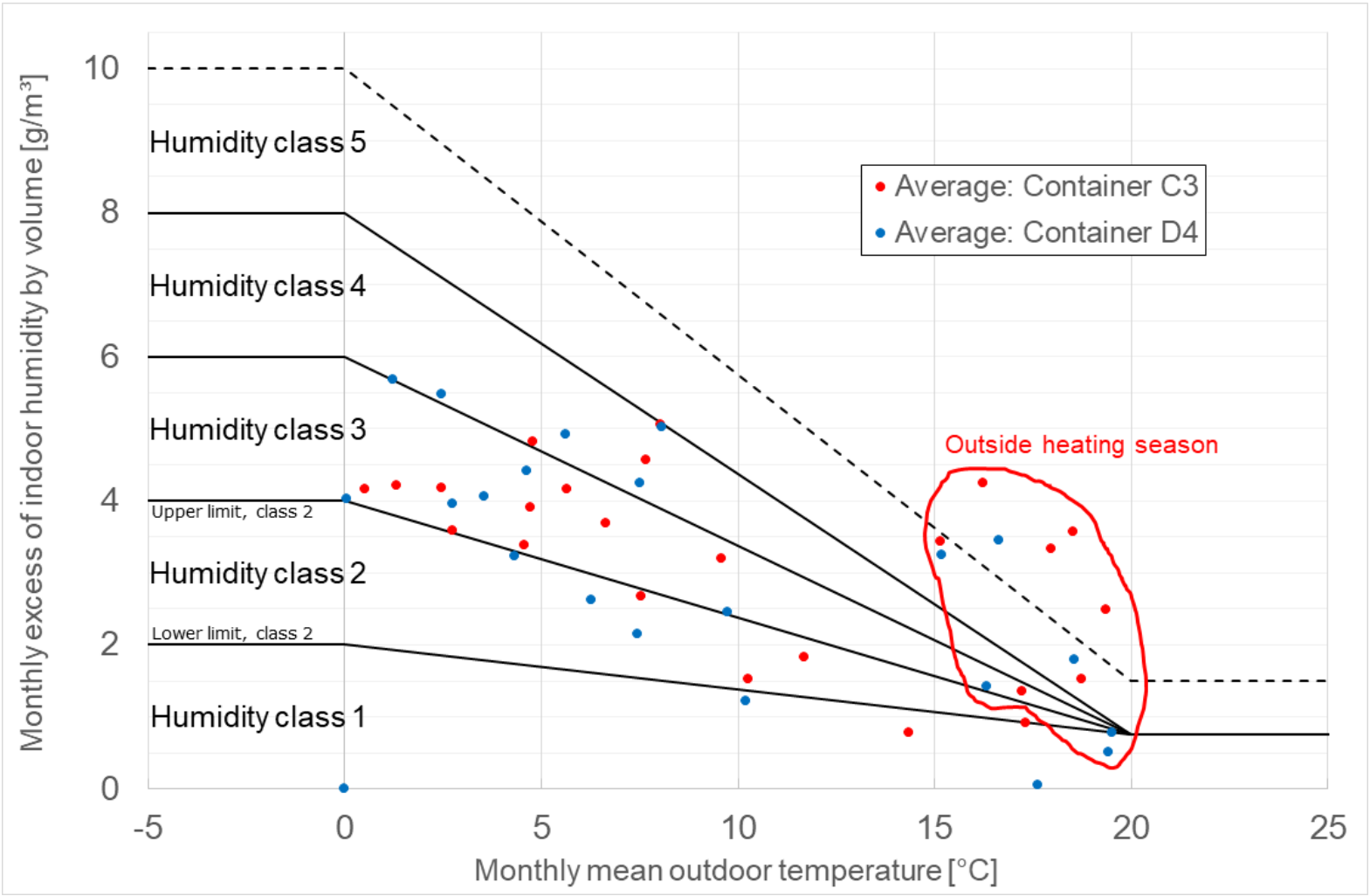


*Figure 151 Enlarged version of Figure 81 on page 118.*

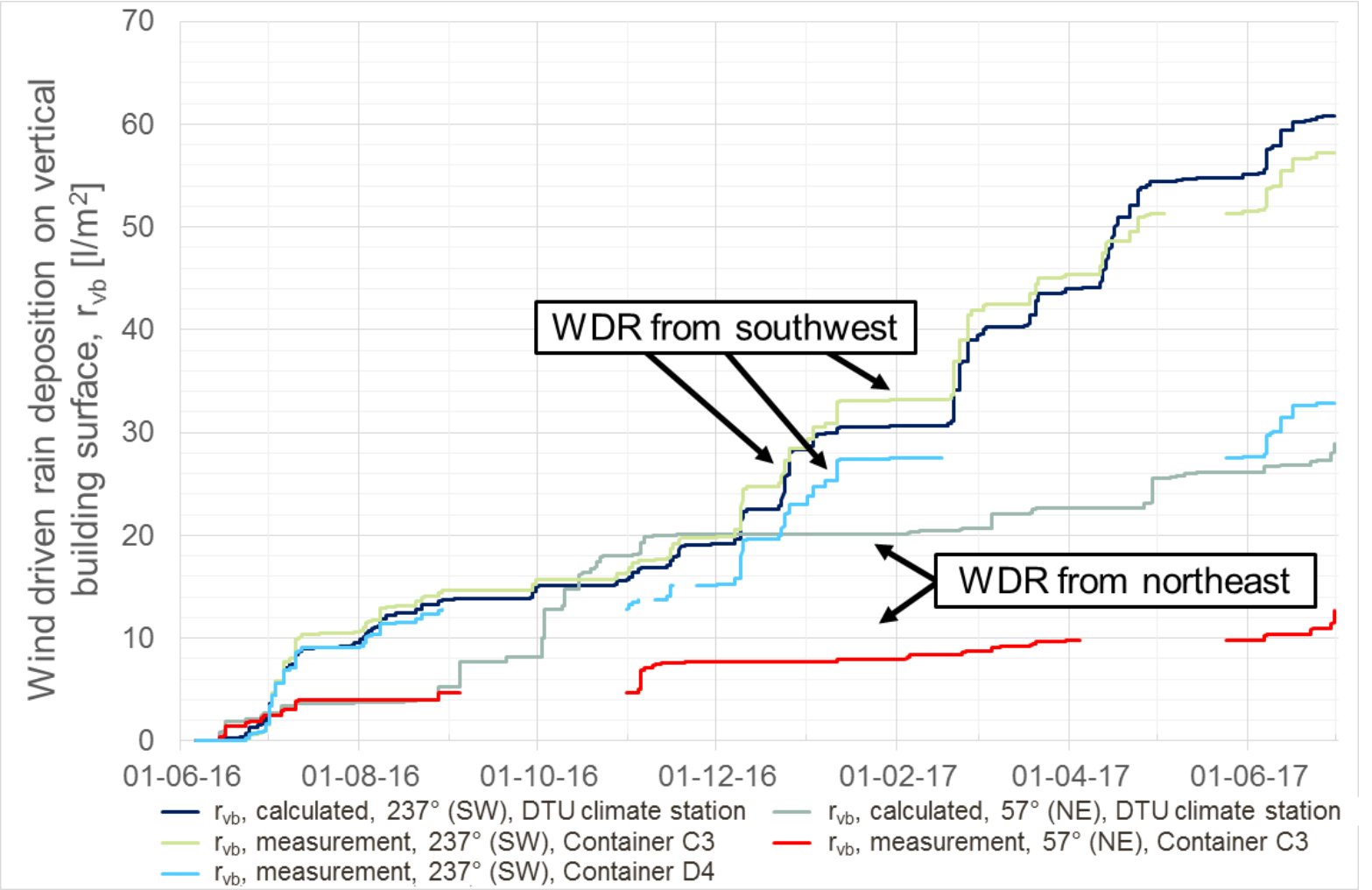


Figure 152 Enlarged version of Figure 83 on page 120.

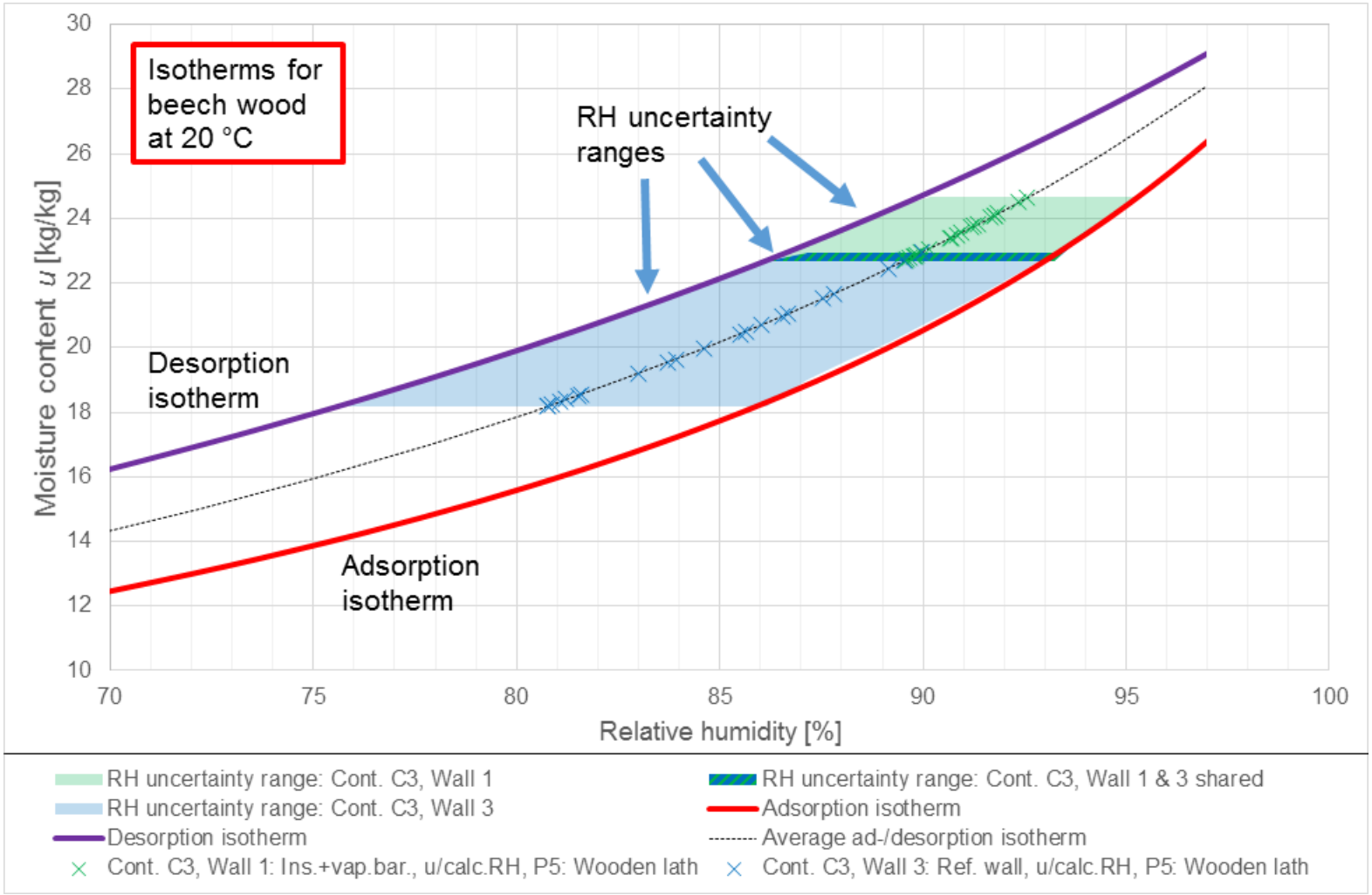


*Figure 153 Enlarged version of Figure 116 on page 150.*

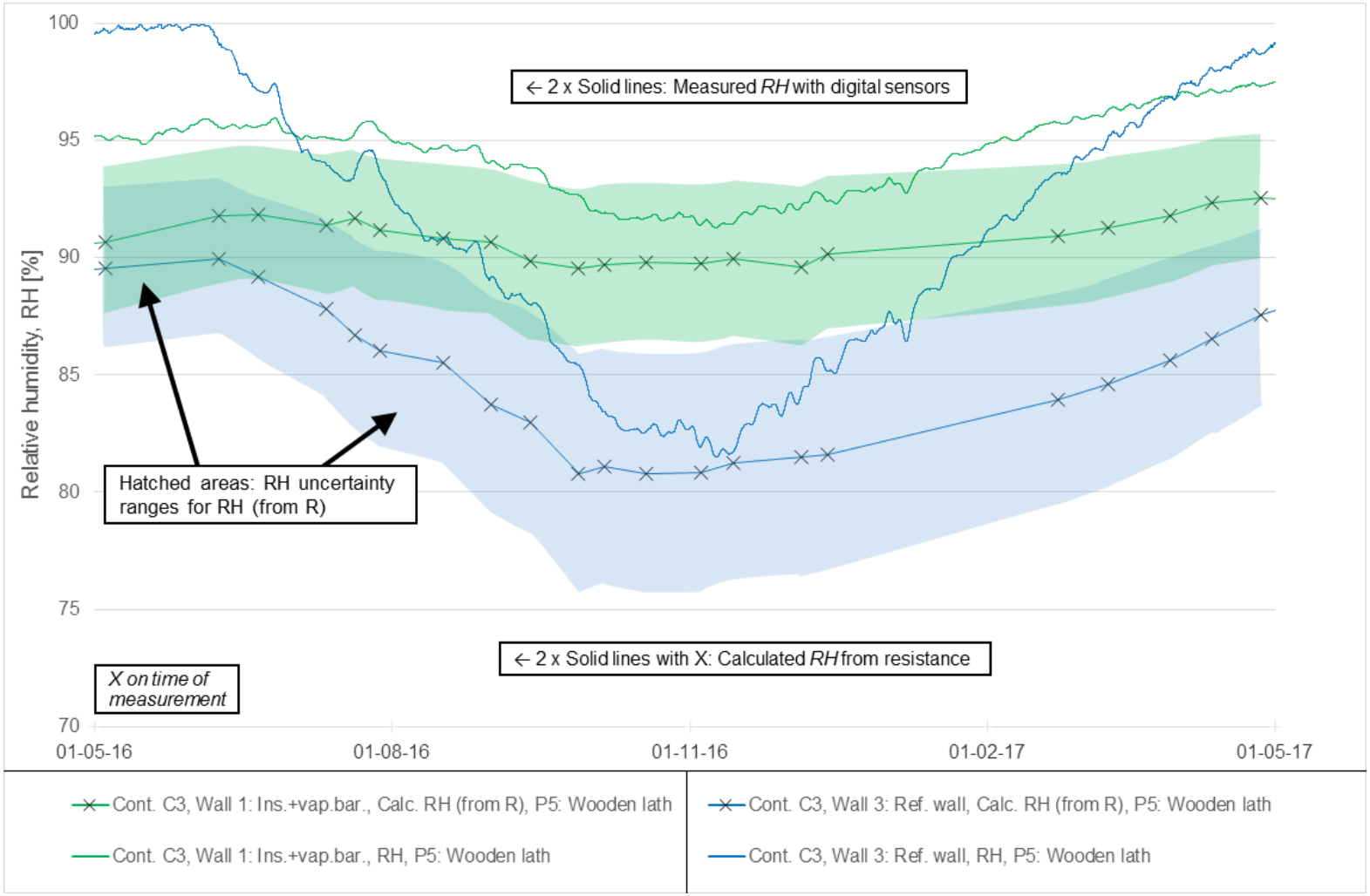


*Figure 154 Enlarged version of Figure 117 on page 152.*

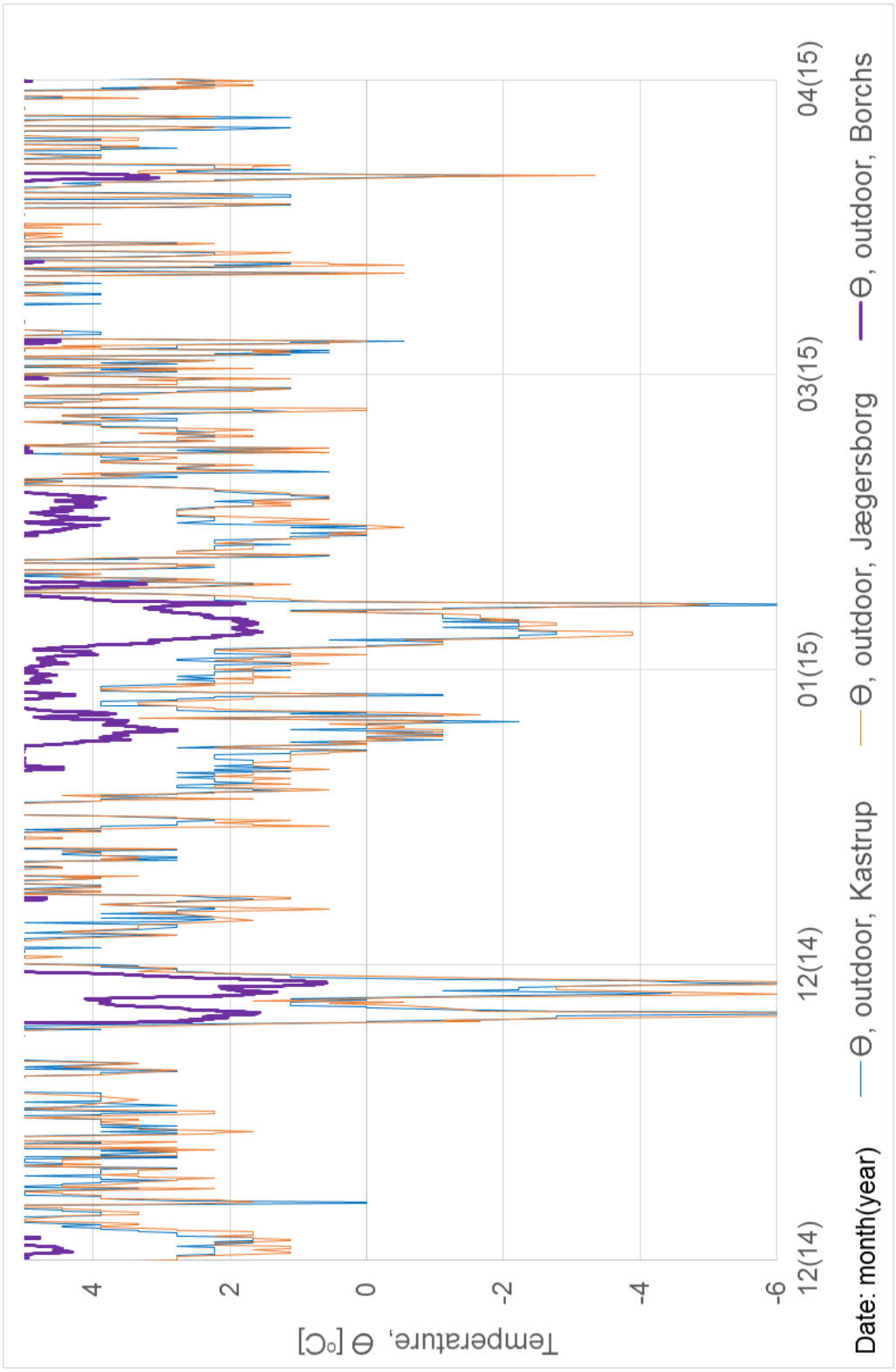


*Figure 155 Enlarged version of Figure 131 on page 173.*

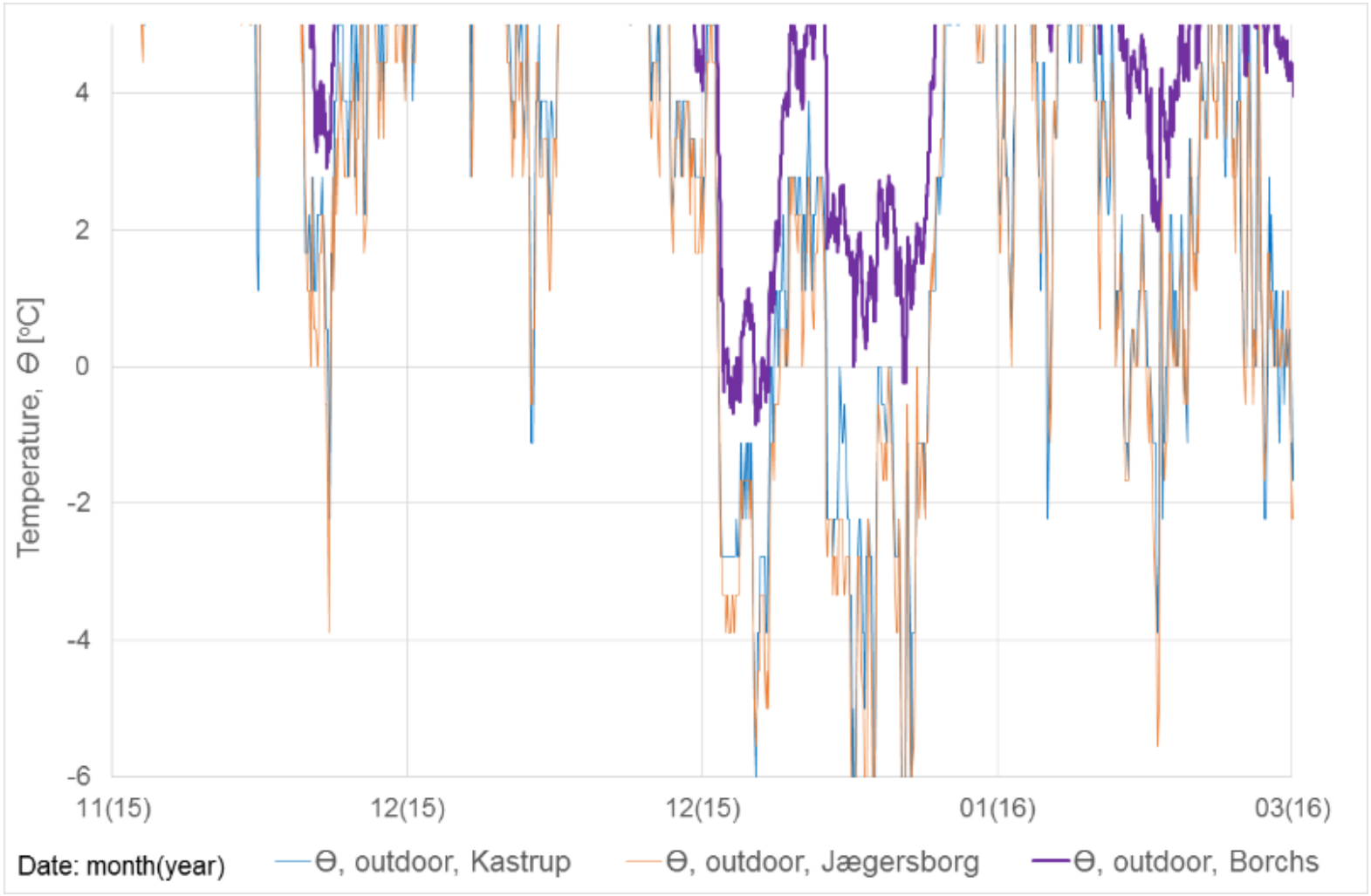


*Figure 156 Enlarged version of Figure 132 on page 173.*

| Number of residents | | | | | |
|---|---|---|---|---|---|
| Room 09: Insulated | 1 | 1 | 2 | 1 | 1 |
| Room 12: Un-insulated | 1 | 2 | 1 | | 1 |

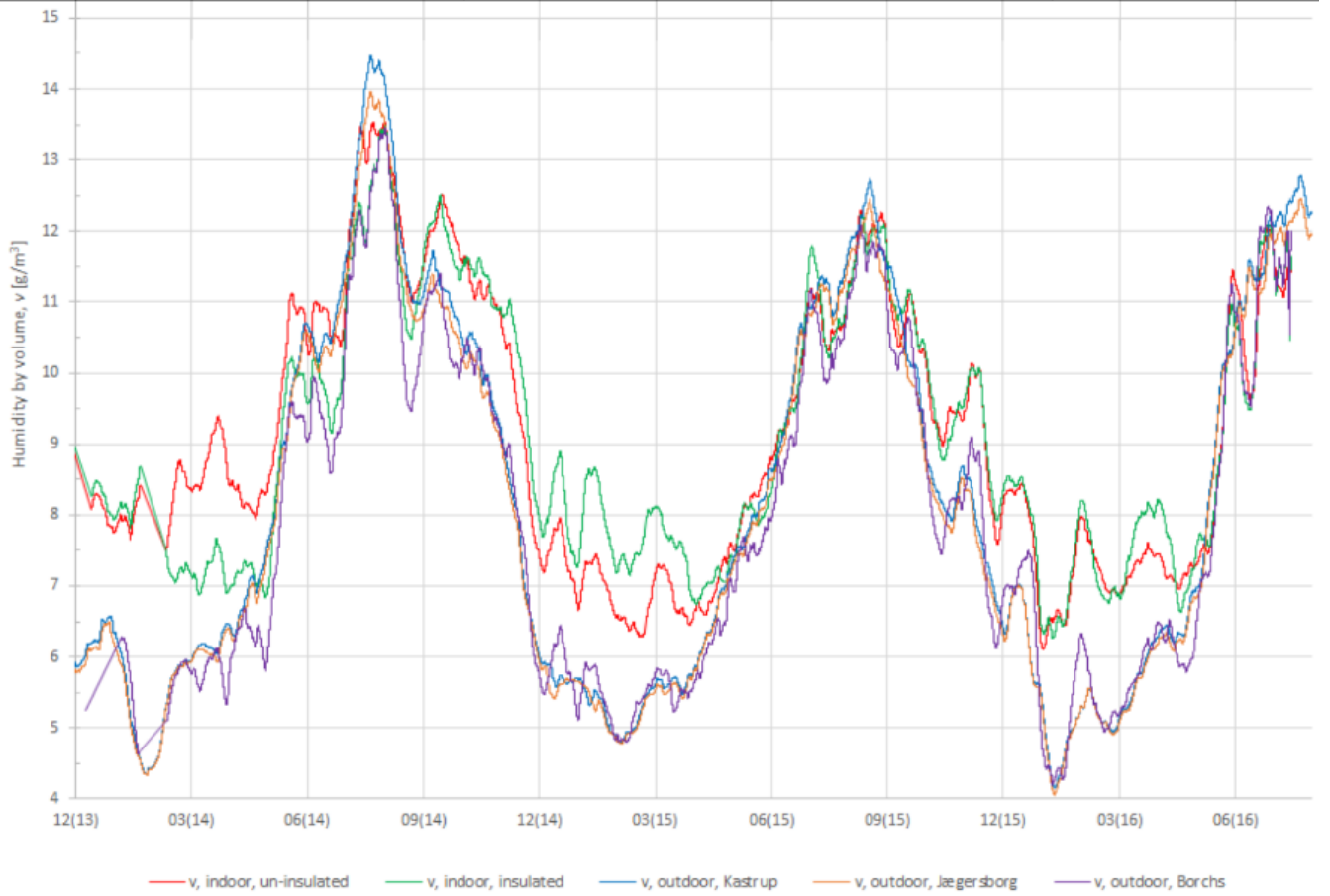


*Figure 157 Enlarged version of Figure 133 on page 174.*

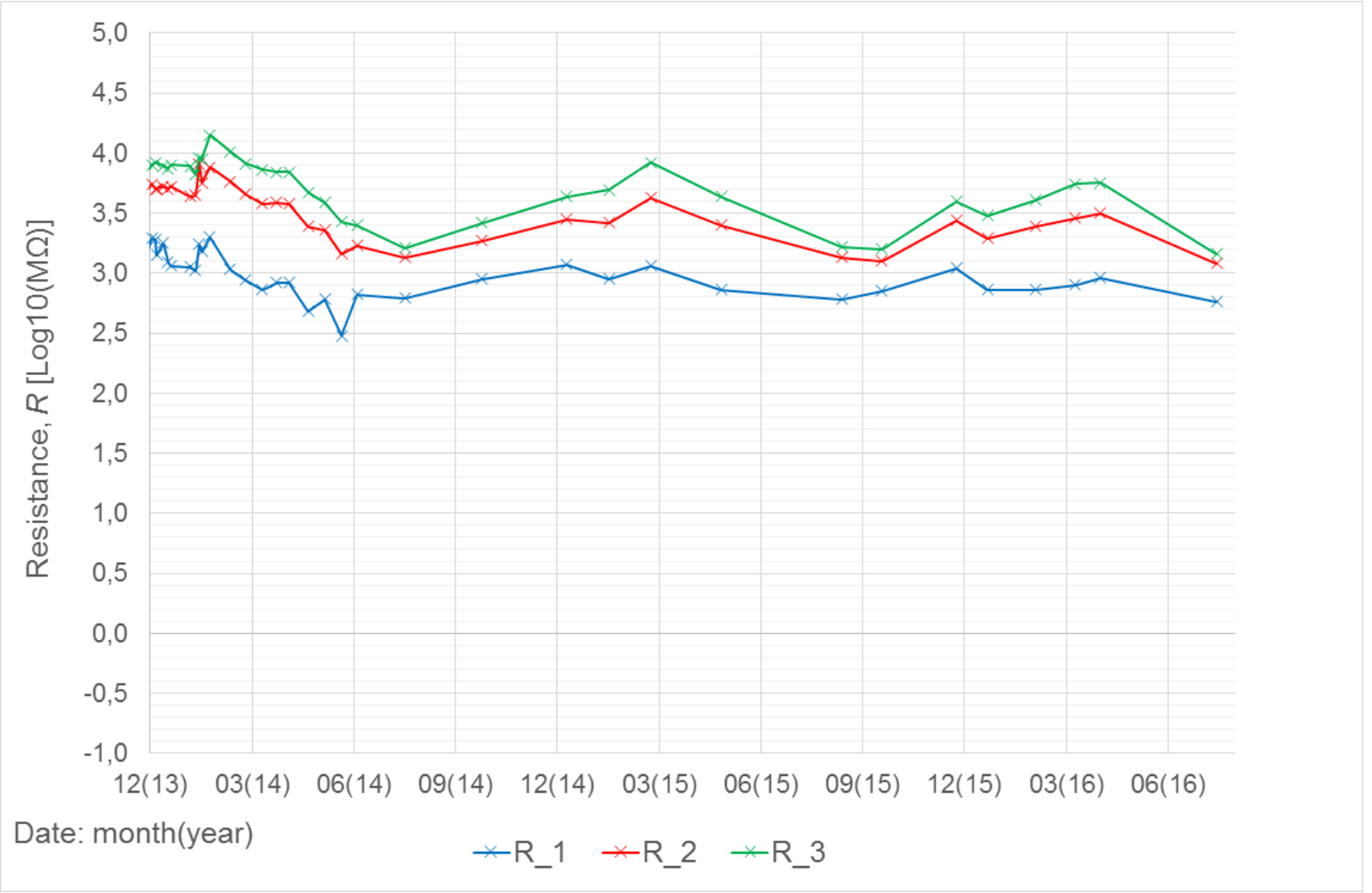


*Figure 158 Enlarged version of Figure 135 on page 176.*

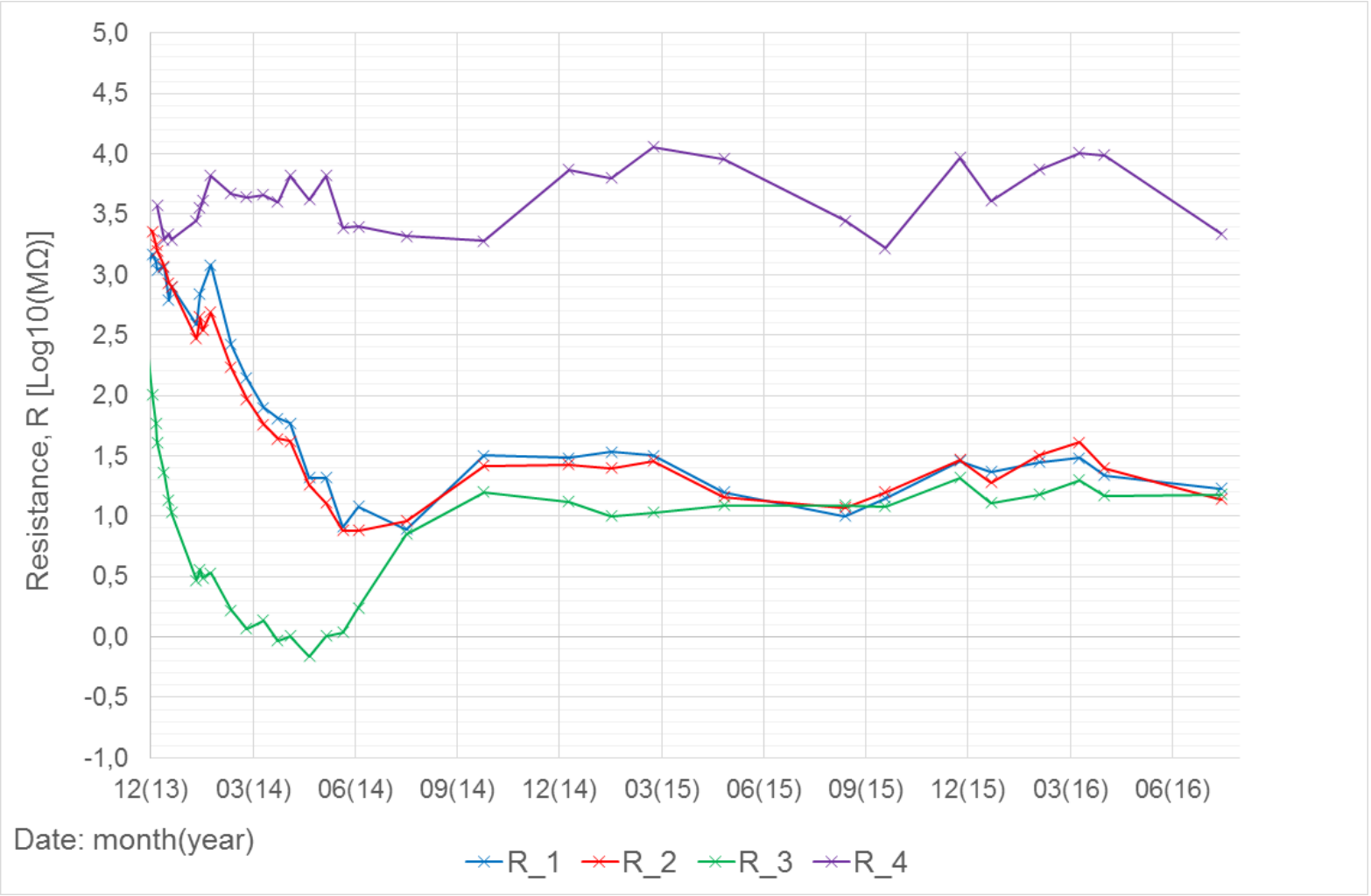


*Figure 159 Enlarged version of Figure 136 on page 176.*

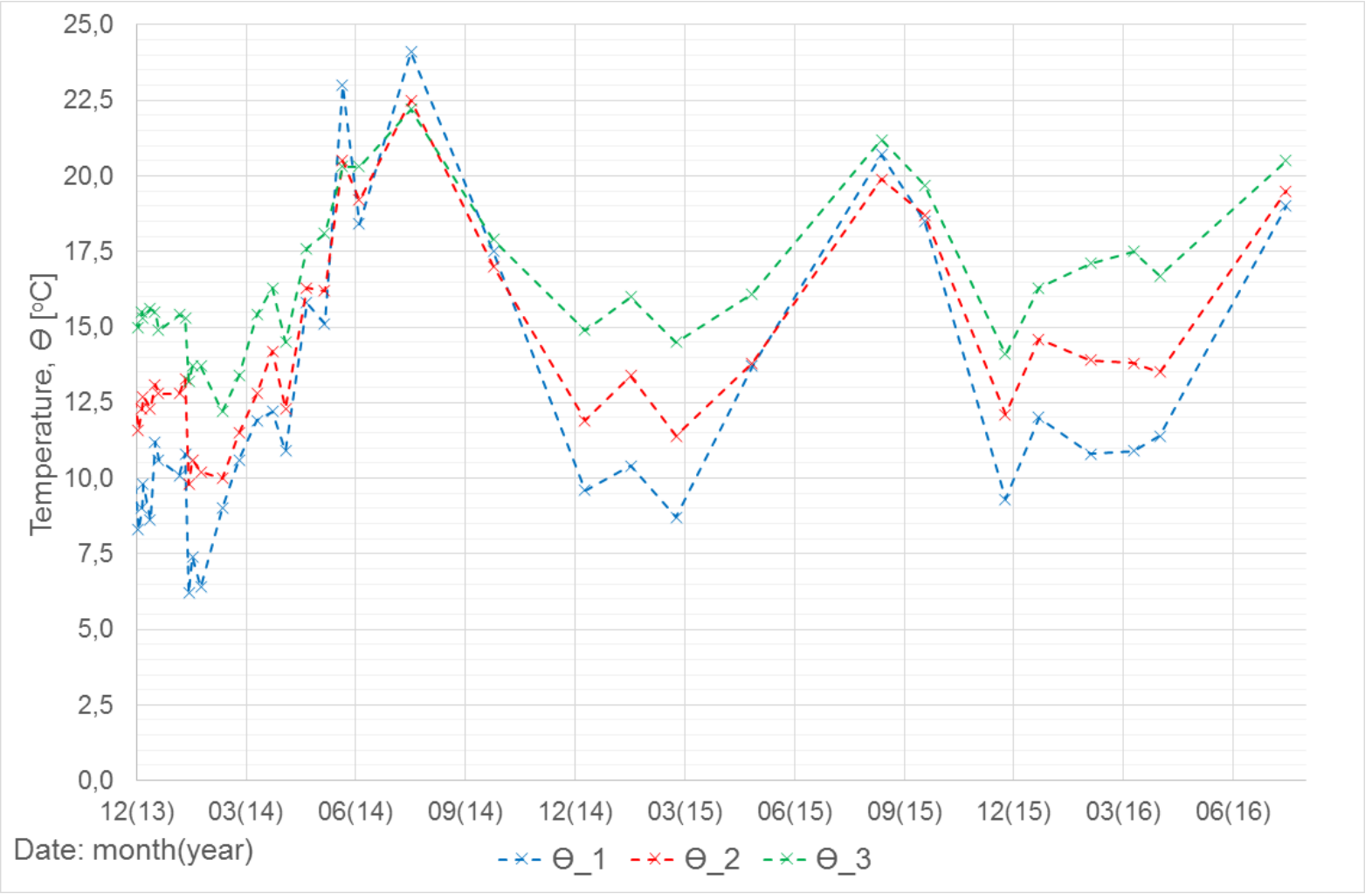


*Figure 160 Enlarged version of Figure 137 on page 177.*

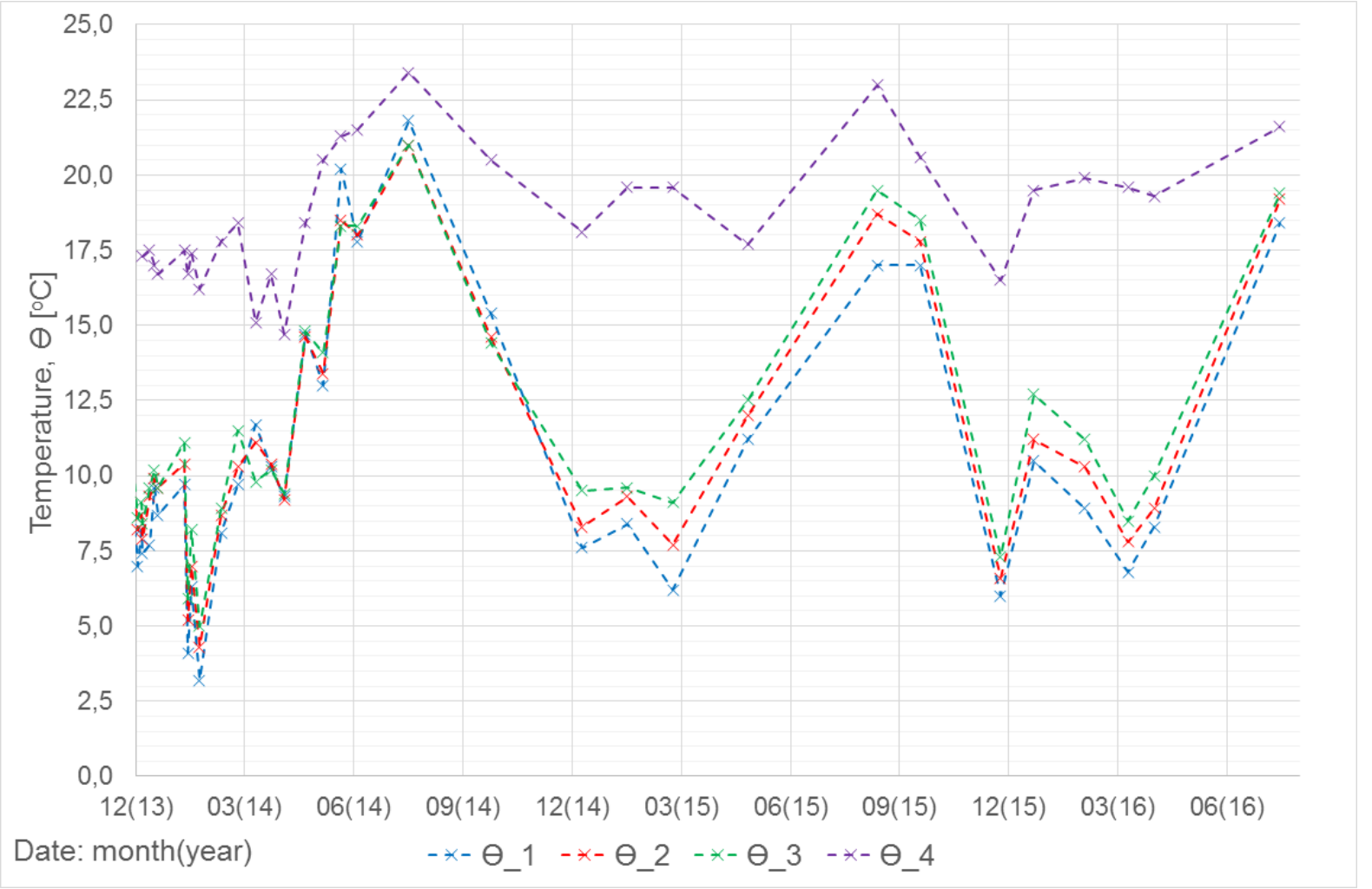


*Figure 161 Enlarged version of Figure 138 on page 177.*

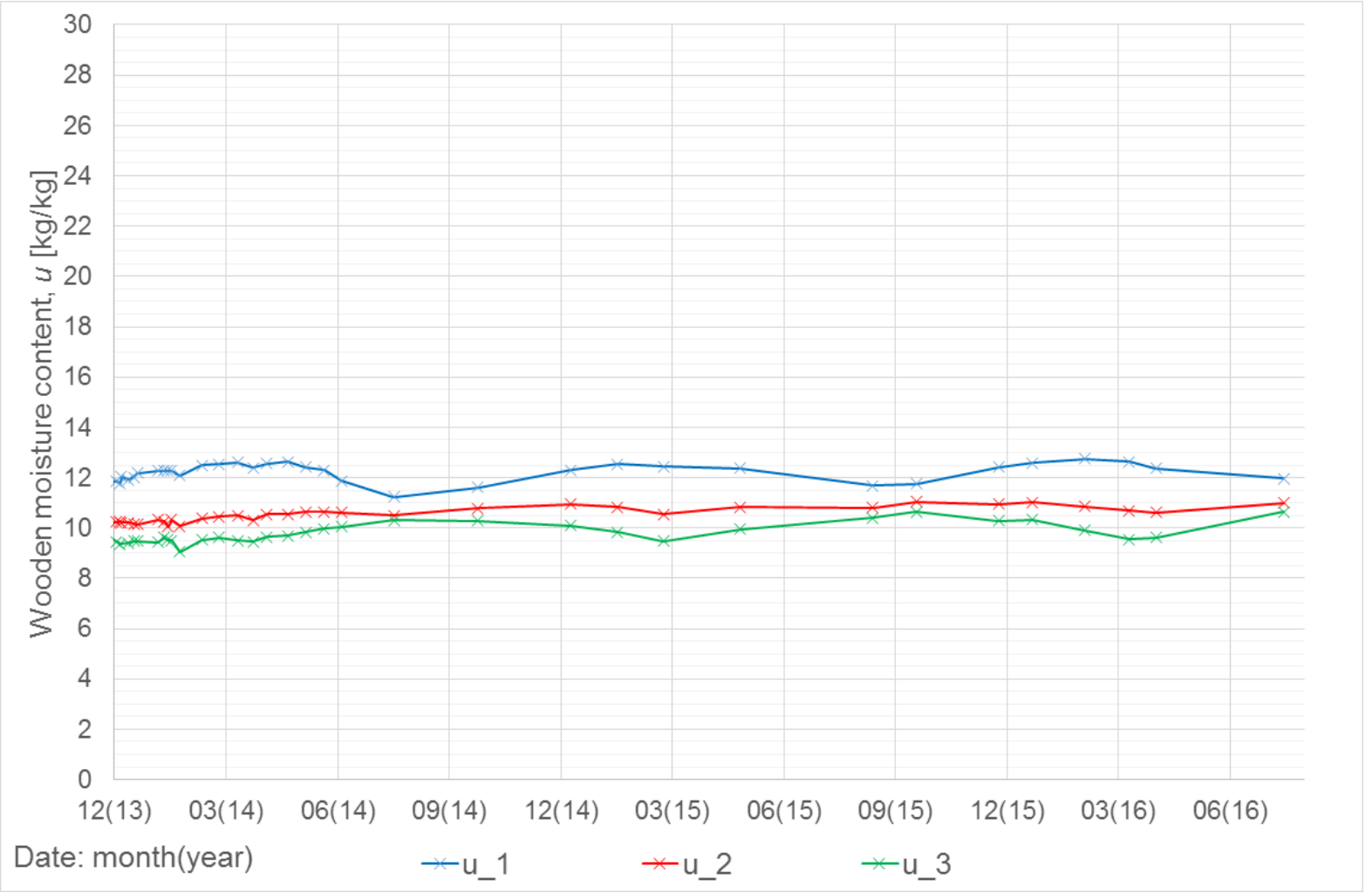


*Figure 162 Enlarged version of Figure 139 on page 178.*

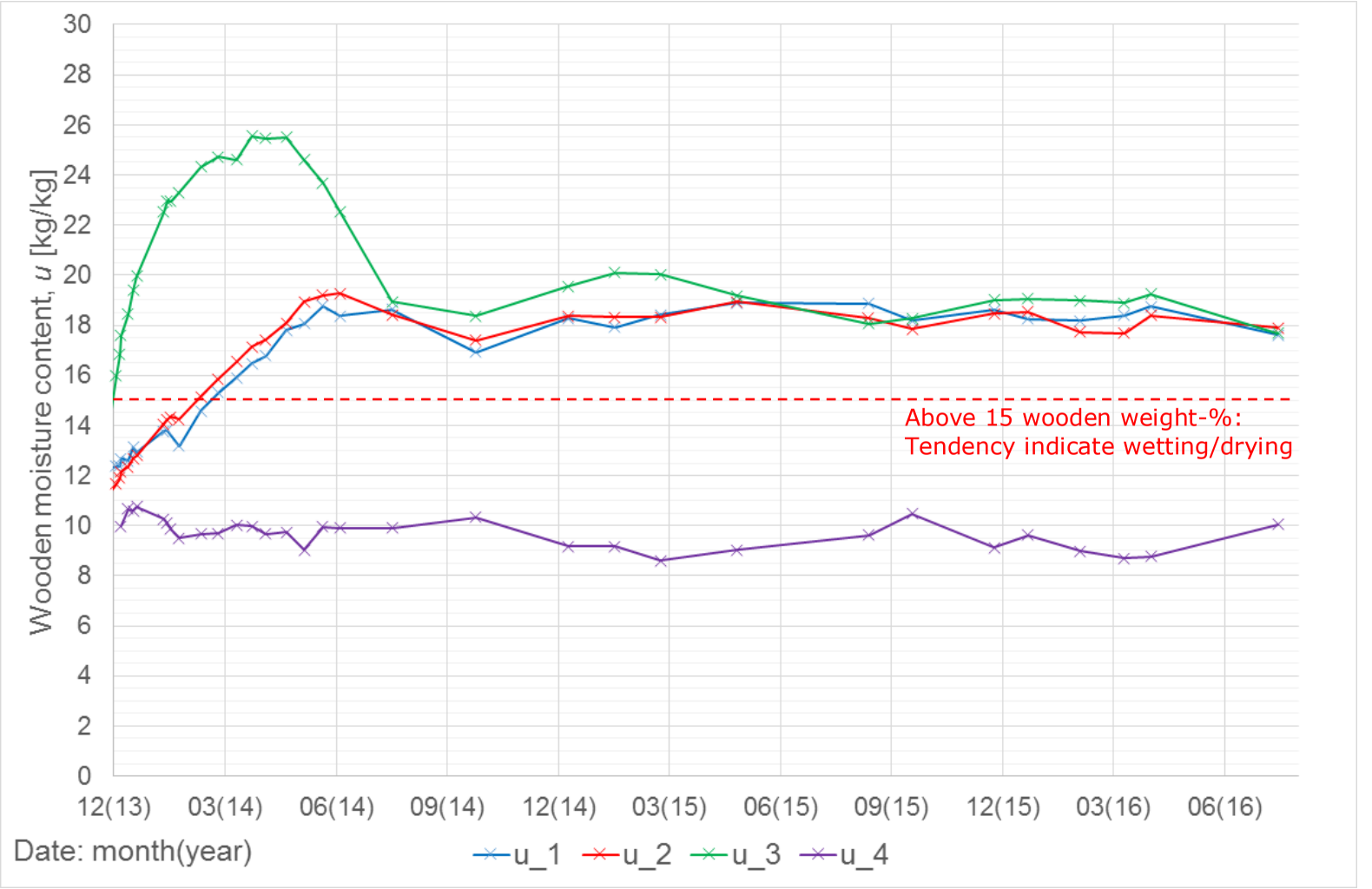


*Figure 163 Enlarged version of Figure 140 on page 178.*

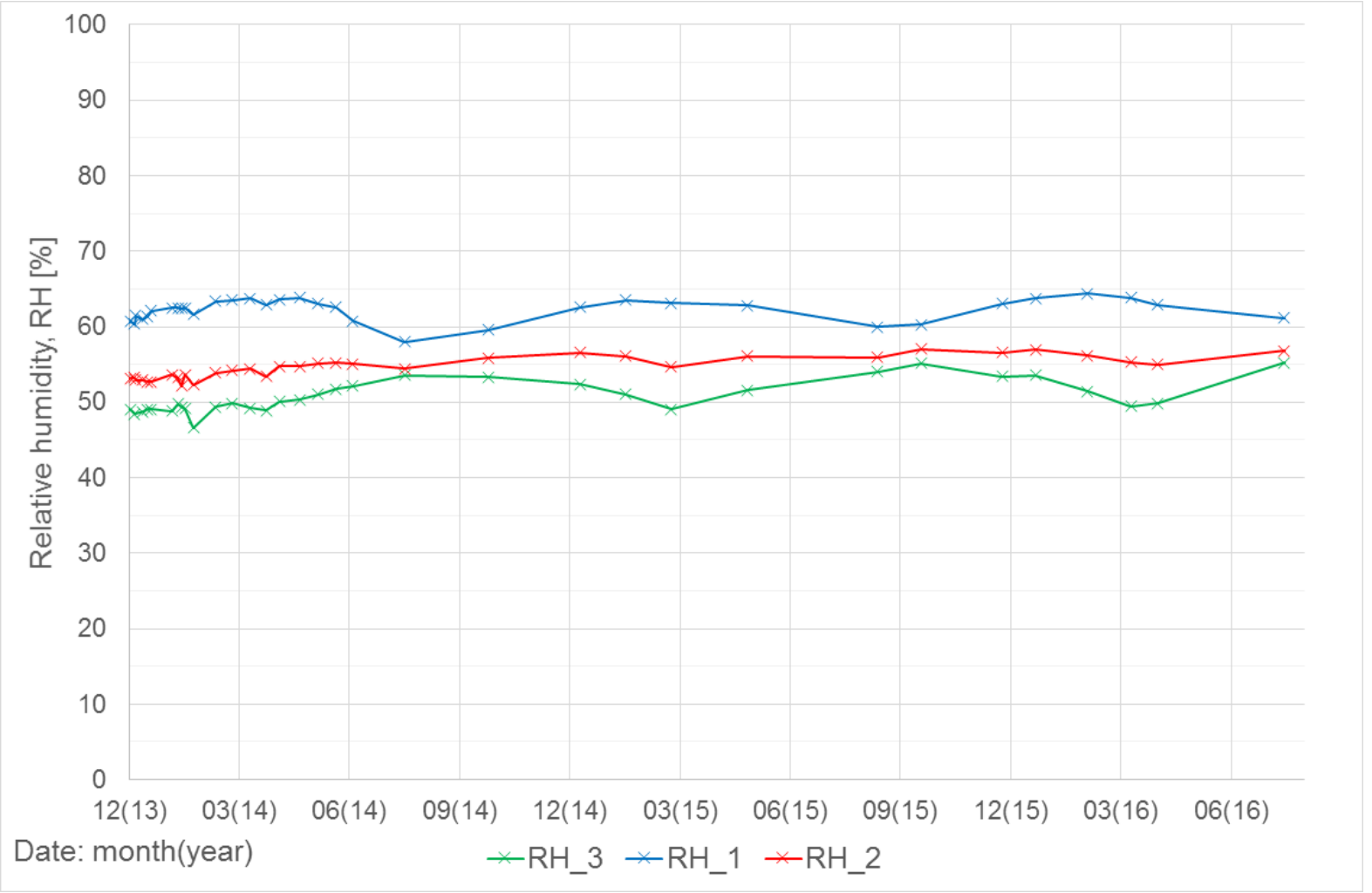


*Figure 164 Enlarged version of Figure 141 on page 179.*

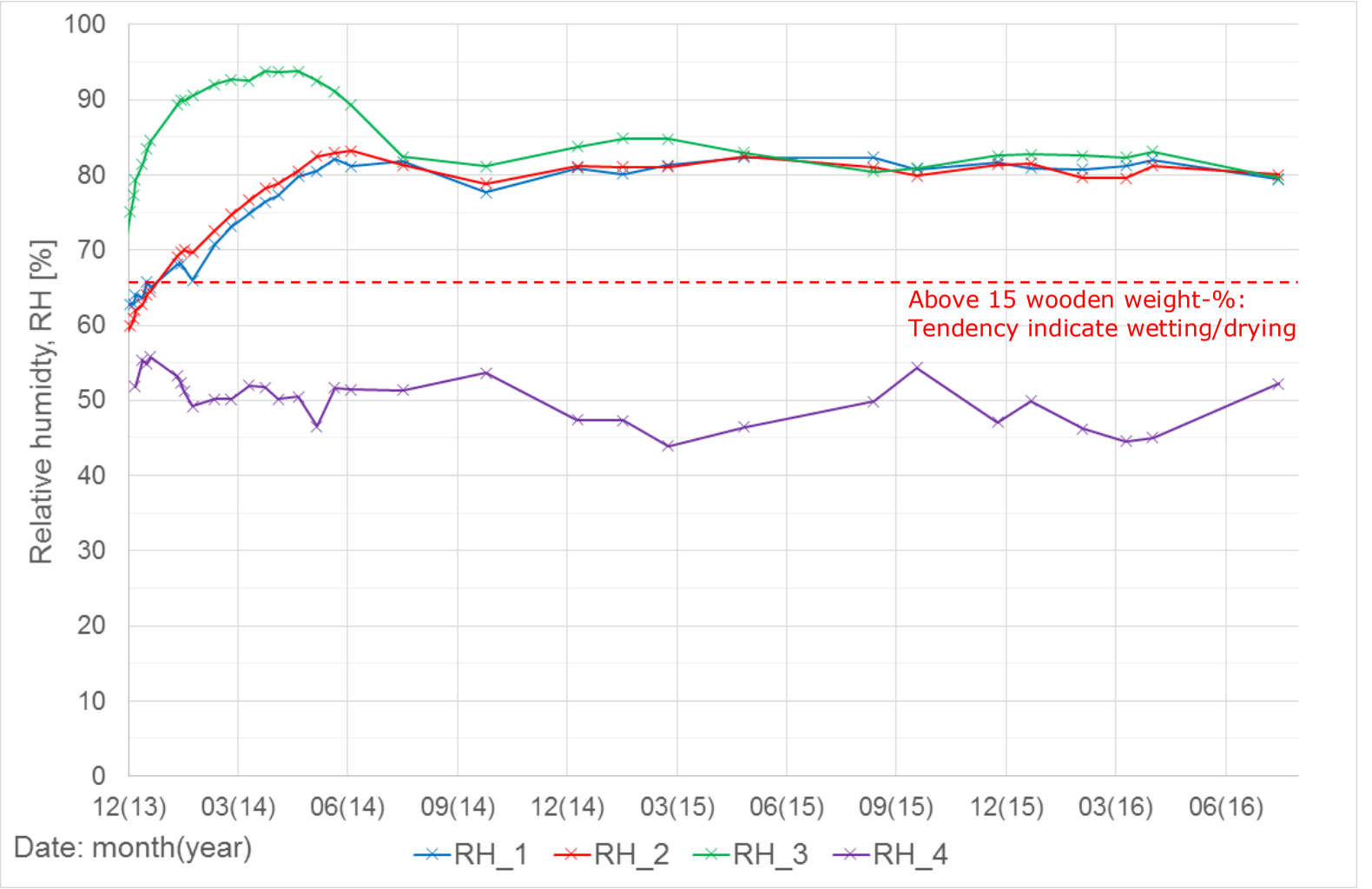


*Figure 165 Enlarged version of Figure 142 on page 179.*


*Figure 166 Enlarged version of Figure 143 on page 180.*

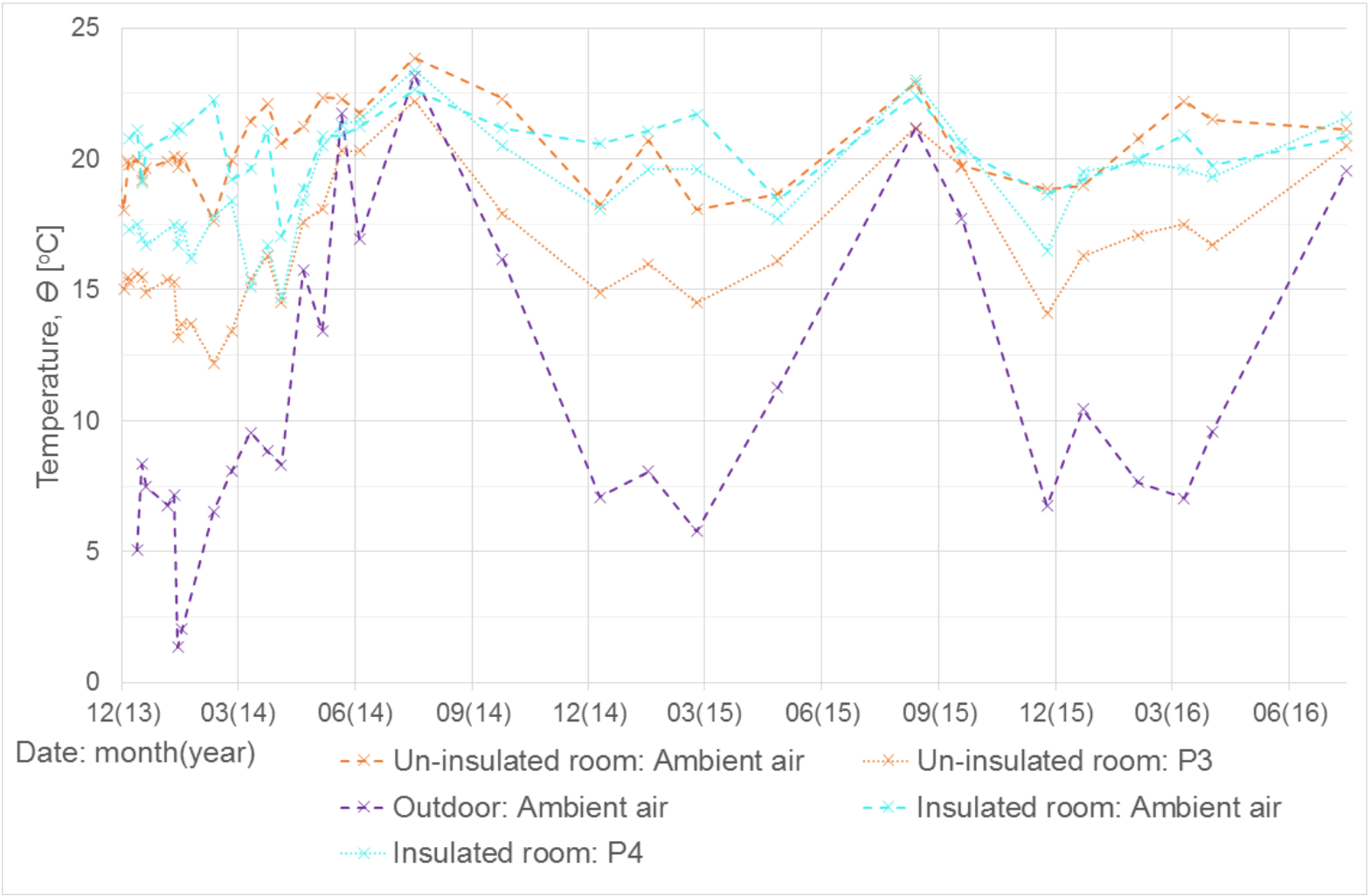


*Figure 167 Enlarged version of Figure 149 on page 185.*

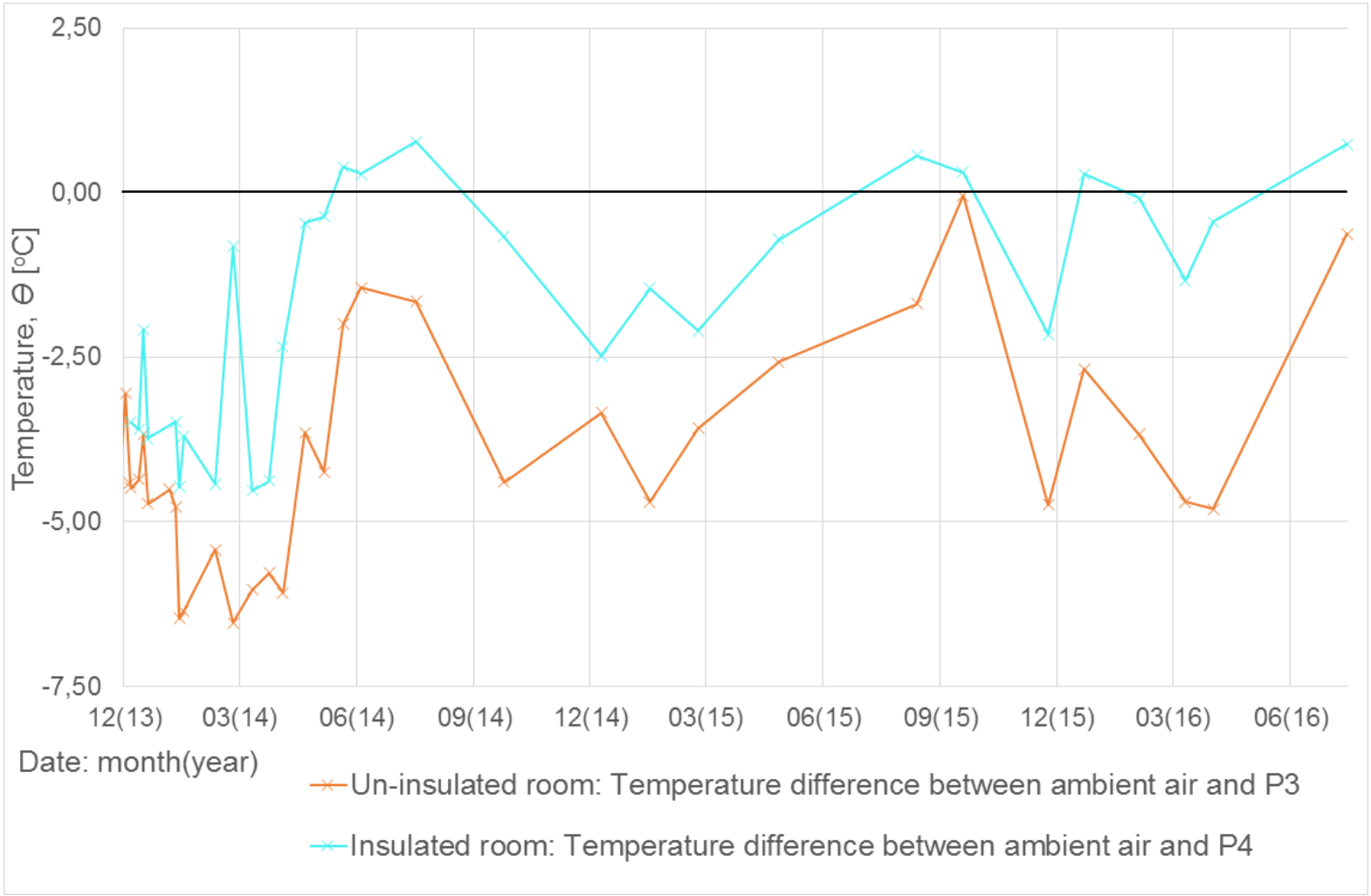


*Figure 168 Enlarged version of Figure 150 on page 185.*

# APPENDIX B EXTENDED DESCRIPTION OF DATA PROCESSING: EXPERIMENTAL SETUP → DATA FILES AND GRAPHS

The script/code for processing data from the experimental setup, written entirely by the PhD student from scratch, comprise of approximately 90 source files, comprising a total of 11500 lines of code and comments. The code has been written with a focus on future usability for later PhD students or technical staff. The work has included a large amount of code optimization and variable type declaration, to prevent the computer/server running the script to run out of storage capacity, while keeping run-time within a reasonable timeframe.

The overall process of the data treatment and script can be seen in Figure 169 and Figure 170.

The actions of the Matlab script is controlled by the 23 parameters presented in Table 8, under the main Matlab file "containerDataNormal.m". Each variable control if various parts of the code should be used or ignored.

| Parameter no | Parent parameter | Possible settings | Description |
|---|---|---|---|
| 1 | | ON \| OFF | Turn on to load data. Else will previously loaded data be used, if available. |
| 2 | | ON \| OFF | Turn on for specific plots, collating various configuration of walls and sensor points into the same graph. |
| 3 | | ON \| OFF | Turn on to plot:<br>> Each wall, including all sensor points.<br>> Each sensor point, including all walls.<br>> All measurement in one plot. |
| 4 | | ON \| OFF | Turn on to plot individual measurement points. |
| 5 | 2 \| 3 \| 4 | ON \| OFF | Child parameter: Control if relative humidity should be plotted in the defined parent parameters. |
| 6 | 2 \| 3 \| 4 | ON \| OFF | Child parameter: Control if temperature should be plotted in the defined parent parameters. |
| 7 | 2 \| 3 \| 4 | ON \| OFF | Child parameter: Control if humidity by volume should be plotted in the defined parent parameters. |
| 8 | 2 \| 3 \| 4 | ON \| OFF | Child parameter: Control if resistance should be plotted in the defined parent parameters. |
| 9 | 2 \| 3 \| 4 | ON \| OFF | Child parameter: Control if values calculated from resistance measurements should be plotted in the defined parent parameters. |
| 12 | | ON \| OFF | Controls if climate values should be plotted. |
| 13 | | ON \| OFF | Parent parameter: Control if any values from damage models should be plotted. |
| 14 | 13 | ON \| OFF | Child parameter: Control if calculated wooden decay should be plotted. |

| | | | |
|---|---|---|---|
| 15 | 13 | ON \| OFF | Child parameter: Control if calculated mould index should be plotted. |
| 16 | 13 | ON \| OFF | Child parameter: Control if T/RH isopleths should be plotted. |
| 17 | 25 | ON \| OFF | Child parameter: Control if plots should include wall/sensor numbers. |
| 18 | 25 | ON \| OFF | Child parameter: Control if separate graphs with legend should be created in sub-directory. |
| 19 | | ON \| OFF | Debug mode. |
| 21 | | ON \| OFF | Turn on to save data to .csv format. |
| 22 | | ON \| OFF | Turn on to smooth data. |
| 23 | 21 \| 26 | 1-7 | Define the receiver, will be created in individual sub-directories. |
| 24 | 22 | ON \| OFF | Child parameter: Control if non-smoothened data should also be included in output. |
| 25 | | ON \| OFF | Turn on if graphs should be plotted. |
| 26 | | ON \| OFF | Turn on to save data to Delphin .out format. |

*Table 8 Parameter entries in control variable of Matlab script: scriptRun*

The time period of plots is controlled in the Matlab file "startTimesteps.m". It is possible to set up multiple plot periods, to various receivers, which can then be shared automatically via cloud services. An example of a plot period is illustrated in the following bullet list:

- dateCustomSet{end+1}{1} = '01-May-2015'; (start date in plot)
- dateCustomSet{end}{2} = '01-May-2017'; (end date in plot)
- dateCustomSet{end}{3} = [5,7]; (code for receiver)

The period in which the damage models are calculated are set individually with similar settings, as illustrated here:

- dateDamage{1} = '01-May-2016';
- dateDamage{2} = '01-Jul-2017';

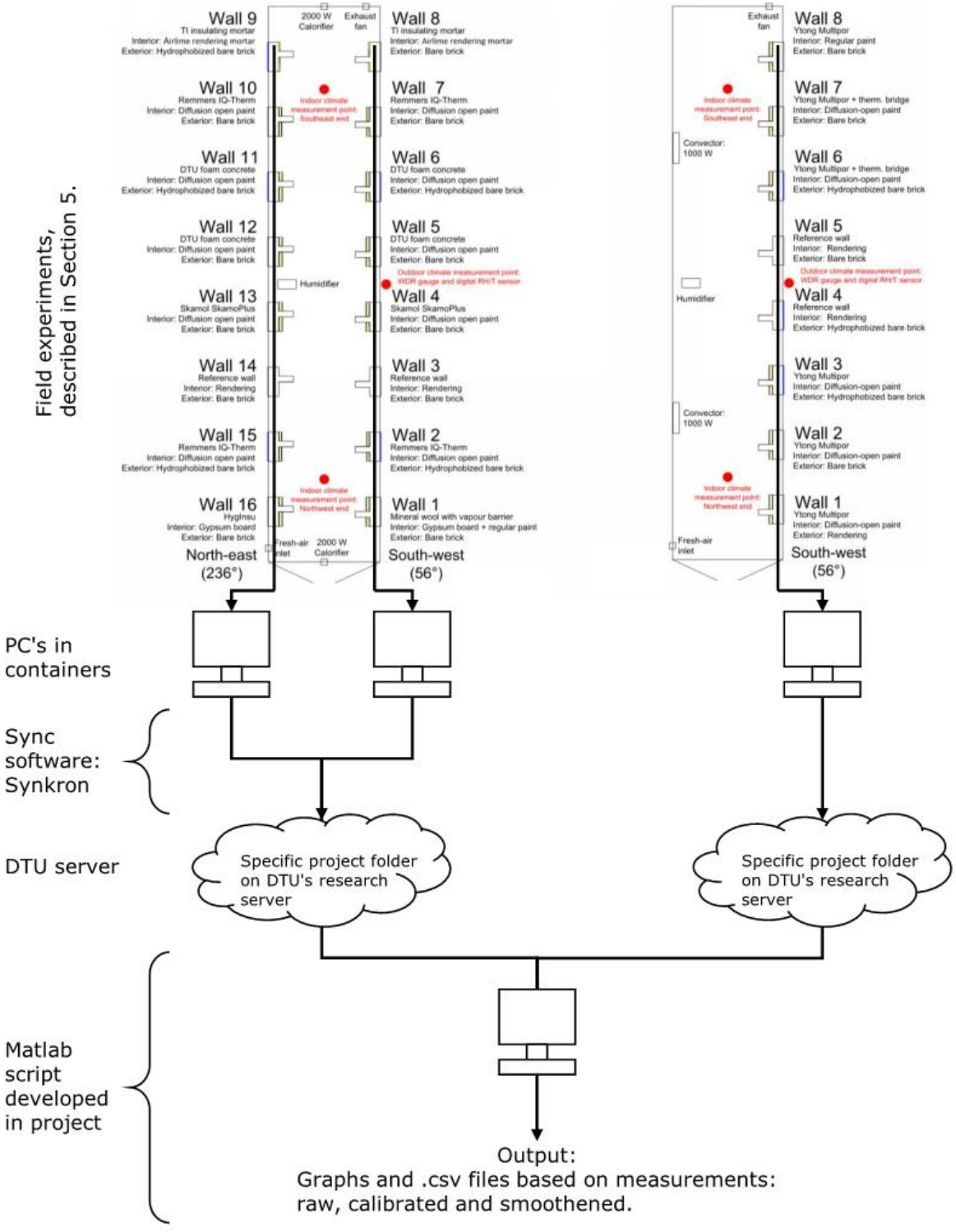


*Figure 169 Overall setup of data processing from field experiments.*

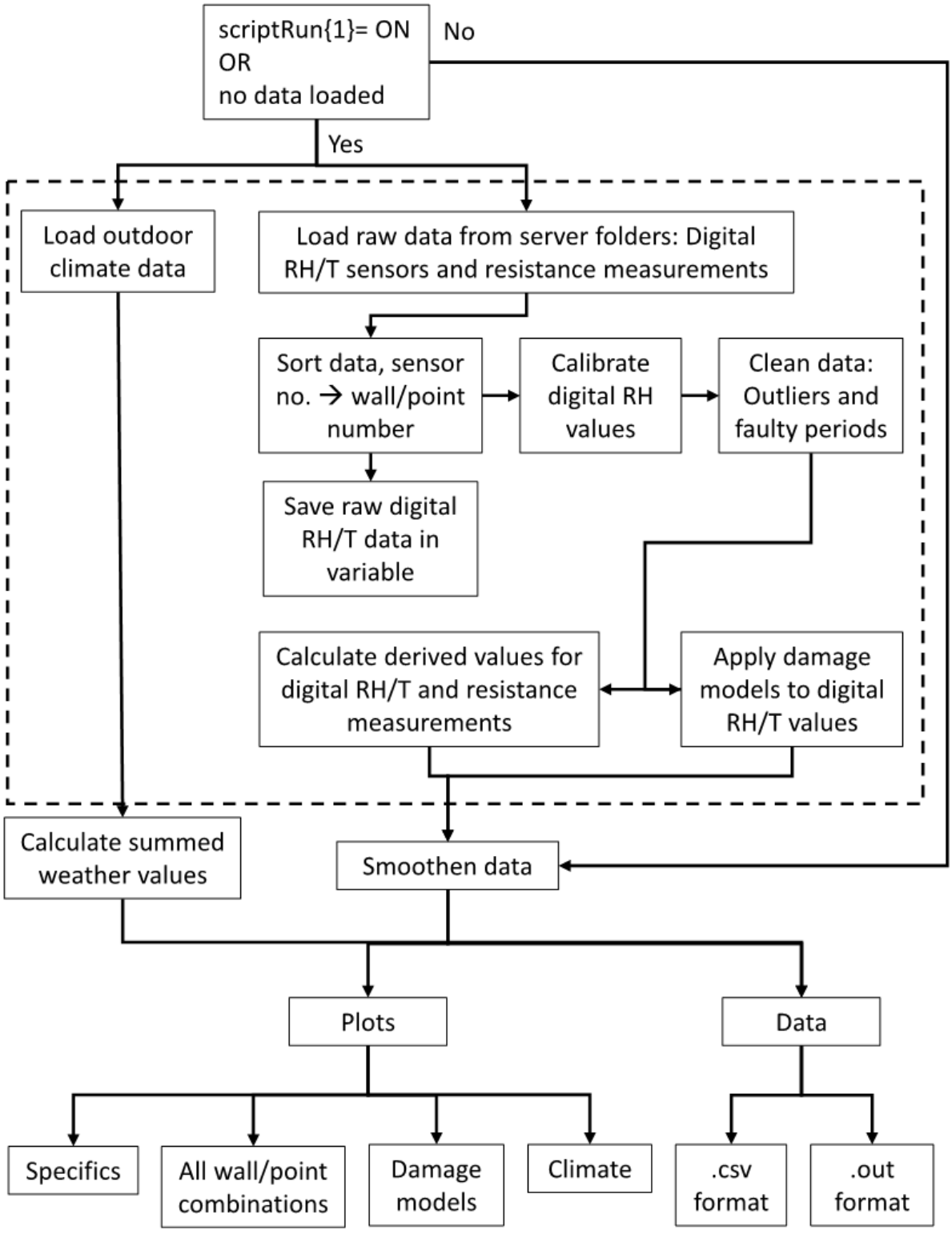


*Figure 170 Flowchart of overall functions in Matlab script for processing measurements.*

# APPENDED PAPERS

A. Paper #1: Interior insulation – Characterisation of the historic, solid masonry building segment and analysis of the heat saving potential by 1d, 2d, and 3d simulation

B. Paper #2: Interior insulation - Experimental investigation of hygrothermal conditions and damage evaluation of solid masonry façades in a listed building

C. Paper #3: Influence of hydrophobation and deliberate thermal bridge on hygrothermal conditions of internally insulated historic solid masonry walls with built-in wood

The outline and state of the papers have been described in the section before the introduction, on page xxi and xxii. The individual content has been summarised in the start of relevant sections.

# A. PAPER #1: INTERIOR INSULATION – CHARACTERISATION OF THE HISTORIC, SOLID MASONRY BUILDING SEGMENT AND ANALYSIS OF THE HEAT SAVING POTENTIAL BY 1D, 2D, AND 3D SIMULATION

Energy and Buildings 162 (2018) 1–11

Contents lists available at ScienceDirect

Energy and Buildings

journal homepage: www.elsevier.com/locate/enbuild

# Interior insulation—Characterisation of the historic, solid masonry building segment and analysis of the heat saving potential by 1d, 2d, and 3d simulation

Tommy Odgaard [a,b,*], Søren Peter Bjarløv [a], Carsten Rode [a]

[a] Technical University of Denmark, Department of Civil Engineering, Brovej 118, 2800 Kongens Lyngby, Denmark
[b] COWI A/S, Parallelvej 2, 2800 Kongens Lyngby, Denmark

ARTICLE INFO

*Article history:*
Received 11 April 2017
Received in revised form 1 December 2017
Accepted 4 December 2017
Available online 9 December 2017

*Keywords:*
Multi-storey
Segment
Saving potential
Historical
Internal insulation
Simulation
Multi-dimensional

ABSTRACT

When considering interior insulation of historic, multi-storey buildings with solid masonry walls, it is important to focus on two important factors: How big is the building segment to which it can be applied, and what is the significance of how the multi-dimensional geometry of these façade walls is considered in the assessment of the heat saving potential.

The findings show that a large proportion of Danish multi-storey dwellings with solid masonry walls, high energy consumption, and uniform characteristics were found to originate from the period 1851–1930. This segment accounts for 25% of all multi-storey apartments in Denmark. It was investigated, which relative reduction of the average thermal transmittance could be obtained by interior insulation when simulated in different dimensions, degrees of insulation and thickness. The analysis showed that partial insulation of the spandrels below windows on the 2nd/3rd highest storeys accounted for up to 40% of the average thermal transmittance reduction achievable by fully insulating inside walls, while covering 17% of the space needed in the full insulation strategy. Furthermore, the analysis showed an underestimation of average thermal transmittance by 2-dimensional compared to 3-dimensional simulation by up to 57%, indicating that 3-dimensional analysis is needed to obtain realistic results.



## 1. Introduction

The Danish government has a vision of becoming fossil fuel free by year 2050. Numbers from the Danish Energy Agency [1] estimated that the climate adjusted energy consumption in multi-family households in Denmark in 2013 accounted for 13.87 TWh. Compared to a total energy consumption of 168.61 TWh in Denmark, multi-family housing accounted for 8.2% of the total energy use. The distribution was the same when focusing on the energy used for heat consumption and domestic hot water, where multi-storey housing accounted for 8.3% of the consumption with 11.35 TWh compared to a total of 137.40 TWh.

With today's focus on reducing energy consumption, Danish multi-storey buildings with solid masonry walls receive increasing attention due to their large potential for energy conservation and consequent reduction of $CO_2$ emissions [2,3]. Multi-storey buildings have previously been studied extensively [4,5], and it was found that a great part of the buildings with solid masonry walls were typically built in the period 1850–1930, and to some degree in the period 1930–1950. Multi-storey buildings from 1850–1930 and 1930–1950 have a high energy consumption for space heating and domestic hot water of approximately 155 kWh/m$^2$, which could potentially be reduced to approximately 60 kWh/m$^2$, which is almost the level required for rather new buildings built according to the Danish Building Regulations 2010 [3]. In a later work [2] the space heating and domestic hot water demands for buildings from the same period was calculated to be 150 kWh/m$^2$. Total energy consumption, for all multi-storey building from the periods 1851–1930 and 1931–1950, was calculated to be 4.35 TWh/year and 2.35 TWh/year respectively, corresponding to approximately 3.2% and 1.7% of the total energy used for space heating and domestic hot water in Denmark. When comparing with the specific energy used for space heating and domestic hot water in all multi-storey buildings, the energy use of buildings from these periods corresponds to 38.3% and 20.7% respectively.

Heat loss is one aspect accounting for a large part of the total energy consumption for multi-storey dwellings from the period

* Corresponding author at: Parallelvej 2, 2800 Kongens Lyngby, Denmark.
*E-mail addresses:* TOOG@COWI.dk (T. Odgaard), SPB@byg.dtu.dk (S.P. Bjarløv), CAR@byg.dtu.dk (C. Rode).

https://doi.org/10.1016/j.enbuild.2017.12.008
0378-7788/

1850–1930. The heat loss can be simplified to a vertical component through roof and ground, and a horizontal component through the façade, including the gables, when exposed. There has previously been a focus on the façade, showing that considerable energy savings can be achieved by applying thermal insulation to the facades [6,7]. The best solution from a building physics point of view is to insulate the exterior surface of existing buildings [8,9]. Exterior insulation is, however, rarely suitable for buildings from the segment, as most are to some degree worthy of preservation. The lowest Danish preservation class is "worth-to-preserve", where the preservation of original architectural features of the exterior facade is mandatory. External insulation is therefore not included in the present paper. In the segment of "worth-to-preserve" buildings, occupants are able to obtain indoor climate and comfort levels that meet modern standards by means of interior insulation. However, interior insulation approaches have a range of disadvantages that must be acknowledged: 1) Thermal bridges cannot be eliminated; 2) Reduction of the indoor space; 3) Alteration of interior expression; 4) Risk of increased moisture content in the materials [10–13]; 5) The temperature in the original wall drops severely [12,14].

To support the intention of the government to reduce energy, and to obtain deeper knowledge on these building segments, the present paper identifies the number and distribution of multi-storey buildings and apartments in Denmark from the period 1850–1950 and describes the architectural and structural features they have in common. A minor study of typical building characteristics and country-wide segment size was performed in [15]. The aim of the present paper is to focus on a regional segment analysis in Denmark, and to perform a further clarification of building characteristics. This clarification of segment size and regional placement in Denmark can serve as a basis for development of general energy reduction strategies that could apply to buildings from the period, with possible large-scale application to reduce energy consumption.

Previous research has focused on how to install interior insulation in old masonry constructions [6,16–19], but it did not clarify the degree to which thermal bridges, such as floor structure and geometry around windows, would influence the resulting efficiency of the interior insulation. Thermal bridges do not influence the construction when it is considered from a 1-dimensional point of view, but will have an increasing influence when 2- and 3-dimensional aspects are taken into account. The present paper determines the influence of typical thermal bridges that are found in these segments on the efficiency of different interior insulation methods when modelled in 2 and 3 dimensions.

## 2. The traditional Danish multi-storey housing, year 1850–1930

The following section comprises a literature study into the compositions and characteristics of historical multi-storey buildings in Denmark built in the pre-war period before the Second World War. The building style of this building segment has been extensively researched and documented in Danish by J. Engelmark [4,5], who has provided detailed documentation about the composition of this type of buildings.

The first building code in Denmark took effect in 1856 [5,20]. This collection of regulations was ground breaking, due to clear formulations covering construction details and choice of materials and thought through in such a manner that the general dimensions and construction techniques did not change until the 1930′s, when a new building code was passed. The buildings from the period 1850–1950 were generally built after the same strict principles because of this building legislation, gradually changing to more modern building methods through the last 20 years of the period.

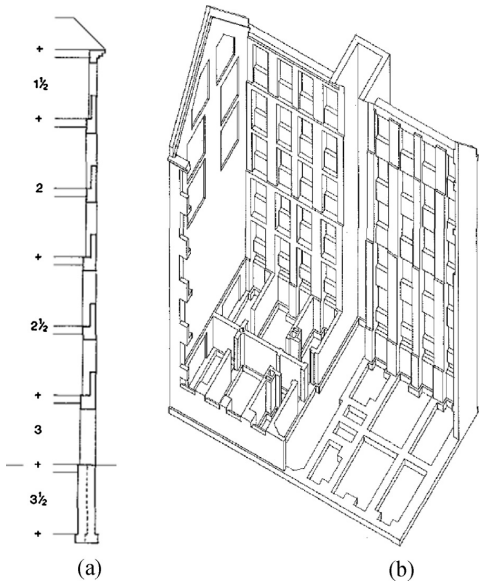


**Fig. 1.** (a) Thickness of wall columns in bricks (~0.24 m per brick). (b) Maximum penetration of outer leaf. Both illustrated in courtesy of J. Engelmark, extracts from Danish literature [4].

This change of methods that was introduced with the new building code in 1930, included the use of cavity walls, and concrete and steel as building materials [5]. The building geometries however generally followed the same principles as in the earlier period. Initially, the legislation applied to construction in Copenhagen, but the regional boroughs of Denmark quickly adopted the regulations.

The general working procedure in the period was that architects designed the multi-storey buildings, usually cutting margins to the limit permitted by the regulations, based on short handbooks. Engineers were rarely involved in the design of standard multi-storey building, and then only if special details were needed. Due to this custom, the majority of buildings from the period were constructed with the same general characteristics.

The buildings were typically made with facades of brick, with or without render, and with some wooden members, e.g. as supports of the floor beams. The floor decks were constructed with wooden beams between the façades, with wooden floorboards on top, clay pugging placed on wooden pugging boards between the beams and wooden furring strips below as underlay for a rendered ceiling. One important parameter, which was defined in the building code, was the composition of the façade, including the minimum thickness of load bearing wall columns and the dimensions of spandrels under windows. Danish masonry is constructed after modular dimensions revolving around brick dimensions (228 × 108 × 54) mm with mortar joints in the horizontal direction of 12 mm and in the vertical direction of (3 bricks + 3 mortar layers) = 200 mm. The thickness of the wall columns varied within the building and was defined as shown in Fig. 1(a), with 1½ bricks' thickness (348 mm) at the highest floor, increasing downwards as illustrated in the figure. Windows were placed between the wall columns, and spandrels completed the façade in the areas between the windows and the floor decks. The spandrels are of special interest in this study, since they were always 1 brick thick (228 mm) regardless of the floor number, and thus constitute the thinnest part of the façade. The wall above the window had a thickness corresponding to the column size at the given floor. The building code stated a maximum

permissible degree of penetration of the facade for windows and doors to be 2/3′s of the surface in the horizontal direction and 1/2 of the surface in the vertical direction. This maximum allowance was aimed for when designing buildings to yield the highest floor space and lowest material use, which thereby resulted in very perforated facades. Fig. 1(b) shows the outer shell of a typical construction from the time, with the maximum allowed degree of penetration and minimum size of column and spandrel. The only place where large undisturbed wall areas were present was in the gables, but the gables were generally shared with the next building, and thus not exposed to the exterior. The heat loss of the gable wall was therefore negligible.

## 3. Method, segment size, floorplans and heat flux models

The investigation took place in three parts. The amount and national distribution of relevant buildings and apartments were documented, using a major database managed by the Danish Government [21]. The previously described characteristic building design was investigated based on a range of randomly selected floor plans. A theoretical thermal simulation study was performed, which focused on the possible areas for application of interior insulation in single apartments, using assumptions based on the construction legislation that had been in force and validated in the floor plan analysis.

### 3.1. Investigation of segment size

To discover the segment size and nationwide distribution, data for this paper were collected from the national Danish Building and Dwelling Register, shortened "BBR". The register was administered at a governmental/ministry level, and contained information on all buildings in Denmark [21].

The BBR register was used to investigate the segment size of typical old multi-storey dwellings in Denmark. The raw data from the BBR were sorted according to different criteria to remove irrelevant apartment areas and to quantify the size of the segment at the national, regional and local scale. The data were initially prepared by:

1. Including only buildings containing multi-storey apartments.
2. Including only non-demolished buildings.
3. In some buildings, the original attic and basement rooms have been converted into apartments. These areas have been removed from the dataset, as focus is on the original apartments.

The data were then further categorised as described in the following subsections.

#### 3.1.1. Construction year

The data were sorted after three different ranges of construction year, where the first two were defined according to when shifts in prevailing building style/characteristics had taken place, shifts which have previously been identified in literature [2,3,5]. The third sorting mechanism included all construction years in the database, acting as a point of reference, for illustrating the size of the first two segments, compared to all current multi-storey dwellings in Denmark.

The definitions used in this paper are the following:

1. 1851 to 1930: Solid walls.
2. 1931 to 1950: Introduction of cavity walls and new materials: concrete and steel.
3. $-\infty$ to January 25, 2017: Point of reference, all units in register.

#### 3.1.2. Storeys in building

The definition of multi-storey houses in the register were households split vertically. To exclude minor town houses, the investigation was limited to multi-storey buildings with a minimum of 3 storeys.

#### 3.1.3. Regional location

Denmark was at the time of the analysis divided into 98 municipalities with unique municipality ID-numbers, distributed over 5 regions. Neither the municipalities nor the regions were equivalent in size or population. Municipalities with high density of multi-storey buildings in the period 1851–1930 were extracted from the regional summations and documented separately. An illustration of the regional division and separate municipality values can be seen in Fig. 5.

#### 3.1.4. Facade composition

For the 1851–1930 and 1931–1950 periods, only buildings with brick façade were included in the datasets. The point-of-reference dataset described in Section 3.1.1 comprises all registered units with all façade types.

#### 3.1.5. Decomposition into individual apartments/buildings

In the dataset, all apartments and buildings had unique ID numbers. The data were decomposed by isolating unique apartment/building ID.

### 3.2. Investigation of actual façade composition from floorplans

A range of floorplans from different parts of Copenhagen were analysed to see if a correlation between different parameters existed. The following parameters were registered for each individual apartment: Amount of rooms, amount and width of windows, apartment area including walls, length of thermal envelope and length of gable.

43 apartments divided over 9 buildings were analysed. The buildings had the following construction years: 1874, 1886, 1886, 1880, 1890, 1892, 1897, 1904, 1914, 1920. One of the buildings included a mansion apartment.

There were two purposes of the floorplan investigation:

1. To validate the characteristics of the traditional Danish multi-storey housing.
2. To identify a possible correlation between the segment size investigation in Section 3.1 and the total amount/width of windows in the Danish multi-storey building stock from the relevant period.

### 3.3. Thermal heat flux models, based on Danish construction legislation and different insulation strategies

A 3-dimensional model [22], representing the characteristic geometry of a façade element from the 1850–1930 period, as illustrated in Fig. 1(b), was set up in the simulation software COMSOL Multiphysics [23]. The model was used to perform a thermal investigation and to calculate the relative reduction in average thermal transmittance (U-value) for the masonry part of the model, achieved by applying interior insulation that varied in extent and thickness. The model consisted of a wall section, with vertical delimitation in the middle of columns on the left and right side of an spandrel. The horizontal delimitation was underneath the wooden pugging board in the floor structure.

The 1-dimensional model was defined as a point in the 1-brick spandrel consisting of bare brick towards the exterior and rendering on the interior side (total wall thickness 238 mm).

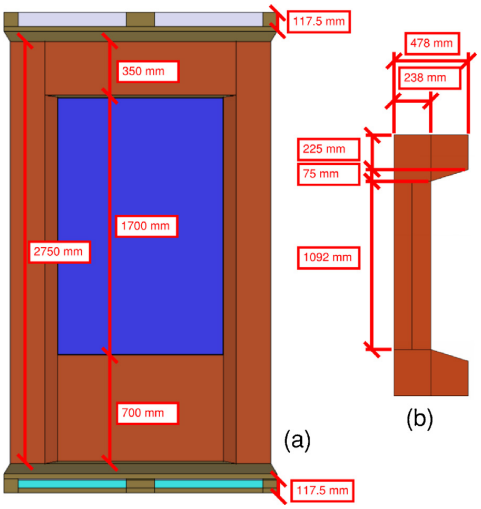


**Fig. 2.** Dimensions of COMSOL model. (a) = vertical section of 3-dimensional model, (b) = 2-dimensional model. Horizontal dimensions of 2- and 3-dimensional model are identical.

The 2-dimensional model was produced as a horizontal cross section of the 3-dimensional model to ensure cohesion. The model was created at the level of the spandrel. Examples of the model can be seen in Fig. 3(a, b).

The 3-dimensional model was made as a parametric model as illustrated in Fig. 2. Examples of model variations can be seen in Fig. 3(c,d,e,f). The models in this study were based on a wall column depth of 2 bricks (478 mm), corresponding to the traditional construction at the second and third floor from the top. The model has a resulting exterior masonry area of 3.83 $m^2$ after subtracting the window area. The vertical composition of the model is based on the illustration on page 84 of [5]. This construction has a total height of 2.985 m, consisting of an interior surface height of 2.75 m. The window has a height of 1.70 m, with 0.70 m of spandrel below and 0.35 m of interior wall above. The horizontal composition of the model was based on conversations with J. Engelmark, on his thesis [4] and on the floorplan investigation described in Section 3.2. The width of the construction consist of two half wall columns of 0.30 m on each side of 4½ bricks (1.092 m) of spandrel or window structure, resulting in a total width for one window sections of 1.692 m.

The floor structure consisted of pugging, air, a 100 × 100 mm wooden beam in the middle and 2 50 × 100 mm wooden beams at right and left edge of the model. The beams embedded in masonry in the columns did not have any air surrounding them in the model as these areas have in practice become full of dust and dirt. The beam between the columns had air and pugging surrounding it, as the beam would be lying freely and not in direct contact with the wall.

1-, 2- and 3-dimensional models are abbreviated as “1d”, “2d” and “3d” in the graphs, tables and caption text in this paper.

The parametric 2- and 3-dimensional models include a wide range of different insulation strategies, as it can be seen in Fig. 3. The models are abbreviated in graphs, tables and caption text with the following words: Spandrel, sides, front. The abbreviations have the following meaning:

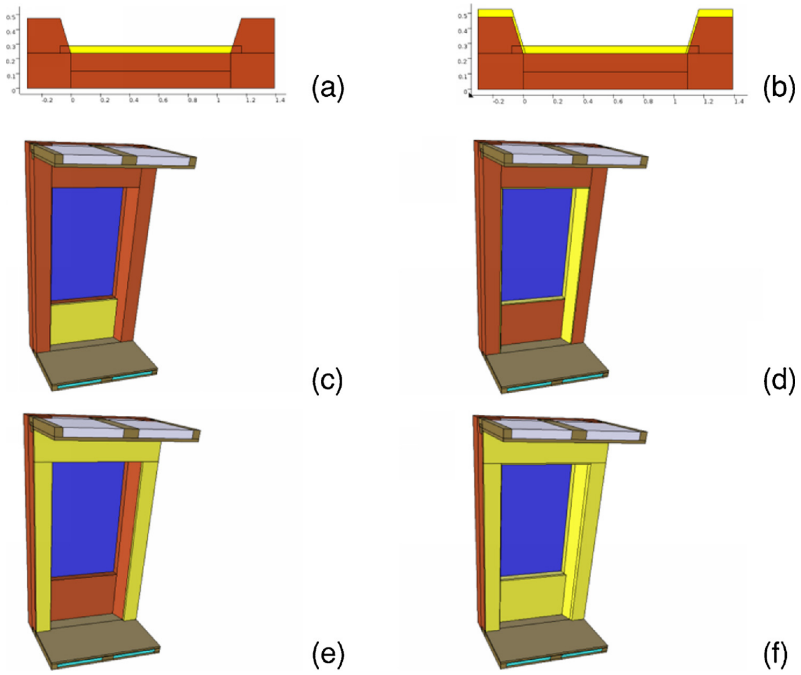


**Fig. 3.** Examples of the models used in the simulations [22]. The text describes simulation dimension and placement of insulation as presented in Section 3.3: (a) 2d, spandrel. (b) 2d, spandrel, sides, front. (c) 3d, spandrel. (d) 3d, sides. (e) 3d, front. (f) 3d, spandrel, sides, front.

- Spandrel: Insulation placed in front of the spandrel. Can be seen in Fig. 3(a,b,c,f).
- Sides: Insulation placed on the slant side of the columns. Has a maximum thickness of 15 mm. Can be seen in Fig. 3(b,d,f).
- Front: Insulation placed at the front of the column and at the wall area above the window. Can be seen in Fig. 3(b,e,f).

The masonry area within the floor structure was left uninsulated in the models, as this area is rarely opened and insulated when performing refurbishment of multi-storey buildings in Denmark.

The thermal conductivity values of the materials in the model were mainly obtained from the Delphin material database [24,25]: Masonry (brick + mortar), $\lambda = 0.8$ W/(m·K), shown in red in the models; Thermal insulation, $\lambda = 0.045$ W/(m·K), shown in yellow in the models; Wood (longitudinal), $\lambda = 0.194$ W/(m·K), shown in brown in the models; Sandy clay, used as pugging, $\lambda = 1.76$ W/(m·K), shown in cyan in models.

The properties of air was defined in COMSOL Multiphysics [23]. The heat transfer through the air was thereby not limited to conduction, but also included radiation and convection, depending on the dimensions of the object. Air was coloured grey in models.

The window is shown in dark blue in the models, with a defined frame thickness of 115 mm. The resulting heat loss through the window was subtracted from the results, as focus was on the potential average reduction in thermal transmittance of the masonry part of the total external wall area.

## 4. Results

### 4.1. Segment analysis through the Buildings and Dwellings Register

The Danish Building and Dwelling Register [21] was used to evaluate the number of multi-storey buildings in Denmark. All results have been based on data extracted on January 25, 2017.

A segmented illustration of the total number of apartment units in Denmark, not situated on basement or attic level, is shown in Fig. 4, illustrating the large number of apartment units in Denmark

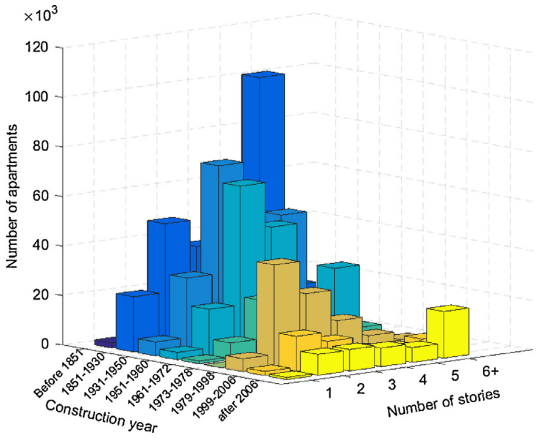


**Fig. 4.** Apartment units, sorted after construction year and number of storeys. The time steps represent shifts in building style, inspired by Wittchen & Engelmark [2,5].

with construction year in the period 1851–1930, and 1931–1950, compared to other periods. The apartment units are grouped according to construction year along the x-axis, storeys along the y-axis and the number of apartments within the respective groups on the z-axis.

The data on which Fig. 4 is based can be seen in Table 1 for the periods 1851–1930 and 1931–1950, with additional information regarding the number of individual buildings in the described periods. The numbers in the larger period $-\infty$ until data extraction in Table 1 serve as a reference number, for illustrating the share of multi-storey buildings/apartments which origin from the earlier periods.

The number of apartments with construction period 1851–1930 in Table 1 were further analysed according to the regional location. This data were plotted on a map of Denmark in Fig. 5(a). The map

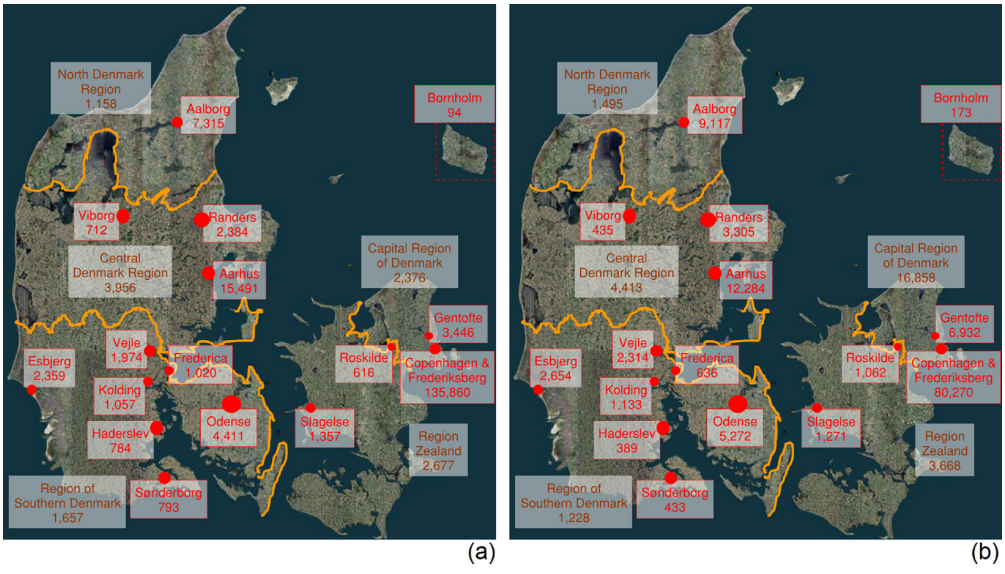


**Fig. 5.** Brick facade, multi-storey apartments >2 storeys. Periods: (a) = 1851–1930, (b) = 1931–1950.

**Table 1**
Segment analysis, number of multi-storey buildings and apartments.

| Sorting criteria | Period | Unique | 3 storeys | 4 storeys | 5 storeys | 6+ storeys | Sum |
|---|---|---|---|---|---|---|---|
| Brick façade | 1851 to 1930 | Buildings | 5,962 | 2,994 | 5,381 | 640 | 14,977 |
| | | Apartments | 38,961 | 31,118 | 103,414 | 18,004 | 191,497 |
| Brick façade | 1931 to 1950 | Buildings | 4,177 | 1,123 | 1,412 | 172 | 6,884 |
| | | Apartments | 72,821 | 22,984 | 49,427 | 10,110 | 155,342 |
| All façade types | $-\infty$ to 2016.11.28 | Buildings | 18,836 | 7,534 | 8,044 | 2,004 | 36,418 |
| | | Apartments | 299,175 | 159,593 | 196,572 | 105,725 | 761,065 |

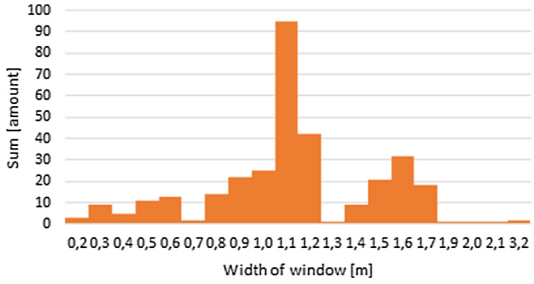


**Fig. 6.** All registered window widths from floorplan investigation.

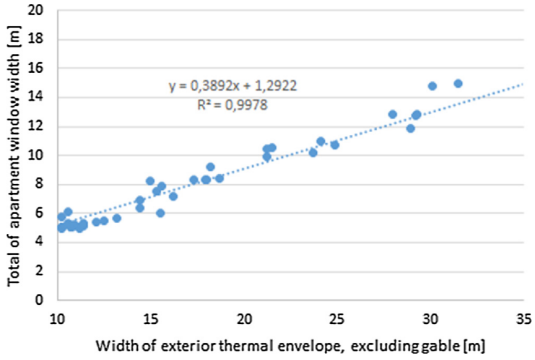


**Fig. 7.** Total window width and width of exterior thermal envelope for apartments from floorplan investigation. One mansion apartment is situated outside the axis, with coordinates (241.2, 94.8).

shows the regional borders with orange lines, including the number of apartment units in the regions outside the abstracted cities with orange text in unframed boxes. The number of apartment units in the abstracted cities are shown in red framed boxes connected to the red dot illustrating the location of the individual cities. A similar figure for the later period 1931–1950 can be seen in Fig. 5(b).

### 4.2. Façade investigation based on 43 floorplans

Each window was analysed and the results can be seen in Fig. 6. In this figure, it can be seen that the most registered window width is 1.1 m, and that windows with widths of 1.0, 1.1 and 1.2 m make up 50% of all registered windows.

The window width is summed up for each apartment, with windows shared between apartments, e.g. due to shared staircases, being divided with 50% width to each apartment. The apartment's total width of windows is then compared to the total width of thermal envelope, excluding gable walls, in Fig. 7, and the apartment area, including walls, in Fig. 8. The gable wall had to be removed from the apartment's thermal envelope in all cases. Amount of windows and amount of rooms showed no clear correlation with other registered parameters.

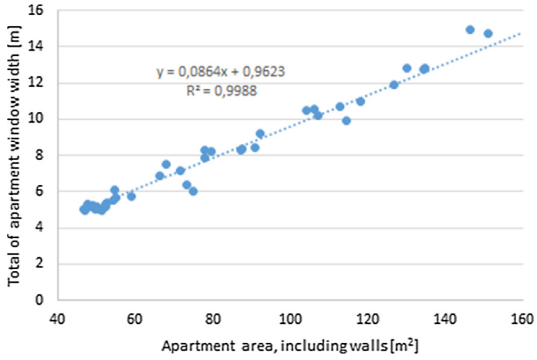


**Fig. 8.** Sum of window width and apartment area from floorplan investigation. One mansion apartment is situated outside the axis, with coordinates (1089, 94.8).

### 4.3. Heat loss investigation of interior insulation of a typical façade

The output of the simulated 1-, 2- and 3-dimensional models presented in Section 3.3 resulted in a range of specific heat flow rates for each combination of insulation degree/thickness as can be seen in Fig. 9. The influence of the window has been subtracted, and the result has been divided by the exterior masonry area to obtain the average thermal transmittance of the masonry part of the wall. The calculated relative reductions can be seen in Fig. 10, defined as the difference between the average thermal transmittance of the uninsulated model, compared to the average thermal transmittance of the increasing insulation thickness. The output of the simulations in Figs. 9 and 10 show results with different geometrical dimension and degrees of insulation coverage.

## 5. Discussion

### 5.1. Segment size

As it can be seen graphically in Fig. 4, a large proportion of the Danish multi-storey apartments were constructed in the period 1851–1930 and 1931–1950. Table 1 shows the specific numbers of multi-storey dwellings with more than 2 storeys constructed within these periods. The ratio of the number of apartments from the two periods, compared to all currently existing multi-storey apartments, was calculated to illustrate the significant relative size of these segments for the country of Denmark: 25% of the current apartments in multi-storey buildings and 41% of the multi-storey buildings were constructed in the period 1851–1930. For the period 1931–1950, the equivalent numbers were 20% and 19%, respectively. It can thereby be concluded that 46% of the apartments and 60% of the buildings in the current Danish multi-storey dwelling

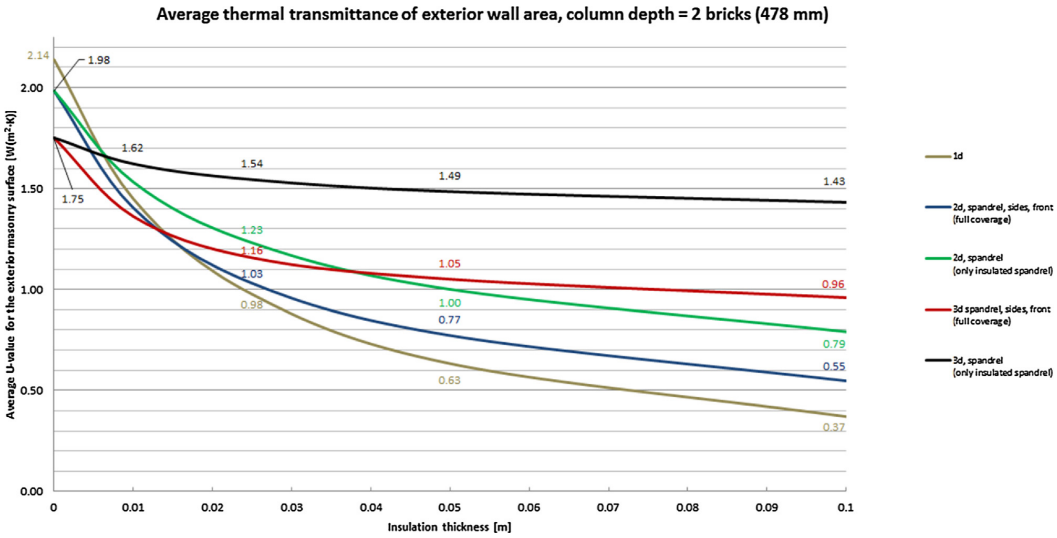


**Fig. 9.** Exterior surface average thermal transmittance as a function of insulation thickness: 10, 25, 50 and 100 mm. Focus on geometrical dimensions and insulation coverage. Abbreviations have been described in depth in Section 3.3.

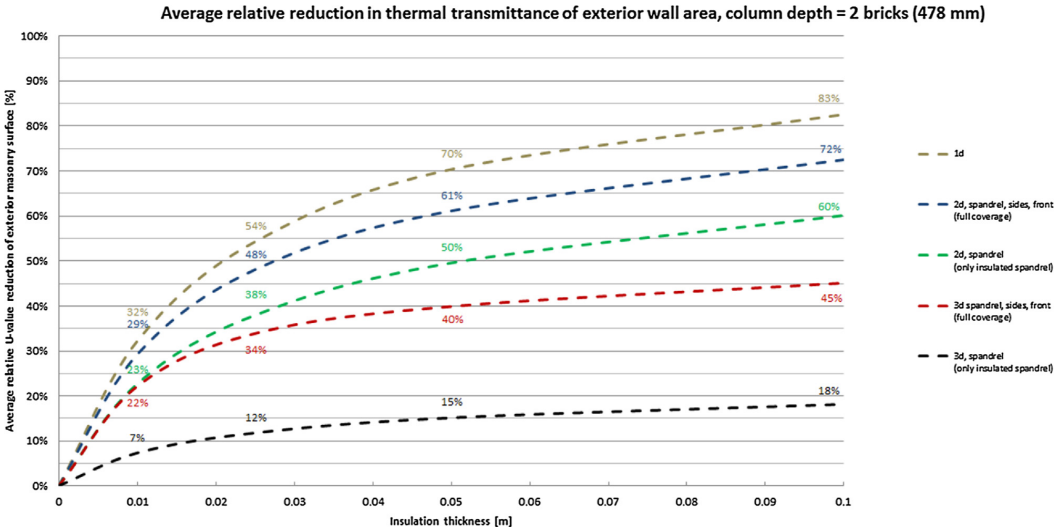


**Fig. 10.** Relative reduction in thermal transmittance compared to the uninsulated as a function of insulation thickness: 10, 25, 50 and 100 mm. Focus on geometrical dimensions and insulation coverage. Abbreviations have been described in depth in Section 3.3.

stock higher than 2 storeys consist of buildings constructed in the period 1851–1950 with brick facades and overall uniform characteristics.

It can be seen from Fig. 5(a) that most of the dwellings constructed in the years 1851–1930 are situated in the larger cities of Denmark: Copenhagen & Frederiksberg; Aarhus; Aalborg; Odense; and Gentofte. The Danish capital, Copenhagen and Frederiksberg, accounted for the largest proportion of all, with 71% of the apartment units accounted for in the figure.

The latter period, 1931–1950, was summarised in Fig. 5(b). The numbers from this period had a distribution of apartments quite similar to the earlier and much longer period. The largest difference can be seen in the Capital Region of Denmark. In this region, it is clear that the smaller municipalities surrounding Copenhagen/Frederiksberg experienced a large increase in units constructed. While Copenhagen/Frederiksberg accounted for a lower proportion of the total amount of apartment units in the latter period (52%), the large increase in the surrounding municipalities meant that the Capital Region of Denmark still contained 67% of the total number of apartments in the period. The ratio in the earlier period was 74%.

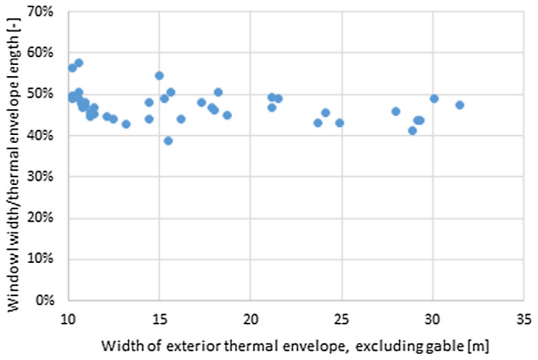


**Fig. 11.** Scatter plot of window/thermal envelope ratio from floorplan investigation. One mansion apartment is situated outside the axis, with coordinates (241.2, 39.3).

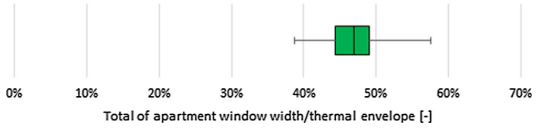


**Fig. 12.** Box plot of window/thermal envelope ratio from floorplan investigation. 25% quartile = 44.4%, median = 46.9%, 75% quartile = 49.0%.

### 5.2. Actual façade composition

As it can be seen in Fig. 7, there is an almost linear relationship between the width of the exterior thermal envelope of individual apartments, excluding gables, and the total of their window widths. The linear trend line has a coefficient of determination of $R^2 = 0.9978$, over the range from 10.2 to 241.2 m of thermal envelope. The distribution between windows and masonry in the horizontal direction was further calculated and visualised in Fig. 11. A box plot of the results including information on the quartiles can be seen in Fig. 12.

The found 25% quartile of 44.4% windows/thermal envelope in Fig. 12 was used to locate a floorplan with similar window/thermal envelope distribution. One that had a window/thermal envelope ratio of 43.0% was found, and details from the floorplan, where interior insulation was not directly applicable, were marked on a Google Street view picture of the façade. This picture can be seen in Fig. 13. The yellow hatches mark windows, the red hatches show the position of solid interior walls separating fire cells from neighbouring apartments/staircases, the blue hatches show the position of interior walls, which could be either timber or solid masonry walls, and the green hatches indicate the position of the floor structure. The 43.0% ratio were below the 25% quartile of the box plot in Fig. 12, illustrating that the possible areas for application of interior insulation are limited. The figure shows the same characteristics as Fig. 1(b), illustrating the high degree of penetration of the façade and the very limited areas available for the application of interior insulation, with surrounding thermal bridges consisting of floor structure and occasional interior walls. It is possible to insulate the floor structure between the wooden beams and the ceiling/floor boards, but this is typically not done in Denmark as it greatly increases the cost of the refurbishment.

The floorplan investigation further showed an almost linear correlation between the summed window width and apartment areas in Fig. 8. The linear trend tendency line had a coefficient of determination of $R^2 = 0.9988$, over the range from 46.7 to 1089.9 m$^2$ apartment area. The width of window per floor area was calculated and visualised in Fig. 14. A box plot of the results including info on the quartiles may be seen in Fig. 15.

### 5.3. Average thermal transmittance and relative reduction potential for interior insulation applied to characteristic facades

The COMSOL models described in Section 3.3 were used to evaluate the resulting average thermal transmittance in Fig. 9 and corresponding relative reduction in thermal transmittance in Fig. 10 by application of different degrees of insulation. A 1-dimensional model, illustrating the theoretical reduction in thermal transmittance of the thin spandrel with increasing insulation, is shown as a reference in Figs. 9 and 10. As it can be seen Fig. 1(b), the buildings from the period 1850–1930 has a high geometric complexity, and as a result thereof, 1-dimensional conditions for assessment of heat transmission through the walls are rarely present in practice.

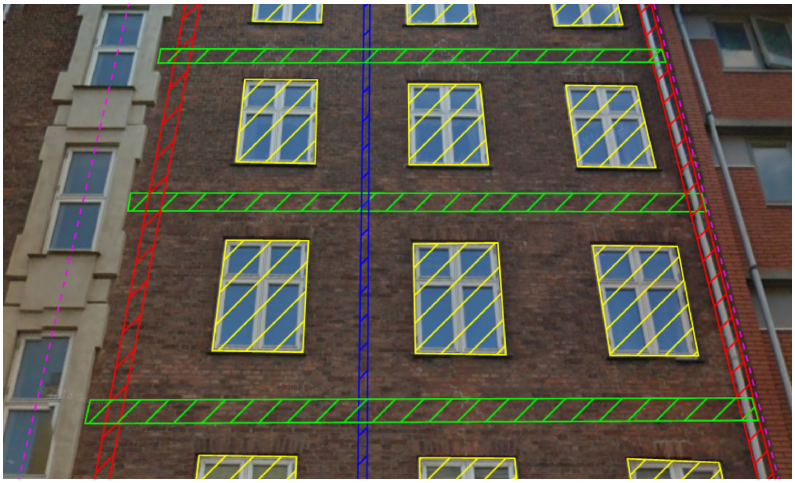

**Fig. 13.** Exterior surface of a 1927 multi-storey building with a window/thermal envelope ratio of 43.0% within the pink dashed lines. Hatches were defined as follows: Yellow = windows, blue = light interior walls, red = solid/fire walls, green = floor structure. Hatches were based on actual floorplan (Original photo by Google street view).

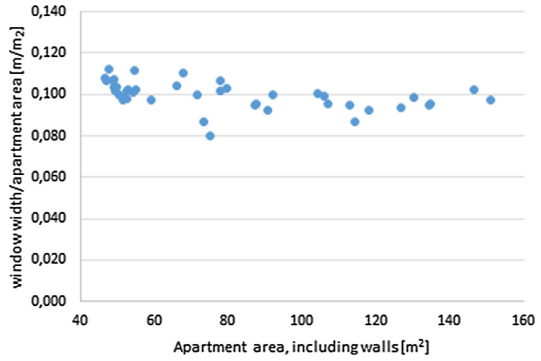


**Fig. 14.** Scatter plot of window width/apartment area ratio. One mansion apartment is situated outside the axis, with coordinates (1089, 0.087).

**Table 2**
Difference in average thermal transmittance from simulating with 2d instead of 3d. Values under 100% means higher average thermal transmittance for 3d.

| | Insulation thickness [mm] | | | | |
|---|---|---|---|---|---|
| | 0 | 10 | 25 | 50 | 100 |
| spandrel | 113% | 94% | 80% | 67% | 55% |
| spandrel, sides, front | 113% | 103% | 89% | 73% | 57% |

The 2- and 3-dimensional models were evaluated based on different insulation strategies, presented in Section 4.2 and illustrated in Fig. 3. As it can be seen in Figs. 9 and 10, there was a large difference between simulating the construction in 1d, 2d or 3d. While the 3d model with 100 mm with full insulation coverage of spandrels, sides and front resulted in a 45% relative reduction in average thermal transmittance. The corresponding 2d and 1d model resulted in 72% and 83% respectively. The difference between the average thermal transmittances in 2d and 3d were calculated and may be seen in Table 2. This table indicated that 2d simulation overestimated the constructions average thermal transmittance in the un-insulated case, but underestimated the average thermal transmittance by 55–57% with 100 mm insulation.

Another result that could be seen from Fig. 9 was the potential reduction from insulating only the spandrel, compared to full coverage of spandrel, sides and front. The reduction illustrated in Table 3, showed that for the 3d case, 33–40% of the obtainable reduction in thermal transmittance through the fully covering insulation strategy could be obtained by the cheaper and less complex insulating strategy of only insulating the thin spandrel under the window. To illustrate why the reduced spandrel insulation is cheaper and less complex, a simple measurement of area was performed. In the model, the spandrel insulation has an extent of 0.77 $m^2$, while the fully covering spandrel, sides, front insulation strategy has an extent of 4.65 $m^2$. This means the extent of the spandrel insulation is 17% of that of the fully covering spandrel, sides and front insulation strategy.

A similar calculation were done for the 2d simulation in Table 3, showing that 78–83% of the relative reduction in thermal transmittance from a fully covering insulation strategy on spandrel, sides and front could be achieved by only insulating the spandrel. Even though the heat flow through the window was excluded from the results, the heat flow that was affected by the geometry of the wall around the window yielded a significant increase.

Based on the large variation between 1d, 2d and 3d simulation in Tables 2 and 3, it was concluded that 3-dimensional analysis was needed to obtain realistic results.

### 5.4. Recapitulation of segment size, floorplan investigation for façade composition and potential reduction in average thermal transmittance

The procedure of installing fully covering interior insulation has previously been shown to involve a high capital cost, technical problems due to the many fitting and fixtures, and occupational health problems due to disruption during the conversion [26]. Brannigan and Both deemed these problems, and the resulting reduced room size, prohibitive. A way to persuade occupants to install interior insulation could be the use of the less extensive and generally simpler partial insulation strategy, insulating only the spandrel. Installed on a large scale in the city of Copenhagen/Frederiksberg, where the segment have been shown in Sections 4.1 & 5.1 to be large and to share many characteristics, the energy saving from this smaller intervention was found to offer a large potential energy saving for heating.

The following thermal conductance values for the masonry part of a window section were found by multiplying the found thermal transmittances in Fig. 9 with the external masonry area of the model. The model of interest were a 3-dimensinal model with only spandrel insulation (illustrated in Fig. 3(c)): uninsulated = 6.71 W/K, 100 mm of insulation = 5.49 W/K, savings = 1.22 W/K pr. window section. With 2726 mean degree days in a normal year in Denmark [27], this resulted in an energy saving of $3.33 \frac{kWh}{n_{windowsections} \cdot year}$. The Danish method to calculate degree days is based on an indoor temperature of 17 °C, calculated when the mean outdoor temperature is below 10 °C in spring and 12 °C in autumn for 3 consecutive days. The BBR register was used to find the total floor space in multi-storey apartments over 2 storeys constructed in the period 1851–1930 in Copenhagen/Frederiksberg, being 11,400,000 $m^2$. The analysis of the 43 floorplans in Section 5.2 showed a median of 0.1 m window/$m^2$ apartment area, resulting in 1,140,000 m window. By adding the found distribution in Fig. 6, the total amount of window sections in Copenhagen/Frederiksberg were calculated to be 1,206,000 windowsections. The analysis yielded a final potential energy saving from insulating the spandrel in apartments constructed in 1851–1930 and located in Copenhagen/Frederiksberg:

$$Q_{save,parapet} = 3.33 \frac{kWh}{windowsection} \cdot 1,206,000\ windowsections = 4.02 \frac{GWh}{year}$$

This saving account for 0.1% of the 4.35 TWh/year space heating and domestic hot water energy usage in all Danish multi-storey buildings from the period 1851–1930 [2].

The strategy of installing insulation on the spandrel could pose technical problems, as radiators are often placed in this location. An alternative could be the use of heat shields, which in earlier

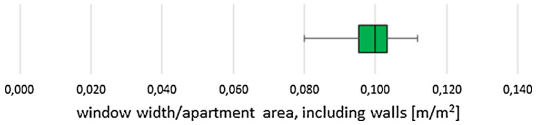


**Fig. 15.** Box plot of window width/apartment area ratio. 25% quartile = 9.5%, median = 10.0%, 75% quartile = 10.3%.

**Table 3**
Thermal transmittance of the different COMSOL models, the reduction from insulation and the possible percentage achievable from insulating spandrel, compared to full coverage with spandrel, sides, front.

| | Physics/savings/extent of insulation system | Unit | Insulation thickness [mm] | | | | |
|---|---|---|---|---|---|---|---|
| | | | 0 | 10 | 25 | 50 | 100 |
| 2-dimensional model | U-value: Spandrel, sides, front | $\left[\frac{W}{m^2K}\right]$ | 1.98 | 1.40 | 1.03 | 0.77 | 0.55 |
| | Reduction by ins.: Spandrel, sides, front | $\left[\frac{W}{m^2K}\right]$ | – | 0.58 | 0.95 | 1.21 | 1.44 |
| | U-value: Spandrel | $\left[\frac{W}{m^2K}\right]$ | 1.98 | 1.53 | 1.23 | 1.00 | 0.79 |
| | Reduction by ins.: Spandrel | $\left[\frac{W}{m^2K}\right]$ | – | 0.45 | 0.75 | 0.98 | 1.19 |
| | **Achieved by spandrel vs. full insulation** | | **–** | **78%** | **79%** | **81%** | **83%** |
| 3-dimensional model | U-value: Spandrel, sides, front | $\left[\frac{W}{m^2K}\right]$ | 1.75 | 1.36 | 1.16 | 1.05 | 0.96 |
| | Reduction by ins.: Spandrel, sides, front | $\left[\frac{W}{m^2K}\right]$ | – | 0.39 | 0.59 | 0.70 | 0.79 |
| | U-value: Spandrel | $\left[\frac{W}{m^2K}\right]$ | 1.75 | 1.62 | 1.54 | 1.49 | 1.43 |
| | Reduction by ins.: Spandrel | $\left[\frac{W}{m^2K}\right]$ | – | 0.13 | 0.21 | 0.27 | 0.32 |
| | **Achieved by spandrel vs. full insulation** | | **–** | **33%** | **35%** | **38%** | **40%** |

studies showed the ability to decrease the heat loss through the thin spandrel considerably [28].

## 6. Conclusion

The following bullets contain the main findings in present paper.

- The results of the segment analysis showed that 25% apartments and 41% buildings of the current Danish multi-storey building stock originates from the period 1851–1930. 71% of those apartment units are situated in the Capital of Denmark.
- The results of the floorplan analysis showed a façade composition median of 47% windows/thermal envelope ratio and a median of 0.1 m window width/$m^2$ apartment area.
- The thermal heat flow analysis showed:
  - ○ 2 dimensional simulation underestimated the heat loss when applying interior insulation by up to 55–57 % with 100 mm insulation, compared to 3 dimensional simulation.
    - 3-dimensional analysis is needed to obtain realistic results.
  - ○ By only insulating the spandrels below the windows, 33–40% of the effect from a full coverage insulation strategy could be achieved.
- Recapitulation of the three analyses showed an energy saving potential from insulating the spandrel of all multi-storey apartments over 2 storeys in Denmark of 4.02 GWh/year, correlating to 0.1% of the space heating and domestic hot water energy usage in all Danish multi-storey buildings from the period 1851–1930.

## Acknowledgements

Many talks with associate professor, emeritus, Jesper Engelmark, concerning the building style and details of Danish multi-storey buildings from 1850 to 1950, are greatly acknowledged.

This work was supported through the Danish industrial PhD program by Innovationsfonden [grant number 1355-00129]; COWIfonden [grant number C-123.01]; and COWI A/S.

## References

[1] Danish Energy Agency, Energystatistics 2013, 1256 Copenhagen K, Denmark, 2015.
[2] J. Kragh, K.B. Wittchen, Development of two Danish building typologies for residential buildings, Energy Build. 68 (2014) 79–86, http://dx.doi.org/10.1016/j.enbuild.2013.04.028.
[3] K.B. Wittchen, J. Kragh, O.M. Jensen, Energy saving potentials ?A case study on the Danish building stock, ECEEE 2011 SUMMER STUDY • ENERGY Effic. FIRST Found. A LOW-CARBON Soc (2011) 1355–1363.
[4] J. Engelmark, Københavnsk etageboligbyggeri 1850–1900. En byggeteknisk undersøgelse, Statens Byggeforskningsinstitut, Hørsholm, 1983.
[5] J. Engelmark, Dansk Byggeskik: Etagebyggeriet gennem 150 år, 1 ed., Realdania Byg, 2013.
[6] M. Morelli, S. Svendsen, Investigation of interior post-insulated masonry walls with wooden beam ends, J. Build. Phys. 36 (2012) 265–293, http://dx.doi.org/10.1177/1744259112447928.
[7] M. Morelli, L. Rønby, S.E. Mikkelsen, M.G. Minzari, T. Kildemoes, H.M. Tommerup, Energy retrofitting of a typical old Danish multi-family building to a nearly-zero energy building based on experiences from a test apartment, Energy Build. 54 (2012) 395–406, http://dx.doi.org/10.1016/j.enbuild.2012.07.046.
[8] E. Brandt, E.B. Møller, T. Bunch-Nielsen, G. Christensen, C. Gudum, M.H. Hansen, SBi Anvisning 224: Fugt i bygninger, 2.0, Statens Byggeforskningsinstitut, SBI, 2013.
[9] J. Munch-Andersen, SBi-anvisning 221 – Efterisolering af etageboliger, 1.0, Statens Byggeforskningsinstitut, SBI, Hørsholm, 2008.
[10] E. Vereecken, S. Roels, A comparison of the hygric performance of interior insulation systems: a hot box–cold box experiment, Energy Build. 80 (2014) 37–44, http://dx.doi.org/10.1016/j.enbuild.2014.04.033.
[11] M. Saïd, Pe.R. Demers, L.L. McSheffrey, Hygrothermal performance of a masonry wall retrofitted with interior insulation, Res. Build. Phys. (2003) 445–454 http://irc.nrc-cnrc.gc.ca/ircpubs.
[12] K. Ueno, J. Straube, R. Van Straaten, Field monitoring and simulation of a historic mass masonry building retrofitted with interior insulation, Therm. Perform. Exter. Envel. Whole Build. XII Int. Conf. (2013) 16.
[13] E. Vereecken, S. Roels, Capillary active interior insulation: do the advantages really offset potential disadvantages? Mater. Struct. 48 (2015) 3009–3021, http://dx.doi.org/10.1617/s11527-014-0373-9.
[14] J. Straube, C. Schumacher, Interior insulation retrofits of load-Bearing masonry walls in cold climates, J. Green Build. 2 (2007) 42–50, http://dx.doi.org/10.3992/jgb.2.2.42.
[15] T. Odgaard, S.P. Bjarløv, C. Rode, M.V. Vesterløkke, Building renovation with interior insulation on solid masonry walls in Denmark –a study of the building segment and possible solutions, Energy Procedia (2015) 830–835, http://dx.doi.org/10.1016/j.egypro.2015.11.003.
[16] G. Christensen, A.P. Kock, E.B. Møller, Indvendig efterisolering – ældre ydervægge af murværk, BYG-ERFA, 2015.
[17] Z. Pavlik, Hygrothermal performance study of an innovative interior thermal insulation system, Appl. Therm. Eng. 29 (2009) 1941–1946, http://dx.doi.org/10.1016/j.applthermaleng.2008.09.013.
[18] G.A. Scheffler, Hygric performance of internal insulation with light-weight autoclaved aerated concrete, in: Proc. 5th Int. Conf. Autoclaved Aerated Concr., Sept. 15–16, 2011, 2011, pp. 323–335 http://www.xella.com/de/docs/2011_Scheffler_InternalInsulation-LightWeightAAC-Multipor.pdf.
[19] J. Toman, A. Vimmrova, R. Cerny, Long-term on-site assessment of hygrothermal performance of interior thermal insulation system without water vapour barrier, Energy Build. 41 (2009) 51–55, http://dx.doi.org/10.1016/j.enbuild.2008.07.007.
[20] A. Nielsen, Samling af Bestemmelser vedrørende Københavns Kommune 1840–1863, Københavns, 1919.
[21] SKAT, KOMBIT, KL, The Building and Dwelling Register, 2012 (Accessed January 19, 2015) http://bbr.dk/bbrkort.
[22] T. Odgaard, C. Rode, S.P. Bjarløv, Parametric COMSOL Model Used for Thermal Investigation of Interior Insulation Effectiveness, 2017 (dataset).
[23] COMSOL, COMSOL Multiphysics, 2015 http://www.comsol.eu/contact.
[24] A. Nicolai, J. Grunewald, Delphin, 2015 http://www.bauklimatik-dresden.de/delphin.

[25] A. Nicolai, G.A. Scheffler, J. Grunewald, R. Plagge, An efficient numerical solution method and implementation for coupled heat, moisture, and salt transport, in: The DELPHIN Simulation Program, 2008, http://dx.doi.org/10.1081/E-EEE2-120046011.
[26] A. Brannigan, C.A. Booth, Building envelop energy efficient retrofitting options for domestic buildings in the UK, in: S.S. Zubir, C.A. Brebbia (Eds.), Sustain. City VIII, WIT PRESS, 2013, pp. 475–486, http://dx.doi.org/10.2495/SC130401.
[27] P.O. Fanger, H. Lund, H.E. Hansen, P.O. Danig, P. Kjerulf-Jensen, B. Elbæk, P.V. Nielsen, S. Aggerholm, F. Antvorskov, J. Gustavsson, O.B. Stampe, T. Lund Madsen, P.O. Danig, P. Worsøe-Schmidt, Danvak Grundbog i varme- og klimateknik, 3rd ed., Danvak APs, Vojens, Denmark, 2006.
[28] O. Madsen, J. Engelmark, M. Bybjerg, Varmeskjold – Nedbringelse af varmetab bag radiatorer, BUR Resumé 25 (1986) 7.

# B. PAPER #2: INTERIOR INSULATION - EXPERIMENTAL INVESTIGATION OF HYGROTHERMAL CONDITIONS AND DAMAGE EVALUATION OF SOLID MASONRY FAÇADES IN A LISTED BUILDING

Building and Environment 129 (2018) 1–14

Contents lists available at ScienceDirect

Building and Environment

journal homepage: www.elsevier.com/locate/buildenv

# Interior insulation – Experimental investigation of hygrothermal conditions and damage evaluation of solid masonry façades in a listed building

Tommy Odgaard[a,b,*], Søren Peter Bjarløv[a], Carsten Rode[a]

[a] Technical University of Denmark, Department of Civil Engineering, Brovej 118, 2800 Kongens Lyngby, Denmark
[b] COWI A/S, Parallelvej 2, 2800 Kongens Lyngby, Denmark

ARTICLE INFO

*Keywords:*
Historical
Masonry
Insulation
Moisture
Damage
Experimental

ABSTRACT

Exterior walls in historic multi-storey buildings compared to walls in modern buildings have low thermal resistance, resulting in high energy loss and cold surfaces/floors in cold climates. When restrictions regarding alteration of the exterior appearance exist, interior insulation might be the only possibility to increase occupant comfort.

This paper describes an investigation of the hygrothermal influence when applying 100 mm of diffusion open interior insulation to a historic multi-storey solid masonry spandrel. The dormitory room with the insulated spandrel had a normal indoor climate with a maximum observed monthly average humidity by volume excess of 3.2 g/m$^3$ during the experiment.

Relative humidity and temperature were monitored manually using wooden dowels over 2 years and 8 months in two solid masonry spandrels: one insulated wall and one untreated wall. The investigation showed that installing insulation on a solid masonry spandrel induced hygrothermal changes: Uniformly distributed higher relative humidity and lower temperature throughout the masonry, compared to an un-insulated wall. The relative humidity of the un-insulated masonry wall was in the range 50% on the inside to 60% on the outside, while the insulated wall showed uniformly distributed values around 80%.

The risk of moisture-induced damage was evaluated based on mathematical models for mould and decay of wood, visual inspection for frost and mould, and on-site measurements for presence of mould spores. The damage evaluation showed no risk of damage from the changed hygrothermal conditions when applying interior insulation to a solid masonry spandrel.

## 1. Introduction

With today's focus on reducing heat loss, Danish multi-storey buildings with solid masonry walls receive increasing attention due to their large potential for reducing heat loss and consequent reduction of $CO_2$ emissions [1,2]. The overall heat loss can be simplified to a vertical component through roof and ground, and a horizontal component through the façade, including the gables when exposed. Research shows that considerable energy savings can be achieved by applying thermal insulation to the solid masonry walls of historic multi-storey buildings [3,4]. The spandrels underneath the windows are the thinnest walls in traditional multi-story buildings and are responsible for a considerable part in the overall heat loss of the facade. The walls are characteristically 1-stone thick (238 mm), and have an interior layer of plaster [5,6]. 1-D hygrothermal simulation in WUFI of an uninsulated spandrel showed a minimum temperature on the inside of 9.2 °C [7] when simulating with a Danish design year [8]. Occupants staying in rooms with cold surfaces can suffer from discomfort due to asymmetric radiation from surfaces when larger than 10 °C [9,10], cold floors [11,12] and draught. Occupant comfort will increase, when the exposure to cold surfaces are reduced.

From a building physics point of view, the best location for adding insulation to a solid masonry wall is on the exterior side [13–15]. However, from a building preservation point of view, exterior insulation is often not a possibility. E.g., preservation of the exterior appearance of listed and worth-to-preserve buildings is a mandatory requirement in Denmark. With worth-to-preserve buildings, interior insulation is therefore often the only possibility.

Previous research has focused on how to add interior insulation on old masonry structures and the performance of the insulation material [3,16–22]. Aiming for energy reduction and temperature increase of the thinnest parts of the façade, Odgaard et al. showed that for a multi-storey building with 2-stone (468 mm) wall columns with interior rendering, up to 40% of the possible U-value reduction by applying

* Corresponding author. Parallelvej 2, 2800 Kongens Lyngby, Denmark.
*E-mail addresses:* TOOG@COWI.dk (T. Odgaard), SPB@byg.dtu.dk (S.P. Bjarløv), CAR@byg.dtu.dk (C. Rode).

https://doi.org/10.1016/j.buildenv.2017.11.015
Received 8 August 2017; Received in revised form 6 November 2017; Accepted 8 November 2017
Available online 02 December 2017


**Fig. 1.** Picture of façade used in experiment. Overview courtesy of Maps from COWI.

interior insulation to the entire interior masonry wall, could be achieved by insulating the spandrels [23].

Hygrothermal conditions in the original solid masonry wall become worse when adding thermal insulation to the interior side. The heat flow from the room to the original wall will be reduced [24], possibly causing condensation to form behind vapour open insulation [15,25]. The moisture content increases in the original wall, and leads to high moisture content on the cold side of the newly added insulation material [15,22,24,26–29].

The changed hygrothermal conditions will increase the risk of damages. One being the risk of frost damage [15], governed by 3 criteria occurring at the same time [30]: Temperature below freezing; wet masonry; and material sensitivity to frost. Another being the risk of mould and decay of wood occurring, governed by Ref. [31]: temperature; relative humidity; exposure time; and material.

Mould risk can be assessed mathematically based on monitored relative humidity and temperature, or based on on-site measurements. A large amount of different mathematical mould models exist in literature. Comparison of models have previously been done in Ref. [32] for wood, whereas review of the models including other material surfaces were included in Ref. [33]. A transfer model that converts the "growth-in-mm" results from the bio-hygrothermal model of Sedlbauer [34,35], the model used in WUFI, to the mould index model developed by Ojanen et al. [36], the model used in Delphin were described in Ref. [37]. Mathematical mould risk evaluation in this paper was based on the model from VTT [36,38], with risk evaluation based on the defined limits for maximum allowed mould index values at the interior side and interstices in the structure [37]. Different approaches for on-site measurements exist [39–41]. As the aim of present investigation is to detect if mould growth occurs, and not to detect specific mould species, it was decided to use the Mycometer®-test method [42].

A review of different mathematical decay models were performed by Brischke and Thelandersson, with a focus on outdoor conditions. As the models were based on temperature, relative humidity and exposure time, the models must also be appropriate for wood performance in other positions where oxygen is available. A range of parameters, which should be included in an appropriate model for decay of wood, were described in Ref. [43]: The importance of wood type, the need for inclusion of lag/activation process and how dose-response functions are appropriate for the biological field. The model of H. Viitanen et al. [44] included the mentioned parameters, where the inclusion of the activation process, defined as an index "$\alpha$", resulted in a dose-response function that comprises the lag effect. The model in Ref. [44] was based on Pine Sapwood, the structural lumber in historic Danish Multi-storey buildings traditionally consist of Pomeranian Pinewood, both heartwood and sapwood [5,6]. Oxygen will be naturally present in the traditional floor constructions of historic multi-storey buildings, which consist of layers of open air and clay.

Hygrothermal conditions in the experiment were monitored using wooden dowels drilled into the walls of interest. The use of wooden dowels to monitor hygrothermal conditions in structures is well-known and has proven as a stable methodology for long-term measurements [45–47], with examples of sensors working for a minimum of 20 years [48]. The conversion of resistance and temperature measurements in wooden dowels to wood moisture content is described both in Danish [49–52] and international literature stating the applicability of wooden dowels for slow and long term-measurement of relative humidity [53,54].

The aim of this paper is to present the results of an investigation of changed hygrothermal conditions when applying interior insulation to a reduced part of the interior surface, specifically the spandrels of a historic solid masonry wall. This has been conducted experimentally by installing interior insulation in the old historic Borchs Dormitory from 1823, situated in the Danish capital, Copenhagen. The dormitory consists of solid masonry walls with a rendered and painted facade. The study focused on reduction of heat loss and improvement of the indoor climate without risk of damage by frost, mould or decay of wood. The hygrothermal conditions were monitored in two walls, one with and one without interior insulation. Døi and Nielsen started the monitoring period in November 2014 with 1½ months of measurements [55]. The hygrothermal conditions continued to be monitored as reported in the present study, and comprises a total monitoring period of 2 years and 8 months.

## 2. Method

### 2.1. Experimental setup - building composition

Borchs dormitory was built in year 1823 and is situated at the coordinates (55.6805°N, 12.5744°E). A picture of the façade and overview of the area can be seen in Fig. 1. The buildings north and northwest of the garden/courtyard in front of the façade have a height of 4–5 stories + roof, which limits the influence from dominant western winds and wind driven rain. The exterior façade consists of solid masonry walls, constructed from historic red clay bricks and lime mortar, with no built in thermal insulation. The windows do not have an external sill. The position of the windows follow building tradition, situated approximately 4 cm from the exterior surface into the building, leaving 4 cm of masonry at the bottom, top and sides of the wall around the window exposed to rain. The infiltration of rainwater is reduced by a layer of rendering and paint covering the exterior side of the masonry wall. This rendering was originally performed with lime mortar, which might have been repaired with rendering systems with content of Portland cement at later stages. The masonry wall is also rendered and painted on the interior side. The building has four storeys, three of which have rendered and painted vertical facades and a 4th storey

below the sloped roof. The façade in each of the North-West facing rooms on the floor above ground used for the experiment, Room 9 and 12, consists of two spandrels. One spandrel in each room has a radiator in front; the other spandrel is blank and is used for the experiment. The exterior surface of the spandrels used in the experiment was inspected from ground level and showed no visible cracks in the façade.

The preservation class of the dormitory was at the time of investigation defined as “Listed” [56], a classification demanding for preservation of the interior and exterior expressions. A range of energy saving measures were discussed with representatives from the Danish Agency for Culture and Palaces in Ref. [55]. The only possible energy saving measure, which could be allowed by the Agency for Culture and Palaces, was internal insulation of an spandrel, where the limited extend of insulation coverage was defined by architectonic components on the inside surface. The material usage had to be limited to products with possibility for re-establishment at a later stage, a criterion that 100 mm of the diffusion open thermal insulation system “Ytong Multipor Mineral Insulation Boards” fulfilled. The manufacturer has provided the material characteristics: Density, $\rho = \sim 115$ kg/m$^3$, thermal conductivity, $\lambda = 0.045$ W/(m·K), water vapour resistance factor, $\mu = 3$ (light mortar $\leq 10$). The insulation was installed by the manufacturer, following their normal specifications by fully bonding the insulation board to the original interior rendering and covering the interior side of the insulation board with the same light mortar.

The insulation system was installed on the inside of the blank spandrel in Room 9, while the blank spandrel in Room 12 was kept untreated, as seen in Fig. 1. A detailed drawing of the insulated wall can be seen in Fig. 2. The un-insulated wall was similar to the insulated wall, without the insulation system.

### 2.2. Indoor and outdoor humidity by volume [v]

The measured indoor conditions in both rooms were assessed, to determine if the monitored moisture conditions in the experiment were within normally expected values. The values were assessed according to the internal humidity classes in Appendix A.2 of [57] and Chapter 3.3.3 of [13], based on interpolated values from the indoor and outdoor temperature and relative humidity loggers. The interpolation ensured similar data steps for the comparison. The outdoor values were based on monthly average values from a locally placed logger, as can be seen in Fig. 1. The average indoor excess of humidity by volume was found by subtracting the summarized monthly outdoor humidity by volume from the summarized indoor humidity by volume and dividing the result by the number of data points in the month. The vapour pressure and humidity by volume was determined mathematically by the empirical expressions from Ref. [57].

### 2.3. Measuring equipment

The conditions in the walls were monitored in three sensor points by manual readings. The measurement strategy was based on DC electrical resistance measurements in wooden dowels and thermal measurements in soldered copper and constantan wire, both measured with a T301.COW instrument [58,59]. A measurement period of 20 s [52] was used for the electrical resistance measurements, whereafter the value was noted. All wooden dowels were pushed as long as possible into drilled holes of various depths from the interior side, as illustrated in Figs. 2 and 3. All holes were closed with acrylic sealant on the surface of the interior masonry to hinder convective exchange of air between the air in the drilled hole and the inside environment. The sealant was applied from the top of the wires, reaching 1-2 cm into the holes with possible small voids along/underneath the wire. The wires and dowels were placed loosely in the drilled holes without additional sealant around the wire and dowel. The depths of the drilled holes were defined in Ref. [55], and the locations of the wooden dowels were measured at the end of the experiment. Only sensors 1, 2 and 3 in the un-insulated

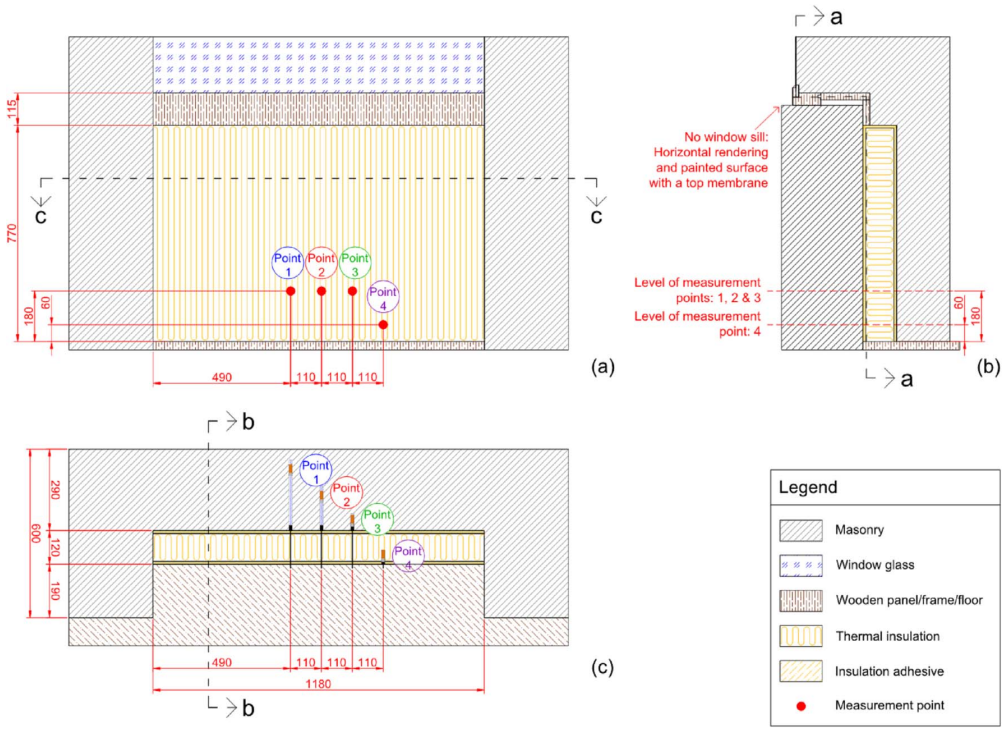


**Fig. 2.** 2-dimensional sketches of construction.

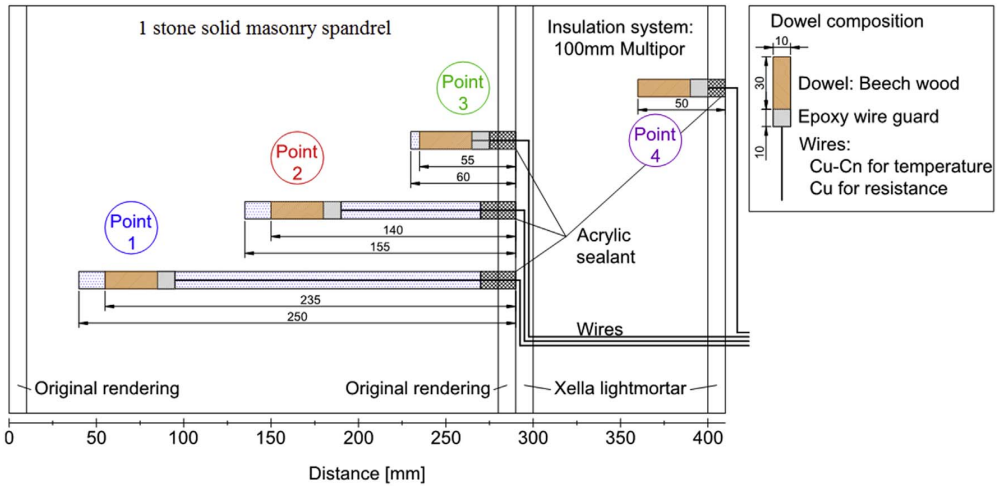


**Fig. 3.** Illustration of dowel placement. Resistance is measured in the wooden dowel; temperature is measured in the epoxy wire guard. Blue = air, brown = wooden dowel. Colours of point numbers are consistent throughout the paper. (For interpretation of the references to colour in this figure legend, the reader is referred to the Web version of this article.)

wall and sensor 4 from the insulated wall were removed, as the insulation board was left in place. For the insulated case, the wires were run to the floorboards and into the room, where after the insulated board was installed, covering the drilled holes.

Monitoring of the hygrothermal conditions in the wall ran from November 2013 until July 2016. The insulation was installed in December 2013. The resistance and temperature measurements of the wooden dowels were performed with the following intensity: 2013-11-25 → 2014-01-23 every ~3-5 days; → 2014-06-04 every ~14 days; → 2016-07-15 every ~1-2 months.

The indoor and outdoor climates were monitored by three Onset HOBO U12-012 temperature and relative humidity data loggers [60]. The loggers were placed as illustrated in Fig. 1, inside in Room 9 & 12 and outside in a nearby open bicycle shed. The conditions were monitored at minimum every 15 min in the entire monitoring period. The outdoor climate was further monitored by 2 nearby weather stations [61]. A station situated in Kastrup (Copenhagen Airport), 9 km south-southeast from Borchs dormitory, and a station situated in Jægersborg, 10 km north-northwest from Borchs dormitory. Running averages of the measured indoor and outdoor relative humidity and temperature boundary conditions were calculated with different time spans for the running average to better illustrate the values in graphs. The running averages were calculated as averages of the boundary condition values 0.5 x time span back and 0.5 x time span ahead of time for each data point.

#### 2.3.1. Conversion, measured wooden resistance [R] to relative humidity [RH]

The calculation from DC electrical resistance to wooden moisture content by weight is based on [50], illustrated in equations (1) and (2). The equations fit with the graph for conversion of resistance to wooden moisture content by weight supplied with the dowels [62].

$$R_{adjusted}\,[log10M\Omega] = R\,[log10M\Omega] - (0.029 + 0.005{\cdot}R\,[log10M\Omega]) \cdot(20 - \theta\,[^{\circ}C])[50] \quad (1)$$

$$u\left[\frac{kg}{kg}\right] = 10\text{^}\left(\frac{12.63 - R_{adjusted}\,[log10M\Omega]}{9.196}\right)[50] \quad (2)$$

where: $R$ = measured DC electrical resistance $[log10M\Omega]$, $R_{adjusted}$ = electrical resistance adjusted to 20 °C $[log10M\Omega]$, $u$ = wooden moisture weight percent $\left[\frac{kg}{kg}\right]$.

Equation (3) is used to transform wooden moisture into relative humidity by curve fitting to the sorption isotherm for 750 kg/m$^3$ beech wood in Refs. [63,64]. The relative humidity was determined as the mean result from the adsorption and desorption curves.

$$\mathrm{RH}(u)\,[\%] = 0.5{\cdot}\left(\left(C_{adsorption}{\cdot}\exp\left(1 - \left(\frac{u\left[\frac{kg}{kg}\right]}{A_{adsorption}}\right)^{B_{adsorption}}\right)\right) + \left(C_{desorption}{\cdot}\exp\left(1 - \left(\frac{u\left[\frac{kg}{kg}\right]}{A_{desorption}}\right)^{B_{desorption}}\right)\right)\right) \quad (3)$$

where: $RH$ = Relative humidity [%], $A$, $B$ & $C$ being the following factors for ad- and desorption: $A_{adsorption}$ = 7.608, $B_{adsorption}$ = -1.353, $C_{adsorption}$ = 42.960, $A_{desorption}$ = 12.690, $B_{desorption}$ = -0.8945, $C_{desorption}$ = 57.440.

### 2.4. Investigation of cold surfaces, wall and floor

An investigation of the thermal envelope of the dormitory building was performed in the start of the project in October 2013, before installation of interior insulation. The investigation was performed by a professional company, ISOLINK [65] with focus on detection of thermal irregularities of interior building envelope via infrared/thermographic pictures [66].

### 2.5. Mathematical model for calculation of mould risk [M]

It has been decided to base the mathematical mould evaluation in the present paper on the method developed by the Technical Research centre of Finland (VTT), and by Tampere University of Technology, Finland for wood based materials [38], later extended to evaluate other material types [36].

The mould index, abbreviated "$M$", is calculated based on a dataset with 60 min interpolated values of the original measurements. The mould index is defined as a value in the range 0 → 6, with each integer defining as a state of the mould growth [38]. The following basic factors were defined for the analysed case:

- Surface quality ($SQ$) and wood species ($W$): Only non-wood materials were modelled, resulting in $SQ = W = 0$ [37].

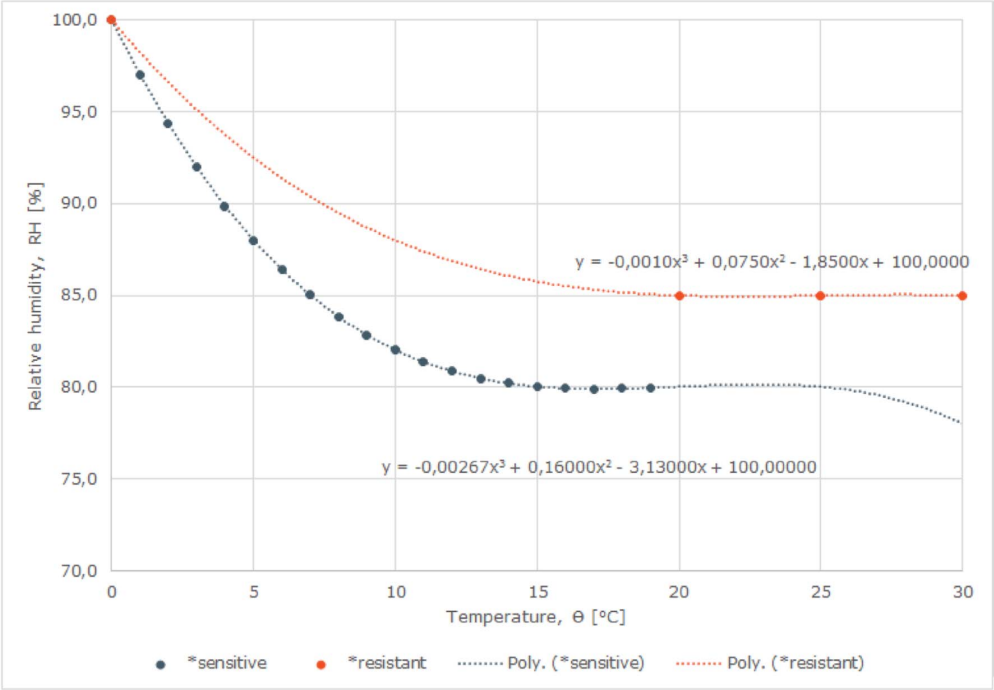


**Fig. 4.** Development of simple expression for mould limit of *resistant materials. *sensitive = limit from Ref. [36].

- Material class: "Medium resistant", as the Multipor and adhesive material is defined as cement based/aerated concrete [36].

The combined temperature and relative humidity limit for mould growth when using a “very sensitive” and “sensitive” material were defined in Ref. [36] by a limit of 80% RH with a curve in the temperature range $\theta = 0\ ^oC \rightarrow 20\ ^oC$ as illustrated with label "*sensitive” in Fig. 4. For a medium resistant material, a limit of 85% RH was defined [36], but only from 20 °C and above. In order to cover the temperature range $\theta = 0\ ^oC \rightarrow 20\ ^oC$, we suggest a 3rd degree polynomial curve fit to the following defined points: ($\theta$, RH) = (0, 100; 20, 85; 25, 85; 30, 85). This resulted in the following equation: $RH(\theta) = -0.001 \cdot \theta^3 + 0.075 \cdot \theta^2 - 1.85 \cdot \theta + 100$. Points and resulting fit can be seen in Fig. 4 with the label "*resistant”. There will be no mould growth for temperatures below 0 °C.

Prediction of mould growth in boundary layers between materials were described in Ref. [36]. This work of Ojanen et al. further included the possibility for reduction of the mould index when the combined temperature and relative humidity conditions were outside the limit for mould growth, based on mould declination factors for a range of different materials. As a large spread existed in the declination factors for materials situated in the medium resistance category, the results in the present paper were modelled with the factor set to “almost no decline”, “relatively low decline”, and “significant relevant decline”, being 0.1, 0.25 and 0.5 respectively [36].

The mould model was applied to two measurement points. Point 3 being the wooden dowel placed in the wall closest to the original interior surface, and Point 4 in the insulation board. The points are illustrated in Figs. 2 and 3.

### 2.6. Physical test for mould on-site via Mycometer®-test

Mould growth was tested on-site 1 year after termination of monitoring hygrothermal conditions. The investigations were performed on the interior surface, and in the interface between masonry and interior insulation. Mould growth was assessed using the method of Mycometer, with instructions by trained specialists at the consultancy firm COWI A/S and from the webpage of Mycometer [67,68].

The outcome of the test is FLouresence Units (*FLU*), a value that can be related to the N-acetylhexosaminidase activity found in mould. The magnitude of FLU defines a category interrelated to the presence of mould (spores), based on interpretation criteria set up by Mycometer [41,42,69].

The 3 categories of mould occurrence are [41,42,69]:

1. A: Below background level.
2. B: Above background level: " … *typically due to high concentrations of spores in dust deposits."* [69], " … *likely depositied fungal debris, which can often be found in older Mortar/Concrete materials."* [69].
3. C: High above background level: " … *due to mould growth* … " [69].

The performance of the Mycometer-test have been validated in relation to linearity and repeatability [70].

### 2.7. Model for calculation of irreversible mass loss by decay of wood [ML]

Evaluation of the risk for decay of wood is done with the extended mathematical model developed at the Technical Research centre of Finland (VTT) [44]. The model is based on an activation process, $\alpha$, increasing from $\alpha = 0 \rightarrow 1$ during favourable condition for decay of wood, and decreasing $\alpha \rightarrow 0$ during non-favourable conditions. The percentage of irreversible mass loss of wood, abbreviated "*ML*", increase when activation process $\alpha = 1$.

The decay model was calculated based on a dataset with 60 min interpolated values of the original measurements. The model was started at an initial activation process of $\alpha = 0$ in the three measurement points in the masonry wall, Point 1, 2 & 3.

## 3. Results

The results in this paper are experimental measurements obtained from a 2 year and 8 months monitoring period, together with inspections and on-site investigations. All raw and analysed measurement data from the experiment, have been provided in Ref. [71].

The following suffixes have been used to illustrate the different variations of data.

- "_Point = #", e.g. _Point = 1, denote the measurement point, as described earlier in section 2.3.
- "_int" describe interpolated values. These interpolated values are calculated every 60 min, are used as input for calculation of mould index, *M*, activation process, *α*, and decay mass loss, *ML*.

The date x-axis is for all graphs formatted as: “month (year)".

### 3.1. Boundary conditions

The measured boundary conditions, relative humidity, *RH*, and temperature, *Θ*, in the two indoor rooms and three outdoor locations can be seen in Fig. 5. Relative humidity is illustrated with solid lines, temperature with dashed lines. The 2 y-axes show the same range with the purpose to isolate the relative humidity and temperature data and increase the readability.

### 3.2. Measurements in walls

The measured raw data with the T301.COW instrument, resistance, *R*, and temperature, *Θ*, have been calculated into relative humidity, *RH*, using the method described in Section 2.3.1. The values from the 4 sensor points in the insulated solid masonry spandrel can be seen in Fig. 6. The values from the 3 sensor points in the un-insulated solid masonry spandrel can be seen in Fig. 7. The location of the sensor points can be seen in Figs. 2 and 3. Relative humidity is illustrated with solid lines, temperature with dashed lines.

### 3.3. Thermal images of cold surfaces at start of project

An investigation of cold surface temperatures observed on the interior building envelope via thermographic pictures was performed before installing interior insulation. Thermographic pictures of the original spandrels in Room 9 and 12 can be seen in Fig. 8 and Fig. 9 respectively. A photograph of the measured area is inserted in the bottom left corner and a temperature scale is inserted on the right-hand side. The top left corner of Fig. 9 show an additional thermographic picture of the spandrel in Room 12. The spot measurements (*Sp1 to Sp4*) in the figures indicate points where temperatures have been measured, with values given in the figure captions.

### 3.4. Visual inspection of frost damage to the exterior façade

The exterior façade of the insulated spandrel was visually inspected to determine if frost damage occurred during the experiment and up until 1 year after termination of the monitoring period. A photograph of the last visual inspection can be seen in Fig. 10.

### 3.5. Results from on-site investigation of mould via Mycometer®-test

Eight Mycometer tests were performed in the room with an insulated spandrel, 3 years and 8 months after installation of interior insulation. The tests consisted of five Mycometer-surface and three Mycometer-material tests. The results of the tests were reported as FLouresence Units (FLU) and a category defining presence of mould (spores), as described in Section 2.6.

The Mycometer-tests were performed after the procedure defined in the following numerated list, with results extracted from the laboratory report [72] as bullet points.

1. Test of interior surface, location: Between columns, 60 cm from floor.
   - Mycometer surface test resulting in FLU = 0 = Category A.
2. Test of interior surface, location: Next to P4, 6 cm from floor.

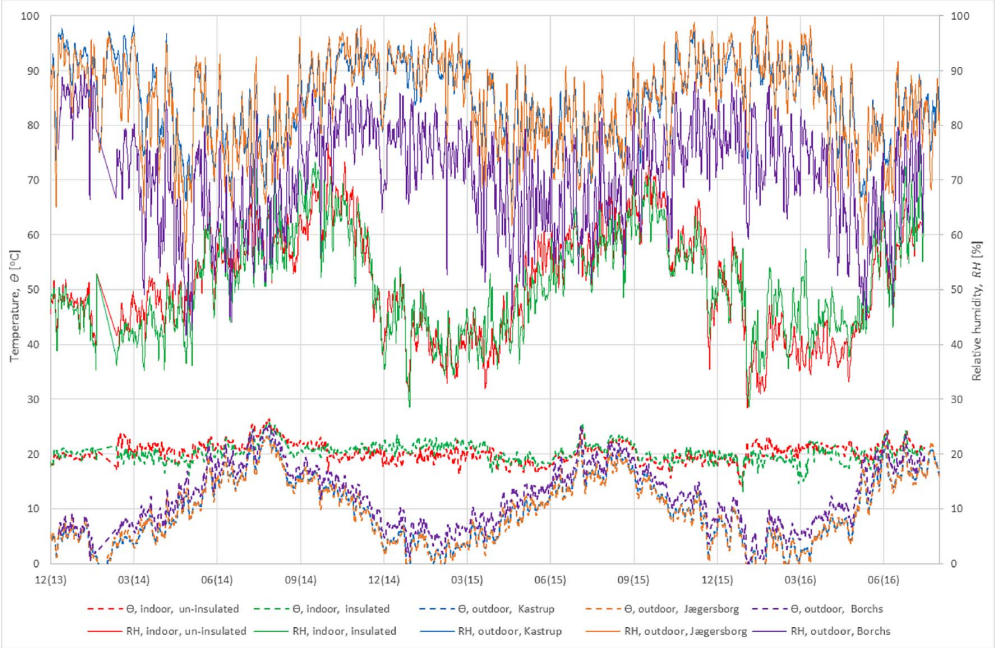


**Fig. 5.** 2-day averages of measured indoor and outdoor climate conditions.

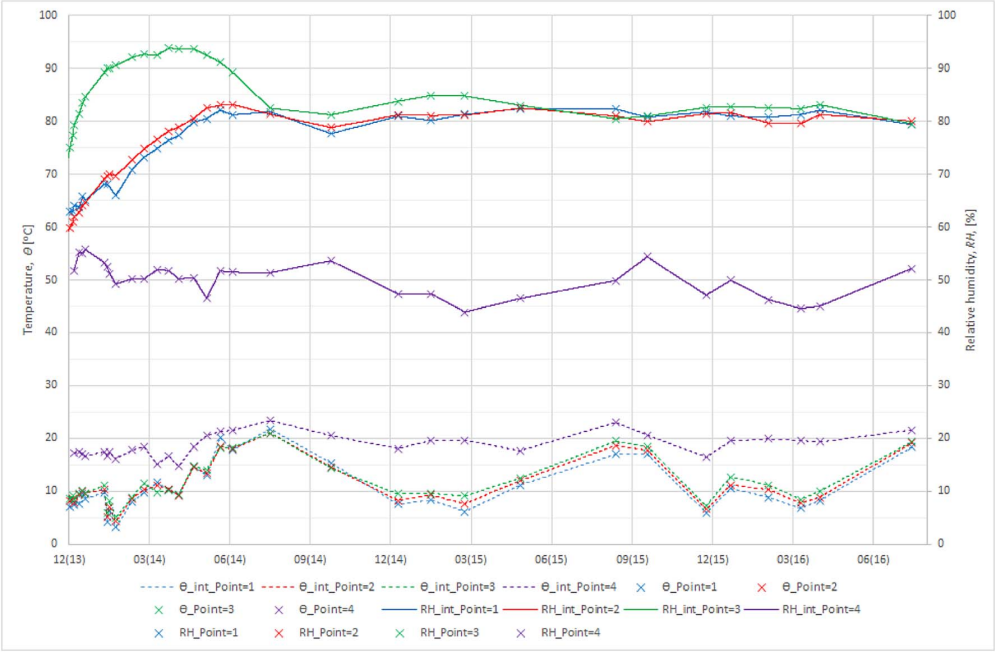


**Fig. 6.** Measured temperature, Θ, and calculated relative humidity, RH, for insulated spandrel in Room 9.

- Mycometer surface test resulting in FLU = 0 = Category A.

3. Test of interior surface, location: Other spandrel in same room, next to radiator.
   - Mycometer surface test resulting in FLU = 4 = Category A.
4. Clean ø105 mm Core-bit with alcohol: First in bath, then with freshly soaked paper towel. Drill core horizontally between columns, 60 cm from floor. Drilled through insulation system and original rendering, into original masonry wall.
   - Test of brick/mortar surface, behind original interior rendering.
     - Mycometer surface test resulting in FLU = 6 = Category A.
   - Material sample from extracted core, layer between original interior rendering and insulation adhesive.
     - Mycometer analysis of mould growth inside cement containing materials resulted in FLU = 18 = Category A.

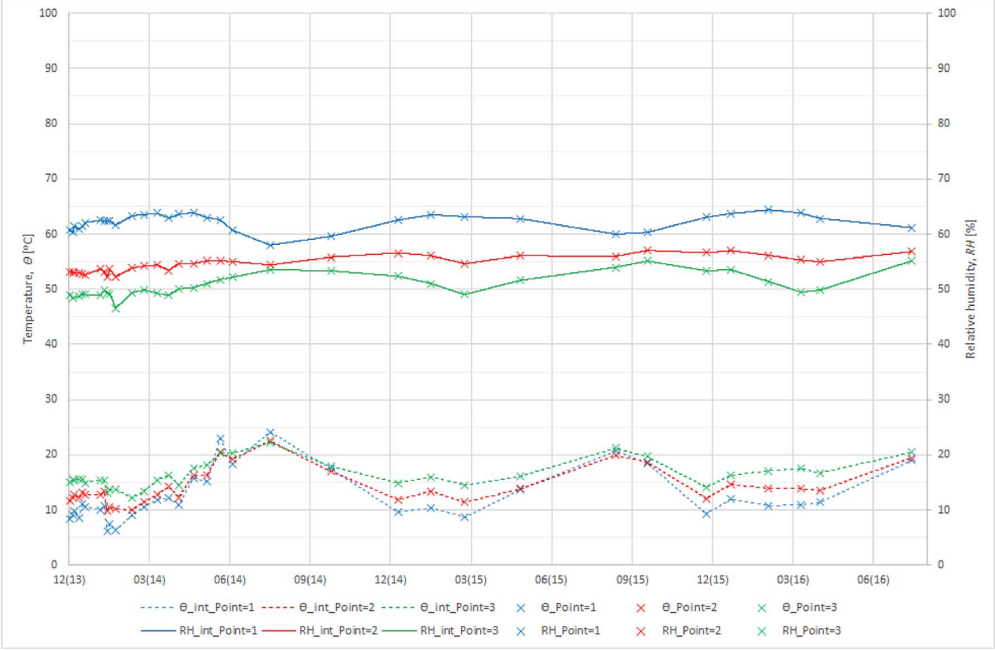


**Fig. 7.** Measured temperature, Θ, and calculated relative humidity, RH, for un-insulated spandrel in Room 12.

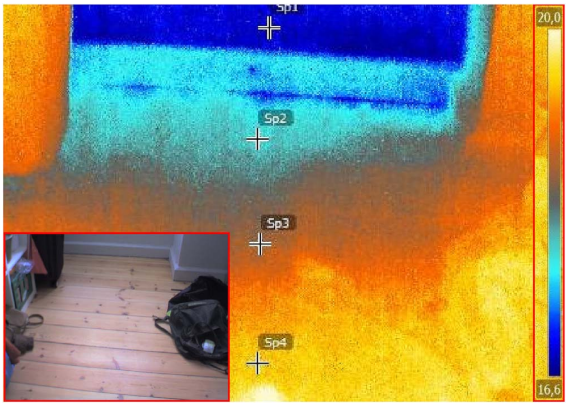


**Fig. 8.** Thermal image in Room 9. Bottom left: Photograph. $\Theta_{Sp1}$ = 16.7 °C, $\Theta_{Sp2}$ = 17.8 °C, $\Theta_{Sp3}$ = 18.5 °C, $\Theta_{Sp4}$ = 19.5 °C. Outdoor temperature at time of investigation: $\Theta_{out}$ = 13.7 °C. Material by courtesy of ISOLINK & Erik Møller Arkitekter.

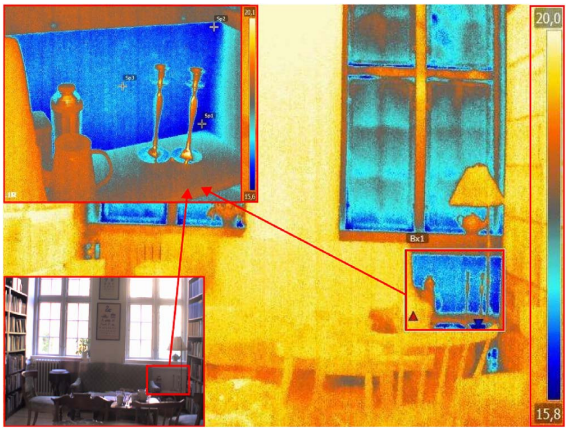


**Fig. 9.** Thermal image in Room 12. Bottom left: Photograph. Top left: Thermal image of Bx1. $\Theta_{Sp1}$ = 15.6 °C, $\Theta_{Sp2}$ = 15.8 °C, $\Theta_{Sp3}$ = 16.7 °C. Outdoor temperature at time of investigation: $\Theta_{out}$ = 13.7 °C. Material by courtesy of ISOLINK & Erik Møller Arkitekter.

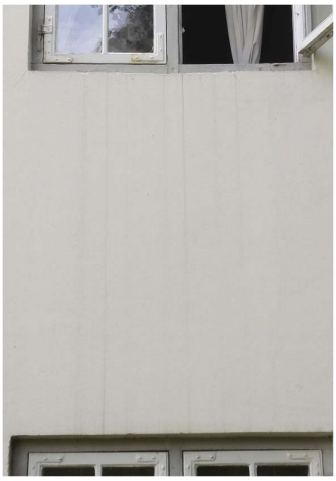

**Fig. 10.** Last visual inspection of exterior surface of insulated spandrel on 2017-07-24.

- Material sample from extracted core, joint between two insulation boards.
  - Mycometer analysis of mould growth inside cement containing materials resulted in FLU = 29 = Category A.

5. Clean ø105 mm Core-bit with alcohol: First in bath, then with freshly soaked paper towel. Drill core in P4, edge of Core-bit on floor. Drilled through insulation system, stopped with original interior rendering intact and insulation adhesive removed.
   - Test of original interior rendering surface.
     - Mycometer surface test resulting in FLU = 131 = Category B.
   - Material sample from extracted core, adhesive and insulation material.
     - Mycometer analysis of mould growth inside cement containing materials resulted in FLU = 91 = Category B.

## 4. Discussion

The discussion is split into six parts in the following subsections, each dealing with a part of the results from the experiment. The sections include the boundary conditions of the experiment, evaluation of the monitored temperature and relative humidity at the 7 sensor points, evaluation of risk of damage based on frost, mould and decay of wood, and evaluation of cold surfaces.

The following suffix has been used to illustrate the different variations of data.

- "_decline = #", e.g. decline = 0.05, refers to declination factors when calculating mould index, *M*, as described in Section 2.5.

### 4.1. Boundary conditions

To validate the measured outdoor values, a comparison between the data from the outdoor HOBO logger at Borchs dormitory and the weather stations in Kastrup and Jægersborg is shown in Fig. 5. This comparison was initiated because unexpected low relative humidity and high temperature were measured locally at Borchs dormitory. The humidity by volume for each station were calculated and plotted in Fig. 11. The comparison showed low difference between the three stations. The measured local outdoor conditions were assessed to be valid for calculating the excess humidity by volume from outdoor to indoor in the two rooms. These values were used to evaluate the moisture load in the rooms, based on humidity classes [13,57].

Differences between the humidity by volume in the two rooms appear from the beginning of 2014 until beginning of 2015, but with opposite sign in the two years. We found that this originated from the number of residents inhabiting the rooms. During the monitoring period, the residents in the rooms changed several times. The period each resident(s) has lived in the room is marked with merged cells in Table 1, with text stating gender and age when moving in and out in brackets.

The indoor humidity by volume of the two rooms, Fig. 11, shows values following the outdoor climate, with a moisture excess to the indoor air caused by the occupant activity. The calculated monthly mean indoor excess of humidity by volume over the monthly mean outdoor temperature for both rooms can be seen in Fig. 12. The results show that the room with an insulated spandrel has an excess of indoor humidity by volume in the coldest months lower than humidity class 2, following the slope of class 2. The room does not exceed humidity class 2, defined as *"Offices, dwellings with normal occupancy and ventilation"* [57].

The values in Fig. 12 show that the experimental conditions for the insulated room can be classified as being within the expected normal climate conditions for dwellings.

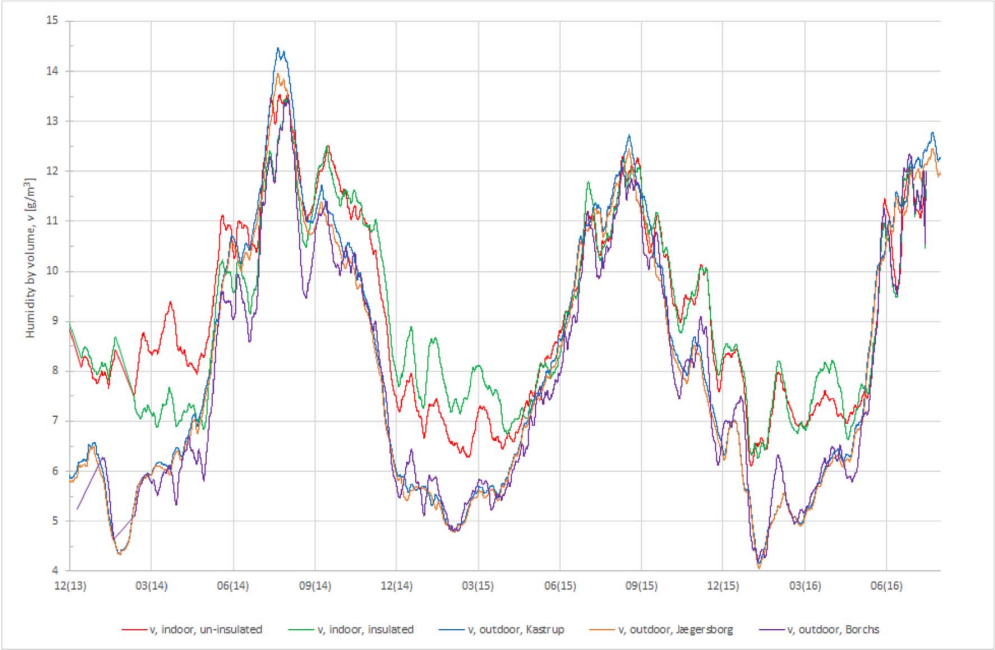


**Fig. 11.** 28-day average of calculated humidity by volume for the indoor and outdoor climates.

### 4.2. Measured temperature and relative humidity in masonry wall

The difference and magnitude of the measured hygrothermal conditions in the masonry part of the insulated and un-insulated wall have been compared. When comparing the insulation-induced change in temperature from Figs. 7 and 6, the main temperature drop takes place in the insulation layer, as expected. This results in notable lower temperatures throughout the masonry with a low difference from inside to outside. A similar change can be seen for relative humidity, with insulation resulting in high relative humidity throughout the wall and a low difference from inside to outside. The changed hygrothermal conditions are especially seen during the winter periods. E.g. in the second winter, the relative humidity and temperature at the time of measurement in the original un-insulated wall in Fig. 7 lies within a band ranging from 63% RH and 10 °C at the outside to 52% RH and 15 °C at the inside of the masonry wall. The relative humidity and temperature measured at the same time in the insulated wall in Fig. 6 lies within a narrow band ranging from 84% RH and 8 °C on the outside to 86% RH and 10 °C at the masonry wall towards the inside.

The generally changed humidity level induced by applying interior insulation to the walls can be seen by evaluating the average relative humidity in the period after initial dry-out (July, 2014) until the end of the monitoring experiment. The values for the Points 1/2/3 of the un-insulated wall show 62/56/52% RH. The equivalent values for Points 1/2/3 in the insulated wall show uniformly distributed values of 81/81/82% RH.

### 4.3. Evaluating risk of frost damage

As stated in the introduction, evaluation of frost damage is governed by 3 criteria occurring at the same time [30], of which two have been evaluated in this investigation: Temperature below freezing and wet masonry. As it can be seen in Fig. 6, the interior insulated masonry wall becomes wetter than the un-insulated wall in Fig. 7, but as the maximum measured relative humidity in the exterior masonry measurement Point 1 = 82% RH, we presume that the masonry does not reach a wet state (RH > 98%) in the time between the manual measurements. The temperature conditions have been evaluated by plotting the raw data for locally measured temperature in the nearby bicycle shed in Fig. 13. While the climate stations show periods with temperature down to -10 °C over some days in consecution (not shown in paper), the local temperatures only go below freezing 2 times during the 3 monitored winters, to a minimum temperature of -2 °C. The wall will have a significant contribution of heat from the inside, as only part of the wall is insulated. From this, we presume the temperature in the outer layer of the masonry do not drop below the freezing point in the time between the manual measurements.

A final visual inspection was carried out one year after the termination of the monitoring experiment. As can be seen in Fig. 10, no frost damage of the external wall was observed during the experiment.

### 4.4. Evaluating risk of mould: mathematical and measured on-site

The VTT mould model [36] described in Section 2.5, was applied to the measured values of Point 3 and 4 for the insulated wall presented in Fig. 6 and Point 3 for un-insulated wall presented in Fig. 7. The outcomes with mould index > 0 can be seen in Fig. 14, with a maximum mould index of $M = 0.3$ obtained at Point 3 for the insulated wall during the initial dry-out period. Using the evaluation scheme described in Ref. [37] for the interface layer, it becomes clear that even if the installed insulation system had not been based on cementitious material, then the calculated mould index would still have resulted in the category $0 < M < 2$ = “acceptable”. As the Xella Multipor insulation board were mounted with light mortar, which according to [73], contains more than 20 weight-% Portland cement, the glue can be categorized as a cementitious material. Ojanen et al. found that during construction with cementitious materials, the alkaline conditions prohibit mould formation on new surfaces [37]. Based on this, a new starting point for mould growth was defined at the date of initial drying: 2014-07-17. The mould models with this new starting point did not show risk of mould growth. Evaluation of mould for the un-insulated wall indicated no risks of mould growth.

**Table 1**
Residents during experiment.

| | 2013 | 2014 | | | | | | | | | | | 2015 | | | | | | | | | | | | 2016 | | | | | |
|---|---|---|---|---|---|---|---|---|---|---|---|---|---|---|---|---|---|---|---|---|---|---|---|---|---|---|---|---|---|---|
| | Dec | Jan | Feb | Mar | Apr | May | Jun | Jul | Aug | Sep | Oct | Nov | Dec | Jan | Feb | Mar | Apr | May | Jun | Jul | Aug | Sep | Oct | Nov | Dec | Jan | Feb | Mar | Apr | May | Jun | Jul |
| Room 09: Insulated<br>Room 12:Un Insulated | Female (27-28)<br>Male (27) | | | Male (27-28) & Female (29-30) | | Female (28-29) | | | | Female (28-29) & Female (23)<br>Male (26-27) | | | | | | | Male (26-27) | | | | | | | | | | | | Male (27-28)<br>Female (27) | | | |

On-site investigation of mould growth of the insulated wall using Mycometer tests showed 6 of 8 samples within category A: below background level. The two samples taken behind the insulation in P4, close to the floor, had results within category B: above background level. Thereby, no physical mould growth was found on or behind the insulation board.

### 4.5. Evaluating risk of mass loss by decay of wood

It is important to emphasise that the traditional solid masonry spandrels did not contain wooden elements. Evaluation of risk of mass loss by decay of wood was based on the hypothesis that increase of moisture in the masonry could influence nearby wooden components. The wooden components being the wooden floor and the load bearing structure underneath. The added interior insulation to the masonry spandrel join the existing wooden floor, as can be seen in Fig. 2. The load bearing structure of the historic multi-storey buildings consisted of wooden beams, holding the floor and supported by the solid masonry façade columns, or on a wooden exchange running parallel to the façade [5,6].

The model to calculate decay of wood described by Viitanen et al. [44] was applied to the measured values of the un-insulated wall in Fig. 7 and the insulated wall in Fig. 6. The model showed an activation process not exceeding 0 in the monitoring period at either of sensor Point 1, 2 or 3. As the activation process did not reach a value of 1, this indicates no calculated risk of decay of wood at either point in the solid masonry wall.

As the open floor structure experiences better hygrothermal conditions than the masonry/interior insulation interface, there appears to be no risk of decay of the wooden components. The better hygrothermal conditions derive from the natural ability of wood to distribute moisture along the fibres and evaporate excess moisture to the adjacent air, being the room air and the air volume on top of and below the traditional floor structure, compared to the closed masonry/insulation interface.

### 4.6. Cold surfaces

An investigation of thermal irregularities was performed in the beginning of the project, before interior insulation was installed at the spandrel of Room 9. The outdoor temperature was measured to be $\Theta_{out}$ = 13,7 °C at the time of the investigation. The temperatures recorded at the un-insulated surfaces of the spandrels were (Fig. 8:$\Theta_{Sp1}$) = 16.7 °C in Room 9 and (Fig. 9:$\Theta_{Sp1}$) = 15.6 °C in Room 12.

The floor temperatures were recorded by thermal imaging in Room 9, indicating low floor temperatures in front of the spandrel and into the building, with a measured floor temperature of (Fig. 8:$\Theta_{Sp2}$) = 17.8 °C in between the columns and (Fig. 8:$\Theta_{Sp3}$) = 18.5 °C approximately 0.5 m from the spandrel. It is stated in Ref. [11] that an acceptable temperature range for bare feet/socks combined with pinewood floor of 18.5–31 °C for short term exposure and 22.5–28 °C for long term exposure, with an additional temperature increase in both cases of +1/2 °C for sedentary activity. Temperature ranges when wearing light shoes were treated in Ref. [12], stating an acceptable floor temperature range for indoor environment category A/B being 19–29 °C, and C being 17–31 °C. Based on the temperature ranges and monitored temperatures, the temperature in the case was on the limit of the lowest indoor class for occupants wearing light shoes. Putting the numbers in perspective: Traditional indoor footwear for Danish occupants are bare feet/socks, and the external design temperature is $\Theta_{out,design}$ = -12 °C [8].

It is evident that comfort can be improved for both asymmetric radiation and floor temperature by reducing the cold surface, such as by application of interior insulation. Such comfort improvement will increase the deviation from the limit for asymmetric radiation and act

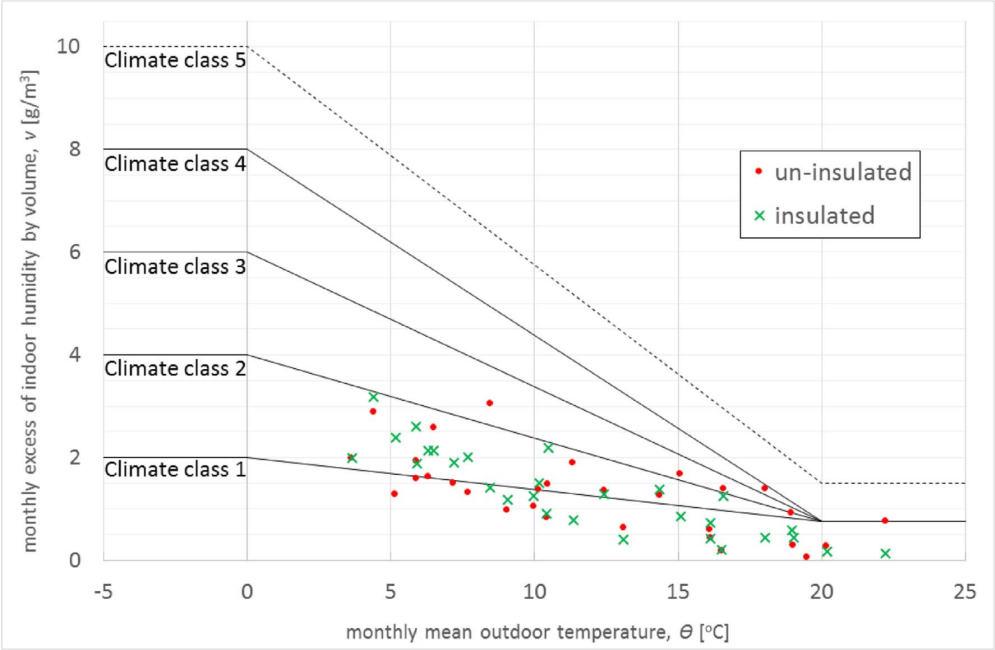


**Fig. 12.** Excess of indoor humidity by volume in rooms, based on outdoor climate. Humidity classes from Refs. [13,57].

positively regarding the indoor environment class in respect to floor temperature. An example of the effect from applying interior insulation is illustrated by the increased surface temperature compared to the room air temperature seen in Fig. 15. The values in Fig. 15 include the values for the interior surface temperature, inside ambient air temperature and outdoor ambient air temperature at the time of manual measurements.

Based on the temperature differences seen in Fig. 15, it can be concluded that the surface temperature on the un-insulated spandrel was within the 10 °C limit for asymmetric radiation [9,10], but the deviation between surface and ambient air temperature decreased when interior insulation was applied.

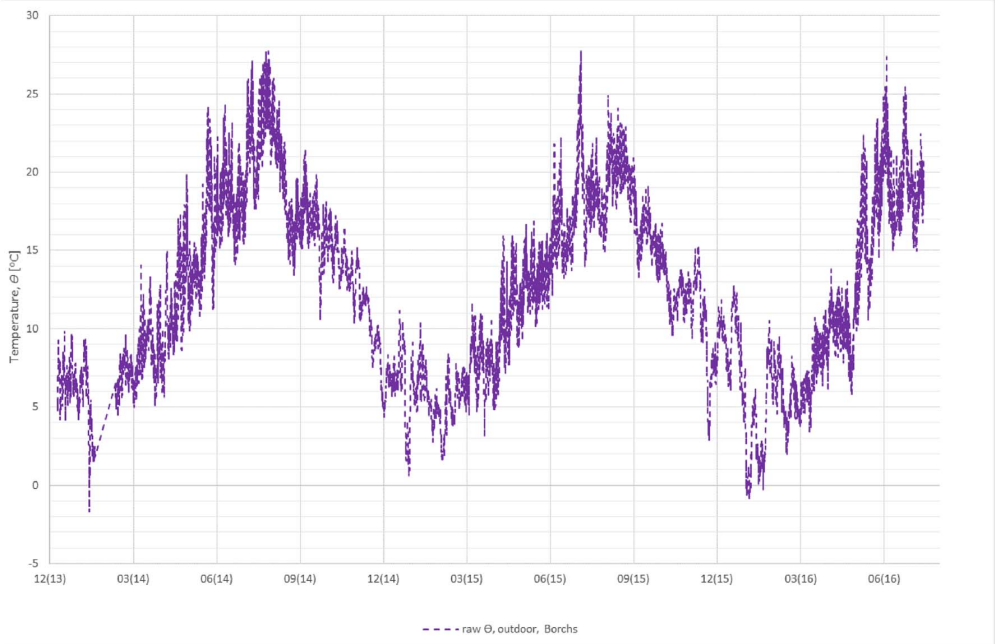


**Fig. 13.** Measured outdoor temperature in nearby open bicycle shed.

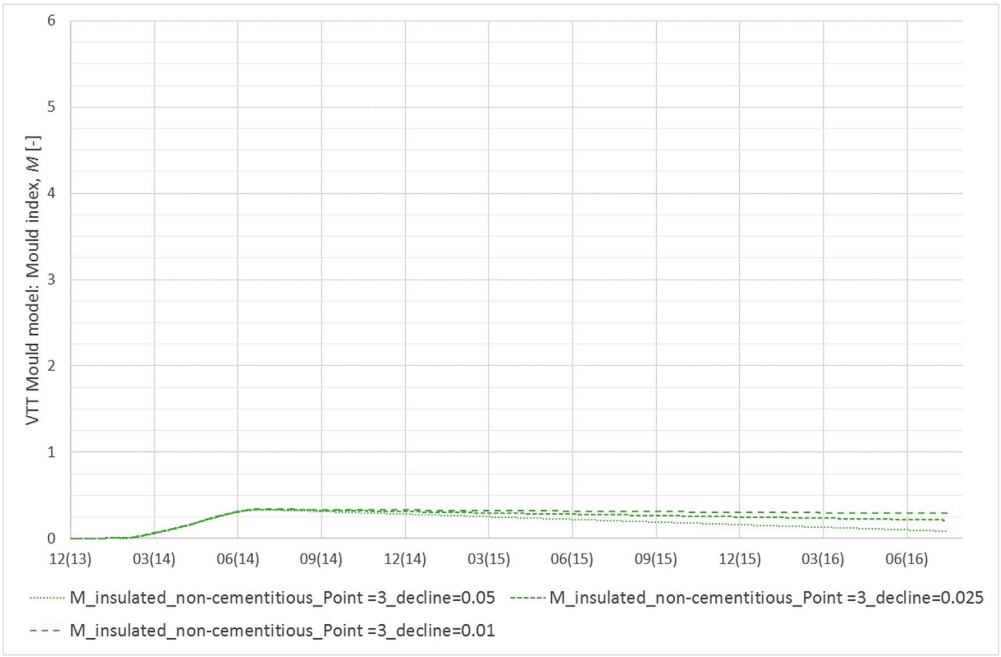


**Fig. 14.** Results from calculated VTT mould and decay models > 0, based on values for insulated (Fig. 6) and un-insulated (Fig. 7) wall.

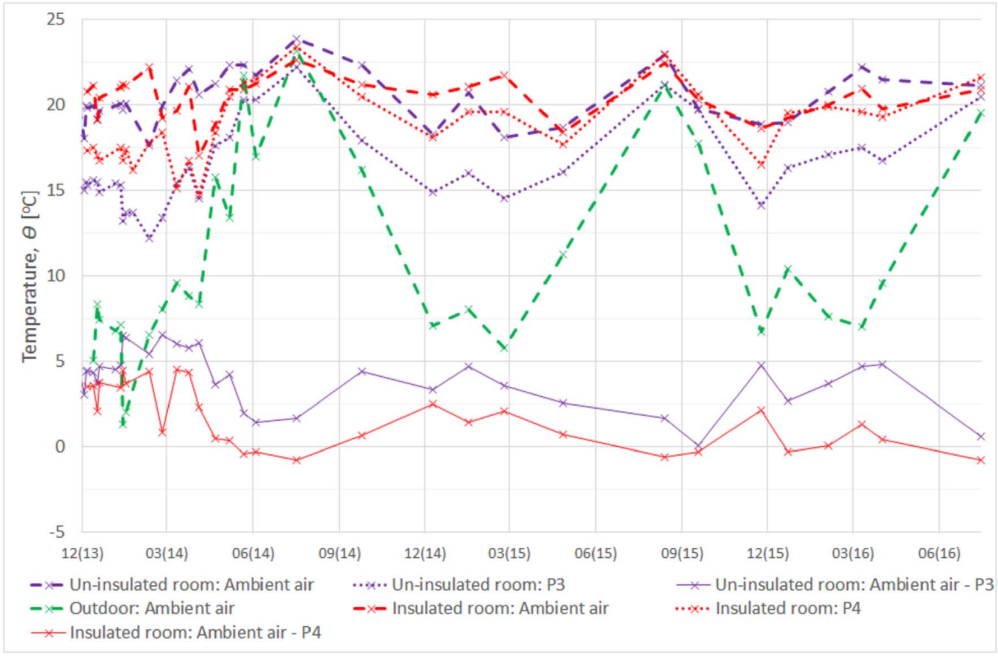


**Fig. 15.** Ambient air temperature, interior surface temperatures and difference between the two at the time of manual measurements.

## 5. Conclusion

This study has described an experimental investigation into the effect of installing interior insulation to the spandrels of a historic listed multi-storey dormitory building with solid masonry walls in the Danish capital, Copenhagen. Before the application, low interior surface temperatures of floors and façade walls were registered via thermal imaging. During the experiment, temperatures were monitored continuously on the inside of the un-insulated spandrel of a room that showed seasonally low surface temperatures and high difference between room air and surface temperature. Another room of the dormitory had an insulated spandrel, which had an increased surface temperature and a smaller difference between indoor air and surface temperatures.

The overall outcome of the results show that when applying interior insulation to the spandrel of a solid masonry wall subject to expected normal indoor climate, then the magnitude of relative humidity throughout the wall increases and temperature decreases, and there will be only small differences between inside and outside. The changed hygrothermal conditions have been evaluated visually for frost and mould, supplemented by on-site inspections for mould and mathematical predictions of risk of mould and decay of wood. Neither of the evaluated damage criteria showed damage after application of interior insulation.

It must be noted that conclusions in this paper are based on a healthy apartment with beneficial boundary conditions on the inside and outside, similar to a large segment of buildings in historic town centres [23]. The façade had a low impact of wind driven rain, combined with a rendered and painted façade. The temperature conditions in the courtyard were high, so the wall did not experience temperatures below freezing point. The indoor excess of humidity by volume in the room with an insulated spandrel did not go beyond humidity class 2 *"Offices, dwellings with normal occupancy and ventilation"* [13,57]. If the inside and outside boundary conditions get worse, then the risk of moisture induced damage, such as mould [20], decay of wood, and frost can increase.

## Acknowledgements

Allan Ulrick Døi and Rasmus von Wurstemberger Nielsen for the initial work, conducted during their B.Sc. thesis [55].

Jan Ringgaard from J E R Byggeservice/BMT Instruments provided wooden dowels and helped with installation.

Xella Denmark for installation of Multipor system to the spandrel of Room 9.

This work was supported through the Danish industrial PhD program by Innovationsfonden [grant number 1355-00129]; COWIfonden [grant number C-123.01]; and COWI A/S.

## Appendix A. Supplementary data

Supplementary data related to this article can be found at http://dx.doi.org/10.1016/j.buildenv.2017.11.015.

## References

[1] J. Kragh, K.B. Wittchen, Development of two Danish building typologies for residential buildings, Energy Build. 68 (2014) 79–86, http://dx.doi.org/10.1016/j.enbuild.2013.04.028.

[2] K.B. Wittchen, J. Kragh, O.M. Jensen, Energy saving potentials – a case study on the Danish building stock, ECEEE 2011 SUMMER STUDY · ENERGY Effic. FIRST Found. A LOW-CARBON Soc. (2011) 1355–1363.

[3] M. Morelli, S. Svendsen, Investigation of interior post-insulated masonry walls with wooden beam ends, J. Build. Phys. 36 (2012) 265–293, http://dx.doi.org/10.1177/1744259112447928.

[4] M. Morelli, L. Rønby, S.E. Mikkelsen, M.G. Minzari, T. Kildemoes, H.M. Tommerup, Energy retrofitting of a typical old Danish multi-family building to a "nearly-zero" energy building based on experiences from a test apartment, Energy Build. 54 (2012) 395–406, http://dx.doi.org/10.1016/j.enbuild.2012.07.046.

[5] J. Engelmark, Københavnsk Etageboligbyggeri 1850–1900. En Byggeteknisk Undersøgelse, Statens Byggeforskningsinstitut, (1983) Hørsholm.

[6] J. Engelmark, Dansk Byggeskik: Etagebyggeriet Gennem 150 År, 1. edition, Realdania Byg, 2013.

[7] G.R. Finken, S.P. Bjarløv, R.H. Peuhkuri, Effect of facade impregnation on feasibility of capillary active thermal internal insulation for a historic dormitory - a hygrothermal simulation study, Constr. Build. Mater 113 (2016) 202–214, http://dx.doi.org/10.1016/j.conbuildmat.2016.03.019.

[8] DS 418:2011, Beregning Af Bygningers Varmetab/Calculation of Heat Loss from Buildings, (2011) Charlottenlund.

[9] P.O. Fanger, H. Lund, H.E. Hansen, P.O. Danig, P. Kjerulf-Jensen, B. Elbæk, P.V. Nielsen, S. Aggerholm, F. Antvorskov, J. Gustavsson, O.B. Stampe, T. Lund Madsen, P.O. Danig, P. Worsøe-Schmidt, Danvak Grundbog I Varme- Og Klimateknik, third ed., Danvak APs, Vojens, Denmark, 2006.

[10] P.O. Fanger, B.M. Ipsern, G. Langkilde, B.W. Olesen, N.K. Christensen, S. Tanabe, Comfort limits for asymmetric thermal radiation, Energy Buildigns 8 (1985) 225–236, http://dx.doi.org/10.1016/0378-7788(85)90006-4.

[11] DS/ISO/TS 13732–2:2011, Ergonomics of the Thermal Environment – Methods for the Assessment of Human Responses to Contact with Surfaces – Part 2: Human Contact with Surfaces at Moderate Temperature, 1. edition, Dansk Standard/Danish Standards, Charlottenlund, 2011.

[12] DS/EN ISO 7730:2006, Ergonomics of the Thermal Environment – Analytical Determination and Interpretation of Thermal Comfort Using Calculation of the PMV and PPD Indices and Local Thermal Comfort Criteria, 2. edition, Dansk Standard/Danish Standards, Charlottenlund, 2006.

[13] E. Brandt, E.B. Møller, T. Bunch-Nielsen, G. Christensen, C. Gudum, M.H. Hansen, SBi Anvisning 224: Fugt I Bygninger, 2.0, Statens Byggeforskningsinstitut, SBI, 2013.

[14] J. Munch-Andersen, Sbi-anvisning 221-Efterisolering Af Etageboliger, 1.0, Statens Byggeforskningsinstitut, SBI, Hørsholm, 2008.

[15] H.M. Kuenzel, Effect of interior and exterior insulation on the hygrothermal behaviour of exposed walls, Mat. Struct. 31 (1998) 99–103.

[16] G. Christensen, A.P. Kock, E.B. Møller, Indvendig Efterisolering - Ældre Ydervægge Af Murværk, BYG-ERFA, 2015.

[17] Z. Pavlik, Hygrothermal performance study of an innovative interior thermal insulation system, Appl. Therm. Eng. 29 (2009) 1941–1946, http://dx.doi.org/10.1016/j.applthermaleng.2008.09.013.

[18] G.A. Scheffler, Hygric performance of internal insulation with light-weight autoclaved aerated concrete, Proc. 5th Int. Conf. Autoclaved Aerated Concr. Sept. 15-16, 2011, 2011, pp. 323–335 http://www.xella.com/de/docs/2011_Scheffler_InternalInsulation-LightWeightAAC-Multipor.pdf.

[19] J. Toman, A. Vimmrova, R. Cerny, Long-term on-site assessment of hygrothermal performance of interior thermal insulation system without water vapour barrier, Energy Build. 41 (2009) 51–55, http://dx.doi.org/10.1016/j.enbuild.2008.07.007.

[20] J. Zhao, J. Grunewald, U. Ruisinger, S. Feng, Evaluation of capillary-active mineral insulation systems for interior retrofit solution, Build. Environ. 115 (2017) 215–227, http://dx.doi.org/10.1016/j.buildenv.2017.01.004.

[21] M. Harrestrup, S. Svendsen, Full-scale test of an old heritage multi-storey building undergoing energy retrofitting with focus on internal insulation and moisture, Build. Environ. 85 (2015) 123–133, http://dx.doi.org/10.1016/j.buildenv.2014.12.005.

[22] A.A. Hamid, P. Wallent En, Hygrothermal assessment of internally added thermal insulation on external brick walls in Swedish multifamily buildings, Build. Environ. 123 (2017) 351–362, http://dx.doi.org/10.1016/j.buildenv.2017.05.019.

[23] T. Odgaard, S.P. Bjarløv, C. Rode, Segment size, distribution, characteristics and 1d/2d/3d heat saving potential of multi-storey buildings with solid masonry walls in Denmark, (under review), Energy Build. (n.d.).

[24] K. Ueno, J. Straube, R. Van Straaten, Field monitoring and simulation of a historic mass masonry building retrofitted with interior insulation, Therm. Perform. Exter. Envel. Whole Build. XII Int. Conf. (2013) 16.

[25] J. Straube, C. Schumacher, Interior insulation retrofits of load-bearing masonry walls in cold climates, J. Green Build. 2 (2007) 42–50, http://dx.doi.org/10.3992/jgb.2.2.42.

[26] E. Vereecken, S. Roels, A comparison of the hygric performance of interior insulation systems: a hot box–cold box experiment, Energy Build. 80 (2014) 37–44, http://dx.doi.org/10.1016/j.enbuild.2014.04.033.

[27] M.N.A. Saïd, R.G. Demers, L.L. McSheffrey, Hygrothermal performance of a masonry wall retrofitted with interior insulation, Res. Build. Phys. (2003) 445–454 http://irc.nrc-cnrc.gc.ca/ircpubs.

[28] E. Vereecken, S. Roels, Capillary active interior insulation: do the advantages really offset potential disadvantages? Mat. Struct. 48 (2015) 3009–3021, http://dx.doi.org/10.1617/s11527-014-0373-9.

[29] T. De Mets, A. Tilmans, X. Loncour, Hygrothermal assessment of internal insulation systems of brick walls through numerical simulation and full-scale laboratory testing, 11th Nord. Symp. Build. Physics, NSB2017, Trondheim, Norway, 2017, pp. 11–14.

[30] M. Van Aarle, H. Schellen, J. Van Schijndel, Hygro thermal simulation to predict the risk of frost damage in masonry; effects of climate change, Energy Procedia 78 (2015) 2536–2541, http://dx.doi.org/10.1016/j.egypro.2015.11.268.

[31] H. Viitanen, J. Vinha, K. Salminen, T. Ojanen, R. Peuhkuri, L. Paajanen, K. Lahdesmaki, Moisture and bio-deterioration risk of building materials and structures, J. Build. Phys. 33 (2010) 201–224, http://dx.doi.org/10.1177/1744259109343511.

[32] K. Gradeci, N. Labonnote, J. Köhler, B. Time, Mould models applicable to wood-based materials – a generic framework, 11th Nord. Symp. Build. Physics, NSB2017, 2017, pp. 11–14.

[33] E. Vereecken, S. Roels, Review of mould prediction models and their influence on mould risk evaluation, Build. Environ. 51 (2012) 296–310, http://dx.doi.org/10.1016/j.buildenv.2011.11.003.

[34] K. Sedlbauer, Prediction of mould growth by hygrothermal calculation, J. Build. Phys. 25 (2002) 321–336, http://dx.doi.org/10.1177/0075424202025004093.

[35] K. Sedlbauer, Prediction of Mould Fungus Formation on the Surface of and inside Building Components, Frauenhofer Institute, 2001.

[36] T. Ojanen, H. Viitanen, R. Peuhkuri, K. Lähdesmäki, J. Vinha, K. Salminen, Mold growth modeling of building structures using sensitivity classes of materials, Therm. Perform. Exter. Envel. Build. XI (2010) 1–10 http://web.ornl.gov/sci/buildings/2012/2010 B11 papers/104_Ojanen.pdf.

[37] H. Viitanen, M. Krus, T. Ojanen, V. Eitner, D. Zirkelbach, Mold risk classification based on comparative evaluation of two established growth models, Energy Procedia, Elsevier B.V., 2015, pp. 1425–1430, , http://dx.doi.org/10.1016/j.egypro.2015.11.165.

[38] A. Hukka, H.A. Viitanen, A mathematical model of mould growth on wooden material, Wood Sci. Technol. 33 (1999) 475–485.

[39] A.M. Reeslev, M. Miller, Måling af skimmelsvampe i bygninger – hvorfor og

hvordan? Byggeindustriens Byggeforum (2002) 18–19.
[40] M. Miller, M. Reeslev, Skimmelsporer og skimmelvækst er ikke det samme, Dan. Kemi 1 (2003) 20–23 http://www.kemifokus.dk/skimmelsporer-og-skimmelvaekster-ikke-det-samme/.
[41] J.D. Krause, Analytical instrument performance criteria application: application of a fluorometric method for the detection of mold in indoor environments, Appl. Occup. Environ. Hyg. 18 (2003) 1–5, http://dx.doi.org/10.1080/10473220301457.
[42] M. Reeslev, M. Miller, The MycoMeter(TM)-Test: a new rapid method for detection and quantification of mold in buildings, Proc. Heal. Build. 1 (2000) 589–590.
[43] C. Brischke, S. Thelandersson, Modelling the outdoor performance of wood products - a review on existing approaches, Constr. Build. Mater 66 (2014) 384–397, http://dx.doi.org/10.1016/j.conbuildmat.2014.05.087.
[44] H. Viitanen, T. Toratti, L. Makkonen, R. Peuhkuri, T. Ojanen, L. Ruokolainen, J. Räisänen, Towards modelling of decay risk of wooden materials, Eur. J. Wood Prod. 68 (2010) 303–313, http://dx.doi.org/10.1007/s00107-010-0450-x.
[45] G. Christensen, J. Kolbe, E. Brandt, Langtidsmåling Af Fugtforhold - I Bygninger Og Bygningskonstruktioner, BYG-ERFA, 1999.
[46] E. Brandt, G. Christensen, M.H. Hansen, Fugtindhold I Træ - Måleudstyr, Metoder Og Vurdering, BYG-ERFA, 1999.
[47] E. Brandt, M. Hjorslev Hansen, Fugtindhold I Beton Og Murværk - Måling Og Fejlkilder, BYG-ERFA, 2005.
[48] G. Christensen, Albertslund gårdhavehuse – opfølgende målinger i trætagkonstruktioner, TOR-NYT I/2001 (2001) 12–14.
[49] E. Brandt, M.H. Hansen, O.H. Hansen, P. Mossing, Måling af træfugt ved modstandsmåling, Byggeindustrien (1998) 26–30.
[50] E.J.D.P. Hansen, Supplerende Undersøgelser Til SBI-rapport 268-Byggematerialers Frostbestandighed, Statens byggeforskningsinstitut (SBI), 1996.
[51] U. Lohse, SBI-Rapport 176: Laboratorieforsøg Med Fuger Omkring Trævinduer, (1986) Hørsholm.
[52] J.F. Munch-Petersen, Fugtmåledyvler, Rapport Nr. 198, Lyngby, (1990).
[53] K. Ueno, J. Straube, Laboratory calibration and field results of wood resistance humidity sensors, Proc. BEST 1 Conf. June 10-12, Minneapolis, 2008.
[54] R. Walker, S. Pavía, M. Dalton, Measurement of moisture content in solid brick walls using timber dowel, Mat. Struct. 49 (2016) 2549–2561, http://dx.doi.org/10.1617/s11527-015-0667-6.
[55] A.U. Døi, R.V.W. Nielsen, Optimering Af Indeklimaforhold I Fedede Bygninger Med Fokus På Ydervægskonstruktionen, The Technical University of Denmark, 2014.
[56] Agency for Culture and Palaces, Fredede & bevaringsværdige bygninger, Bygning: collegium mediceum 1691, www.kulturarv.dk/fbb/bygningvis.pub?bygning=3180332, (1995) , Accessed date: 22 March 2017.
[57] DS/EN ISO 13788:2013, Hygrothermal Performance of Building Components and Building Elements — Internal Surface Temperature to Avoid Critical Surface Humidity and Interstitial Condensation — Calculation Methods, 2. edition, Dansk Standard/Danish Standards, Charlottenlund, 2013, http://www.iso.org/iso/catalogue_detail.htm?csnumber=51615.
[58] Bygge og Miljøteknik, Fugtmåler, T 301 COW, (2008) 2 pages.
[59] BMT Instruments ApS, COW T301, Vedbæk, 2017.
[60] Onset Computer Corporation, HOBO® U12-012 Logger, (2016) 2 pages. http://www.onsetcomp.com/files/data-sheet/Onset HOBO U12 Data Loggers.pdf.
[61] NCEI GIS Agile Team, National oceanic and atmospheric administration (NOAA), national centers for environmental information, hourly/sub-hourly observational data map, version 1.8.2, https://gis.ncdc.noaa.gov/maps/ncei/cdo/hourly, (2017) , Accessed date: 8 February 2017.
[62] Bygge- og Miljøteknik, BM - dybel: Elektrisk ledningsevne i afhængighed af fugtindhold, 1 page.
[63] K.K. Hansen, Technical Report 162/86 Sorption Isotherms a Catalogue 86 Build. Mater. Lab. Tech. Univ, Denmark, 1986.
[64] L. Ahlgren, Report 36: Fuktfixering I Porösa Byggnadsmaterial/Moisture Fixation in Porous Building Materials, (1972) Lund, Sweden.
[65] L. Due, Bygningsundersøgelseaf Borchs Kollegium, KBH. Sags. Nr. 2682, Boeslunde, (2013).
[66] DS/EN 13187:1999, Thermal performance of Buildings – Qualitative Detection of Thermal Irregularities in Building Envelopes – Infrared Method, DK-2920 Charlottenlund, (1999).
[67] mycometer, Mycometer Surface: On-Site Fungal Contamination Assessment, (2012), p. 2 http://cdn.mycometer.com/fileadmin/user_upload/Pdf/Mycometer-Surface_Flyer_2012_.pdf.
[68] mycometer, Mycometer®: Instructions for surface sampling, 1 page. http://www.mycometer.com/products/mycometer-surface/surface-sampling/(accessed July 25, 2017).
[69] Mycometer, Interpretation criteria for Mycometer results, http://www.mycometer.com/products/mycometer-surface/interpretation-criteria/(accessed July 25, 2017).
[70] M. Schrock, C. Riffle, A. Dindal, J. Mckernan, J. Enriquez, Environmental Technology Verification Report: Mycometer ®-test Rapid Fungi Detection and Bactiquant ®-test Rapid Bacteria Detection Technologies, (2011).
[71] T. Odgaard, S.P. Bjarløv, C. Rode, Measured and Analyzed Data from Borchs Dormitory, (2017).
[72] S.A. Elborne, Hussvamp Laboratoriet ApS, Mikrobiologisk Analyse, Case: 26996–1, Borchs kollegie, Birkerød, 2017.
[73] G.M.B.H. Fels-Werke, Product Safety Data Sheet for Light Mortar, Int. ref.: SDS_LM_X_e1073, Goslar (2013) https://www.fels.de/en/img/Leichtmoertel_englisch.pdf.

# C. PAPER #3: INFLUENCE OF HYDROPHOBATION AND DELIBERATE THERMAL BRIDGE ON HYGROTHERMAL CONDITIONS OF INTERNALLY INSULATED HISTORIC SOLID MASONRY WALLS WITH BUILT-IN WOOD

Energy & Buildings 173 (2018) 530–546

Contents lists available at ScienceDirect

Energy & Buildings

journal homepage: www.elsevier.com/locate/enbuild

# Influence of hydrophobation and deliberate thermal bridge on hygrothermal conditions of internally insulated historic solid masonry walls with built-in wood

Tommy Odgaard[a,b,*], Søren Peter Bjarløv[a], Carsten Rode[a]

[a] Technical University of Denmark, Department of Civil Engineering, Brovej 118, Kongens Lyngby 2800, Denmark
[b] COWI A/S, Parallelvej 2, Kongens Lyngby 2800, Denmark

ARTICLE INFO

*Article history:*
Received 25 October 2017
Revised 18 May 2018
Accepted 30 May 2018
Available online 15 June 2018

*Keywords:*
Field study
Interior insulation
Impregnation
Thermal bridge
Solid masonry
Historic

ABSTRACT

A large share of the Danish building stock contains historic multi-storey buildings. A considerable energy saving potential exists, achievable through thermal insulation of the façades. Previous research has elucidated problems regarding poor hygrothermal conditions when interior thermal insulation is applied to the façade, but examples exist with positive results.

Eight 1 × 2 m solid masonry test walls with wooden members were installed in an insulated container. The hygrothermal implication of applying 100 mm AAC as interior thermal insulation system was investigated with variations including use of hydrophobation and substitution of insulating material with a deliberate thermal bridge.

Relative humidity and temperature were monitored in the walls over 2 years in 10 measurement points. The amount of wind driven rain was monitored with rain gauges and calculated from climate station data. The indoor excess of humidity by volume corresponded to the highest indoor climate class for dwellings.

Damage models indicated risk of mould growth in the insulation/masonry interface, and risk of wooden decay in the wall plate for the reference and insulated case. Hydrophobation of the exterior surface in tempered cold climate reduced the overall relative humidity, although it increased during winter due to a reduced dry-out potential towards the outside.



## 1. Introduction

A large field study concerning eight solid masonry test walls with wooden members constructed in cut-out 1 × 2 m holes in an insulated container was setup up for experimentation with interior thermal insulation. The experiment was based on a large public interest in finding ways to reduce heating expenses and improving occupant comfort, while preserving the exterior expression of buildings that are renovated. The study focused on historic multi storey buildings from 1850–1950, an extensively investigated segment with similar characteristics during the period [1,2], which constitutes a large share of the Danish building stock [3]. The segment has been shown to have a large overall potential for reduction of heat loss [4,5], with considerable energy saving potential from applying thermal insulation to the solid masonry façade [6,7].

Previous research has focused on how to add interior thermal insulation to old masonry constructions and the performance of the insulation material [6,8–14]. Hygrothermal conditions in the original solid masonry wall are made worse when adding thermal insulation on the inside of constructions in cold climates, as the temperature of the original wall drops severely [15–17], increasing the risk of condensation at the original masonry surface behind the thermal insulation [15,18]. This effect, combined with reduced possibility for two-sided drying [17,19], result in increased moisture content of the wall at the cold side of the interior thermal insulation [13,16,18–23]. The degree to which the conditions are exacerbated is influenced by the interior and exterior boundary conditions, and increases with the thickness of insulation [24] and the amount of moisture entering the construction from both sides. The application of interior thermal insulation to an area limited to the spandrels below windows has been shown possible while avoiding damage from mould, wooden decay and frost [25], and may still achieve 40% of the potential reduction in thermal transmittance with a full covering strategy, although it covers only 17% of the surface [3].

* Corresponding author at: COWI A/S, Parallelvej 2, Kongens Lyngby 2800, Denmark.
*E-mail addresses:* TOOG@COWI.dk (T. Odgaard), SPB@byg.dtu.dk (S.P. Bjarløv), CAR@byg.dtu.dk (C. Rode).

https://doi.org/10.1016/j.enbuild.2018.05.053
0378-7788/

Moisture influencing the interior boundary condition can be expressed as the indoor excess of moisture. The amount of moisture excess has been shown to vary within building style [26] and occupant behaviour and room type [27]. Based on this, an interior thermal insulation system must be able to cope with low and high indoor excess of moisture.

Moisture influencing the exterior boundary can be expressed as the outdoor humidity by volume and wind driven rain (WDR) affecting the façade. The WDR have been shown to have a large influence the average moisture level in internally insulated masonry walls [6,28], with increasing amount of water entering the façade as cracks and deficiencies of the exterior masonry surface are introduced [29].

Heaters and a humidifier were installed, ensuring a controlled level of indoor relative humidity and temperature. The outdoor wall surfaces were exposed to the local climate. The indoor and outdoor boundary conditions were monitored. Similar field tests were used in other European projects at BBRI, Belgium [23] and UCEEB, Czech Republic [30]. The paper presenting results from the field study at BBRI showed how the application of insulation to the interior surface of a solid masonry wall increased the moisture content in the masonry, especially for vapour tight insulation strategies, resulting in increased risk of hygrothermal damage. With diffusion open strategies, the influence from the inside environment was increased. Simulation based on the results obtained at BBRI showed that WDR had an important influence on the hygrothermal conditions in the wall. The paper presenting results from an ongoing field study at UCEEB was focusing on the conditions in the air gap around the embedded wooden beam end, showing that a high observed RH, and thereby risk of mould growth, could be reduced by sealing the air gap from the high influence of the inside environment towards the gap.

The measurements of boundary conditions at DTU included monitoring and calculation of WDR on the façade. An overview and comparison of state of the art WDR models has been performed by [31], comparing 2 semi-empirical models and a CFD model. We have in the present study chosen to model WDR using the semi-empirical model originally developed by Lacy [32], and later extended by Straube [33,34].

As a mean to decrease the wetting of the masonry wall by WDR, hydrophobation of the exterior surface have been introduced by application of a water-repelling agent. The use of hydrophobation has shown to reduce the amount of moisture in walls and thereby also to decrease the thermal transmittance of the structures [24]. An experimental study was performed on the effect of applying the hydrophobizing agent "Funcosil FC" to bricks [35]. Engel et al. found that the application of agents with 10–60% active ingredient changed the properties regarding capillary saturation and water uptake, while water vapour diffusion resistance was nearly unchanged. The changes in properties were shown to highly influence the drying curves of brick, lowering the rate of drying/return transport of water with increasing active ingredient in the hydrophobizing agent.

The aim of this paper is to present an investigation of how the hygrothermal conditions in the wall system are affected by the application of thermal insulation on the interior surface; the influence from applying a hydrophobic façade treatment to the exterior masonry surface and by applying a deliberate thermal bridge next to embedded wooden elements.

The field study is based on measured hygrothermal conditions in four identical solid masonry walls with built in wooden elements, with the same base thermal insulation system on the interior side. The interaction between the interior thermal insulation system and two means have been investigated. The first mean was the application of a hydrophobizing agent to the exterior masonry surface. The second mean concerned replacing a share of thermal insulation material with a deliberate thermal bridge. The hygrothermal conditions were continuously measured during a monitoring period of 2 years.

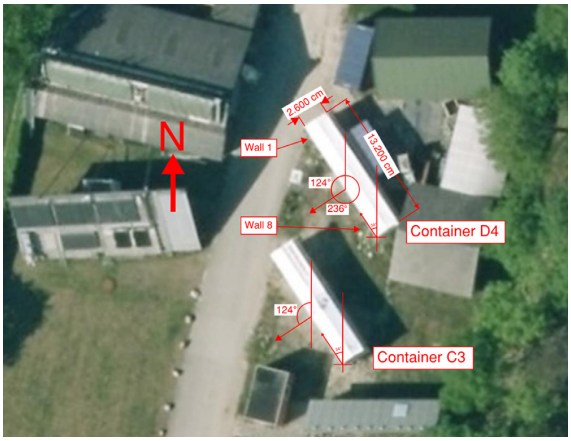


**Fig. 1.** Ortofoto of field study at the test site of the Technical University of Denmark. This paper focus on results from container D4. Photo courtesy of Maps from COWI.

## 2. Method: description of field study set-up and measured data

### *2.1. The base: perforated container with solid masonry walls*

A large-scale field study was built at the field test site of the Department of Civil Engineering at the Technical University of Denmark (DTU) in Kongens Lyngby, Denmark (55.79°N, 12.53°E). The set-up was constructed as an adjusted sample of the traditional Danish multi storey building from the period 1850 to 1930. The main idea for the field study was based on the use of a castoff 40 feet insulated container, similar to two previous field studies at DTU [36]. The façade of the field study was oriented towards the critical direction in Denmark, south-west, based on dominating winds from west [6,37], yielding critical wind driven rain, combined with solar exposure from the south, resulting in potential transport of moisture towards the indoor climate. The exact angle of the façade can be seen from aerial photos illustrated in Fig. 1, showing an actual direction of west-southwest, with a compass angle of 237°. Holes of 1 m width × 2 m height were cut in the facade for the construction of 8 identical base walls for experimentation with thermal insulation.

Construction of the masonry walls were finished on September 18th 2014, from when a forced dry-out period started. The dry-out was performed to remove the moisture induced from the building process, by heating up the indoor climate to 40–50 °C with two 2000 W caloriferes, resulting in an indoor relative humidity in the range 10–30%. The dry-out conditions from the external side were achieved by establishing a tent, open at both ends, and apply heat with one 9000 W calorifere in the period December 2014 to April 2015. The walls were assessed as dried out based on Troxler measurements at the interior side of container C3, showing counts similar to 1 (±0.5) weight-% moisture in masonry, and measured RH under saturation in the embedded digital RH/T sensor points in the masonry. The thermal insulation systems were installed on February 24th and 25th, 2015, with the different means to change the hygrothermal conditions illustrated in Fig. 3. As mentioned later in Section 3.3, the first year of relative humidity measurements was used as a stabilization year. It must be acknowledged that the applied forced dry-out have changed the initial carbonation process,

as high temperature and low relative humidity (RH < 30%) have previously shown to reduce the speed of the carbonation process of the used lime mortar [38]. The carbonation of the masonry walls during the first period is therefore limited, whereas carbonation of the outmost layers, which provide the protection against wind driven rain, is expected sufficient during the first year of stabilization. No additional $CO_2$ have been applied to the experiment, even though literature show promising results [39].

A humidifier to keep the chosen indoor moisture level was started on May 21st 2015, marking the beginning of the experiment. Data for use in the present paper were drawn on May 1st, 2017, for the 2-year period 01–05–2015 until 01–05–2017. In order to stress the experiment, the set point of the humidifier was set to 70% relative humidity in the first period, May until August 2015, then adjusted to 60% relative humidity for the rest of the period which can be considered as a high but not un-realistic value for Danish dwellings in the winter. This set point has traditionally been used as indoor climate conditions for building envelope experiments in Denmark. Yet to be published research from Hansen and Møller, altering the previously found transformation of indoor excess of moisture for indoor experiments [40] to DRY data [37], show that the highest climate class 3 for dwellings [41,42] in Denmark correspond to minimum 60% RH during the year.

### 2.1.1. Setup of base walls in field study

The 8 identical base walls were designed to resemble the intersection of two façade wall columns with a room dividing solid interior wall at the highest floor and a floor structure, including a wooden beam, of a characteristic Danish multi-storey building. Illustrations of the base walls can be seen in Fig. 3 (a–c). The horizontal design of the base walls had a width of 948 mm, equal to 4 stones of brick, and a thickness of 358 mm, 1½ stones, with a layer of rendering on the inside. The rendering and mortar joints were made of the same material: lime mortar. The masonry walls were constructed as massive brick walls in a characteristic cross bond with lime mortar joints by professional masons. An interior wall was built with a thickness of 128 mm, ½ stone, with a layer of rendering on both sides. The vertical design of the base walls had a height of 1987 mm, 30 courses, with a floor structure having a top point at the vertical middle of the wall. The floor structure consisted of a 100 × 100 mm wall plate with a 175 × 175 mm wooden beam resting on top of this. 15 mm OSB boards on all sides except towards the interior wall encapsulated the wooden beam. 100 mm of mineral wool was placed in the OSB board enclosure to emulate a pugging layer. The wooden beam/OSB board construction was constructed to the left of the interior wall, while the space on the right side was kept empty, also for walls where insulation systems were applied.

### 2.1.2. Insulation systems and surface treatments

All thermal insulation systems used in the field study were based on a system of lightweight AAC. The system was installed with variations, as it can be seen in Fig. 2. The notation next to each wall describe the installed interior insulation system and internal/external surface, specific materials are described in Section 2.1.3. The used descriptions in Fig. 2 denote:

- First line: description of the interior surface.
  - Reference wall: no insulation installed, identical to base walls.
  - Interior insulation: Diffusion open thermal insulation system based on lightweight AAC.
  - Interior insulation + therm. bridge: diffusion open thermal insulation system based on lightweight AAC, supplemented with a 100 × 200 mm AAC with higher density in the top 200 mm underneath the floor structure. This block was implemented to create an intentional thermal bridge, meant to protect the wall plate and beam behind. A detail drawing of the system can be seen in Fig. 3(a).
- Second line: description of the exterior surface.
  - Rendering: Rendered surface of the base wall.
  - Diffusion-open paint: a silicate based interior paint.
- Third line: description of the exterior surface.
  - Bare brick: bare brick surface, identical to the base wall.
  - Hydrophobized bare brick: hydrophobic facade treatment of the bare brick masonry. The hydrophobizing agent was rolled onto the exterior masonry surface in April 2015. The exterior surface of the experiment was protected against rain with a tent at the time of application, and the surface and environment temperatures were sufficient according to instructions, backed up by a calorifere in the tent relating to the forced dry-out procedure.

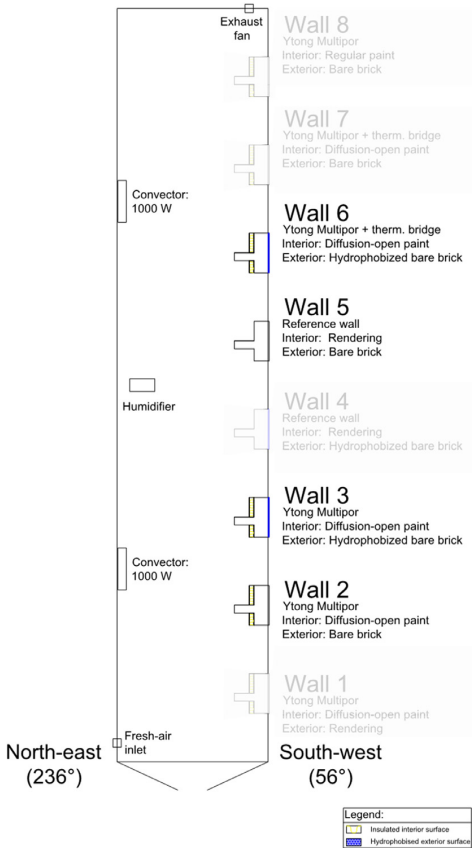


**Fig. 2.** Overview of investigated wall/insulation compositions in container D4. The meaning of the text next to the walls are described in Section 2.1.2. Results from the un-shaded Walls 2, 3, 5 and 6 are investigated in this paper.

### 2.1.3. Materials in field study

Material samples were sent to the Technische Universität Dresden (TUD) for characterization in their material laboratory, as part of a collaboration between DTU and TUD.

The materials used in this study, with parameters measured at TUD if not stated otherwise, can be seen in Table 1.

### 2.2. Measuring equipment

Two measurement systems were installed in the field study, one based on digital sensors logging every 10 min and one based on

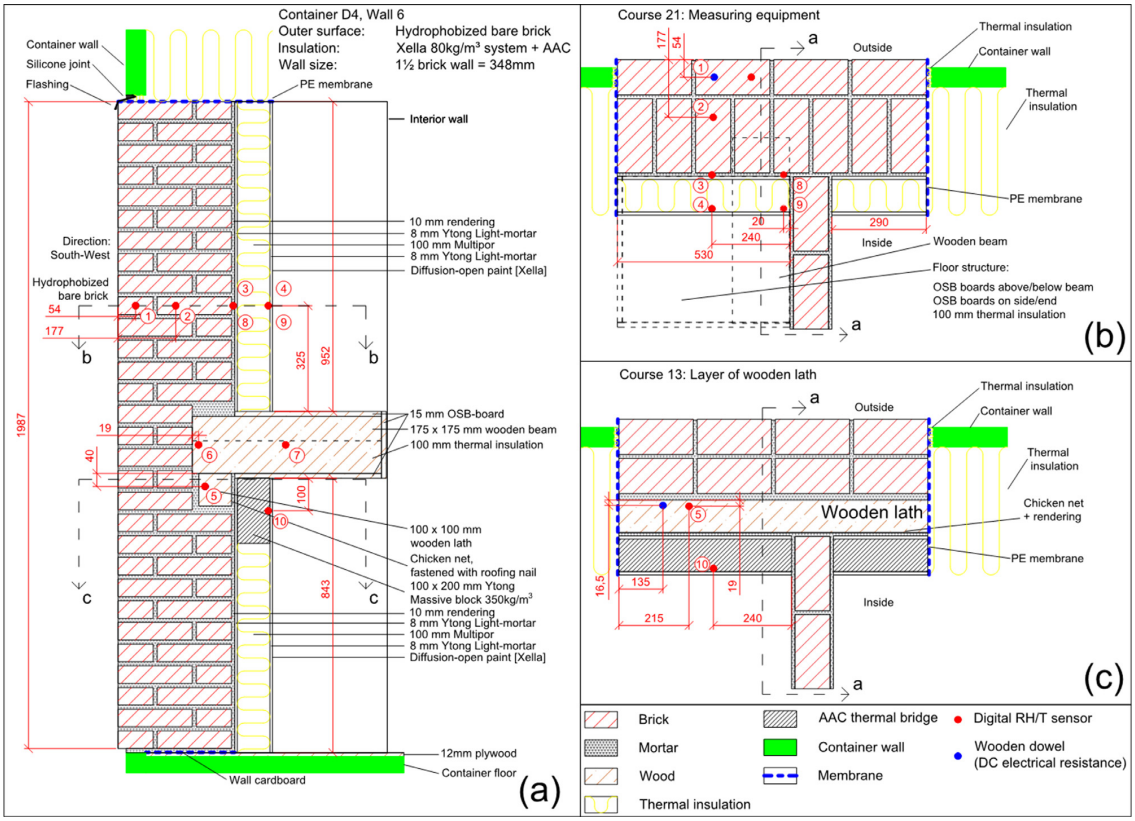


**Fig. 3.** Illustration of wall composition and location of measurement points in Wall 6. Masonry, rendering, wooden elements and insulation on boundaries are identical for all walls. Installed thermal insulation on Wall 2 & 3 are equivalent, but with insulation in front of wall plate instead of AAC. Wall 5 is un-insulated. (a) Show a vertical cut in the wooden beam, (b) & (c) show courses with measuring equipment. Data from the measurement points 1, 2, 3, 4, 5, 6 & 10 are investigated in this paper. Pictures from construction of experiment can be seen in [43].

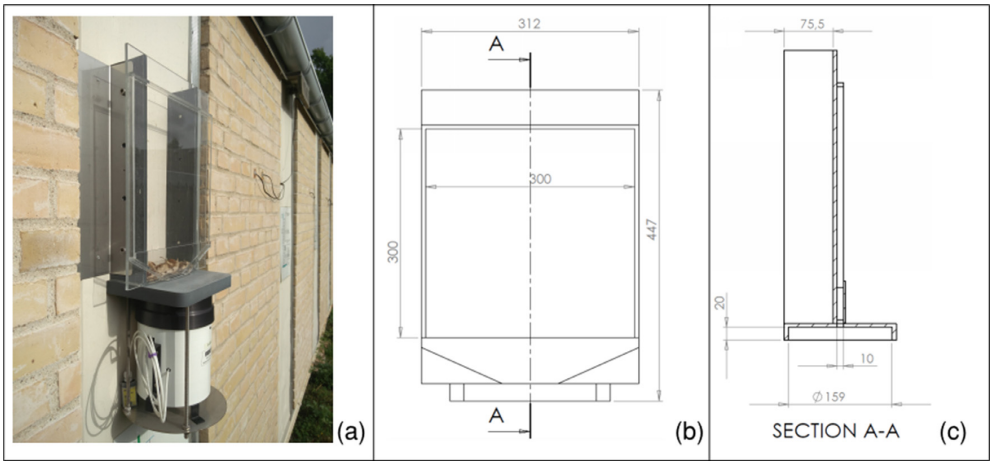


**Fig. 4.** Picture (a) and drawings (b) & (c) of wind driven rain (WDR) gauge developed and used for the field study. The bottom white bucket with integrated tipping gauge and datalogger is a commercial product for logging vertical rain. Drawings produced by Linatex A/S.

**Table 1**
Hygrothermal properties for materials used in field study. * denote material properties stated by producer, non-marked parameters are measured at TUD.

| Name | Density [kg/m³] | $\lambda_{dry}$ [W/(m² K)] | $\mu_{dry}$ [-] | $A_w$ [kg/(m² $s^{0.5}$)] |
|---|---|---|---|---|
| Yellow soft-moulded brick from Helligsø Teglværk | 1640 | 0.60 | 16.91 | 0.278 |
| 7.7% lime adjusted mortar (air lime), grain size 0–4 mm from Wewers A/S designed to resemble mortar used in historic buildings | 160 | 0.08 | 18.75 | 0.764 |
| Ytong Multipor interior mineral insulation boards | 100 | 0.04 | 6.73 | 0.006 |
| Ytong Multipor light mortar | 830 | 0.16 | – | 0.003 |
| Ytong massive block | 340* | 0.08* | 5/10* | |
| Wall plates and wooden beams of Pomeranian pine wood. | | | | |
| OSB board | | | | |
| Ytong Multipor silicate interior paint Remmers Funcosil FC (Concentration = ~40% w/w). | | | | |

manual measurements of electrical resistance of wooden sensors. This paper will mainly present results from the digital system. Results from the system based on electrical resistance is used for validation of results from the digital system.

Wind driven rain sensors with built-in data loggers were installed on the external south-west oriented wall of container C3 and D4. The placement of the containers can be seen in Fig. 1.

*2.2.1. Placement of measuring equipment*

The measurement points investigated in present paper are described in the following bullet list, with positions illustrated in Fig. 3(a–c).

- Point 1: digital RH/T sensor, mounted in brick, near exterior masonry surface.
- Point 2: digital RH/T sensor, mounted in brick, in middle of masonry wall.
- Point 3: digital RH/T sensor, mounted on interior masonry surface, covered by rendering.
- Point 4: digital RH/T sensor, mounted in 10 mm deep cut channel in the interior insulation, covered with the mortar belonging to the insulation system.
- Point 5: digital RH/T sensor and wooden dowel for electrical resistance measurement, mounted in wall plate from the bottom and sealed with silicone.
- Point 6: digital RH/T sensor, mounted in wooden beam and sealed with silicone. Hole drilled horizontally from opposite side of the interior wall, with measurement point in the beam centre.
- Point 10: digital RH/T sensor exclusively in Wall 6 & 7. Mounted in 10 mm deep cut channel in the AAC thermal bridge, covered with the mortar belonging to the insulation system.

*2.2.2. Setup of digital RH/T sensor system*

The system was based on Arduino boards, reading measurements from sensors connected to the same main cable and logging the values to a computer. The digital RH/T sensors used in the experiment were constructed from modules and cables from two different companies, both mentioned in the acknowledgements. The module to sensor cable connection was protected using adhesive shrink tubing, covering the module and sensor cable, but uncovered at the sensing area of the module, a process which may be followed in [43]. The resulting sensor dimensions are approximately ($b \times h \times l$) = 15 × 10 × 60 mm. The producer of the sensor module stated an operating range of 0–100% RH, with an accuracy of ±1.8% RH in the range 0–90% RH. Accuracy in the range >90% RH was not accessed as important for the experiment, as this is above the limits for mould growth and wooden decay. The long-term drift of the modules was stated as <0.5% RH/year.

*2.2.2.1. Calibration and post processing of digital RH.* Each individual sensor was calibration at the start of the project. This was done after protecting the module/sensor cable connection with adhesive shrink tubing, prior to installing the sensor in the field study.

The measured relative humidity for each sensor was calibrated with four saturated salt solutions in ad- and desorption. The calibration was performed in a vapour tight box with an internal fan for ensuring homogeneity of the air. The relative humidity at each step was validated using a Rotronic Hygrometer A2, calibrated prior to the process over certified Rotronic ampoules.

The following saturated salt solutions were used for the calibration, with the resulting relative humidity in brackets: potassium carbonate $K_2CO_3$ (44%); sodium chloride NaCl (75%); potassium nitrate $KNO_3$ (93%); potassium sulfate $K_2SO_4$ (97%). Focus was on relative humidity from 75% and up, as the intention was to investigate if conditions amenable to mould growth and decay conditions would be met [44–46]. The sensors were exposed to each saturated salt solution until steady conditions were achieved, before changing to next salt solution. In the end, a unique linear trend line was fitted to the measurements from each sensor, yielding an equation to convert from measured relative humidity to real relative humidity. Sensors with diverging calibration equations or outliners were discarded.

The individual calibration values of each sensor were applied and results were truncated to be between 0.00 and 99.99% RH. Corrupted data with unrealistic values and outliers from failing sensors and power cuts were removed.

The resulting unique calibration equations had the form illustrated in Eq. (1), and an example of some calibration values for the sensors monitoring the environment can be seen in the following bullet list.

$$RH_{calibrated} = RH_{measured} * a_{calibration} + b_{calibration} \quad (1)$$

> $RH_{calib-inside_{NW}} = RH_{meas-inside_{NW}} \cdot 0.995 + 1.739$

> $RH_{calib-inside_{SE}} = RH_{meas-inside_{SE}} \cdot 0.986 + 1.177$

> $RH_{calib-outside} = RH_{meas-outside} \cdot 0.989 + 0.079$

### 2.3. Climate conditions

#### 2.3.1. Indoor climate conditions

The indoor climate was maintained by installing two heaters and one humidifier, while cooling and dehumidification were not carried out. Indoor set points of 20 °C and 60% relative humidity were maintained by two 1000 W electric convectors and a "Brune B125″ humidifier, supplied with demineralized water. Sensors similar to those used in the walls, hanging from the roof in each end of the field study, 20 cm from the roof, 2 m from the ends, monitored the indoor climate. The output from the two indoor climate sensors was averaged. Air change in the field study was ensured via a fresh-air valve in the north-west end, and an exhaust fan in the southeast end, with a capacity of maintaining an air change of 0.5/h. The fan was in operation outside of the heating season to reduce humidity and temperature in the field study. A circulation fan was installed in the southeast corner of the field study to ensure constant air movement.

#### 2.3.2. Outdoor climate conditions

The exterior wall surfaces were exposed to the local climate. Rain run-off from the roof was ensured not to affect the walls by installing a gutter. The nearest building was a similar field study located in the south-west direction, at a distance of 6.7 m and a height of 3.1 m. Located straight west in a distance of 7.6 m was another building, with a height of 6.5 m. The local temperature and relative humidity were monitored by one sensor similar to those used in the walls, placed behind a wooden cladding under the gutter between Wall 4 & 5. The climate of the local area was monitored by DTU's climate station [47], situated 160 m to the west-southwest, at an altitude 16 m above the field study.

*2.3.2.1. Wind driven rain.* Three wind driven rain (WDR) gauges were installed, one between Wall 4 and 5, two on nearby container C3 (see Fig. 1), same direction as on container D4 and opposite by 180°. The gauges are based on a commercial vertical rain gauge mentioned in the acknowledgements, mounted in custom-built frames to monitor horizontal rain. Considerations defining the design may be seen in [48]. The frame was constructed from acrylic glass (PMMA) with a raised border of 10 mm around the 300 × 300 mm collector area. The WDR hitting the vertical collection area drained into the closed tipping bucket, logging time and tips. The rain gauges were calibrated before installation, to define the amount of liquid per tip. All rain gauges were in function from June 6th, 2016.

The experiment was in operation 13 months earlier than the rain gauges were installed. To obtain information regarding the WDR influencing the façade before June 2016 and during errors on the WDR gauges, the WDR model methodology of [34] was applied to the data from the weather station in Eq. (2).

The transformation from horizontal rain in the free wind field to rain impinging on the specific facade is based on a multiplication with building and environment dependent factors [34]. The multiplied factors in this project are determined from fitting the model to measured WDR. The resulting effect of the fitted $Factor_b = 0.49$, can be seen later under presentation of boundary conditions in Section 3.2, Fig. 5 and in the WDR discussion in Section 3.4, Figs. 14 and 15.

$$r_{vb} = Factor_b \cdot r_v = Factor_b \cdot DRF \cdot V(z) \cdot \cos(\Theta) \cdot r_h \cdot \quad (2)$$

where: $V(z)$ is wind speed at height of interest, defined as $V(z) = V_{10} * (\frac{z}{10})^{\alpha_V}$, $V_{10}$ is standard wind speed from weather station [m/s], $z$ = height of interest [WDR gauge = 1.75 m], $\alpha_V$ = exposure coefficient (0.25 for suburban area [34]), $\Theta$ = angle between wind direction and wall surface [°], $r_h$ = horizontal rain [mm or l/m²].

The DRF (driving rain factor) defines the wind speed/raindrop fall speed interaction. The DRF is used in multiple WDR models, tending to be a fixed standard parameter defined from average conditions, varying from 0.20 to 0.25. But as raindrop fall speed changes with drop size, DRF can vary in the range from 0.15 to 0.50 when drizzles or cloudbursts are studied [34].

DRF has been calculated for 1 minute data steps based on the methodology described by Straube [33]. The median relative frequency of raindrop size is determined from the rain intensity [49]. The median raindrop size is used to determine the raindrop terminal fall speed [50]. Finally, DRF is determined as the reciprocal of the fall speed [33,34] resulting in the varying DRF over rain intensity. Calculation of varying DRF has been incorporated in an Excel sheet with embedded VBA scripts, available here [51].

### 2.4. Implementation of damage modelling

The results of the field study show how the different insulation systems have an influence on the measured relative humidity and temperature. While damage models have previously been shown unable to precisely predict mould growth in constructions, for example by Møller et al. showing no mould activity during constant critical conditions for mould growth in a laboratory experiment [52], the models are still valuable tools when assessing the significance of combined hygrothermal conditions. The models have been used to transform the combination of non-smoothened measurements and exposure time into theoretical risk of damage with two different damage models, with the purpose of comparing the different insulation strategies to the measurements in the reference wall. The damage models are only presented briefly and the sections mainly serve for defining the used parameters, as we will refer to another paper where we gave an in-depth presentation and discussion of the implemented damage models [25], while other researchers have done broader review and discussion of more damage models [53–55].

#### 2.4.1. Mould modelling

The risk of mould occurring on the interior surface and behind the interior insulation is modelled based on the VTT model [44,56,57]. The output of the model is a mould index, *M*, ranging between 0 and 6, with each integer defining a state of mould growth [44]. The measurement points were modelled as non-wood, medium resistant materials, using a limit curve as suggested in [25].

#### 2.4.2. Decay modelling

The risk of wooden decay is evaluated based on the extended VTT model [46]. The model has two outputs: "Activation process", $\alpha$, which is the state of the decay process, and "irreversible wooden mass loss", *ML*, which increases when $\alpha = 1$. The alpha value in all calculations have been started at $\alpha = 1$.

## 3. Results and discussion

The results and discussion have been combined in the present paper, to simplify the presentation of results and allow for placement of discussion near plots of measures data. The results presented in this paper can be seen in Figs. 5–10, Figs. 12 and 13. The presented results are obtained from a 2-year monitoring period: 01–05–2015 until 01–05–2017.

Raw relative humidity data will not be presented, measurements from the digital sensors have been adjusted based on unique sensor calibration equations and filtering settings described in Section 2.2.2.1 The presented results are based on smoothened 96-h running average values, in order to communicate the trends in the field study.

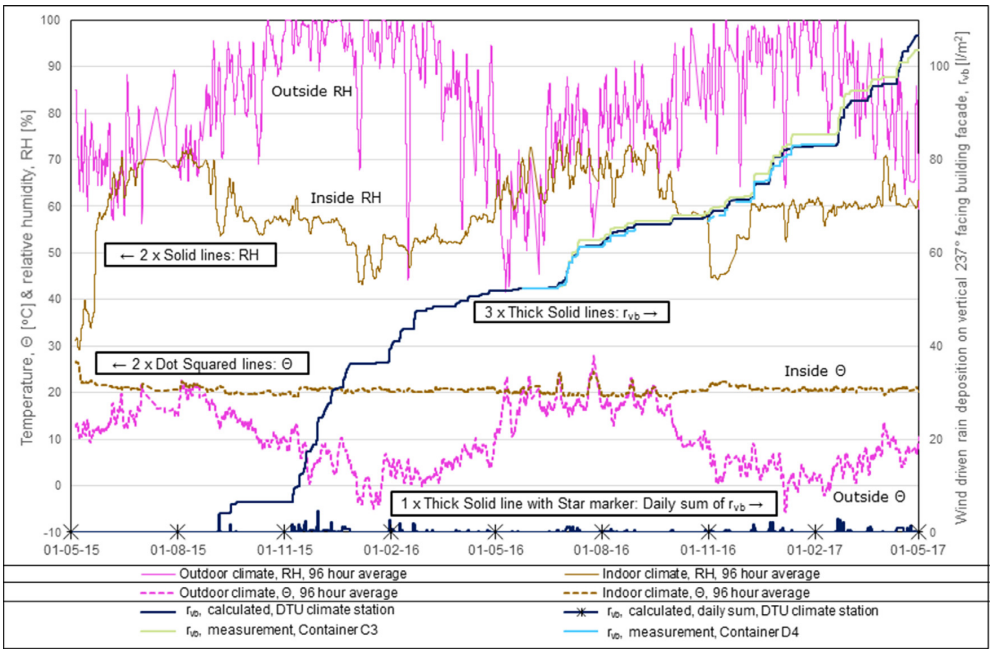


**Fig. 5.** Measured in- and outdoor boundary conditions in field study. The temperature and relative humidity are measured inside and just outside the field study. The WDR data, expressed as $r_{vb}$ values, are measured at the exterior surface of the field study, and calculated from logged values at a nearby climate station. The measured $r_{vb}$ follow the equivalent calculated values in periods with missing data.

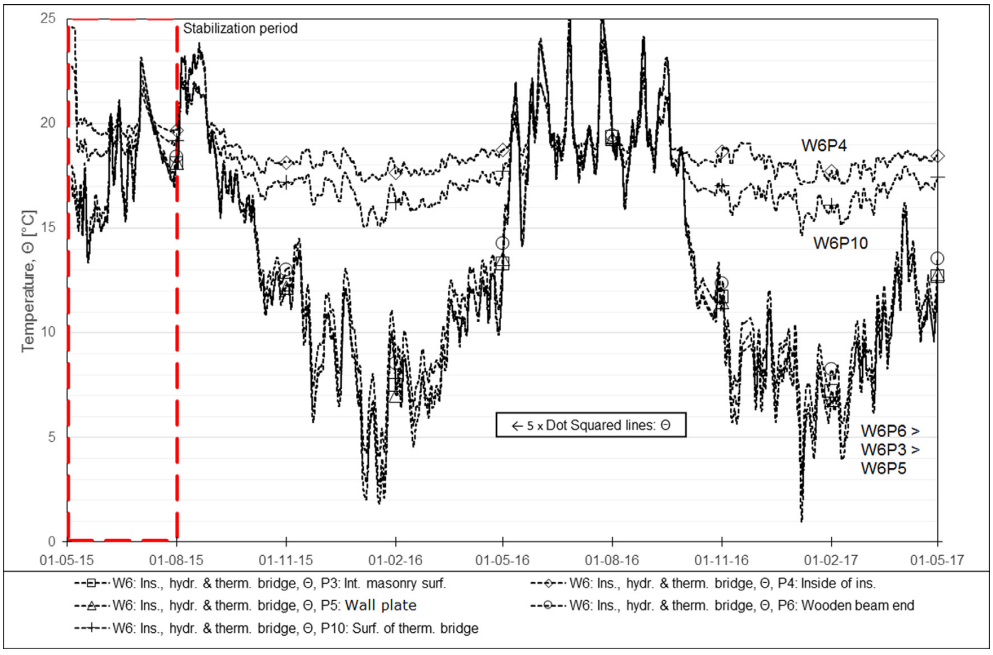


**Fig. 6.** Measured Θ throughout monitoring period. Measurement from sensor points in Wall 6: Insulated, hydrophobized and with deliberate thermal bridge. The measurements in Points 3, 5 and & 6 are difficult to distinguish, but follow each other within a band of 1.5 °C during winter. Additional plots have been produced for other combinations of walls and points can be found in the supplied dataset [58].

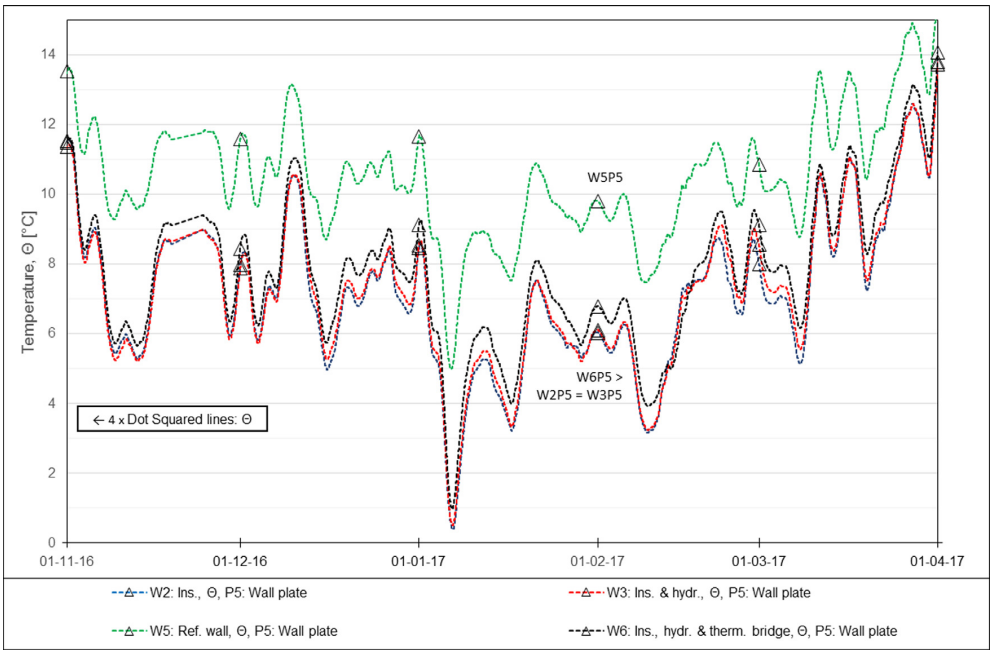


**Fig. 7.** Measured Θ during second winter period. Measurements from Wall 2, 3, 5 & 6 in Point 5: Wall plate. Additional plots have been produced for other combinations of walls and points can be found in the supplied dataset [58].

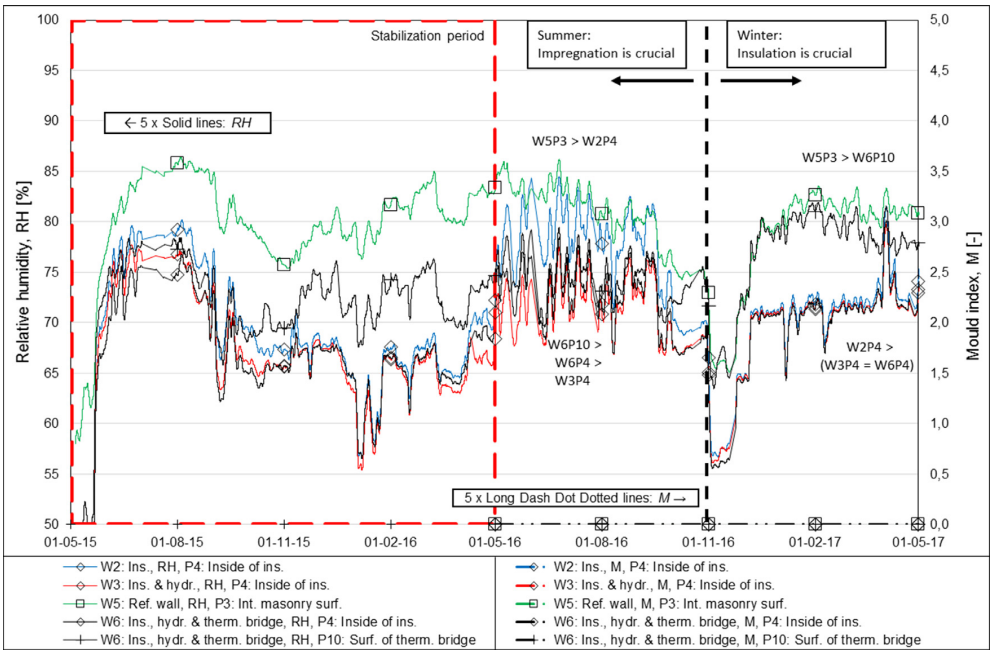


**Fig. 8.** Measured RH and calculated M throughout monitoring period. Sensor points at interior surface: Point 3 for reference wall 5, Point 4 for insulated walls 2, 3 and 6 and Point 10 for Wall 6 with deliberate thermal bridge. Measurements within stabilization period are influenced by initial conditions.

The results and discussion is composed from the following subsections:

- A consistent plot setup used throughout the paper.
- The boundary conditions of the field study.
- Evaluation of the measured temperature, relative humidity and appropriate damage models of the different points. The sensor points are evaluated based on measured temperature and relative humidity, as these values are used when evaluating the implemented mould and decay models described in

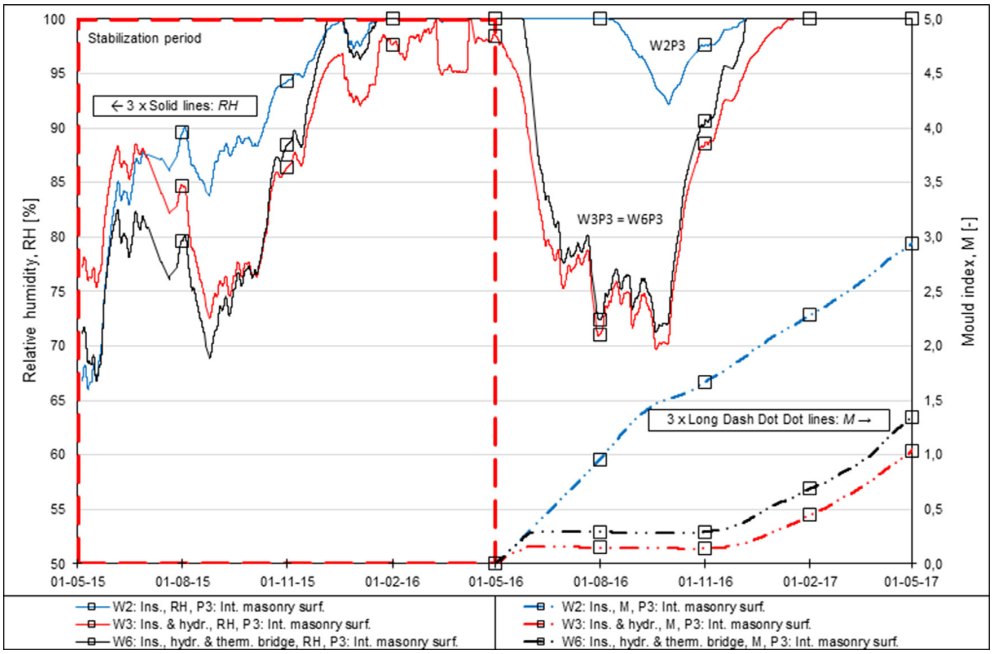


**Fig. 9.** Measured RH and calculated M throughout monitoring period. Sensor point in interior masonry surface, Point 3, in insulated walls 2, 3 and 6. Measurements within stabilization period are influenced by initial conditions.

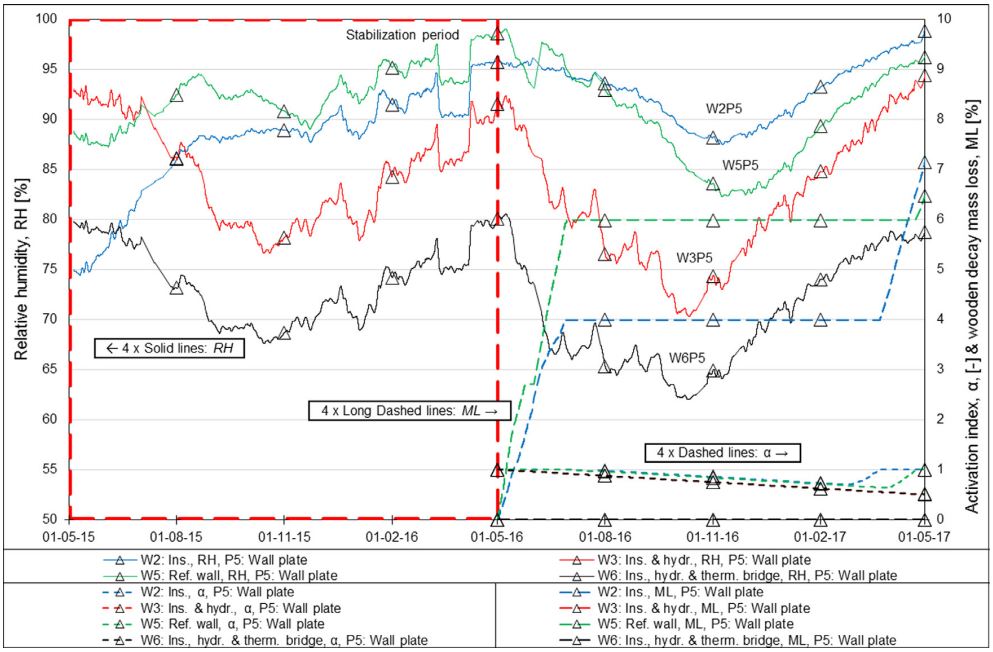


**Fig. 10.** Measured digital RH, calculated $\alpha$ and ML from digital measurements throughout monitoring period. Sensor point in wall plate, Point 5, in reference and insulated walls. Measurements within stabilization period are influenced by initial conditions.

Sections 2.4.1 and 2.4.2 respectively. The outputs of the mould model is included in plots for the interior surface and the interior masonry surface behind insulation (abbreviated: masonry/insulation interface). The outputs of the wooden decay modelling is included in plots for wall plate and wooden beam end.

- A study into the effect of the hydrophobic treatment by comparison of the non-smoothened relative humidity to wind driven rain (WDR).

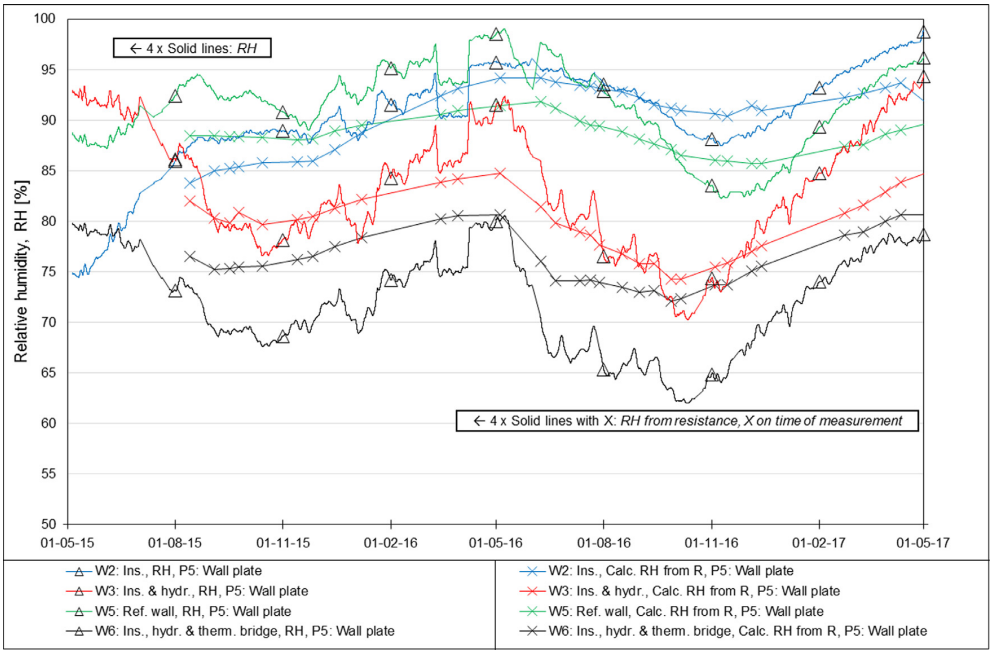


**Fig. 11.** Measured digital RH and RH calculated from electric resistance measurements throughout monitoring period. Sensor point in wall plate, Point 5, in reference and insulated walls.

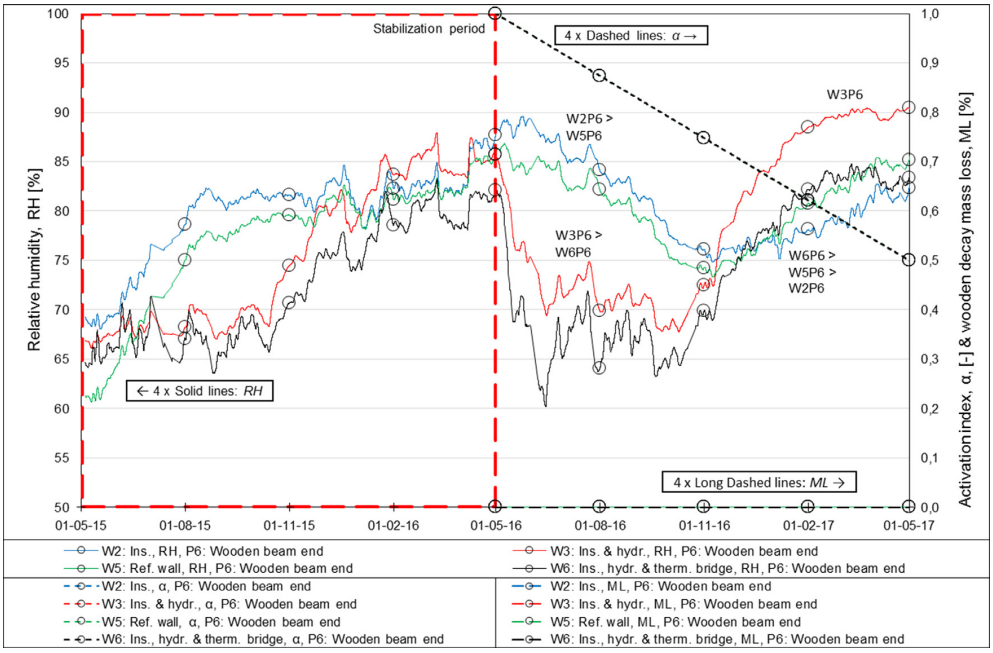


**Fig. 12.** Measured RH, calculated $\alpha$ and ML throughout monitoring period. Sensor point in wooden beam end, Point 6, in reference and insulated walls. Measurements within stabilization period are influenced by initial conditions.

The starting point for the moisture conditions deviated for the four walls. By inspection of measurements from the masonry walls in Fig. 13 it is observed that the moisture conditions vary and do not stabilize until the 2nd summer, in May 2016. Determination of moisture stabilization in the 2nd summer is based on similar values in May of 2016 and 2017. All measurements have been included, but measurements prior to May 2016 are marked with "stabilization period" and the discussion of the results are based on the period after stabilization. The thermal conditions stabilize faster, showing stable results as of August 2015. The damage mod-

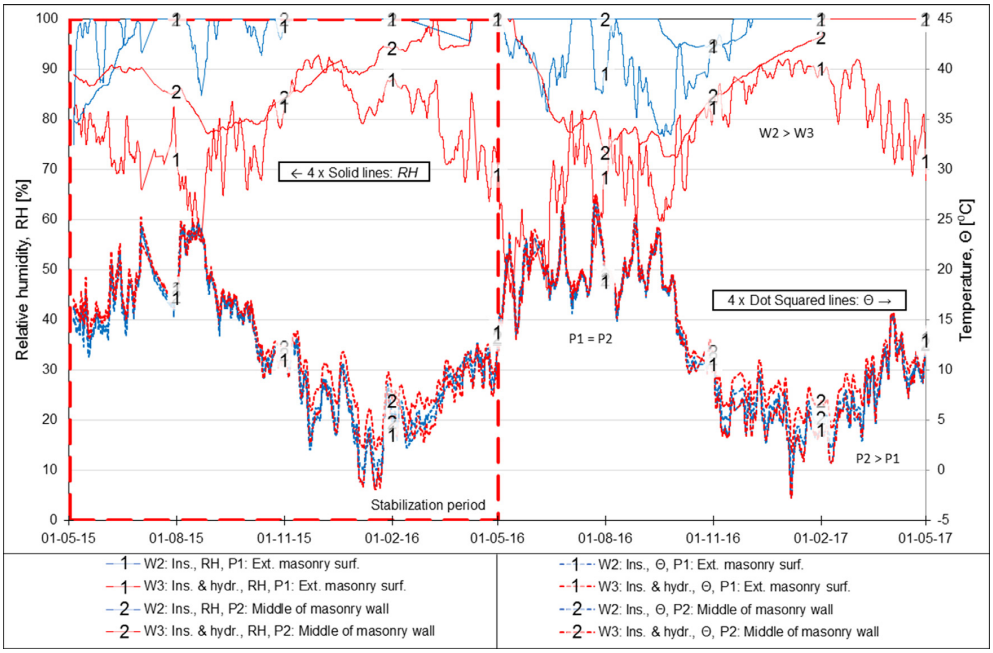


**Fig. 13.** Measured RH and Θ throughout monitoring period. Sensor points in masonry wall: Point 1 & 2. Un-hydrophobized and hydrophobized insulated Wall 2 & 3. Measurements within stabilization period are influenced by initial conditions.

**Table 2**
Description of consistent line colour, style and markers used in all plots in present paper. The different wall compositions are illustrated in Fig. 2. The location of measurement points are illustrated in Fig. 3.

| Line colour | Line style | Line marker |
|---|---|---|
| Blue = W2: Ins. | Solid = RH | 1 no. 1 = P1: Ext. masonry surf. |
| Red = W3: Ins. & hydr. | Dot Squared = Θ | 2 no. 2 = P2: Middle of masonry wall |
| Green = W5: Ref. wall | Long Dash Dot Dot = M | □ Square = P3: Int. masonry surf. |
| Black = W6: Ins., hydr. & therm. bridge | Dash = α | ◇ Diamond = P4: Inside of ins. |
| Pink = Outdoor climate | Long Dash = ML | △ Triangle = P5: Wall plate |
| Brown = Indoor climate | Solid, thick = $r_{vb}$ | ○ Circle = P6: Wooden beam end |
| Dark blue = $r_{vb}$, calculated, DTU climate station | | + Plus = P10: Surf. of therm. bridge |
| Turquise = $r_{vb}$, measurement, Container D4 | | ⁎ Star = $r_{vb}$, daily sum |
| Lime = $r_{vb}$, measurement, Container C3 | | |

els: wooden decay mass loss and mould index have been calculated with starting point at the time of stabilization.

### 3.1. Plot setup, consistent line colour, style and markers used throughout paper

The figures throughout the paper are consistently marked from line colour, style or marker, as illustrated in Table 2.

- The specific line colour indicate the wall number or specific WDR station.
- The line style indicate the variable.
- The line marker indicate the measuring point or daily sum of WDR.

The clear distinction in line format are implemented to allow for identification of the wall composition, measurement point and variable without need to consult the legend.

The date stamps in all figures are defined as "dd–mm–yy". The position of the line markers are defined based on the position of the date stamps on the *x*-axis.

### 3.2. Boundary conditions in field study

Measured boundary conditions can be seen in Fig. 5, where the indoor conditions are averages of two measurements: one from each end of the field study. Horizontal rain measurements from DTU's climate station [47] were fully operational as of 2015.09.05. WDR deposition on vertical building façade angled 237° from north ($r_{vb}$) have been calculated from this point in time and onwards, illustrated with a thick dark blue line. Measured $r_{vb}$ is illustrated with thick turquoise and lime colour lines for container D4 and C3 respectively. Periods with fault on the individual WDR gauges are illustrated by removing the line. The cumulative values for faulty sensors follow the increase of the calculated WDR based on DTU's climate station.

The indoor set points were: Temperature = 20 °C and relative humidity = 70% in the first 3 months, 60% during the remaining period. As dehumidifier and cooling units were not fitted, fluctuations were possible in periods with impact from high outdoor temperature/solar radiation and humidity.

During the monitoring period, the water tank for the humidifier ran out two times, resulting in decreased indoor relative humid-

**Table 3**
Temperatures in measurement points of presented walls during winter periods, compared to reference wall. Investigated based on figures in supplied dataset [58] and Figure 7.

| | Point 3 & 4: Interior surface | Point 3: Original masonry surface | Point 5: Wall plate | Point 6: Wooden beam end |
|---|---|---|---|---|
| Wall 5: reference wall | Reach running average surface temperatures down to 13 °C. | | | |
| Wall 2: insulated | Reach a minimum of 17 °C. The surface temperature of the deliberate thermal bridge is in the range between insulated and un-insulated, with a minimum of 15 °C | The average temperature of the original masonry surface behind the insulation decreases by up to 10 °C | The average temperature in the wall plate is decreased by 2–5 °C. | The average temperature in the wooden beam end is decreased by 1–4 °C. |
| Wall 3: insulated & hydrophobized | | | | |
| Wall 6: insulated, hydrophobized & deliberate thermal bridge | | | Partly replacing thermal insulation with a thermal bridge change the decrease to 2–4 °C. | Partly replacing thermal insulation with a thermal bridge change the decrease to 1–3 °C. |

ity in the periods: 2016.01.02 until 2016.01.26 and 2016.10.30 until 2016.12.07.

The indoor excess of moisture in the field study was assessed based on humidity classes [41,42]. The resulting humidity class within the heating season was class 3 "Buildings with unknown occupancy" [41], defined as an indoor excess of moisture of 6 g/m³ at 0 °C, falling linearly to 0.75 g/m³ at 20 °C.

### 3.3. Measured relative humidity and temperature, combined with damage model calculations

The following results and discussions are split into various points of interest, being either specific sensor points or locations on the wall (e.g. the interior surface, which will have varying sensor point number depending if insulation have been applied or not).

#### 3.3.1. Temperatures from digital RH/T sensors. Two graphs, additional in dataset

Investigation of the changed temperatures when installing interior thermal insulation is not the purpose of the present paper. The temperatures are however a key component to understand the magnitude of the measured relative humidity. The two graphs included in this subsection are examples of the material supplied in [58], including 30 temperature plots for additional combinations of walls/sensor points, the full monitoring period and two winter periods. The discussion of the temperatures in the current section are based on investigations into the full dataset, based on graphs and data in .csv format [58], analysing various combinations of sensor points and walls individually.

The graphs included as examples of the presented walls/points and periods can be seen in Figs. 6 and 7. Fig. 6 include measurements from sensor Points 3–6 and 10 in the insulated and hydrophobized Wall 6 with a deliberate AAC thermal bridge next to the wall plate in the full monitoring period. Fig. 7 include measurements in Point 5, the wall plate, in all analysed walls during the first winter period.

The average temperatures in the summer period from May until October do in general show similar values for all measurement points. Studying the measured boundary conditions in Fig. 5, it can be seen that the difference in temperature between indoor and outdoor climate is low, explaining the similar measurements at wall points.

The order of temperature conditions in the points/walls change during the winter periods. A zoom on the winter period to emphasize the changes has been illustrated for the wall plate in Fig. 7 with similar zooms for other measurement points and walls in [58]. Taking the temperatures in the un-insulated wall as reference, the changes presented in Table 3 are observed when installing thermal insulation.

The measurements from the digital RH/T sensors have been validated by simple steady state calculations at two time steps, similar to the procedure used in [17]. The calculations have been based on the thermal material properties listed in Section 2.1.3, with an in- and outdoor convective heat transfer coefficient of 0.13 $\frac{m^2K}{W}$ and 0.04 $\frac{m^2K}{W}$ respectively. The measured and calculated temperatures for measurement points in the reference Wall 5 can be seen in Table 4, while similar measured and calculated values for the insulated Wall 2 can be seen in Table 5. Comparing the simplified steady state calculations based on $\lambda$dry to the measurements in the transient field study, it is concluded that the measurements from the field study are validated and follow theory.

#### 3.3.2. Relative humidity from digital RH/T sensors and calculated mould index on interior surface

Measured relative humidity and calculated mould index in the point closest to the interior surface can be seen in Fig. 8. The sensor point differs for insulated and reference walls, being Point 3 for reference Wall 5, Point 4 for insulated Walls 2, 3 and 6 and Point 10 for Wall 6 (the deliberate AAC thermal bridge).

No risk of calculated mould growth is observed at the interior surfaces. The relative humidity on the interior surface of the walls are influenced by the following factors: The moisture content and material properties of the surface material, the surface temperature and the humidity of the indoor air. All walls are influenced by similar humidity from the indoor climate, while the surface temperature and material differ for the masonry surface of the reference wall (sensor Point 3 of Wall 5), the interior insulation surface (Point 4 of Walls 2, 3 and 6) and the interior surface of the deliberate thermal bridge (sensor Point 10 of Wall 6). The relative humidity on the interior surfaces (Fig. 8) follow the indoor conditions (Fig. 5) with an excess to the surface relative humidity caused by the surface temperature and moisture content of the different wall configurations.

The effect of exterior façade impregnation and interior thermal insulation can be observed in Fig. 8. During the summer period, the highest surface relative humidity is observed at the surface of the un-hydrophobized walls: The reference Wall 5 and the insulated Wall 2. The surface of the insulation and thermal bridge of the insulated and hydrophobized Walls 3 and 6 show relative humidity which are 5–10% RH lower than the surface of the reference wall. The measured relative humidity at the surface of the insulated and un-hydrophobized Wall 2 is between those of the

**Table 4**
Comparison between simplified steady state calculations of temperature and temperature measurements from transient field study in wall sensor points. Reference Wall 5.

| Time | | Outside amb. air | Point 1 | Point 2 | Point 3 | Point 4 | Inside amb. air |
|---|---|---|---|---|---|---|---|
| 2016.10.10 12:00 | Meas. | 9.3 °C | 11.6 °C | 13.4 °C | 16.5 °C | – | 19.7 °C |
| | Calc. | – | 10.8 °C | 13.3 °C | 16.7 °C | – | – |
| | Dif. | – | −0.8 °C | −0.1 °C | +0.2 °C | – | – |
| 2017.02.01 12:00 | Meas. | 2,6 °C | 6.1 °C | 9.6 °C | 15.0 °C | – | 20.1 °C |
| | Calc. | – | 5.2 °C | 9.3 °C | 15.0 °C | – | – |
| | Dif. | – | −0.9 °C | −0.3 °C | 0 °C | – | – |

**Table 5**
Comparison between simplified steady state calculations of temperature and temperature measurements from transient field study in wall sensor points. Insulated Wall 2.

| Time | | Outside amb. air | Point 1 | Point 2 | Point 3 | Point 4 | Inside amb. air |
|---|---|---|---|---|---|---|---|
| 2016.10.10 12:00 | Meas. | 9.3 °C | 10.5 °C | 10.7 °C | 11.7 °C | 18.2 °C | 19.7 °C |
| | Calc. | – | 9.7 °C | 10.3 °C | 11.1 °C | 19.1 °C | – |
| | Dif. | – | −0.8 °C | −0.4 °C | −0.6 °C | +0.9 °C | – |
| 2017.02.01 12:00 | Meas. | 2,6 °C | 4.1 °C | 5.1 °C | 6.9 °C | 17.4 °C | 20.1 °C |
| | Calc. | – | 3.2 °C | 4.2 °C | 5.6 °C | 19.2 °C | – |
| | Dif. | – | −0.9 °C | −0.9 °C | −1.3 °C | +1.8 °C | – |

reference and the hydrophobized walls, peaking at values similar to that of the reference wall.

During the winter period, the highest surface running average relative humidity is observed on the un-insulated interior surfaces: The masonry surface of Wall 5 (84% RH) and the surface of the deliberate thermal bridge of Wall 6 (82% RH). The surface of the insulation on Walls 2, 3 and 6 show running average relative humidity values 10–15% RH lower than those of the reference wall.

*3.3.3. Relative humidity from digital RH/T sensors and calculated mould index on interior masonry surface, behind insulation*

Measured relative humidity and calculated mould index in Point 3, masonry/insulation interface, can be seen in Fig. 9.

The heat flow to the masonry wall is reduced by applying thermal insulation to the interior surface. The combination of reduced heat flow and diffusion open insulation, allowing diffusion of moisture from the indoor climate, can cause condensation to form on the interior masonry surface.

This effect can be seen in Fig. 9 with condensation during the winter in Point 3 for all insulated Walls 2, 3 and 6. The diffusion open system is designed to allow drying to the interior side, but the un-hydrophobized Wall 2 never drops below a running average of 85% RH. Reduction of rain intrusion by hydrophobation gives a positive effect during summer in Wall 3 and 6, resulting in a minimum of the running average of 70% RH. The calculated mould indexes for the insulated walls show worsened conditions, resulting in a calculated mould index of $M = 2.9$ for Wall 2 and expected similar results of $M = 1.0$ and $M = 1.3$ for Wall 3 and 6. The results are obtained after 1 year of mould index calculation, with a rising tendency in the winter period. Mould index exceeding 3 in interfaces is unacceptable as defined by Viitanen et al. [44], which is expected when analysing longer datasets.

The measured relative humidity is in accordance with results of previous research describing that the hydrophobation has a positive effect for the application of interior insulation [24]. The effect is however not sufficient to ensure that moisture induced damage do not occur with the boundary conditions applied in the field study.

*3.3.4. Relative humidity from digital RH/T sensors and calculated wooden decay mass loss in wall plate*

Measured relative humidity, calculated activation process and wooden decay mass loss in Point 5, the wall plate, can be seen in Fig. 10. Comparison between digital and electrical resistance based measured values in the wall plate have been done later in this section.

The running average relative humidity in the wall plate in Fig. 10 is analysed based on observations from the increasing components in the wall compositions.

1. Reference Wall 5 shows high RH in winter, decreasing during summer. Calculation of wooden decay shows risk of damage in the period May until July.
2. Applying interior insulation in Wall 2 increases the RH as the temperature decreases. This effect is clearest during winter when the temperature difference is the largest, as seen in Fig. 7. Calculation of wooden decay shows risk of damage in the period April until July.
3. Hydrophobation of the exterior surface in Wall 3 reduces the RH in the wall plate during the summer period to a lower level than reference Wall 5. A rapid increase is seen in the winter period, peaking close to the level of both of the un-hydrophobized Walls 2 and 5. Calculation of wooden decay shows that hydrophobation reduces the risk, with no calculated damage.
4. Inserting a deliberate thermal bridge next to the wall plate in Wall 6 increases the temperature during the winter period in the wall plate, compared to the insulated cases in Wall 2 and 3 resulting in reduced RH. Calculation of wooden decay shows that the deliberate thermal bridge further reduce the risk, with no calculated damage.

The damage observed in the reference Wall 5 emphasise the need to control the indoor humidity load in buildings, for instance by installing mechanical ventilation.

Correlation between measurements in the wall plate in Fig. 10 and in the masonry wall in Fig. 13 is observed. Based on this observation, it can be concluded that the moisture content in the masonry wall influences the conditions in the wall plate.

The measured RH from the digital sensors have been compared against the resulting calculated RH from manual electrical resistance measurements in the wall plate in Fig. 10. Similar results were observed from the resistance-based measurements, including the shift of highest relative humidity between Wall 2 and 5.

*3.3.5. Relative humidity from digital RH/T sensors and calculated wooden decay mass loss in wooden beam end*

Measured relative humidity, calculated activation process and wooden decay mass loss in Point 6, the wooden beam end, can be seen in Fig. 12.

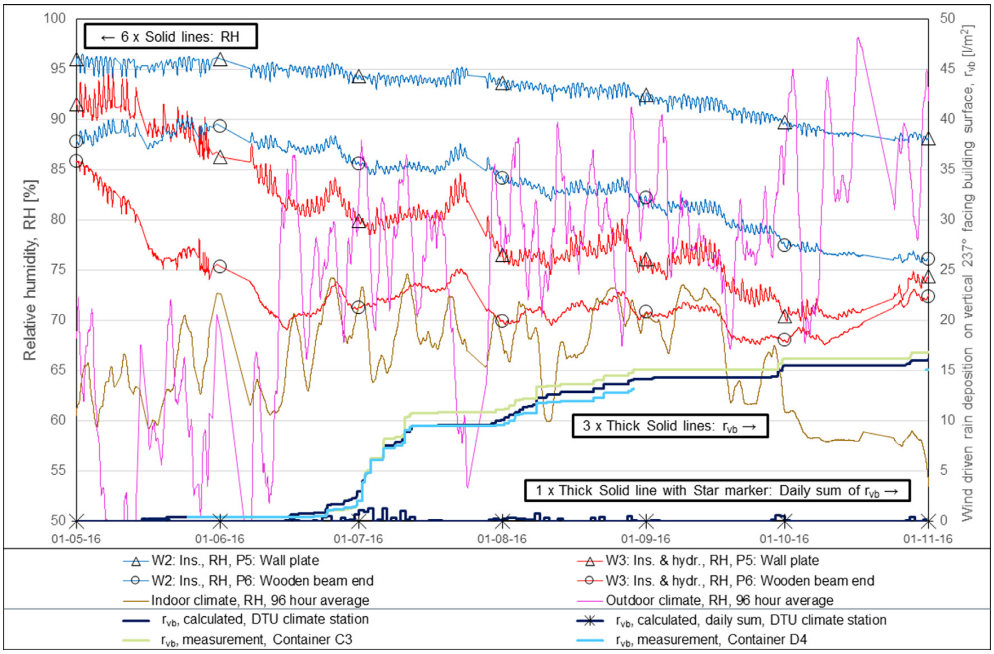


**Fig. 14.** Non-smoothened measurement in walls during 2nd summer period together with in- and outdoor RH and WDR. Measurements from wooden elements, Point 5 & 6, in insulated Walls 2 & 3.

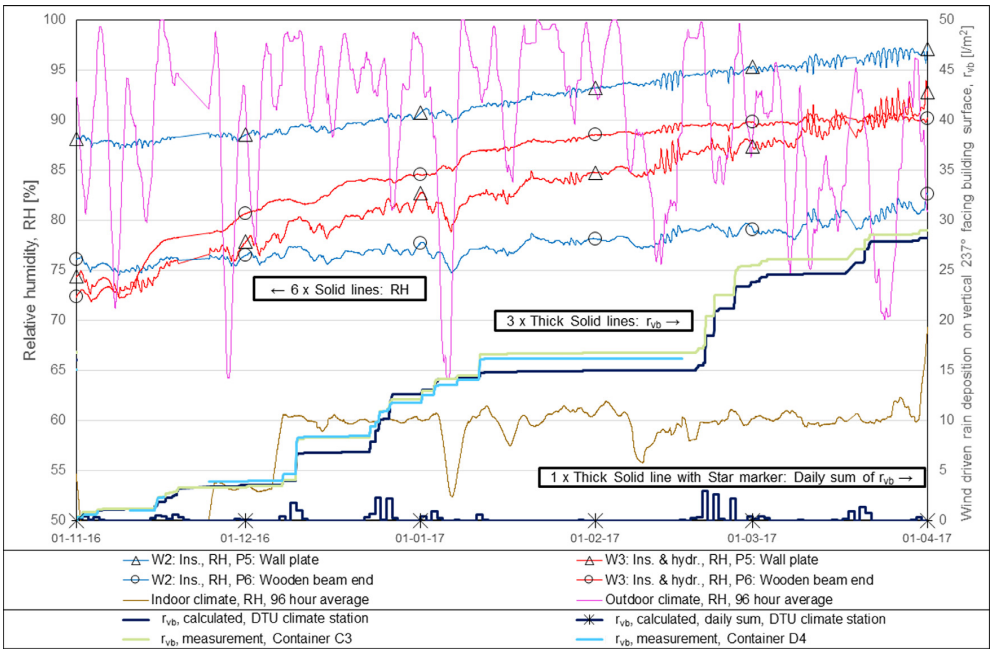


**Fig. 15.** Non-smoothened measurement in walls during 2nd winter period together with in- and outdoor RH and WDR. Measurements from wooden elements, Point 5 & 6, in insulated Walls 2 & 3.

No risk of calculated wooden decay is observed in the wooden beam end. We observe that the un-hydrophobized walls: Reference Wall 5 and insulated Wall 2 show similar running average relative humidity in Fig. 12, deviating within ±5% over the course of the summer. Hydrophobation of the exterior surface in Wall 3 induced a reduction of the relative humidity during the summer period May 2016 until November 2016, while an increase occurred during the winter period November 2016 until May 2017. The relative humidity in the wooden beam end of an insulated and hydrophobized wall could generally be reduced by increasing the temper-

ature via insertion of a deliberate thermal bridge in Wall 6, thus reducing the increase during the winter period to that of the un-hydrophobized Walls 2 & 5. The effect of the hydrophobation is further discussed in Section 3.3.7.

Correlation between the measurements in the wooden beam end in Fig. 12 and the masonry wall in Fig. 13 is observed. Based on this observation, it can be concluded that the conditions in the wooden beam end follow the moisture content in the masonry wall influence.

*3.3.6. Relative humidity from digital RH/T sensors mounted in brick near exterior masonry surface and in middle of masonry wall*

Measured relative humidity and temperature in bricks in Points 1 and 2, Wall 2 and 3, can be seen in Fig. 13.

The temperatures measured in the insulated and un-/hydrophobized Wall 2 and 3 in [58] and Fig. 13 show similar temperatures in Point 1, close to the exterior masonry surface, and temperatures approximately 1 °C higher in the hydrophobized Wall 3 in Point 2, the middle of the masonry wall, during the winter period.

The relative humidity measured in the two walls follow the same tendency, with higher values observed in the un-hydrophobized Wall 2, averaging at 90% RH during summer and saturation (100% RH) during winter. The similar measurements from the hydrophobized Wall 3 show averaging at 70% RH during summer, peaking at 90% RH during winter. Relative humidity measured in the middle of the masonry wall indicate saturation in the un-hydrophobized Wall 2 in Fig. 13, while the hydrophobized Wall 3 show measurements following the exterior side during summer and saturation during winter.

*3.3.7. Summing up on exterior hydrophobation*

The application of interior diffusion open insulation pose a risk of condensation on the interior surface of the masonry, as can be seen in Fig. 9. As hydrophobation reduce the rate of drying of water through the hydrophobized depth at the exterior surfaces [35], this potential condensate water will have reduced possibility to evaporate to the cold and dry outdoor Danish winter climate. The result of the hydrophobic façade treatment can be seen in the rapidly inclining RH in winter period for hydrophobized walls. This effect was especially seen on the wooden beam end in Fig. 12, discussed in Section 3.3.5.

*3.4. Influence of rain deposited on building façade*

A study on the influence of wind driven rain deposited on the building façade has been performed based on plotting non-smoothened point measurements against wind driven rain and running average indoor and outdoor relative humidity. The following two stabilized periods have been emphasized: 2nd summer period in Fig. 14, and 2nd winter period in Fig. 15. The measurements include the wall plate and the wooden beam end, Point 5 and Point 6 respectively, from the insulated and un-hydrophobized Wall 2 and hydrophobized Wall 3.

A large rain event can be seen in Fig. 14, in the beginning of July 2016, depositing an average $r_{vb}$ of 7.3 l/m² over 10 days from the 1 calculated and 2 measured WDR amounts. The rain event results in a short-term increase in relative humidity 9 days after the end of the rain event. A similar, but smaller increase can be seen from the less intense but longer rain event in August 2016. Based on this result, it is concluded that large rain events during the summer period only lead to temporary increases in relative humidity in wooden elements with a time gap between the event and the reaction. The relative humidity measurements in the hydrophobized Wall 3 declines at a faster rate in the summer than the un-hydrophobized Wall 2, while the rain events have a larger temporary influence on the relative humidity recorded in the hydrophobized wall.

During the winter period in Fig. 15, the rain events do not result in similar temporary increases in relative humidity. A more general increase induced from the winter period is seen throughout the period. The hydrophobation issue for cold climate discussed in Section 3.3.7 results in the increase in relative humidity for the wooden beam end of the hydrophobized Wall 3, exceeding values of the un-hydrophobized Wall 2 as the hydrophobation decreases the liquid transport and thereby drying potential to the outdoor cold and dry air.

## 4. Conclusion

The paper presents the first results from a large field study, investigating the effect of applying thermal insulation to the interior side of characteristic historic solid masonry walls. The study includes combining measures to cope with the changed moisture conditions when applying interior thermal insulation. One being application of a hydrophobizing agent to the exterior masonry surface, another being the implementation of a material/thermal bridge with a higher thermal conductivity next to the wall plate and wooden beam, to increase the heat flow to the wooden elements.

The investigated thermal insulation consisted of 100 mm lightweight AAC, installed strictly following the producer's description, to a 360 mm thick solid masonry wall. The exterior surface was exposed to a Danish climate, with an indoor climate of 20 °C and 60% RH. Continuous digital RH/T measurements were performed at multiple positions throughout the masonry wall, in the insulation and in the wooden elements.

The hydrophobizing agent has a varying effect on the measured conditions in the walls depending on season, where the hydrophobation limits the transport of moisture towards the exterior surface during winter, and thereby the evaporation to the cold and dry Danish climate. In the summer, when moisture transport is towards the interior side, the hydrophobation reduces the measured RH in the measurement points.

Damage models were implemented to evaluate the different hygrothermal responses when installing thermal insulation to the interior masonry surface in different variations. Even though the models cannot be expected able to precisely predict evolution of damage, they still show a reference value higher or lower than the initial conditions in the reference wall. Measurements at the masonry surface, behind the interior insulation, showed that the hygrothermal conditions were worsened as the investigated thermal insulation product would not be able to keep the RH below critical levels during the winter period, resulting in unacceptable calculated mould index >3. Based on the found mould indexes behind the thermal insulation material in Section 3.3.3, compared to no calculated mould germination/growth on the un-insulated wall in Section 3.3.2, only the un-insulated wall indicate a viable construction.

Measurements in the wall plates showed a calculated risk of wooden decay for the reference and insulated wall, but also showed that hydrophobation and implementation of a deliberate thermal bridge could improve the hygrothermal conditions in the construction.

The deliberate thermal bridge is shown to reduce the RH in the wooden elements, reducing the increase in RH from hydrophobation during winter to that of the reference and insulated wall in the wooden beam end and to a maximum level under 80% RH for the wall plate.

Investigation of wind-driven rain showed that even though hydrophobation overall reduced the RH in measurement points, it

was not possible to see an effect after large rain events in the wooden elements.

## Conflict of interest

We wish to confirm that there are no known conflicts of interest associated with this publication and there has been no financial support for this work that could have influenced its outcome.

## Acknowledgements

Ph.D. student Tessa Kvist Hansen and Linatex A/S for the collaboration on development of wind driven rain measurement systems.

Lars Kokholm Andersen for developing the physical system and programming between computer and sensors.

Xella Denmark for installation of Ytong Multipor system on the interior surface of the walls.

Intro Flex ApS for application of Remmers Funcosil FC on the exterior surface of the walls.

The data logging systems have been bought from the following respective companies: the vertical rain gauges are "RG3-M HOBO Rain Gauge" from "ONSET". The digital RH/T sensor module are "HYT 221″ from "Innovative Sensor Technology IST AG". The connection from the sensor module was established with "sensorcable for EK-H3/H4″ from "Sensirion AG".

The field study was supported by Realdania, planned in cooperation with Xella Denmark.

Xella, Ytong and Intro Flex have not had any influence on the results and analyses presented in this paper.

This work was supported through the Danish industrial Ph.D. program by Innovationsfonden [grant number 1355-00129]; COWIfonden [grant number C-123.01]; and COWI A/S.

## References

[1] J. Engelmark, Københavnsk etageboligbyggeri 1850–1900, En Byggeteknisk Undersøgelse, Statens Byggeforskningsinstitut, Hørsholm, 1983 http://www.danskbyggeskik.dk/pdf/open.action?pdf.id=188.

[2] J. Engelmark, Dansk Byggeskik : Etagebyggeriet gennem 150 år, first ed., Realdania Byg, 2013.

[3] T. Odgaard, S.P. Bjarløv, C. Rode, Interior insulation—characterisation of the historic, solid masonrybuilding segment and analysis of the heat saving potential by 1d, 2d,and 3d simulation, Energy Build. 160 (2018) 1–11, doi:10.1016/j.enbuild.2017.12.008.

[4] J. Kragh, K.B.B. Wittchen, Development of two Danish building typologies for residential buildings, Energy Build. 68 (2014) 79–86, doi:10.1016/j.enbuild.2013.04.028.

[5] K.B. Wittchen, J. Kragh, O.M. Jensen, Energy saving potentials – a case study on the Danish building stock, in: ECEEE 2011 SUMMER STUDY • ENERGY Effic. FIRST Found. A LOW-CARBON Soc., 2011, pp. 1355–1363.

[6] M. Morelli, S. Svendsen, Investigation of interior post-insulated masonry walls with wooden beam ends, J. Build. Phys. 36 (2012) 265–293, doi:10.1177/1744259112447928.

[7] M. Morelli, L. Rønby, S.E. Mikkelsen, M.G. Minzari, T. Kildemoes, H.M. Tommerup, Energy retrofitting of a typical old Danish multi-family building to a 'nearly-zero' energy building based on experiences from a test apartment, Energy Build. 54 (2012) 395–406, doi:10.1016/j.enbuild.2012.07.046.

[8] Z. Pavlik, Hygrothermal performance study of an innovative interior thermal insulation system, Appl. Therm. Eng. 29 (2009) 1941–1946, doi:10.1016/j.applthermaleng.2008.09.013.

[9] G.A. Scheffler, Hygric performance of internal insulation with light-weight autoclaved aerated concrete, in: Proc. 5th Int. Conf. Autoclaved Aerated Concr. Sept. 15-16, 2011, 2011, pp. 323–335. http://www.xella.com/de/docs/2011_Scheffler_InternalInsulation-LightWeightAAC-Multipor.pdf.

[10] J. Toman, A. Vimmrova, R. Cerny, Long-term on-site assessment of hygrothermal performance of interior thermal insulation system without water vapour barrier, Energy Build. 41 (2009) 51–55, doi:10.1016/j.enbuild.2008.07.007.

[11] J. Zhao, J. Grunewald, U. Ruisinger, S. Feng, Evaluation of capillary-active mineral insulation systems for interior retrofit solution, Build. Environ. 115 (2017) 215–227, doi:10.1016/j.buildenv.2017.01.004.

[12] M. Harrestrup, S. Svendsen, Full-scale test of an old heritage multi-storey building undergoing energy retrofitting with focus on internal insulation and moisture, Build. Environ. 85 (2015) 123–133, doi:10.1016/j.buildenv.2014.12.005.

[13] A.A. Hamid, P. Wallent En, Hygrothermal assessment of internally added thermal insulation on external brick walls in Swedish multifamily buildings, Build. Environ. 123 (2017) 351–362, doi:10.1016/j.buildenv.2017.05.019.

[14] G. Christensen, A.P. Koch, E.B. Møller, Erfaringsblad (31)151115: indvendig efterisolering - ældre ydervægge af murværk, BYG-ERFA. (2015).

[15] J. Straube, C. Schumacher, Interior insulation retrofits of load-bearing masonry walls in cold climates, J. Green Build. 2 (2007) 42–50, doi:10.3992/jgb.2.2.42.

[16] K. Ueno, J. Straube, R. Van Straaten, Field monitoring and simulation of a historic mass masonry building retrofitted with interior insulation, in: Therm. Perform. Exter. Envel. Whole Build. XII Int. Conf., ASHRAE, 2013, pp. 1–16.

[17] P. Johansson, S. Geving, C.-E. Hagentoft, B. Petter Jelle, E. Rognvik, A.S. Kalagasidis, B. Time, Interior insulation retrofit of a historical brick wall using vacuum insulation panels: Hygrothermal numerical simulations and laboratory investigations, Build. Environ. 79 (2014) 31–45, doi:10.1016/j.buildenv.2014.04.014.

[18] H.M. Kuenzel, Effect of interior and exterior insulation on the hygrothermal behaviour of exposed walls, Mater. Struct. 31 (1998) 99–103.

[19] G. Scheffler, A. Worch, S. Bäumler, J. Beck-Bazlen, A. Binder, R. Borsch-Laaks, K. Burcek, M. Elbel, J. Engel, M. Epple, F. Eßmann, J. Gänßmantel, C. Hecht, M. Hildebrand, D. Hofmann, D. Kehl, C. Lenker, S. Plumanns, A. Range, H. Riggert, G. Rudolph, U. Ruisinger, T. Steiner, D. Vogt, P. Wegerer, W. Walther, D. Zirkelbach, WTA-Merkblatt 6-5: interior insulation according to WTA II : evaluation of internal insulation systems with numerical design methods, 2014.

[20] E. Vereecken, S. Roels, A comparison of the hygric performance of interior insulation systems: a hot box–cold box experiment, Energy Build. 80 (2014) 37–44, doi:10.1016/j.enbuild.2014.04.033.

[21] M.N. Saïd, R.G. Demers, L.L. McSheffrey, Hygrothermal performance of a masonry wall retrofitted with interior insulation, Res. Build. Phys. (2003) 445–454. http://irc.nrc-cnrc.gc.ca/ircpubs.

[22] E. Vereecken, S. Roels, Capillary active interior insulation: do the advantages really offset potential disadvantages? Mater. Struct. 48 (2015) 3009–3021, doi:10.1617/s11527-014-0373-9.

[23] T. De Mets, A. Tilmans, X. Loncour, Hygrothermal assessment of internal insulation systems of brick walls through numerical simulation and full-scale laboratory testing, in: 11th Nord. Symp. Build. Physics, NSB2017, Trondheim, Norway, Elsevier Ltd, 2017, pp. 753–758, doi:10.1016/j.egypro.2017.10.022.

[24] G.R. Finken, S.P. Bjarløv, R.H. Peuhkuri, Effect of facade impregnation on feasibility of capillary active thermal internal insulation for a historic dormitory - a hygrothermal simulation study, Constr. Build. Mater. 113 (2016) 202–214, doi:10.1016/j.conbuildmat.2016.03.019.

[25] T. Odgaard, S.P. Bjarløv, C. Rode, Interior insulation – Experimental investigation of hygrothermal conditions and damage evaluation of solid masonry façades in a listed building, Build. Environ. 129 (2018) 1–14, doi:10.1016/j.buildenv.2017.11.015.

[26] E.J.deP. Hansen, E.B. Møller, Moisture supply in Danish single-family houses – the influence of building style, in: 11th Nord. Symp. Build. Physics, NSB2017, Trondheim, Norway, Elsevier Ltd, 2017, pp. 147–152, doi:10.1016/j.egypro.2017.09.663.

[27] E.B. Møller, E.J.deP. Hansen, Moisture supply in Danish single-family houses – the influence of occupant behavior and type of room, in: 11th Nord. Symp. Build. Physics, NSB2017, Trondheim, Norway, Elsevier Ltd, 2017, pp. 141–146, doi:10.1016/j.egypro.2017.09.661.

[28] A. Nielsen, E.B. Møller, T.V. Rasmussen, E.J.deP. Hansen, Use of sensitivity analysis to evaluate hygrothermal conditions in solid brick walls with interior insulation, in: Proc. 5th Int. Build. Phys. Conf., Kyoto, Japan, Kyoto University, 2012, pp. 377–384.

[29] K. Calle, N. Van Den Bossche, Towards understanding rain infiltration in historic brickwork, in: 11th Nord. Symp. Build. Physics, NSB2017, Trondheim, Norway, Elsevier Ltd, 2017, pp. 676–681, doi:10.1016/j.egypro.2017.10.005.

[30] P. Kopecký, K. Staněk, M. Bureš, J. Richter, J. Tywoniak, Experimental investigations of wooden beam ends in masonry with internal insulation, in: 11th Nord. Symp. Build. Physics, NSB2017, Trondheim, Norway, Elsevier Ltd, 2017, pp. 682–687, doi:10.1016/j.egypro.2017.10.006.

[31] B. Blocken, J. Carmeliet, Overview of three state-of-the-art wind-driven rain assessment models and comparison based on model theory, Build. Environ. 45 (2010) 691–703, doi:10.1016/j.buildenv.2009.08.007.

[32] R.E. Lacy, Driving-Rain maps and the onslaught of rain on buildings, in: Proc. RILEM/CIB Symp. Moisture Probl. Build., 1965, p. 29.

[33] J.F. Straube, Moisture Control and Enclosure Systems, University of Waterloo, 1998.

[34] J. Straube, Simplified prediction of driving rain on buildings : ASHRAE 160P and WUFI 4.0, Build. Sci. Dig. (2010) 1–16.

[35] J. Engel, P. Heinze, R. Plagge, Adapting hydrophobizing impregnation agents to the object, Restor. Build. Monuments 20 (2014) 433–440, doi:10.12900/RBM14.20.6-0042.

[36] S.P. Bjarløv, C.J. Johnston, M.H. Hansen, Hygrothermal conditions in cold, north facing attic spaces under the eaves with vapour-open roofing underlay in a cool, temperate climate, Build. Environ. 95 (2016) 272–282, doi:10.1016/j.buildenv.2015.09.009.

[37] P. Grunnet Wang, M. Scharling, K. Pagh Nielsen, C. Kern-Hansen, K.B. Wittchen, 2001â€"2010 Danish Design Reference Year: Reference Climate Dataset for Technical Dimensioning in Building, Construction and other Sectors, 2013 http://vbn.aau.dk/ws/files/81253042/DMI_TR13_19.pdf (accessed 23 July 2014).

[38] R.M. Dheilly, J. Tudo, Y. Sebaibi, M. Quéneudec, Influence of storage conditions on the carbonation of powdered Ca(OH)2, Constr. Build. Mater. 16 (2002) 155–161, doi:10.1016/S0950-0618(02)00012-0.

[39] G. Cultrone, E. Sebastián, M.O. Huertas, Forced and natural carbonation of lime-based mortars with and without additives: mineralogical and textural changes, Cem. Concr. Res. 35 (2005) 2278–2289, doi:10.1016/j.cemconres.2004.12.012.

[40] T. Hansen, E.B. Møller, Full scale laboratory test building for examining moisture penetration through different ceilings, in: K.K. Hansen, C. Rode, L.-O. Nilsson (Eds.), Proc. Int. RILEM Conf., Lyngby, Denmark, RILEM Publications S.A.R.L., 2016, pp. 59–68.
[41] DS/EN ISO 13788:2013, Hygrothermal Performance of Building Components and Building Elements — Internal surface Temperature to Avoid Critical Surface Humidity and Interstitial Condensation — Calculation methods, second ed., Dansk Standard/Danish Standards, Charlottenlund, 2013 http://www.iso.org/iso/catalogue_detail.htm?csnumber=51615.
[42] E. Brandt, E.B. Møller, T. Bunch-Nielsen, G. Christensen, C. Gudum, M.H. Hansen, SBi anvisning 224: fugt i bygninger, 2.0, Statens Byggeforskningsinstitut, SBI, 2013.
[43] T.R. Odgaard, Interior Insulation of Buildings from 1850 to 1930 With Solid Masonry Facade Walls and Embedded Wooden Floor Structure, Technical University of Denmak, 2018.
[44] H. Viitanen, M. Krus, T. Ojanen, V. Eitner, D. Zirkelbach, Mold risk classification based on comparative evaluation of two established growth models, in: Energy Procedia, Elsevier B.V., 2015, pp. 1425–1430, doi:10.1016/j.egypro.2015.11.165.
[45] H. Viitanen, Improved Model to Predict Mold Growth in Building Materials, in: Build. X, ASHRAE, 2007, pp. 1–8.
[46] H. Viitanen, T. Toratti, L. Makkonen, R. Peuhkuri, T. Ojanen, L. Ruokolainen, J. Räisänen, Towards modelling of decay risk of wooden materials, Eur. J. Wood Prod. 68 (2010) 303–313, doi:10.1007/s00107-010-0450-x.
[47] E. Andersen, J. Dragsted, T.V. Kristensen, L.K. Andersen, Upgrade and extension of the climate station at DTU Byg, (2014).
[48] Department of Civil Engineering at the Technical University of Denmark, Technische Universität Dresden, Rønby.dk, Ekolab, E&P service, Kingspan, Introflex, Airmaster, COWI, Results and experience from the project: EUDP 2013-II 'Energy efficient comfort in older apartment blocks', Kongens Lyngby, 2016 Final Report.
[49] A.C. Best, The size distribution of raindrops, Q. J. R. Meteorol. Soc. 76 (1950) 16–36.
[50] N. Dingle, Y. Lee, Terminal fallspeeds of raindrops, J. Appl. Meteorol. 11 (1972) 877–879, doi:10.1175/1520-0450(1972)011⟨0877:TFOR⟩2.0.CO;2.
[51] T. Odgaard, S.P. Bjarløv, C. Rode, Excel workbook with Visual Basic script for WDR calculation, 2018.
[52] E.B. Møller, B. Andersen, C. Rode, R. Peuhkuri, Conditions for mould growth on typical interior surfaces, in: 11th Nord. Symp. Build. Physics, NSB2017, Trondheim, Norway, Elsevier Ltd, 2017, pp. 171–176, doi:10.1016/j.egypro.2017.09.680.
[53] E. Vereecken, S. Roels, Review of mould prediction models and their influence on mould risk evaluation, Build. Environ. 51 (2012) 296–310, doi:10.1016/j.buildenv.2011.11.003.
[54] C. Brischke, S. Thelandersson, Modelling the outdoor performance of wood products - a review on existing approaches, Constr. Build. Mater. 66 (2014) 384–397, doi:10.1016/j.conbuildmat.2014.05.087.
[55] K. Gradeci, N. Labonnote, J. Köhler, B. Time, Mould models applicable to wood-based materials – a generic framework, in: 11th Nord. Symp. Build. Physics, NSB2017, Trondheim, Norway, Elsevier Ltd, 2017, pp. 177–182, doi:10.1016/j.egypro.2017.09.751.
[56] T. Ojanen, H. Viitanen, R. Peuhkuri, K. Lähdesmäki, J. Vinha, K. Salminen, Mold growth modeling of building structures using sensitivity classes of materials, Therm. Perform. Exter. Envel. Build. XI (2010) 1–10. http://web.ornl.gov/sci/buildings/2012/2010B11papers/104_Ojanen.pdf.
[57] A. Hukka, H.A. Viitanen, A mathematical model of mould growth on wooden material, Wood Sci. Technol. 33 (1999) 475–485. http://link.springer.com/article/10.1007/s002260050131. (accessed 29 July 2014).
[58] T. Odgaard, S.P. Bjarløv, C. Rode, Data and additional graphs from field study at the Technical University of Denmark. For paper: "Influence of hydrophobation and deliberate thermal bridge on hygrothermal conditions of internally insulated historic solid masonry walls with built-in wood", (2018).

# KEYWORDS

A large share of the current building stock consists of multi-storey buildings from the period 1850-1930. These buildings cannot provide a level of thermal comfort and energy use equivalent to modern standards, leaving the possibility of improvement for occupants, owners and the government. As alterations of the exterior façade are often unwanted, retrofitting the interior masonry surfaces with thermal insulation is investigated.
Only limited areas are available for retrofitting thermal insulation on the interior surfaces due to unavoidable thermal bridges and it was found to worsen the hygrothermal conditions. The area below the window, the spandrel, showed low temperatures which could result in risk of thermal discomfort. It was investigated to only insulate the spandrel under the window, showing that a large share of the total energy saving potential could be achieved with this strategy. A case study showed that retrofitting thermal insulation in the interior surface of the spandrel resulted in worsened hygrothermal conditions in the construction, not reaching a critical level when evaluating mould, wooden decay and frost.

Civil Engineering

Brovej, Building 118
2800 Kongens Lyngby
Tel. 45251700

www.byg.dtu.dk

8778775094